Assembly of intermediate-mass black holes along star formation

Thesis by
Yanlong Shi

In Partial Fulfillment of the Requirements for the
Degree of
Ph.D. in Physics

CALIFORNIA INSTITUTE OF TECHNOLOGY
Pasadena, California

2023
Defended June 1, 2023

Yanlong Shi
ORCID: 0000-0002-0087-3237

ACKNOWLEDGEMENTS

This thesis would not have been possible without the guidance, support, and especially contributions to the field from my thesis advisor, Dr. Philip Hopkins. Like many other students and collaborators, I am always fascinated by Phil's creativity and knowledge in the many fields of astrophysics, not only on the theory side but a broader view connecting observations and computations. I am also largely influenced by his passion for science, which let me finally realize the importance of curiosity and self-motivation in scientific investigation. This is definitely a rough process for me, but it could have been even messier without Phil's patience.

I thank Dr. Jim Fuller, Dr. Olivier Doré, and Dr. Chen Heinrich for their roles as research advisors who led me to explore asteroseismology and observational cosmology, through which I got in touch with different research styles and built new skills. Much of these works proceeded during the pandemic and would not have been possible without their encouragement, which was very important during my Ph.D. I also thank Dr. Charles Steidel for his role on my candidacy and thesis committee.

Research projects presented here also include efforts from other collaborators, Dr. Michael Grudić and Dr. Kyle Kremer. This thesis would also have been literally impossible without many contributors in the FIRE collaborations that I unfortunately seldom or never directly interacted with.

I benefited from the great administrators of PMA and TAPIR, especially Dr. Nam Ung and JoAnn Byod. Their work was essential for this thesis. I also thank my friends for their help and tolerance in many ways, e.g., Linhao is a good driver.

Last but not least, I always owe a lot to my parents and sister who always support me to the best as they can.

ABSTRACT

Intermediate-mass black holes (IMBHs) are poorly observed and not as well understood as stellar-mass black holes (BHs) and supermassive black holes (SMBHs). However, they can be important to complement the formation scenario of massive BHs other than stellar-mass ones and reconcile the existence of some high-energy sources in the Universe. The thesis studies the assembly of IMBHs in star-forming giant molecular clouds (GMCs) of $\sim 5 - 500\,\mathrm{pc}$ and $\sim 10^4 - 10^{10}\,\mathrm{M}_\odot$, which are realistic environments for some scenarios of IMBH formation, including runaway collisions in dense star clusters and super-Eddington accretion onto $\sim 100\,\mathrm{M}_\odot$ BH seeds like remnants of massive stars.

We first inspect the runaway-collision scenario where IMBHs form as remnants of "quasi-stars" after stellar collisions. Density profiles of young massive clusters can be important for this scenario but are missing observational hints. We measure density profiles of cluster populations in star-formation simulations in GMCs and conduct both analytic derivations and Monte-Carlo simulations to estimate the mass of the quasi-star in different clusters. The analytic expression is in approximate agreement with observations.

The following three chapters are about the super-Eddington accretion scenario. The first question to solve is the availability of super-Eddington accretion in turbulent and star-forming environments. We run simulations of BH accretion in GMCs with star formation based on FIRE-2 physics. We find that dense clumps generated by stellar feedback and turbulence can feed BHs at high accretion rates. We also conclude that GMCs with high surface densities are favored for super- or hyper-Eddington accretion, in which self-gravity dominates over stellar feedback.

After convincing the availability of super-Eddington accretion in dense GMCs, we study the self-regulation of BH accretion through its feedback. We construct a sub-grid model of BH accretion and feedback, including radiation, winds/jets, and relativistic diffusive cosmic rays. We find that super-Eddington accretion is still achievable with proper radiative feedback models but is challenged by BH mechanical feedback. We also quantify BH feedback effects and find that they can be analytically explained with momentum-driven arguments. Moreover, we study the effects of multiple sub-grid parameters and BH feedback's impact on star formation in GMCs.

Finally, we study another mode of accretion due to steady gas inflow towards BHs. This complements the missing interaction between stars and BHs in previous studies. Along with star formation, star clusters form and merge hierarchically, creating deep potential wells to capture BHs. At the late stage of the simulation, a $\sim 10\,\mathrm{pc}$ disk structures form. The gas inflow rate can be $\sim 10\,\mathrm{M}_\odot/\mathrm{yr}$. We find a non-trivial strong toroidal magnetic field in the disk, which is thermally heated and ionized by feedback from stars.

PUBLISHED CONTENT AND CONTRIBUTIONS

Shi, Y. et al. (Jan. 2023). "Hyper-Eddington black hole growth in star-forming molecular clouds and galactic nuclei: can it happen?" MNRAS 518.3, 3606–3621. DOI: 10.1093/mnras/stac3245. arXiv: 2208.05025 [astro-ph.GA].

Shi, Y., M. Y. Grudić, and P. F. Hopkins (Aug. 2021). "The mass budget for intermediate-mass black holes in dense star clusters". MNRAS 505.2, 2753–2763. DOI: 10.1093/mnras/stab1470. arXiv: 2008.12290 [astro-ph.GA].

TABLE OF CONTENTS

LIST OF ILLUSTRATIONS

LIST OF TABLES

Chapter 1

INTRODUCTION

Black holes (BHs) are fascinating objects in the Universe. In the astrophysical sense, BH is a "terminal station" of cosmological structure formation: once the self-gravity of a structure is overwhelmingly dominant over all other counterforces (e.g., thermal/radiation pressure, magnetic/turbulence support, electron/neutron degeneracy pressure), it gravitationally collapses into a BH (Inayoshi et al., 2020). Astrophysical BHs can be classified based on their masses: stellar-mass BHs ($\lesssim 100\,\mathrm{M}_\odot$), supermassive black holes (SMBHs; $\gtrsim 10^6\,\mathrm{M}_\odot$), and intermediate-mass black holes (IMBHs; about 100 – $10^6\,\mathrm{M}_\odot$). The formation and dynamics of BHs is a problem of high interest to astrophysicists (Volonteri et al., 2021).

Stellar-mass BHs are thought to be the remnant of massive stars ($\gtrsim 3\,\mathrm{M}_\odot$) at the end of their evolution track with strong evidence from both observations and theory (Heger et al., 2023). However, not all massive stars are predicted to leave remnants as BHs. If the star's mass is between ~ 140 – $260\,\mathrm{M}_\odot$, it will be a pair-instability supernova at the end of evolution when the energy from electron-positron annihilation could disrupt the star completely, without leaving any remnants (Heger et al., 2003). This results in a prohibited region of the BH mass spectrum, which is the "mass gap" that is roughly in 50 – $130\,\mathrm{M}_\odot$ (Heger and Woosley, 2002). More massive stars, which are predicted to be metal-poor and considered first stars (Population III stars), can produce even more massive BHs, but these stars are never observed (Bromm and Larson, 2004).

SMBHs are in the classical paradigm of galaxies (Kormendy and Ho, 2013). There is convincing evidence of galactic SMBHs. For example, from the motions of stars (S-stars) near Sagittarius A*, the Milky Way central BH is measured to be $4 \times 10^6\,\mathrm{M}_\odot$ (Eckart et al., 2002). More recently, the Event Horizon Telescope collaboration imaged the vicinity of SMBHs of M 87 (Event Horizon Telescope Collaboration et al., 2019) and the Milky Way (Event Horizon Telescope Collaboration et al., 2022), providing even more direct proof. For galaxies outside the Milky Way, central SMBHs are hypothesized from the rotation curves, since a component of $v(r) \propto 1/r$ is required. Galaxies also co-evolve with their central SMBHs, inferred from scaling relations found between BH mass and galaxy properties, e.g., $M_{\rm BH}$–$M_\star$ and $M_{\rm BH}$–

$\sigma_\star$ (Kormendy and Ho, 2013). Moreover, active galactic nuclei (AGNs), which are constrained to be SMBH accretion activities in galaxies, produce emissions in the wavelengths from radio to X-ray and gamma-ray, providing even more information about SMBHs.

Why are IMBHs interesting? IMBHs fill the gap between the stellar-mass BHs and SMBHs (Greene et al., 2020), but this is not the only reason to study them. The formation of BHs is an intriguing problem since observations have found evidence of BH in a wide range of the mass spectrum: from light BHs of a few solar masses, to SMBHs of $\sim 10^9\,\mathrm{M}_\odot$ at high redshift $z \sim 7$ (Fan et al., 2001; Wang et al., 2021), and even in the mass gap (Abbott et al., 2020). The problem is robustly reconciled for stellar-mass BHs from the theory of stellar evolution. For SMBHs, observations of the quasar luminosity show that they have an accretion history, in which their mass grows by orders of magnitudes (Yu and Tremaine, 2002). This only explains why they got more massive through cosmic evolution but have no insights into their progenitors. In view of high-redshift quasars (Fan et al., 2001), which is theoretically challenging since they were at the very early stage of the Universe (0.7 Gyr) and BH accretion is challenging (Haiman and Loeb, 2001), "seed" BHs are considered to fall in the category of IMBHs. Understanding the formation of IMBHs is thus important to complement the larger picture of massive BH formation.

In the remaining sections of the chapter, we first develop a more extensive introduction to the IMBH, including their observational evidence and formation scenarios, and then discuss the motivation of this thesis research.

1.1 Intermediate-mass black holes: observations

There is not as much observational evidence for IMBH as that for stellar-mass BHs or SMBHs (Greene et al., 2020). The origin of stellar-mass BHs is theoretically solid, and since they are remnants of stars, there are ample observations like X-ray binaries, tidal disruption events, and other transients in the local Universe, to support their existence. Massive BHs (including IMBHs and SMBHs) do not have a well-constrained formation scenario. However, SMBHs are easier to detect because they are much more massive, which implies more violent accretion and feedback activities (e.g., high reshift AGNs, AGN variability with time), larger dynamical scales (e.g., stellar dynamics), and even sufficiently large ISCO radii (e.g., EHT direct imaging). The SMBH also coevolves with the host galaxy through its gravity, accretion, and feedback, proving even more observational tools (e.g., the M_{BH}–$\sigma_\star$

and $M_{\rm BH}$–$M_\star$ relation). IMBHs are not benefited from any of these advantages: they are not as populous as stellar-mass BHs, their accretion rates are much lower than SMBHs, the region dominated by their gravity is small compared with that of SMBHs, and their host galaxies (if any) are dwarf and faint, with $M_\star \lesssim 10^{10}\,{\rm M}_\odot$ (Greene et al., 2020).

Still, some observations are directly or indirectly correlated with IMBHs, either due to their interaction with the nearby stellar system, or emission from their accretion activities.

Sub-$L_\star$ galaxies. IMBHs can be hosted by sub-$L_\star$ (less massive than the Milky Way, $\lesssim 10^{10}\,{\rm M}_\odot$) galaxies at their center. This is supported by the dynamical modeling of these galaxies, where the mass profile can be obtained through the mass-to-light ratio (M/L) and the velocity dispersion from the spectrum (Greene et al., 2020). There are already some candidates galaxies with IMBH at the center, for example, with dynamical modeling Nguyen et al., 2019 found an IMBH candidate of $6800\,{\rm M}_\odot$ in NGC 205.

Another hint for the existence of IMBHs in these galaxies is the "extrapolation" of scaling relations between the central BH mass and galactic properties for massive galaxies, like the $M_{\rm BH}$–$\sigma_\star$ and $M_{\rm BH}$–$M_\star$ relations (Kormendy and Ho, 2013). There are already some studies that compare the data from $\lesssim 10^{10}\,{\rm M}_\odot$ galaxies with the traditional scaling relations, and found no violation of these relations (Greene et al., 2020). If the extrapolation is finally validated, galaxies with $M_\star \lesssim 10^{10}\,{\rm M}_\odot$ or $\sigma_\star \lesssim 50\,{\rm km/s}$ are possible to host $\lesssim 10^6\,{\rm M}_\odot$ IMBHs.

Due to galaxy evolution (like mergers), not all nucleus IMBHs can retain in sub-$L_\star$ galaxies at the time of observation. Still, studies found that the fraction of these nuclei with an IMBH is high: e.g., $> 50\%$ for 10^9 – $10^{10}\,{\rm M}_\odot$ galaxies (Miller et al., 2015; Nguyen et al., 2019).

Low-mass AGNs. Active galactic nuclei (AGNs) are luminous sources that are powered by accreting massive BHs at the center of galaxies. Observations of AGNs have revealed the existence of SMBHs (e.g., the extreme case, Fan et al., 2001), and a natural way to search for IMBH candidates is through low-mass AGNs. There are already some samples of low-mass AGNs, for example, with optical spectroscopic selection people found AGNs with sub-$L_\star$ hosts (Greene et al., 2008), and with reverberation mapping, there are some IMBH candidates in galaxies like NGC 4395,

whose mass is $\sim 4 \times 10^5\,M_\odot$ (Peterson et al., 2005). Moreover, with correlations among the X-ray luminosity (L_R), the radio continuum luminosity (L_R), and the BH mass (the "fundamental plane," Merloni et al., 2003; Gültekin et al., 2019), there are also some IMBH candidates like NGC 404 whose mass is $\sim 5 \times 10^5\,M_\odot$ (Nyland et al., 2012). The method is also used to study off-nucleus sources that can be powered by IMBHs (Tremou et al., 2018).

Globular clusters. Dense globular clusters can also be hosts of IMBHs, which are theoretically hypothesized to be results of runaway collisions (Portegies Zwart and McMillan, 2002; Gürkan et al., 2004). Through the dynamical modeling of clusters, there are signatures of central massive (yet dark) objects at the center. There are many examples of such candidates, which are listed in Table 2.1 in Chapter 2, where we compare our theoretical estimates of runaway IMBHs with observations (Shi et al., 2021).

Hypervelocity stars. Hypervelocity stars (HVS) are stars moving at very high velocities ($\sim 1000\,\mathrm{km/s}$) observed in the Milky Way. The origin of HVS is theoretically hypothesized to be interactions with massive BHs, such as the central SMBH of the Milky Way, as well as IMBHs either near Milky Way BH or not (Hills, 1988; Yu and Tremaine, 2003). Observations found HVS without a Galatic Center origin, which implies the possibility of off-nucleus IMBH (Gualandris and Portegies Zwart, 2007).

Ultra-luminous X-ray sources. From X-ray observations, people identified some off-nucleus ultra-luminous X-ray sources (ULXs), which typically have $L_X \sim 10^{39}$ – 10^{41} erg/s. These luminous sources are off-nucleus and thus can not be powered by SMBHs. Some ULXs are hypothesized to be accreting IMBHs or stellar-mass BHs. With further spectral studies, people found that most ULXs are more likely to be powered by stellar-mass BHs at high accretion rates (Greene et al., 2020). Still, there are some very luminous sources that can only be explained with IMBHs. For example, HLX-1 at the galaxy ESO 243-49 is suspected to be an IMBH candidate, with its mass measured as 10^4 – $10^5\,M_\odot$ depending on the specific method utilized (Webb et al., 2012).

Young stars at the Galactic Center. Stars at the Galactic Center of the Milky Way are typically old, though some observations have identified some ensemble of young

stars, which is hard to explain from the star formation theory (Ghez et al., 2003). Theoretical studies then hypothesize that these stars are embedded in a cluster that is dominated by an IMBH at the center. Due to dynamical friction and tidal forces, the IMBH sinks to the Galactic Center along with the entire cluster, explaining the existence of these young stars (Hansen and Milosavljević, 2003; Yu et al., 2007), while the existence of IMBHs in young clusters is also theoretically hypothesized (Portegies Zwart and McMillan, 2002; Gürkan et al., 2004).

Gravitational waves. So far, the most convincing and direct evidence for IMBH is probably from gravitational waves. The LIGO-Virgo collaboration discovered a gravitational-wave event of binary BH merger, where an $85^{+21}_{-14}\,M_\odot$ BH merges with a $66^{+17}_{-18}\,M_\odot$ BH, producing an $142^{+28}_{-16}\,M_\odot$ BH (Abbott et al., 2020). The $85^{+21}_{-14}\,M_\odot$ BH and the final $142^{+28}_{-16}\,M_\odot$ BH are approximately in the IMBH regime. More interestingly, both progenitor BHs are in the "mass gap" ($\sim 50 - 130\,M_\odot$) that is prohibited due to pair-instability (Heger and Woosley, 2002). The existence of such BH thus brings up reflections of its formation scenario (e.g., Kremer et al., 2020).

1.2 Intermediate-mass black holes: formation scenarios

Besides the observational efforts to find IMBHs, there have been some (baryonic) formation scenarios of IMBHs (Inayoshi et al., 2020; Volonteri et al., 2021), which are either related to massive stars (collapses of Population III stars), pristine gas (the direct collapse), dense stellar environments (runaway mergers in globular clusters and galactic nuclei), or BH accretion physics (super-/hyper-Eddington accretion).

Collapses of Pop III stars. A natural extrapolation from the formation of stellar-mass BH to the IMBH is the collapse of a massive star. These massive stars are typically assumed to form in metal-poor environments in the early Universe (Madau and Rees, 2001). If the massive star is above the mass gap ($\sim 140 - 260\,M_\odot$, where it will be a pair-instability supernova instead of collapsing Heger and Woosley, 2002; Heger et al., 2003), it can form IMBHs of $\gtrsim 100\,M_\odot$ (e.g., simulation work like Greif et al., 2011).

There are some issues if these IMBHs are considered SMBH seeds. For example, these IMBHs are not massive enough to reconcile high-redshift quasars, since the number of e-foldings between $100\,M_\odot$ and $10^9\,M_\odot$ is comparable with that between 45 Myr ($\epsilon_{\rm ref} t_{\rm Sal}$ with $\epsilon_{\rm ref} = 0.1$) and 0.8 Gyr ($z \sim 7$), while the sustainable high accretion rate through the entire history is questionable. Moreover, unlike estimated

before by Madau and Rees, 2001 that one Population III remnant form in one dark matter halo, simulations suggest that multiple stars form in a wide spectrum of masses (Greif et al., 2011; Volonteri et al., 2021). Other mechanisms to make massive seeds are also proposed.

Direct collapse. The direct collapse mechanism assumes that the pristine dense gas clump collapses to an IMBH either without going through the stellar evolution, or undergoing a phase of quasi-star (Bromm and Loeb, 2003; Begelman et al., 2006). To hold the clump massive enough, it must avoid efficient cooling and fragmentation. A typical requirement is that a sufficient Lyman-Werner (LW) background ($\sim 10^4$ K) dissociates molecular hydrogen (Omukai, 2001), such that the clump is embedded in an atomic cooling halo (ACH). The background can come from nearby star formation or galaxy mergers (Dijkstra et al., 2008). The direct collapse mechanism typically generates massive IMBHs of $\sim 10^4 - 10^6$ $M_\odot$ (Inayoshi et al., 2020).

There are also some debates about the scenario. For example, the supply of the LW background is not well-constrained; the predicted high mass of IMBHs is also not guaranteed since the realistic gas environment can be turbulent; fragmentation could happen instead of monolithic collapse (Corbett Moran et al., 2018). Moreover, there are studies that try to lift the assumption of LW background through other physics (though the general goal is to avoid fragmentation): e.g., other approaches to dissociate molecular hydrogen, large streaming velocity between the gas (baryon) and dark matter that delay the collapse, rapid galaxy mergers or strong inflow that produces massive and dense clumps (Inayoshi et al., 2020). More recent simulations also argue that turbulence can be sufficient to avoid fragmentation even if the gas is cold (Latif et al., 2022).

Runaway mergers. Another scenario of IMBH formation is the runaway mergers in dense stellar clusters. Due to dynamical friction, massive stars in the cluster will lose angular momentum and sink to the center of the cluster. If the lifetime of the cluster is sufficiently long (i.e., the relation timescale), the sunk massive stars can merge and form a supermassive star (or quasi-star) at the center, which later gives birth to an IMBH (Portegies Zwart and McMillan, 2002; Gürkan et al., 2004). The IMBH mass can be $\sim 10^3 - 10^4$ $M_\odot$ (Inayoshi et al., 2020).

There are some theoretical challenges in this specific mechanism. For example, the anisotropic gravitational wave emission between the IMBH and an incoming stellar-mass BH could eject the IMBH out of the cluster (Holley-Bockelmann et al.,

2008); the physical evolution of the supermassive star is not well-understood: there is a possibility that the supermassive star explodes due to pair-instability (Spera and Mapelli, 2017).

Another possible route to form IMBH in dense clusters is the hierarchical mergers starting from stellar-mass BHs (Fragione and Rasio, 2023). However, the mechanism typically takes a longer timescale than stellar mergers (Gyr versus Myr) and inevitably suffers from the gravitational-wave recoil. IMBHs from the mechanism are thus unlikely to be seeds of SMBHs (Greene et al., 2020).

Super-Eddington accretion. Efficient accretion onto (lighter) stellar-mass BHs or Population III remnants is also possible to explain the existence of some massive IMBHs of $10^4 - 10^5\,\mathrm{M}_\odot$. The classical upper limit for BH accretion in a spherical configuration is the Eddington accretion rate: materials that infall to the BH can release radiative energy that is sufficient to hit the Eddington luminosity, beyond which the radiation pressure overcomes the gravity and expels the gaseous material away. The Eddington accretion rate is formulated as

$$\dot{M}_{\rm Edd} \equiv \frac{M_{\rm BH}}{\epsilon_{\rm ref} t_{\rm Sal}}, \tag{1.1}$$

where $t_{\rm Sal} = \kappa_{\rm es} c/(4\pi G) \approx 0.45\,\mathrm{Gyr}$ and $\kappa_{\rm es}$ is the opacity due to scattering between light and electrons (Thompson scattering); $\epsilon_{\rm ref} = 0.1$ is a constant reference radiative efficiency, defined as the ratio between the energy released as radiative power and the inflow rest-mass energy ($\dot{M}_{\rm BH} c^2$).

Theoretical studies of BH accretion have proved the possibility of breaking the limit of the Eddington accretion rate, like the non-spherical configuration that allows efficient radiation without stalling accretion, and photon-trapping effects that photons are "trapped" along the strong accretion flow rather than being radiated (Begelman, 1979). As a result, the luminosity of the accreting BH is limited even if the accretion rate is very high (Inayoshi et al., 2020), such that the gas inflow towards the BH and super-Eddington accretion can be sustainable. Numerical simulations considering radiation hydrodynamics near BHs (typically $\lesssim 1000 G M_{\rm BH}/c^2$) also validated the possibility of super-Eddington accretion at $\sim 1000 \dot{M}_{\rm Edd}$ (Jiang et al., 2019).

There are proper environments for super-Eddington accretion in the early Universe, like dense molecular clouds and protogalactic cores (Inayoshi et al., 2020). Despite that efficient accretion is theoretically possible, there are many limitations in reality,

e.g., the realistic gaseous medium is turbulent, star formation may affect BH accretion, and BH feedback can be important at large scales. Chapters 3 and 4 will study these problems in detail.

1.3 Star formation in giant molecular clouds

The thesis is based on numerical simulations with the code GIZMO (Hopkins, 2015; Hopkins and Raives, 2016), which is a mesh-free, Lagrangian, Godunov code for hydrodynamics and magnetohydrodynamics (MHD). Moreover, the code is integrated with state-of-the-art treatment of multiple physics that are related to BHs, like star formation and feedback, thermodynamics of the gaseous medium, BH accretion and feedback. Throughout this study, we use the simulation framework FIRE-2 (Feedback In Realistic Environment; Hopkins et al., 2018b).

The basic building block for this study is the simulation of star formation in giant molecular clouds (GMCs), which are generally $\sim 5 - 500\,\mathrm{pc}$ in size and $\sim 10^4 - 10^{10}\,\mathrm{M}_\odot$ in mass. The simulation itself can provide information about star clusters that are related to IMBH formation from runaway collisions (Portegies Zwart and McMillan, 2002). Moreover, star-forming GMC is the realistic environment for BH accretion. Despite some previous work of parsec-scale BH accretion considered physics like MHD and pre-seeded turbulence (Krumholz et al., 2006), the effect of star formation and feedback (e.g., consumption of available gas reservoir for BH accretion, feedback-driven winds, heating, and ionization) is typically not included, but can be important.

Star formation is a key problem in astrophysics, it happens because of gravitational collapse (Krumholz, 2015). Once the baryonic (atomic) cloud cools below $\sim 10^4$ K, molecular hydrogen and CO form, and cooling becomes efficient. The drop in the temperature also implies a drop in the thermal support, so fragmentation and collapse happen, which further generate dense cores and protostars. With further contraction, the core of the protostar is hot enough that nuclear fusion of deuterium ignites, releasing radiation and thermal energy to support the protostars. The protostar then evolves and migrates to the main sequence.

Feedback from stars can also be important even to star formation at the GMC scale (Grudić et al., 2018b; Guszejnov et al., 2020; Grudić et al., 2021b). Feedback is in the form of radiation, winds, and cosmic rays (CRs). Radiation affects the GMC through radiative pressure, heating, and ionization; winds can exert mechanical ram pressure on the GMC; CRs are high-energy electrons and ions that expel the

gas through coupling and diffusion (Zweibel, 2017), and they also heat the gas through energy loss (Guo and Oh, 2008). All these effects change the dynamics and thermodynamics of the GMC, which can break the condition of star formation.

Simulations of star formation in GMCs: key conlusions

Simulations directly related to this study are first performed in Grudić et al., 2018b. They initialize with a GMC of 10^4 K. Turbulence and magnetic field are seeded such that their energy is a fraction (10% by default in our simulations) of the gravitational binding energy ($GM_{\rm cl}^2/R_{\rm cl}$, where $M_{\rm cl}$ and $R_{\rm cl}$ are mass and radius of the GMC). Star formation "happens" when the velocity field near a gas cell is convergent and gravitationally bounded, after which the gas cell becomes a star particle. The stellar feedback is then performed through mass-function-averaged feedback models.

Dense clumps form with star formation. Through these simulations, one basic conclusion is that dense clumps exist in star-forming clouds. Dense clumps or cores can be induced by initial turbulence and perturbations – and they further form stars if the cores are convergent and gravitationally bound. Moreover, there are secondary dense clumps from star formation. Stellar feedback can drive turbulence by introducing mass flows and shocks in the GMC. The turbulence also generates dense clumps in the simulation after collisions of shock fronts. This is visualized in both Grudić et al., 2018b and Shi et al., 2023b.

Saturation of stellar feedback in GMCs. Another important conclusion is related to the global competence between self-gravity and feedback. A simple semi-analytical argument can be made (Grudić et al., 2018b). Assuming that after star formation, the stellar surface is $\Sigma_\star$. The gravity acting on the gas is $F_{\rm g} \sim GM_{\rm gas}M_{\rm cl}/R_{\rm cl}^2 \sim \pi G\Sigma M_{\rm gas}$, where Σ is the initial mean surface density of the GMC. Feedback from stars is characterized by $\langle \dot{p}/M \rangle$, which is the momentum ejection rate per unit stellar mass. This implies a feedback force $F_{\rm fb} \sim \langle \dot{p}/M \rangle \Sigma_\star \pi R_{\rm cl}^2$. Note that $\Sigma_{\rm gas} + \Sigma_\star \sim \Sigma$. Once feedback regulation overcomes the self-gravity, star formation stalls since the GMC is disrupted. The star formation efficiency is then

$$\epsilon_\star \equiv \frac{\Sigma_\star}{\Sigma} \sim \frac{1}{1 + \Sigma_{\rm crit}/\Sigma}, \tag{1.2}$$

where $\Sigma_{\rm crit} \sim \langle \dot{p}/M \rangle/(2\pi G)$. Once the surface density is higher than $\Sigma_{\rm crit}$, feedback from stars is unimportant, or "saturated". At the limit, star formation efficiency is high, and the whole system (stars and gas) is gravitationally bound. The simple

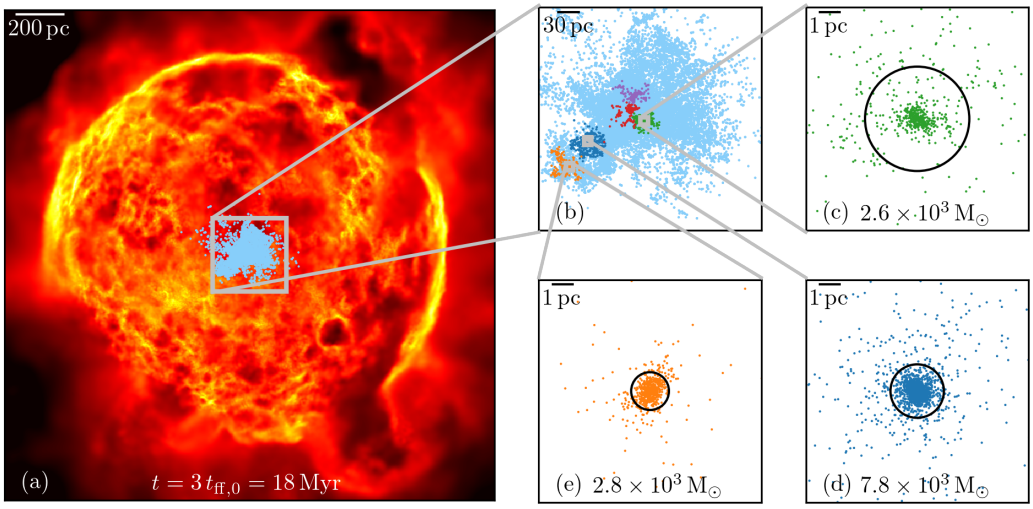

Figure 1.1: Clusters formed in simulations of star formation in GMCs. In panel (a) we show the morphology of gas (the column density is log-scale), which is expelled away by strong feedback from star formation. Panel (b) zooms in at the star-forming region. In the larger stellar assemble (cyan dots), there are some gravitationally bounded clusters, which we highlight in panels (c), (d), and (e). These clusters weigh $\sim 10^3\,{\rm M}_\odot$ with varying half-mass radii (black circles).

argument is in good agreement with star formation simulations by different groups (Chevance et al., 2022).

This discovery shows that the mean surface density of the GMC can be a good representation of self-gravity. It is insightful for BH accretion in two ways. i) In the absence of BH feedback, self-gravity can determine whether the feedback from stars is important. ii) If BH feedback is considered, the competence between self-gravity and the BH feedback will regulate BH accretion in a similar way as the star formation.

Star cluster assembly in GMCs. An even more direct output of star formation simulations is the assembly of star clusters. One example of star formation is presented in Fig. 1.1, which is based on a GMC of $10^6\,{\rm M}_\odot$ and 50 pc. At the late stage of the simulation, stars form in the central $\sim$ 100 pc while gas is expelled by stellar feedback, generating bow shocks. Through searching for gravitationally bounded systems, globular star clusters can be identified. For example, Grudić et al., 2018a and Grudić et al., 2021a show that the treatment of star formation in GMCs can well recover the dynamics of star clusters. Information about star cluster dynamics is useful for estimating IMBH masses form from runaway mergers. We

conduct this research in Chapter 2.

Simulations of cluster formation in GMCs also suggest that clusters form hierarchically like dark matter halos or galaxies (Guszejnov et al., 2022). This is due to gravitational interactions between clusters. Moreover, BH-cluster interactions can also be important, and BH accretion can be affected. This is studied in Chapter 5.

1.4 Black hole accretion and feedback

BH accretion and feedback is a multi-scale physics like star formation. It studies the process that material from large scales ($\sim$ kpc) to arrive at the event horizon of black holes, which value is typically in the unit of gravitational radius $r_{\rm g} = GM_{\rm BH}/c^2 = (M_{\rm BH}/10^8\,{\rm M}_\odot)$ au. Treatments of gas flow at different scales are different.

BH accretion

The simplest condition is that the gaseous material adiabatically and spherically falls to the BH without angular momentum if it is gravitationally bounded to the BH. It is generalized to the Bondi-Hoyle accretion (Hoyle and Lyttleton, 1939; Bondi, 1952), in which the mass accretion rate is

$$\dot{M}_{\rm Bondi} = \frac{4\pi G M_{\rm BH}^2 \rho}{(c_{\rm s}^2 + v_{\rm rel}^2)^{3/2}}. \tag{1.3}$$

Here $c_{\rm s}$ is the sound speed and $v_{\rm rel} = |\mathbf{v}_{\rm gas} - \mathbf{v}_{\rm bh}|$ is the relative velocity between the BH and the gas. This is a crude estimate that is applied to large scales when the angular momentum of gas is unimportant (much smaller than that of the circular orbit of the same radius).

The angular momentum effect is important once the gas flow gets closer to the BH, and accretion disk theory is then developed to solve the problem of angular momentum dissipation, to allow it to enter the innermost stable circular orbit (ISCO) of the BH. The standard disk model first solves the problem with these assumptions (Shakura and Sunyaev, 1973):

1. The disk is light compared to the BH, so the material follows the circular Keplerian motion and the radial advection is negligible.

2. Gas flow loses angular momentum through viscosity that arises from the magnetic field and turbulence. The shear is defined with $T_{r\phi} = -\alpha P$ where P is local gas pressure and α is a constant.

3. The pressure P is the sum of radiative pressure and thermal pressure. It is responsible for the vertical force balance with the gravity.

4. The disk is optically thick, and the opacity comes from Thompson scattering and free-free scattering.

5. Cooling of the disk is in the form of blackbody radiation, in balance with viscous heating.

6. There is an inner boundary condition that the viscosity vanishes at the ISCO.

The standard disk model is optically thick but geometrically thick (Shakura and Sunyaev, 1973). This disk is sub-Eddington. The model achieved great success in many applications in astrophysics (Abramowicz and Fragile, 2013; Abramowicz and Straub, 2014).

However, these assumptions can become invalid in extreme cases. Here are some examples (Abramowicz and Fragile, 2013; Abramowicz and Straub, 2014).

- Radiative cooling can be inefficient even if the optical depth is high. This happens when the accretion rate is high enough, that photons are trapped in the accretion flow (Begelman, 1979), and the radial advection towards the BH becomes the major cooling source.

  Due to the modification in assumption, one significant model is the slim disk (Abramowicz et al., 1988; Sądowski, 2009), which features a high accretion rate (Eddington or super-Eddington). It is also "thicker" than the standard thin disk. Although the accretion rate is high, the luminosity from the disk only grows logarithmically (Watarai et al., 2000).

- It can be optically thin. As a result, the blackbody radiative cooling can become unimportant. Cooling is then dominated by the radial advection that brings the heat to the BH. This results in the advection-dominated accretion flow (ADAF; Narayan and Yi, 1994), which is sub-Eddington. Different from the standard disk, the ADAF is geometrically extended like a corona and is significantly hotter.

- It can be geometrically thick, where the Kerr metric is typically assumed. The vertical structure then becomes important, which can be supported by the radiative pressure. These assumptions generate the "Polish doughnut"

model (Sikora, 1981; Madau, 1988), which has super-Eddington luminosity and super-Eddington accretion rate. However, although the luminosity is high, it only grows sub-linearly with the accretion rate (Madau et al., 2014).

- Other sources of cooling can exist and dominates over the blackbody radiation or advection, like the bremsstrahlung, inverse-Compton radiation, and pair production (Bjoernsson et al., 1996). One extreme case is that at the innermost region of the disk, the density and temperate are both high, and cooling is dominated by neutrinos (Popham et al., 1999; Liu et al., 2017). This extends the slim disk model in accretion rates, reaching hyper-Eddington.

In summary, with small-scale accretion theory, super-Eddington accretion is theoretically possible due to photon-trapping effects (Begelman, 1979), and cooling is then dominated by other non-radiative mechanisms like radial advection or neutrinos. The photon-trapping also naturally implies a limited radiative luminosity.

BH feedback

Energy and mass released from the BH accretion process can damage the conditions for accretion. For example, radiation and cosmic rays can ionize and heat nearby gas, making them unbound to the BH; they can also drive winds, which expel the gas away from the BH. If the feedback is strong, the GMC can be disrupted and super-Eddington BH accretion can be terminated (as will be shown in Chapter 4).

Simulations of BH accretion and feedback: a general view

In numerical simulations, it is difficult to simulate the whole process of BH accretion and feedback, due to the large jump in scales which requires super high resolution, and more importantly, the dominating physics varies vastly at different scales (e.g., from Newtonian to General relativistic, from partially ionized to fully ionized). Numerical simulations of BH accretion typically focus on either small or large scales.

On small scales (much smaller than the Bondi radius, like hundreds of gravitational radius), to reach the super-Eddington accretion (of our interest), the photon-trapping effect (Begelman, 1979) is important. Simulations thus have to consider the radiative transfer (Ohsuga et al., 2005), though additional physics like magnetohydrodynamics (Jiang et al., 2014; Jiang et al., 2019) and general relativity (Sądowski et al., 2015) can also be important, to account for effects like energy loss due to magnetically arrested disk (Narayan et al., 2003) and BH rotation (Blandford and Znajek, 1977).

Moreover, theory and simulations also found that radiation causes instant mass outflow close to the BH (Blandford and Begelman, 1999; Inayoshi et al., 2016; Hu et al., 2022). Still, small-scale simulations found that given sufficient mass supply, the BH accretion rate can be $\sim 1000\dot{M}_{\rm Edd}$, while the radiative luminosity is only $\lesssim 10L_{\rm Edd}$. Super-Eddington accretion is not obscured by small-scale accretion physics.

On larger scales (greater than the Bondi radius), like the galactic scale or GMC scale (pc to kpc), the emphasis is "how much material can be gravitationally bounded to the BH." Naturally, this can be calculated with Eq. (1.3), which is widely used in numerical simulations of SMBHs at the galactic center (Hopkins et al., 2018b; Hopkins et al., 2023), where the BH is in low relative velocity with the gas. However, once the BH is in turbulent, magnetized environment like GMCs, this formulation may fail due to reasons like: i) the BH-gas relative velocity can be large, largely breaking the spherical configuration originally assumed in Bondi, 1952; ii) the gas can be magnetically/turbulently supported (Krumholz et al., 2006; Burleigh et al., 2017).

To estimate the BH accretion in GMC-scale simulation, we instead use the criterion of "gravitational capture" that is natural to Lagrangian codes: a gas cell will be swallowed by the BH if it is gravitationally bounded to the BH. BH is thus a "sink" particle in the simulation. This boundedness is characterized by (Bate et al., 1995; Shi et al., 2023b)

$$u_{\rm thermal} + \frac{v_{\rm A}^2}{2} + \frac{v_{\rm rel}^2}{2} < \frac{GM_{\rm sink}}{r}, \tag{1.4}$$

where $u_{\rm thermal}$ is the specific thermal energy, $v_{\rm A}$ the Alfvén speed. The sink mass $M_{\rm sink}$ here can be the BH mass.

Moreover, the particle must be within a "sink radius", which is the cutoff (or resolution limit) of the BH accretion. This is sufficient for the purpose to determine the amount of fuel towards the BH, though many dynamics inside the sink radius are unresolved. It is also reasonable if the focus is the impact of large-scale and long-term physics, which typically has a much longer dynamical timescale than that near the gravitational radius, making the simulation executable. More details of our simulation of BH accretion in GMCs are included in Chapter 3.

Feedback from BHs is included in the simulation through a "sub-grid model": due to the mass and scale resolution limits of our GMC simulations, small-scale physics ($\ll$ pc, inside the sink radius) like accretion disks can not be modeled.

There are some assumptions about the sub-grid model. First, there is a scale-independent mass flow towards the BH. In realistic conditions, this mass transfer is in the form of an accretion disk (as we introduced earlier). In the simulation, we store the mass bound to the BH in a secondary "disk" reservoir ($M_{\rm disk}$) and then transfer mass within a fixed timescale $t_{\rm dep}$, so the mass transfer/depletion rate is $\dot{M}_{\rm dep} = M_{\rm disk}/t_{\rm dep}$.

Then along the mass inflow, some fraction $f_{\rm acc}$ of mass will reach the BH ($\dot{M}_{\rm BH} = f_{\rm acc}\dot{M}_{\rm dep}$), while the remaining is ejected back to the GMC in the form of mechanical jets. There is also some energy to power the jet, and to be released in the form of radiation and cosmic ray, each is characterized by an energy efficiency that $\epsilon = E/(\dot{M}_{\rm BH}c^2)$. For each BH feedback mechanism, the energy efficiency determines the strength of feedback.

Finally, each feedback mechanism is implemented in a similar way as that in the stellar feedback. This is extensively described in references of Chapter 4.

1.5 This thesis: theoretical studies of IMBH formation

In this section, we summarize the main topics of this thesis, first by defining some open questions in the field, and then summarizing the results from numerical simulations performed in this thesis.

Some open questions

This study tries to tackle some open questions of IMBH formation scenarios, including the runaway mergers and the super-Eddington accretion.

1. In the runaway merger scenario, the density distribution profile of the cluster can be important. Previous works (e.g, Gürkan et al., 2004) typically assumed a flat inner density profile, which can be questionable since they do not essentially reproduce the young clusters at formation. Obtaining this information is thus important.

2. In the super-Eddington accretion scenario, the availability of this fast accretion in a realistic environment remains uncertain. Although theories and simulations of smaller scales ($\ll$ pc) proved that super-Eddington accretion could happen, they assumed sufficient fuel supply (Jiang et al., 2019) from larger scales (e.g, parsec scales). In a realistic turbulent molecular cloud with star formation, this assumption is not guaranteed.

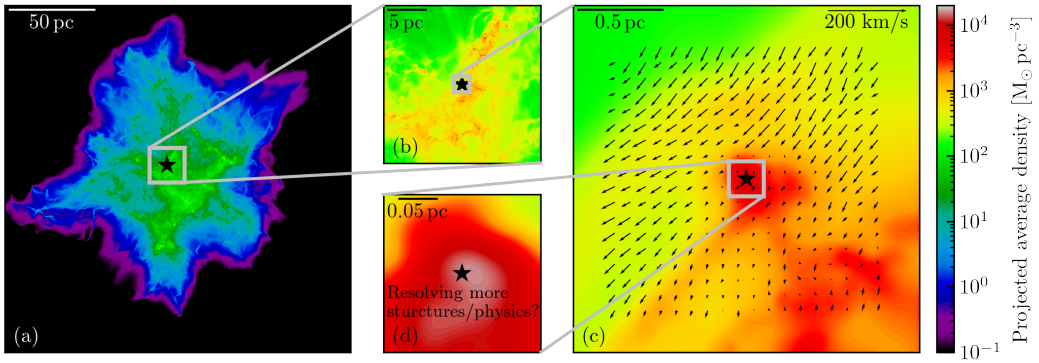

Figure 1.2: Simulations of BH accretion in GMCs. We show the line-averaged density of gas at the snapshot when a BH is having significant accretion. We zoom in from panel (a) to (d), where the gas density is evaluated in the box region centered at the BH. Panel (c) demonstrate the "clump accretion" as in Chapters 3 and 4, that the BH is in low relative speed with a dense clump generated by star formation and turbulence. Panel (d) shows a future direction where zoom-in simulations can bring more information about BH accretion and feedback.

3. Following the previous question. If there is enough fuel supply from a turbulent gaseous environment, there are some limiting factors that may change the result. For example, BH accretion can be regulated by its feedback effects like radiative pressure and heating, mechanical outflows, as well as cosmic ray diffusion and heating, which may affect parsec-scale gas inflow towards the BH. Quantifying these effects is thus essential.

Our attempts

In view of simulations of both star formation and BH accretion, we summarize the major contents of each chapter of the thesis below.

- Chapter 2 studies the runaway mergers in globular clusters with information inferred from simulations of star formation. With density profiles of a population of young massive clusters obtained from star-formation simulations in Grudić et al., 2018b, we conduct both analytic derivations and Monte-Carlo simulations to estimate the mass of quasi-stars. We conclude that these clusters typically have a steep inner slope. The analytic expression is in approximate agreement with observations.

- Chapter 3 studies the availability of hyper-Eddington accretion for seed BHs in GMCs, i.e., whether there is enough gas supply from parsec scales to BHs.

	"Clump accretion"	"Steady accretion"
GMC density	Prefers high-surface density	Stellar feedback saturated
Accretion	Spiky (clump-crossing time)	Linear/sustaining ($\sim$ Myr)
BH initial mass	Weak dependence	Prefer massive BHs
Physical explanation	GMC's gravity dominance	Cluster dynamics

Table 1.1: Comparisons between the "clump accretion" (Chapers 3, 4) and "steady accretion" (Chapter 5) of super-Eddington accretion in GMCs.

We run simulations of BH accretion in GMCs with star formation based on FIRE-2 physics. We confirm that stellar feedback is the dominating factor in generating dense clumps, and the accretion of these clumps provides sufficient fuels to support hyper-Eddington accretion. We also conclude that GMCs with high surface densities are favored for super-Eddington accretion. We show the visualization of clump accretion in Fig. 1.2.

- Chapter 4 studies the self-regulation of BH accretion through its feedback in GMCs with a large suite of simulation varying parameters in a BH feedback sub-grid model. The sub-grid model connects BH accretion at parsec and sub-parsec scales and quantifies feedback mechanisms, including radiation, winds/jets, and relativistic diffusive cosmic rays. We find that super-Eddington accretion is still achievable with proper radiative feedback models but is challenged by the momentum outflow of jets. We also explain BH feedback behavior with semi-analytic arguments.

- Chapter 5 studies a "steady" mode of accretion other than the "clump accretion" studied in previous chapters. Due to potential wells of the star cluster, the gas inflow towards BHs can be steady. This complements the missing interaction between stars and BHs in previous chapters. The gas inflow rate can be $\sim 10\,\mathrm{M}_\odot/\mathrm{yr}$, creating an optimal condition for efficient seed BH accretion. We find a strong toroidal magnetic field in the gas inflow, which is also thermally heated and ionized by feedback from stars.

On the super-Eddington scenario explore in Chapters 3, 4, and 5, we make a comparison between the "clump accretion" (Chapers 3, 4) and "steady accretion" (Chapter 5) that exist for BHs in GMCs, as presented in Table 1.1.

1.6 Outlook

We briefly introduce some extensions of this thesis study. Although we tried to address the problem of BH accretion in GMCs, there are some unsolved follow-up problems. Moreover, advances in numerical simulations can reveal more information about BH accretion, BH feedback, BH seed creation, and more. We think future studies may benefit from two techniques: the super-refinement and the single-star formation simulation.

The super-refinement is a natural technique for solving differential equations: at a "stiff point", more resolution in time or space is required to capture the dynamics. BH accretion problem is exactly of this kind, it is multi-scale and multi-physics, with interactions (accretion/feedback) that links small and large scales. The technique is natural for Eulerian/grid codes but has also been implemented in Lagrangian codes (in different names, like super-Lagrangian), with applications in BH simulations like Talbot et al., 2021 and Hopkins, 2023b; Hopkins, 2023a. There are some problems that can be solved with "zoom-in" simulations using the technique.

Bridging the gap of small and large scale BH accretion. As visualized in Fig. 1.2, the current simulation resolution limit is $\sim 0.01\,\mathrm{pc}$. The uncertainty of the small-scale physics results in our large parameter survey in Chapter 4, without a deciding answer. Super-refinement can help increase the resolution near BHs and can help construct more realistic feedback models.

Are BH accretion disks magnetized in GMCs? The study of the accretion flow in Chapter 5 and AGN simulations (Hopkins, 2023b; Hopkins, 2023a) both show that flux freezing can be prevalent for accreting BHs. It is thus interesting to check the magnetic field near the accretion disk of BHs in the ISM, to infer hints about their observability.

What are the detailed dynamics of "clump accretion"? Another information that can be drawn from zoom-in simulations is the dynamics of the clump accretion mentioned in Chapters 3 and 4. These simulations can also help us get observational signals of this accretion.

Can protogalactic nuclei naturally produce their central SMBH seeds? In Chapter 5 we find that BH seeds in the GMC can be naturally captured and migrated to the center following star formation without fine-tuning. If the mechanism is also

correct for protogalactic nuclei, SMBH seeds can be naturally produced along star formation.

Another booming field is the simulation resolving single-star dynamics, largely advanced by the STAR-FORGE project (Grudić et al., 2021b; Guszejnov et al., 2021). Our current simulations are based on synthesized star formation and feedback models (each "star particle" represents an ensemble of stars), so many details of single-star dynamics, like their formation, evolution, and feedback, are not resolved. BHs are natural remnants after massive stars' evolution. With STAR-FORGE, many detailed physics-related BHs can be revealed.

What is the origin of BH seeds in GMCs? With the simulation resolving single-star dynamics, we can track the evolution of each star and check the accretion of the remnant BH. This can solve the caveat of BH seed origin in current simulations.

What is the runaway merger in globular clusters? In Chapter 2 we study the IMBH formation from runaway stellar mergers in clusters. However, details of the runaway merger are not considered but can be interesting, like their structure, dynamics, and stability. This is possible with single-star simulations.

Other BH-related phenomena in star clusters. Details of stellar remnants in star clusters can be inferred from STAR-FORGE and can be applied to other studies like mergers of BH-BH and BH-neutron stars. This connects the field of gravitational waves and can provide additional observability of the physics we are studying.

Chapter 2

RUNAWAY MERGERS AS PROGENITORS OF IMBHS

Shi, Y., M. Y. Grudić, and P. F. Hopkins (Aug. 2021). "The mass budget for intermediate-mass black holes in dense star clusters". MNRAS 505.2, 2753–2763. DOI: 10.1093/mnras/stab1470. arXiv: 2008.12290 [astro-ph.GA].

Abstract

Intermediate-mass black holes (IMBHs) could form via runaway merging of massive stars in a young massive star cluster (YMC). We combine a suite of numerical simulations of YMC formation with a semi-analytic model for dynamical friction and merging of massive stars and evolution of a central quasi-star, to predict how final quasi-star and relic IMBH masses scale with cluster properties (and compare with observations). The simulations argue that inner YMC density profiles at formation are steep (approaching isothermal), producing some efficient merging even in clusters with relatively low effective densities, unlike models which assume flat central profiles resembling those of globular clusters (GCs) *after* central relaxation. Our results can be approximated by simple analytic scalings, with $M_{\rm IMBH} \propto v_{\rm cl}^{3/2}$ where $v_{\rm cl}^2 = G\,M_{\rm cl}/r_{\rm h}$ is the circular velocity in terms of initial cluster mass $M_{\rm cl}$ and half-mass radius $r_{\rm h}$. While this suggests IMBH formation is *possible* even in typical clusters, we show that predicted IMBH masses for these systems are small, $\sim 100-1000\,M_\odot$ or $\sim 0.0003\,M_{\rm cl}$, below even the most conservative observational upper limits in all known cases. The IMBH mass could reach $\gtrsim 10^4\,M_\odot$ in the centers nuclear star clusters, ultra-compact dwarfs, or compact ellipticals, but in all these cases the prediction remains far below the present observed supermassive BH masses in these systems.

2.1 Introduction

Intermediate massive black holes (IMBHs), which typically weigh 10^2–10^5 $M_\odot$, are believed to be the missing link between stellar mass black holes and super massive black holes (SMBHs). These objects, if they exist, are expected to play an important role in multiple astrophysical processes, e.g., affecting the evolution of globular star clusters and powering off-nuclear ultraluminous X-ray sources (ULXs). More importantly, they are potentially the progenitors of SMBHs which are known to live

in most galaxies (Gebhardt et al., 2000; Volonteri, 2010; Mezcua, 2017; Koliopanos, 2017). Observations of ULXs and stellar kinematics argued that there may be some evidence for such objects in galaxies (Farrell et al., 2009; Kaaret et al., 2017), and globular star clusters (e.g., Portegies Zwart et al., 2004, see more in §2.5). But these claims remain controversial.

Theoretically, several different IMBH formation channels have been proposed. Major ideas include: direct collapse of hyper-mass quasi-stars in isolation (e.g., Volonteri and Begelman, 2010; Schleicher et al., 2013), runaway hyper-Eddington accretion onto stellar mass black holes (e.g., Ryu et al., 2016), and runaway mergers in globular (star) clusters (GCs, e.g., Portegies Zwart and McMillan, 2002; Gürkan et al., 2004; Gieles et al., 2018a). All these mechanisms have challenges. For the direct collapse channel, the fragmentation of molecular clouds may not form quasi-stars instantly, but star clusters (Corbett Moran et al., 2018). For the hyper-Eddington channel, one important question is whether such high-efficiency accretion is sustainable or even possible. Finally, for the runaway merger channel, gravitational recoil due to merging stellar-mass BHs will likely "kick" the IMBH to a high velocity ($\sim$ 1000 km/s, e.g., Holley-Bockelmann et al., 2008), sufficient to make it escape the star cluster. Only relatively massive IMBHs ($\gtrsim 10^3\ M_\odot$) could remain in the galactic field even after the star cluster dissolves and survive such a merger without too-large a "kick" (Fragione et al., 2018), which means the IMBH must be that massive before stellar-mass BH mergers occur. To solve this problem, the runaway merging process must be rapid enough such that massive stars merge together *before* they evolve off the main sequence and become black holes individually.

Previous studies of runaway mergers in star clusters have provided us with a possible scenario: Due to mass segregation, relatively massive main-sequence stars sink to the cluster's center and then merge into a supermassive central object which then self-collapses to an IMBH after ~3 Myr. In Portegies Zwart and McMillan (2002), the authors showed N-body simulations of the process, and found that star clusters with initial half-mass relaxation time scale $t_{\rm rlx} \lesssim 25$ Myr can form IMBHs. More precise simulations in Gürkan et al. (2004) drew a similar conclusion and predicted that the quasi-star's mass could account for $\sim 0.1\%$ of the total cluster mass. More recently, Petts and Gualandris (2017) ran high-resolution simulations of young dense star clusters infalling to the Galactic Center. The clusters undergoes a similar process and the formation and collapse of a very massive star (VMS) was observed, resulting black holes with mass $\sim 20 - 400$ M$_\odot$ (which covers part of the IMBH mass range).

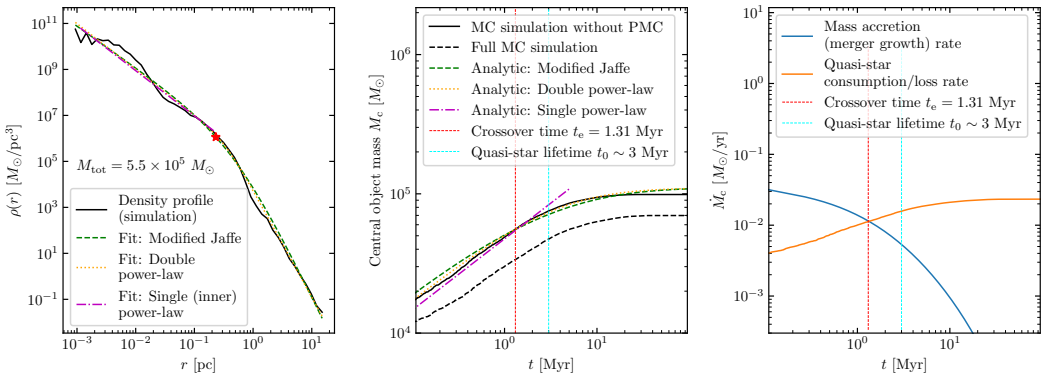

Figure 2.1: Density profiles of globular clusters, and the mass evolution of runaway merger. **Left**: Radial density profile $\rho(r)$ for a young, massive, star cluster (stellar mass $M_{\rm tot} = 5.5\times10^5\ {\rm M}_\odot$) in the studied suite of star-cluster formation simulations, taken just after the peak episode of star formation. We compare three analytic fits to the profile: "modified Jaffe" (Eq. 2.1), "double power-law" (Eq. 2.2), and a single power-law fit only to the "inner" radii within the half-mass radius $r_{\rm h}$ (marked by a red star). **Middle**: Calculated mass growth of the central massive object, owing to mergers of massive stars. *Full MC simulation*: calculating the inspiral of massive stars in the cluster sampling from the IMF and following each orbit as described in (§ 2.2), identifying them as merged when they contact the quasi-stellar radius. *Crossover time*: time when the accretion timescale $\dot{M}_{\rm acc}/M_{\rm c}$ becomes > 3 Myr, an estimate of when mass-loss from the quasi-star might outpace accretion). *MC simulation without PMC*: MC simulation ignoring the "point mass correction" ("without PMC," also refer § 2.2) – i.e. ignoring the effect of the quasi-star itself and finite mass N-body effects in the center of the star cluster on stellar dynamics (instead assuming the density profile is simply the smooth/continuous extrapolation of the continuous $\rho(r)$. This produces systematically higher $M_{\rm c}$ as the PMC causes inspiralling stars to stall, but the effect is relatively small (tens of percents) *Analytic:* Closed-form, approximate solutions for $M_{\rm c}(t)$, using the analytic fits (*left*). These agree well with the MC without PMC model, so the PMC is the dominant correction. **Right:** Mass accretion rate $\dot{M}_{\rm c}$ history of the central massive object. We compare a fuel consumption+stellar mass loss rate for the quasi-star given by a toy model for Eddington-limited growth, with $\dot{M}_{\rm c,\,consumption+loss} \sim -M_{\rm c}/3\,{\rm Myr}$. At early times, growth rates are much larger than this loss rate, while at later times, accretion rates drop rapidly. As a result, the exact assumption about when to "truncate" accretion rates and how to model quasi-star mass-loss make relatively little difference to our predictions for $M_{\rm c}$ (though they are important for models which attempt to predict the *relic* IMBH mass, given some $M_{\rm c}$).

The studies focused on cluster dynamics, while the evolution of the central object is another important key step of the runaway merger scenario. The central object, as the product of runaway collisions, is named “quasi-star" or “very massive star" in different context. For consistency, it will be mentioned as “quasi-star” in this work. Petts and Gualandris (2017) performed runaway-collision simulations with sophisticated descriptions of the quasi-star’s mass loss, and showed that the quasi-star will collapse after $\sim$ 3 Myr. Other studies have found that quasi-stars’ mass ($M_{\rm q}$ hereafter) can reach up to 10^6 $M_\odot$ in principle (given infinite “fuel”), and the remnant BH mass is $M_{\rm BH} \sim 0.1 M_{\rm q}$ (e.g., Begelman, 2010; Ball et al., 2011). These models also find the quasi-stars’ lifetime to be $\sim$ 3 Myr, with only a weak dependence on their masses.

These models, taken at face value, however, would actually imply almost no IMBHs in GCs or other dense stellar systems. The problem is that most GCs (let alone nuclear stellar clusters or galaxy bulges) have half-mass relaxation time scale much longer than 100 Myr (e.g., $t_{\rm rlx} \sim 2.5$ Gyr for M15). However, the studies cited above assumed the *initial* mass profile of GCs was essentially identical to the mass profiles of nearby relaxed clusters observed today (e.g., with a flat King-type central density profile). In short, if one were to assume that the GCs’ present-day mass distribution reflects their mass distribution at formation, this would rule out the runaway merger channel in most globular clusters. However, calculations following the dynamical evolution of globular clusters over cosmological timescales unanimously find that this is not a good assumption (Giersz et al., 2013; Wang et al., 2016; Baumgardt and Hilker, 2018; Kremer et al., 2020). Rather, the combined effects of stellar evolution and mass loss, dynamical ejections, mass segregation and “binary burning,” and tidal heating/stripping all tend to puff up and flatten the central mass profile slope of dense stellar systems (usually on time scales far shorter than the N-body relaxation time), implying that many presently-observed clusters once had much denser inner cores.

Indeed, the closest observable cousins to proto-globular clusters, young massive clusters (YMCs), are generally found to have density profiles that are significantly different from old globular clusters of comparable mass. Their half-mass radii are generally smaller, with a typical half-mass radius of $\sim$ 1 pc that has no clear correlation with mass (Ryon et al., 2015; Ryon et al., 2017), and thus their relaxation times are generally shorter. They also have a relatively compact density profile with an outer asymptotic power-law slope $\rho \propto r^{-\eta_1}$, where η_1 is typically in the range

2 – 3 (Grudić et al., 2018a). Grudić et al. (2018a) further found that hydrodynamical simulations of YMC formation were able to reproduce this density profile robustly, and proposed that these density profiles arise from the star cluster assembly process.

In this article we revisit the basic physical processes involved in the assembly a massive stellar object in the centre of a dense star cluster, using the results of the Grudić et al. (2018a) simulations, which successfully reproduce observed YMC outer density profiles (Ryon et al., 2015; Ryon et al., 2017), as well as a range of giant molecular cloud (GMC) properties including their turbulent structure, magnetic field strengths, and stellar auto-correlation functions or stellar clustering (Guszejnov et al., 2020). These simulations attempt to capture (to the extent possible with state-of-the-art simulations) the cluster properties as they form, which is the most relevant time for potential IMBH formation. Using these simulation results to guide our space of cluster models, we perform a set of Monte Carlo (MC) simulations to track the mass segregation process and study the evolution of the central mass (the quasi-star). Using these methods we predict the mass growth history of the quasi-star and its dependence on the properties of the progenitor cloud or host cluster.

The article is organized as follows: in Section 2.2 we introduce the analytical and numerical methods used to study mass segregation and the runaway growth of massive objects in star clusters; in Section 2.3, we show the numerical results from the MC simulations and discuss some secondary effects; in Section 2.5, we expand the discussion to observational aspects and make predictions; finally, in Section 2.6 we summarize our main findings.

2.2 Models and methods

Initial conditions from cluster formation simulations

For our initial conditions, we extract catalogues of star clusters as they form in the simulations from Grudić et al. (2018b) and Grudić et al. (2018a). These are N-body plus magneto-hydrodynamic (MHD) simulations of cloud collapse and star formation, including detailed models for radiative cooling and chemistry, star formation, and "feedback" once stars form in the form of radiation (e.g., radiation pressure and HII regions), stellar winds, and supernovae. The simulations follow the collapse of giant molecular clouds, the assembly of star clusters, and the eventual dispersal of gas due to stellar feedback. One such simulation of e.g., a massive complex can produce many independent clusters: we identify gravitationally-bound

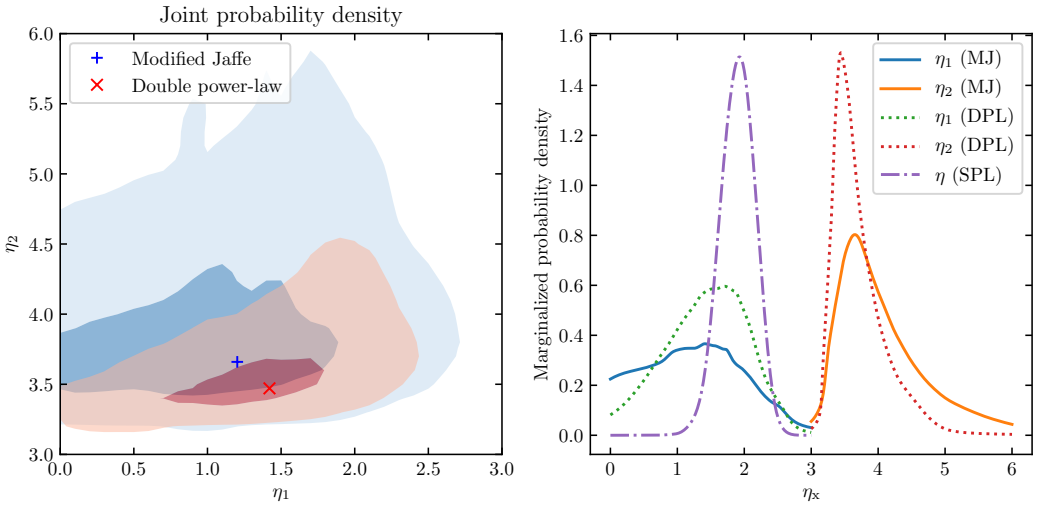

Figure 2.2: Probability distribution function (PDF) of the best-fit analytic density profile innert slopes (η_1, where $\rho \propto (r/r_{\rm h})^{-\eta_1}$ as $r \rightarrow 0$) and outer slopes (η_2, relevant as $r \rightarrow \infty$), fit to our entire library of MHD star cluster formation simulations. We compare both "modified Jaffe" (Eq. 2.1; MJ) and "double power-law" (Eq. 2.2; DPL) and (at *right*) single power-law (SPL) fits to just $r < r_{\rm h}$. **Left**: Joint PDF of η_1 and η_2. Darker (lighter) counters denote the 1 σ (2 σ) inclusion contours, while crosses show the local maxima. **Right:** Marginal 1D PDFs for η_1 and η_2. The MJ, DPL, and SPL fits are statistically consistent, though MJ shows larger covariance between η_1 and η_2 owing to the much less-sharp "knee"; SPL has no covariance by construction. Independent of fitting methodology, the simulations clearly exhibit steep inner profiles at formation with most-common $\eta_1 \sim 1.5-2$, closer to isothermal ($\eta_1 = 2$) than to their post-relaxation King-like ($\eta_1 = 0$) profiles.

star clusters remaining after gas dispersal[1] using a group-finder which associates stars belonging to a common potential well which are also gravitationally bound within that well (see Appendix A in Grudić et al. (2018a) for details). We restrict to clusters which form > 100 bound star particles.

This gives us an ensemble of $\sim$ 1000 clusters "at formation," one of which is shown in Fig. 2.1 Note that this sample of clusters should not be considered statistically representative of a cluster population that would form in a real galaxy: the initial conditions of the simulations were simply uniformly sampled on a logarithmic grid in mass-radius parameter space, which is ideal for our study here.

These simulations are designed to (1) sample an enormous parameter space, and (2) simulate large complexes through the entirety of star formation and stellar evolution:

[1]We have also compared the results extracting clusters at the time of peak star formation; the time difference is sufficiently small that it has little effect on our results.

as such, the numerical resolution is such that individual "star particles" in the original simulations represent an IMF-averaged ensemble of stars. To properly evolve stellar dynamics, we therefore re-sample each star particle into an ensemble of individual stars, drawing probabilistically from the stellar initial mass function (IMF) conserving total stellar mass. By default (since it is the same used for the original simulation stellar evolution models) we adopt a Kroupa (2001) IMF with an upper mass limit of $m_{\rm max} = 100$ M$_\odot$.[2] For this assumption the median stellar mass is $\langle m \rangle \approx 0.38$ M$_\odot$, and the mean is 1.5 M$_\odot$.

Analytic models from the simulations

Although our simulation suite is extensive, it is still limited by (1) finite sampling of parameter space and (2) finite resolution. Especially in cluster centers (particularly important here), the original simulation will always produce finite-resolution effects. Moreover, although the simulated clusters have some non-axisymmetric structure, we generally find this is small and generates torques which are weak compared to dynamical friction (discussed below). Therefore, it is especially useful to also consider general analytic models for the initial conditions, *motivated* by the cluster catalogue from our simulation suite.

We consider three simple, spherically-symmetric analytic density profiles, which we will show allows us to capture almost all of the key behaviors we study. These are shown in Fig. 2.1 as fits to one example profile.[3] First, a "Modified Jaffe" model (from Binney and Tremaine 2008, Eq. 2.64):

$$\rho(r) = \rho_{\rm c} \left(\frac{r}{r_{\rm c}}\right)^{-\eta_1} \left(1 + \frac{r}{r_{\rm c}}\right)^{-\eta_2+\eta_1} . \tag{2.1}$$

with inner power-law slope η_1, outer slope η_2, turnover radius $r_{\rm c}$, and normalization ρ_c (given by e.g., the total mass). We also consider a similar "double power" law model:

$$\rho(r) = \frac{\rho_{\rm c}}{(r/r_{\rm c})^{\eta_1} + (r/r_{\rm c})^{\eta_2}}, \tag{2.2}$$

[2] We have tested and adopting instead a Chabrier (2003) makes negligible difference to our conclusions. Likewise we find that varying the upper "cutoff" mass of the IMF makes only weak (logarithmic) corrections to our predictions (because these stars contribute negligibly to the total massive-star stellar mass budget).

[3] We have experimented with a variety of different methods for fitting the analytic profiles to the simulation outputs, and find the most robust results fitting directly to the spherically-averaged $\rho(r)$ in log-log space with uniform weights but constraining the analytic fit to reproduce the total mass and half-mass radius (specifying ρ_c and $r_{\rm c}$) exactly, so only the slopes $\eta_{1,2}$ are "free."

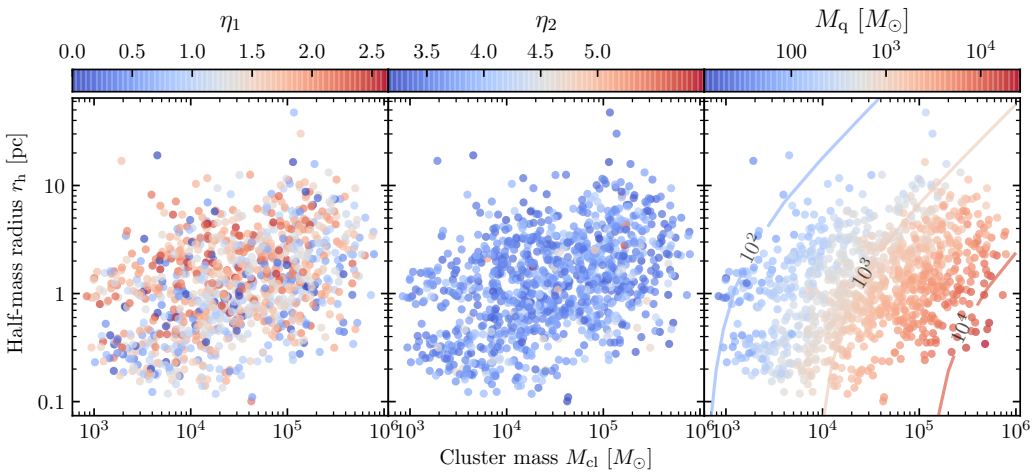

Figure 2.3: Properties and predictions from our cluster catalog with respect to cluster mass $M_{\rm cl}$ and effective radius ($r_{\rm h}$). **Left**: Best-fit inner density profile slope parameter (η_1). **Middle**: Best-fit outer density profile slope parameter (η_2). Notably, there is no significant systematic dependence of the density profile *shape* parameters η_1 or η_2 on the cluster mass and radius, consistent with scale-free predictions for substructure in turbulent gravitational fragmentation (Guszejnov et al., 2018a). **Right**: Predicted central object mass $M_{\rm q}$, measured as $M_{\rm c}(t = t_{\rm c}$, i.e. at the "crossover time" as in e.g., Fig. 2.1, from our "full model," as a function of $M_{\rm c}$ and $r_{\rm h}$. We compare the predicted values (contours, with $M_{\rm q}/{\rm M}_\odot$ labeled) if we assume all clusters have an identical universal double power-law mass profile with the "typical" values of $\eta_1 = \eta_{1*}$ and $\eta_2 = \eta_{2*}$ (§ 2.3). This reproduces the results well, indicating that sub-structure in the simulations, and variation in mass profile shape from cluster-to-cluster, do not strongly influence our conclusions.

which has the same qualitative features as the "Modified Jaffe" model but features a much sharper turnover around $r_{\rm c}$, which is useful in what follows as it dramatically reduces the covariance between the parameters η_1 and η_2.

Finally, we also consider a "single power" law model: $\rho(r) = \rho_{\rm c}(r/r_{\rm c})^{-\eta}$ for $r < r_{\rm c}$. This obviously cannot fit any mass profile over the entire dynamic range of r with finite mass; we therefore restrict the fit only to radii smaller than the half-mass radius (so $\eta \approx \eta_1$). This is included here because it allows us to derive some simple analytic expressions in regimes where the inner profile dominates the behavior.

Sinking and "merging" stars

Even with the simplifications above, integrating the full N-body dynamics of massive stars through a cluster into merger with a central object is computationally impossible (both given our large parameter space of models and sample of "clusters" reaching

$\sim 10^8\,M_\odot$, let alone uncertainties in the actual size/evolution of the central object). However, full N-body studies of a small number of smaller clusters (e.g. Portegies Zwart and McMillan, 2002; Gürkan et al., 2004; Alessandrini et al., 2014) have shown that dynamical friction is an excellent approximation to rate of sinking and merger of massive stars with $m \gg \langle m \rangle$ (which are those that dominate the buildup of a central quasi-star on the timescales of interest). This quickly circularizes the orbits of the massive stars and leads to orbital decay with

$$\dot{r} = -4\pi\, G^2\, m\, \ln\Lambda\, v_c^{-3}\, \rho_b\, r \tag{2.3}$$

where m is the mass of the sinking star, $v_c^2 \equiv G\,M(<r)/r$ reflects the enclosed mass $M(<r)$ inside r, ρ_b is the density of the background stars at radius r (e.g., the $\rho(r)$ in the profiles above), and Λ is a Coulomb logarithm which we take to be $\Lambda(r) \approx 0.1\,M(<r)/\langle m \rangle$. Less massive stars will not sink: we approximate this (conservatively, for now) by simply applying a cutoff ignoring any $\dot{r}$ below $m_{\rm min} = 8\,M_\odot$.[4]

From a MC realization of the ICs (either directly from the formation simulations, or analytic fits), we then evolve the system forward in time. As massive stars approach the center, the first to reach the center (region interior to which there are no other $m > m_{\rm min}$ stars) becomes the "seed" quasi-star (with mass M_c). Because we are interested in mergers *while the massive stars are on the main sequence*, we subsequently "merge" into this any massive star which (1) has not yet reached the end of its main sequence lifetime (adopting the relation from Mottram et al. 2011; typically $\sim 3\,$Myr for the most massive stars), (2) approaches the quasi-star within a radius $r < r_q$ which represents some "interacting binary" or "common envelope" radius (for which we take the value quoted by Hosokawa et al. (2013) for models of a rapidly-accreting protostar: $r_q \approx 2600\,R_\odot\,(M_q/100\,M_\odot)^{1/2}$),[5] and (3) reaches before the quasi-star itself has reached the end of its lifetime. We simply add the merged mass to M_c, neglecting e.g., mass-loss associated with the merger. Note that during collisions the central object mass $M_c(t)$ will contribute to the total enclosed mass $M(<r)$ as an additional point mass, which is included as a

[4] This ignores back-reaction causing lower-mass stars to migrate outwards, but this is a small effect on the timescales we consider, and we show below the exact choice of $m_{\rm min}$ also has relatively weak effects on our conclusions.

[5] This is essentially an extrapolation from "normal" pre-main sequence stars. Of course the sizes of quasi-stars are purely theoretical and uncertain: however varying this by factors of several has very little effect on our conclusions, as the "sinking" times around these radii are relatively small. But we need to include some finite "merger radius" since we do not model effects like gravitational wave emission which could merge point-mass-like particles.

correction when solving Eq. (2.3) in our *full* version of MC simulations. This "point mass correction" (PMC) is not included in our analytical calculation and the corresponding MC simulations.

The quasi-star "lifetime" essentially sets the end of our simulation, and the final mass of the quasi-star. Studies of quasi-star structure (e.g., Goodman and Tan, 2004; Schleicher et al., 2013; Ball et al., 2011) have found that because these stars are approximately Eddington-limited, they have lifetimes $\sim 3\,\mathrm{Myr}$ akin to massive stars. Simulations that include a detailed description of quasi-star's mass loss also show a similar lifetime of typically 3 Myr Petts and Gualandris (2017). We have therefore considered simply taking the mass $M_q = M_c(t = 3\,\mathrm{Myr})$. We have also considered a more sophisticated model motivated by the same pre-main-sequence models described above: some accretion rate $\dot{M}_{\rm acc} = dM_c/dt$ from mergers sustains the quasi-star lifetime and keeps it "puffed up" (allowing efficient mergers) as long as it is larger than the fuel consumption/loss rate from a combination of nuclear burning and stellar mass-loss, which occurs on a characteristic timescale $t_0 \sim 3\,\mathrm{Myr}$. We therefore take the final M_q to be M_c at the first time where $\dot{M}_{\rm acc}$ falls below M_c/t_0. In practice, because the merging stars also have lifetimes $\sim 3\,\mathrm{Myr}$, it makes very little difference which of these assumptions we adopt.

2.3 Results

Density profiles

Grudić et al. (2018a) showed that the simulated clusters here produce a distribution of density profile shapes *after relaxation* in good agreement with observations; however, no analysis of the *inner* density profiles *at formation* was performed. In Fig. 2.2, we show the distribution of the inner (η_1) and outer (η_2) mass profile slopes fit to all clusters. In both "modified Jaffe" and "double-power-law" models, the outer slopes are typically in the range of 3.5-4.5 as found in Grudić et al. (2018a). The inner slopes cluster around $1 - 2.5$ (as compared to post-relaxation profiles, which broadly follow a "flat" Elson et al. 1987 distribution). The best fit distribution for η_1 is most narrowly-peaked (around $\eta_1 \approx 2$) for the "single-power-law" fits (fit to just r within the half-mass radius), and most broad for the "modified Jaffe" fit. Our extensive experimentation with different fitting methods indicates that this directly traces the covariance between η_1 and η_2. The single-power fit, with only one slope, has no $\eta_1 - \eta_2$ covariance. The double-power fit, with a "sharp" break, has weak covariance between η_1 and η_2 which "smears" the best-fit η_1. The modified Jaffe fit exhibits very strong covariance between η_1 and η_2, with a wide range of allowed fits

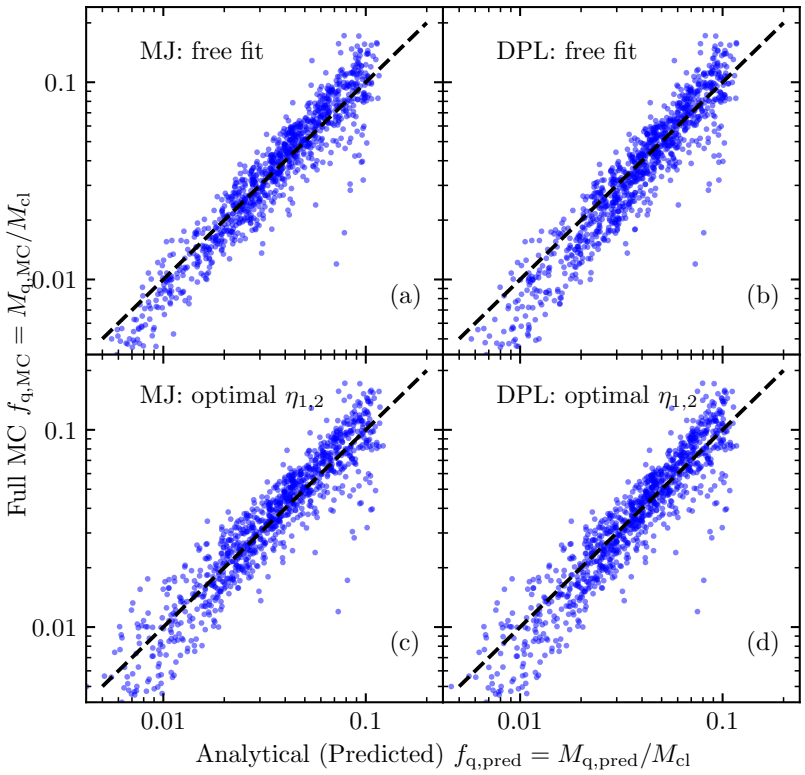

Figure 2.4: Quantitative comparison of the maximum central object mass M_q predicted by different analytic models for the density profile, to that calculated using the full simulation 3D density information, for all $\sim$ 1000 MHD star-formation simulation clusters in our library. We normalize both by cluster mass $M_{\rm cl}$ to reduce the dynamic range and better highlight any discrepancies. Dashed lines show identity (MC equals analytic). **(a)**: Results assuming an analytic modified Jaffe profile with all clusters fitted separately with 4 free parameters. **(b)**: Double power model with all clusters fitted separately with 4 free parameters. **(c)**: Modified Jaffe model assuming a universal profile shape with the slopes η_{1*} and η_{2*} (but allowing $M_{\rm cl}$ and $r_{\rm h}$ to vary, matched to the exact simulation values for each simulation). **(d)**: Double power model assuming a universal profile shape with η_{1*} and η_{2*}. In general, assuming universal, smooth, analytic, 1D density profiles introduces relatively small errors into our estimates of $M_{\rm q}$ (*provided* we adopt the correct "at formation" slopes), suggesting it is reasonable to apply these to YMCs and other young objects for which $M_{\rm cl}$ and $r_{\rm h}$ can be measured but $\rho(r)$ as $r \rightarrow 0$ cannot be resolved.

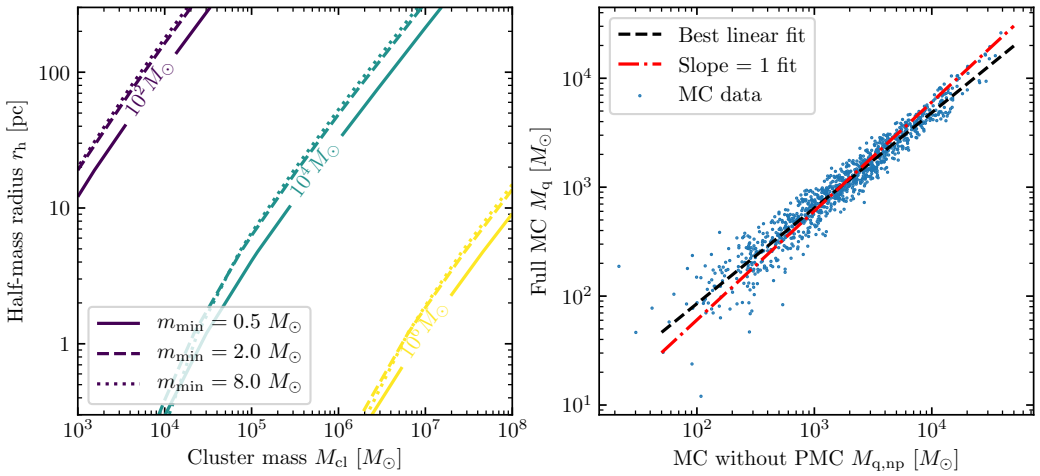

Figure 2.5: The effect of the "lower mass cutoff" (mass limit where dynamical friction remains a good approximation) and point-mass corrections on quasi-star masses M_q. **Left**: Varying m_{min}, the minimum stellar mass where we assume that a dynamical-friction-type orbital decay (Eq. 2.3, requiring stellar masses $m \gg \langle m \rangle \sim 0.38\,M_\odot$) is valid. Lines show the predicted M_q as a function of cluster mass M_{cl} and size r_h, assuming the universal best-fit η_{1*}, η_{2*}, for each m_{min}, and otherwise adopting our "full" model. This produces nearly-negligible differences, as stars with masses $\ll 8\,M_\odot$ sink inefficiently even if dynamical friction were a good approximation for their dynamics. The effects of varying the upper mass-limit of the IMF from $100\,M_\odot$ (not shown) are also negligible. **Right**: Effect of ignoring the "point mass correction" (not accounting for the finite N-body effect of the quasi-star itself, see Fig. 2.1). Even if we ignore these corrections, we obtain $M_{q,np}$ very similar to our full model M_q, just systematically larger by a modest factor – a linear fit gives $M_q \approx 0.6\,M_{q,np}$ (fitting an arbitrary power-law gives $(M_q/2000\,M_\odot) \approx 0.6\,(M_{q,np}/2000\,M_\odot)^{0.9}$, but the difference from the "slope = 1 fit" is not significant). Accounting for these finite N-body effects produces a not-negligible correction to M_q, but it is largely a systematic effect which does not change our qualitative conclusions.

for any given simulation profile.[6]

Fig. 2.3 shows that the best-fit η_1 and η_2 do *not* depend systematically on either cluster half-mass radius r_h or mass M_{cl}. Likewise our cluster catalogue includes simulations with progenitor clouds of different metallicities ($Z/Z_\odot = 0.01 - 1$), and we see no dependence on Z.

Even though the exact values of the "inner slope" η_1 can vary between fits, the

[6]It is important to note that because of the covariance in the fits, models with the modified Jaffe fit with $\eta_1 \sim 0$ give $r_c \ll r_{half}$, i.e. the "rollover" occurs very slowly down to extremely small radii (often below the simulation resolution) – so the central densities are still large.

fact that these are relatively narrowly constrained (within covariances, i.e. all are "good" representations of the data), and that they do not depend systematically on cloud mass/size, means that we obtain reasonably good estimates for the final central object mass from our full MC calculation, using an idealized mass profile fit with either of the fitting functions *or* assuming a "universal" mass profile shape across all clusters (Fig. 2.4). The modal fit values for (η_1, η_2) are $(\eta_{1M}, \eta_{2M}) = (1.2, 3.7)$ for the modified Jaffe, (1.4, 3.5) for the double-power-law, and (1.9) for the single power-law model. Because of the covariances, however, these are not the same as the values which give the best estimate of M_q compared to our full MC calculation. Instead, we should ask which values (η_{1*}, η_{2*}), applied to the entire ensemble of clouds (as a "universal" profile shape), most accurately predict M_q from the MC:[7] these are (η_{1*}, η_{2*})=(1.68, 4.95) for modified Jaffe,[8] (1.81, 3.79) for double power-law, and (1.93) for single power-law, all of which feature a similar, isothermal-like inner slope $\eta_1 \sim 2$.

Central object growth

Fig. 2.1 shows one example of our full MC simulation, with the ensuing growth of the central object as a function of time $M_c(t)$. The results from the spherical analytic model with the modified Jaffe or double-power-law profiles agree very will with the full MC (the single-power-law works well up to $\sim 1-3$ Myr, as well, where most of the accretion is from radii $\ll r_h$). The "crossover point" where $\dot{M}_{acc} = M_c/t_0$ occurs at $t \sim 1.3$ Myr, but the growth rate of M_c is slowing down already at this point, so M_q only differs by a factor of ~ 1.5 if we take M_q to be M_c at $t = 3$ Myr, or a factor of 1.9 if we take M_q as $t \rightarrow \infty$. In any case, this particular cluster, chosen to be relatively extreme (with a total mass $\sim 10^6\,M_\odot$ and initial central density of $\sim 10^{11}\,M_\odot\,pc^{-3}$ at $r \lesssim 0.001$ pc) is able to merge most of its massive stars ($\sim 10\%$ of the total stellar mass) within < 3 Myr.

Fig. 2.3 shows M_q from our full MC calculation for each simulated cluster, as a function of cluster mass and half-mass radius. There is a clear trend where more massive clusters M_{cl} at the same size give larger M_q, and a weaker but still evident trend of larger M_q for more compact clusters at fixed mass. These are expected

[7] Formally we find the (η_{1*}, η_{2*}) which minimize the variance

$$\sum |\log\{M_{q,\,pred}(\eta_{1*},\,\eta_{2*},\,r_h,\,M_{cl})\} - \log\{M_q(MC)\}|^2.$$

[8] The dramatic change in the values for modified Jaffe again indicates the covariance (with the $\eta_2 = 4.95$ value indicating that the outer slope plays a very small role in determining M_q).

if cluster profiles are approximately self-similar: to show this we compare the predicted $M_{\rm q}$ from analytic models with different $M_{\rm cl}$ and $r_{\rm h}$, assuming a universal density profile shape (the double power-law fit with fixed $\eta_1 = \eta_{1*}$, $\eta_2 = \eta_{2*}$).

Fig. 2.4 compares the mass fraction which can merge to the center $f_q \equiv M_q/M_{\rm cl}$ from our full MC calculation to that obtained from the simple spherical analytic models. We compare the results from the modified Jaffe and double-power-law fits, fit individually to each simulation cluster, which predict f_q to within $< 10\%$ on average – this indicates that deviations from symmetry, "lumpiness" or irregular structure in the potential and density profile, or resolution effects (e.g., numerical flattening or shot noise in the central density profile, as compared to the profile generated by a smooth power-law down to $r \rightarrow 0$) do not strongly influence our results. We also show the results assuming a universal profile with $(\eta_1, \eta_2) = (\eta_{1*}, \eta_{2*})$. This increases the scatter (as expected) but only by a modest amount: we can predict M_q to within an rms < 0.15 dex assuming this universal shape at formation.

It is unclear exactly at which mass scale dynamical friction ceases to be a good approximation for the "sinking" of massive stars: Fig. 2.5 varies the minimum mass $m_{\rm min}$ we allow to sink, to show this has only a small effect on our predictions. Varying $m_{\rm min}$ from $0.5 - 8\,{\rm M}_\odot$ changes M_q by a factor ~ 2, because (a) lower-mass stars sink more slowly (even if we allow them to sink), and (b) the Salpeter IMF is not extremely steep, so the total mass of stars "sinking" only changes with $m_{\rm min}^{-0.3}$.

Because most of the mass in the IMF is not in the highest-mass stars, it also makes little difference if we vary the high-mass cutoff (e.g., changing the upper-mass cutoff of the IMF from $100\,{\rm M}_\odot$ to $200\,{\rm M}_\odot$ only produces a $\lesssim 10\%$ difference in $M_{\rm q}$).

Another significant uncertainty in our models is how the actual mergers/coalescence occur in the center: we simply populate stars and merge anything within some large radius in the center (reflecting the envelope size of the quasi-star), implicitly meaning there is some "overlap" between the envelope of the quasi-stars and our populated stars in the models. Properly determining if or how mergers once massive stars sink close to the central quasi-star requires dynamical stellar merger simulations. But even within our simple model, stars can still "stall" near the center. In Fig. 2.5, we consider a model variation where we simply merge any star which reaches the radius where the proto-star *would* dominate (be more than $1/2$ of) the enclosed mass $M(r)$, and ignore the mass of M_q itself in calculating v_c in Eq. 2.3: these changes essentially guarantee that any massive star which approaches small r merges. We see that this systematically increases $M_q/M_{\rm cl}$, as expected, by a factor ~ 2. This in

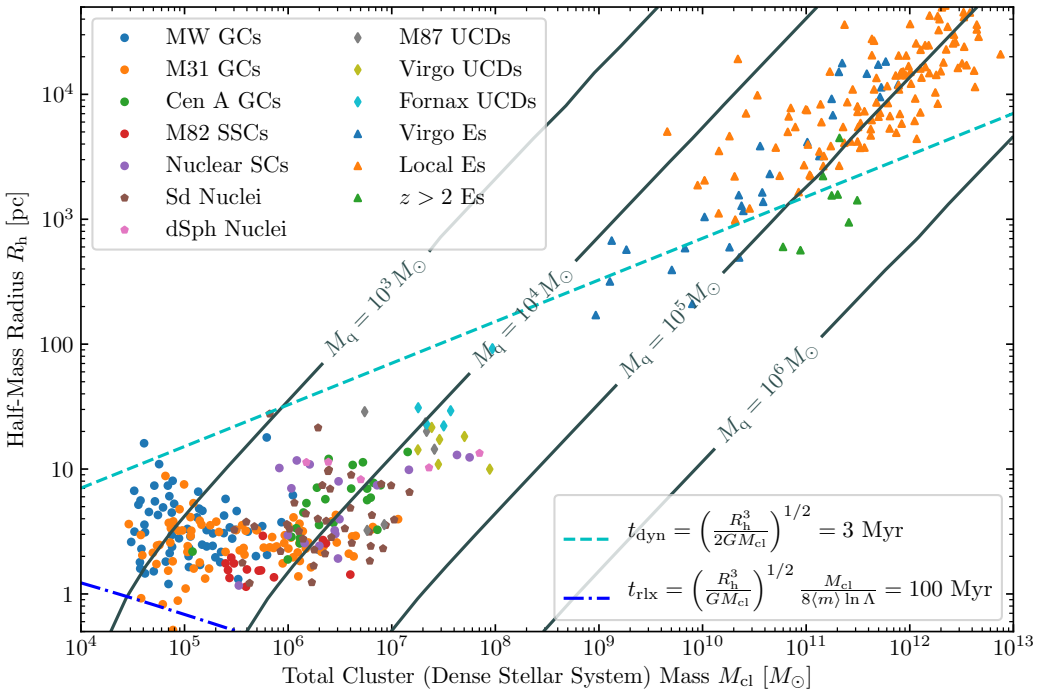

Figure 2.6: Predictions for the peak central object mass M_q given by our full models assuming the best-fit universal at-formation density profile parameters η_{1*}, η_{2*}, and given cluster mass $M_{\rm cl}$ and projected 2D circular half-mass radius $R_{\rm h}$ (solid lines label contours of constant M_q). We note where the dynamical time $t_{\rm dyn} = 3\,$Myr (systems with $R_{\rm h}$ above this line have $t_{\rm dyn} \gg 3\,$Myr, making our assumption that the stars are approximately co-eval on the timescales of interest for quasi-star evolution suspect). We also compare the contour below which the cluster-scale N-body relaxation time $r_{\rm rlx} < 100\,$Myr where "complete core collapse" (requiring full N-body simulations) as opposed to sinking in the center should occur (almost no clusters meet this criteria). We compare the masses and radii of a variety of *observed* dense stellar systems (references in text; § 2.5), including globular clusters (GCs), super star clusters (SSCs), nuclear star clusters (NSCs) and dwarf galaxy stellar nuclei, ultra-compact dwarf galaxies (UCDs) and the elliptical galaxies (Es). If we assume their masses and radii have not evolved dramatically since formation, this gives a rough prediction for their initial quasi-star masses. Although $M_{\rm q}$ could reach as large as $\gtrsim 10^4\,{\rm M}_\odot$ in the most massive SSCs/nuclei/UCDs, this is generally much smaller than the present-day SMBH masses detected in such systems (even moreso for the $M_{\rm q} \gtrsim 10^5\,{\rm M}_\odot$ in the most massive Es, but these also have $t_{\rm dyn} \gtrsim 3\,$Myr).

turn means that our "default" model is predicting an order-unity fraction of massive stars near $r \sim 0$ "stall" or otherwise fail to merge, a reasonable order-of-magnitude approximation to few-body simulations. It also implies that these correction does not change our qualitative conclusions.

2.4 Comparison to previous work

As discussed in § 2.1, Portegies Zwart and McMillan (2002) and Gürkan et al. (2004) considered detailed N-body simulations to follow runaway merging, but used adopted very different mass profile shapes (similar to post-relaxation clusters today). *If* we adopt a similar profile shape to their default (e.g., a Plummer-like $(\eta_1, \eta_2) = (0\ ,\ 5)$), and then run our full model to calculate M_q for a wide range of $M_{\rm cl}$ and $r_{\rm h}$ (sampling the values of our simulation library) then – despite the other simplifications here – we obtain quite good agreement (within a factor of a few) with *both* their requirement that the cluster must have $t_{\rm rlx} \lesssim 25\,{\rm Myr}$ to produce any appreciable growth of $M_{\rm c}$ and the peak mass $M_{\rm q}$ or resulting mass fraction $f_q = M_q/M_{\rm cl}$ in a central massive object produced when this criterion is met. This is reassuring, and implies our methodology is reasonable. The key difference in our predictions, compared to theirs, arises because our MHD star formation simulations predict quite different values of η_1 compared to those they considered.

Some other recent studies have considered runway stellar mergers in initial conditions closer to those here (but with a more limited or ad-hoc choice of initial profiles). Sakurai et al. (2017) adopted a similar approach to that here, using hydrodynamic simulations to select dense ($M_{\rm cl} \sim 10^5\,{\rm M_\odot}$, King-profile core $r_{\rm c} \sim 0.4\,{\rm pc}$) proto-galactic "clouds" and then using those to set up initial conditions for N-body simulations: although our survey is intended to match much later-forming star clusters, where the cloud properties overlap we find similar M_q within a factor ~ 2 for each of the ~ 8 clusters they simulate (assuming a typical $r_{\rm c}/r_{\rm h} \sim 0.1$). Petts and Gualandris (2017), as mentioned in § 2.1, also used King-type profiles to setup the initial cluster density. In those simulations, clusters with mass $M_{\rm cl} \sim 10^5\,{\rm M_\odot}$ and half-mass radius $r_{\rm h} \sim 0.1$ – $0.6\,{\rm pc}$ typically generate quasi-stars of $M_q \sim 100$ – $4000\,{\rm M_\odot}$ and remnant black holes of $M_{\rm BH} \sim 20$ – $400\,{\rm M_\odot}$. The simulations, although with a background potential field near the Galactic Center, generally agree with our analytic estimation in the quasi-star's mass (e.g., when compared with the right panel of Fig. 2.3). However, the central density of the clusters is typically 10^6 – $10^7\,{\rm M_\odot/pc^3}$ while our star formation simulations show significant higher density (e.g., as shown in Fig. 2.1).

In parallel, Devecchi and Volonteri (2009) considered analytic models for cloud/cluster formation, to estimate typical cloud densities in the early universe, coupled to a simple prescription from Portegies Zwart and McMillan (2002) for the fraction of clusters undergoing runaway, to argue f_q could reach ~ 0.05 for dense clusters

formed in the early Universe because these produce steep central profiles ($\eta_1 \gtrsim 5/3$), broadly similar to our conclusions. And recently, Tagawa et al. (2020) performed semi-analytic calculations qualitatively akin to those here, considering a much more limited range of profiles (but taking steep η_1) but much more detailed models for the (proto)-stellar evolution of the quasi-star and merger criteria, but conclude that effective growth ceases at $\sim 3\,$Myr (as we assume here) with a similar effective radius for merger (versus M_q) as we adopt here. More recently, Rizzuto et al. (2021) performed a series of N-body simulations of YMCs based on King-type profiles, indicating that massive stars weighing up to $\sim 400\,M_\odot$ may form within 5–15 Myr and sequentially become IMBHs. The results generally support our semi-analytical model, which is based on a more realistic parameter space of YMC density profiles and limited lifetime for quasi-stars.

2.5 Discussion

We now consider the implications of our results for real dense stellar systems. Fig. 2.6 plots the distribution in $M_{\rm cl}$ and $r_{\rm h}$ of a wide variety of known dense, stellar-dominated, dispersion-supported systems: globulars and YMCs, super-star clusters (SSCs), nuclear star clusters in different dwarf and late-type galaxies (NSCs), ultra-compact dwarf galaxies (UCDs), nearby and high-redshift compact elliptical galaxies and bulge-dominated galaxies (Es). The sizes and masses are compiled in Hopkins et al. (2010), from observations by Harris (1996), Barmby et al. (2007), Rejkuba et al. (2007), McCrady and Graham (2007), Walcher et al. (2005), Böker et al. (2004), Geha et al. (2002), Haşegan et al. (2005), Evstigneeva et al. (2007), Hilker et al. (2007), Kormendy et al. (2009), Lauer et al. (2007), and van Dokkum et al. (2008). We have no way of knowing their properties "at formation," but because our full simulations can be reasonably approximated by assuming a "universal" profile shape at formation, we compare the contours of M_q predicted by our model with a universal at-formation (η_{1*}, η_{2*}). This does assume that the total mass and size have not evolved much since formation, an obviously uncertain assumption, but likely plausible since most of these systems have N-body relaxation times longer than the Hubble time.

From the detailed studies of quasi-star evolution noted in § 2.1, we will also assume in what follows that any quasi-star leaves behind a "relic" BH of mass $M_{\rm BH} \sim 0.1\,\epsilon_{0.1}\,M_q$. This "fudge factor" $\epsilon_{0.1}$ accounts for processes including inefficiency of final mergers, mass loss/ejection during merges, stellar winds and mass loss during collapse from the quasi-star.

Object	$M_{\rm cl}/{\rm M}_\odot$	$r_{\rm h}/{\rm pc}$	$\frac{M_{\rm BH}^{\rm pre}}{\epsilon_{0.1}\,{\rm M}_\odot}$	$M_{\rm BH}^{\rm obs}/{\rm M}_\odot$
ω Cen [1]	3.2×10^6	8.4	600	40,000 [1,8]; <12,000 [9]
47 Tucanae [3]	1.1×10^6	8.2	300	2,300 [13]; <1,700 [3,7]
G1 (M31) [4]	7.6×10^6	6.8	1500	17,000 [14];
				no evidence ($\lesssim 20,000$) [4]
M3 [15]	2.7×10^5	3.4	200	<5,300 [15]
M13 [15]	3.0×10^5	9.5	100	<8,600 [15]
M15 [6]	6.5×10^5	7.7	200	<500 [16]
M92 [15]	2.3×10^5	2.6	200	<1,000 [15]
NGC 1851 [18]	3.7×10^5	2.4	300	<2,000 [18]
NGC 1904 [18]	1.4×10^5	4.0	100	3,000 [18]
NGC 5694 [18]	2.6×10^5	4.4	100	<8,000 [18]
NGC 5824 [18]	4.5×10^5	4.5	200	<6,000 [18]
NGC 6093 [18]	3.4×10^5	3.2	200	<800 [18]
NGC 6266 [18]	9.3×10^5	3.0	500	2,000 [18]
NGC 6388 [2]	6.8×10^5	1.5	700	28,000 [2]; <2000 [10];
				1,500 [11]; <1,200 [12]
NGC 6397 [6]	9.1×10^4	4.6	60	600 [15]
NGC 6624 [5]	1.1×10^5	2.4	100	7,500 [17];
				no evidence ($\lesssim 10,000$) [5]

Table 2.1: Predictions for the relic IMBH mass from runaway merging based on our study here, compared to observational estimates or upper limits for IMBH masses in well-studied clusters. Columns give: (1) Object: cluster name (with reference for its properties); (2) Cluster mass $M_{\rm cl}$; (3) Cluster half-mass radius $r_{\rm h}$; (4) Predicted relic IMBH mass $M_{\rm BH}$ from our models (see e.g., Eq. 2.4) assuming a simple relation between relic BH mass and peak quasi-star mass ($M_{\rm BH} = 0.1\,\epsilon_{0.1}\,M_{\rm q}$); (5) Claimed IMBH "detection" masses or upper limits. References labeled "no evidence" argue there is no positive evidence for an IMBH but set weak upper limits (shown). In all cases our predicted relic $M_{\rm BH}$ is below present upper limits (and claimed detections). References: [1] Zocchi et al. (2017); [2] Lützgendorf et al. (2015); [3] Hénault-Brunet et al. (2020); [4] Baumgardt et al. (2003); [5] Gieles et al. (2018b); [6] Sollima and Baumgardt (2017); [7] Mann et al. (2019); [8] Baumgardt (2017); [9] van der Marel and Anderson (2010); [10] Lanzoni et al. (2013); [11] Cseh et al. (2010); [12] Bozzo et al. (2011); [13] Kızıltan et al. (2017); [14] Gebhardt et al. (2005); [15] Kamann et al. (2016); [16] Kirsten and Vlemmings (2012). [17] Perera et al. (2017). [18] Lützgendorf et al. (2013).

Analytic scalings

Assuming the "universal" profile parameters, the contours of constant M_q are approximately power-laws over most of the dynamic range of interest. We can approximate this quite well via a simple purely-analytic estimate for M_q if we assume a single-power law profile with $\eta_1 = 2$ (isothermal), neglect "edge" effects (assume the stars outside $r_{\rm h}$ are not sinking efficiently), and approximate the effects of various non-linear terms like varying coulomb logarithms, the finite N-body point mass correction, finite IMF sampling, finite size of the quasi-star, and others as a systematic factor of ~ 2 normalization correction (reasonably well-motivated by our comparison in Fig. 2.5). With all of these approximations, we obtain the very simple expression:

$$M_{\rm BH} = 0.1\,\epsilon_{0.1}\,M_q \sim 250\,{\rm M}_\odot\,\epsilon_{0.1}\left(\frac{M_{\rm cl,\,5}}{r_{\rm h,\,pc}}\right)^{3/4} \sim 250\,{\rm M}_\odot\,\epsilon_{0.1}\left(\frac{V_{\rm eff}}{20\,{\rm km\,s^{-1}}}\right)^{3/2} \tag{2.4}$$

where $V_{\rm eff}^2 \equiv G\,M_{\rm cl}/r_{\rm h}$, $M_{\rm cl,\,5} = M_{\rm cl}/10^5\,{\rm M}_\odot$, $r_{\rm h,\,pc} = r_{\rm h}/{\rm pc}$.

Despite the many simplifications involved in deriving this expression, it provides a quite reasonable order-of-magnitude approximation to the most important results from our more detailed full model calculations.

Globulars and "typical" dense star clusters

Fig. 2.6 & Eq. 2.4 do suggest IMBHs could form in massive GCs, with typical masses $M_{\rm BH} \sim 0.0003\,\epsilon_{0.1}\,M_{\rm cl}$. In Fig. 2.6 we also show the criterion $t_{\rm rlx} < 100\,{\rm Myr}$ which Portegies Zwart and McMillan (2002) and Gürkan et al. (2004) argue is required for a GC with an initially *flat* ($\eta_1 = 0$), Plummer-like density profile to undergo any significant runaway merging. We see, as noted in § 2.1, that almost no known present-day massive clusters meet this criterion. The reason our modeling here predicts they *can* form central objects is because we argue they likely had steeper slopes at initial formation (allowing some merging near their center at these early times). But, essentially by definition, any interior region which has a steep enough slope to produce runaway merging within $< 3\,{\rm Myr}$ will, on timescales $\sim {\rm Gyr}$, have undergone relaxation, flattening the central profile seen today.

However, although our models predict runaway merging *could* occur in the centers of almost all clusters at formation, the actual mass which we predict successfully merges (for realistic cluster $M_{\rm cl}$ and $r_{\rm h}$) is quite modest, giving a rather low $M_{\rm BH}/M_{\rm cl}$ compared to the clusters which undergo "complete runaway core collapse" (with

$t_{\rm rlx} < 25\,{\rm Myr}$) in Portegies Zwart and McMillan (2002). In Table 2.1, we explicitly list a number of individual observed GCs from Fig. 2.6 which have claimed detections or upper limits for central IMBHs. Many contradictory observational claims exist for some clusters, a well-known issue in the literature. Using the same models from Fig. 2.6, and the observed cluster properties, we give our best estimate of $M_{\rm BH}$ (approximately given by Eq. 2.4), and compare to these observations. We see that the predicted relic mass from our calculations is typically $\sim 10^{-4} - 10^{-3}\,M_{\rm cl}$, in many cases a factor ~ 10 or more below the claimed detections/upper limits. There is no case where our predicted $M_{\rm BH}$ exceeds even the most stringent upper limits. The most constraining examples we find are M15 and NGC 6388: here our "default" prediction is only a factor ~ 2.5 below the current upper limits or smallest values among the claimed detections. This implies $\epsilon_{0.1} \lesssim 3$ (i.e. $M_{\rm BH} \lesssim 0.3\,M_q$, if our models are to be believed at this level of accuracy).

If some of the most-massive detections (with claimed IMBH masses up to ~ 70 times larger than our prediction) are indeed correct (although almost all of these cases are controversial with much lower limits claimed by other studies), then it would most likely imply that the central BHs grew rapidly after formation via some other process such as gas accretion (from e.g., stellar mass-loss in the cluster).

Connection to SMBHs and more massive stellar systems

The predicted quasi-stars/IMBHs suggested in Fig. 2.6 & Eq. 2.4 become more massive, on average, in more massive systems, reaching $M_{\rm q} \sim 3\times10^4\,{\rm M}_\odot$ in the most massive and dense NSCs and UCDs, and up to $M_q \sim 3\times10^5\,{\rm M}_\odot$ in the centers of the most compact local and high-redshift bulges/Es.

These are systems which are known to host super-massive BHs, with $M_{\rm BH} \sim 10^4 - 10^{10}\,{\rm M}_\odot$ unambiguously detected (with the smallest BHs in dwarf NSCs, the most massive in compact Es), obeying a tight correlation with the velocity dispersion σ of the surrounding stars $M_{\rm BH}^{M-\sigma} \sim 3\times10^8\,{\rm M}_\odot\,(\sigma/200\,{\rm km\,s^{-1}})^{4.3}$ (Kormendy and Ho, 2013). However, noting that $\sigma \approx V_{\rm eff}$ in Eq. 2.4 for an isothermal profile, this implies that the present-day SMBHs observed are much more massive than the IMBH we predict from runaway merging at formation, for any $\sigma \gtrsim 7\,\epsilon_{0.1}^{0.3}\,{\rm km\,s^{-1}}$ (present-day $M_{\rm BH}^{M-\sigma} \gtrsim 100\,\epsilon_{0.1}^{1.5}\,{\rm M}_\odot$). In other words, while the masses here are potentially interesting for very first initial seeds of the SMBHs, runaway merging *cannot* establish most of the mass of *any* observed BHs on the BH-host galaxy (or BH-NSC) scaling relations. It does not substantially reduce the amount of BH ac-

cretion (nor the time required for that accretion, if it occurs at e.g., a fixed Eddington ratio), nor even radically change the initial seed mass relative to commonly-assumed $M_{\rm BH}^{\rm seed} \sim 100\,{\rm M}_{\odot}$ as the "most optimal normal stellar relic" remnant mass.

An important additional caveat in these massive systems is that our models assume the stars are approximately co-eval. This is reasonable in the centers of dense GCs where the dynamical times are $\ll$ Myr. However, in e.g., elliptical galaxy centers, the dynamical times can be $\gg 3\,$Myr; since stars cannot form much faster than the dynamical time, it is almost certainly the case that the massive star formation was extended in time relative to the lifetime $\sim 3\,$Myr of the quasi-star. In the center, later-forming stars can still sink, but they will merge with a central IMBH instead of quasi-star, producing a tidal disruption event and building up an accretion disk rather than directly forming a quasi-star.

2.6 Conclusions

Using the outputs of high-resolution numerical hydrodynamic simulations of star cluster/complex formation and destruction which have been shown to reproduce a wide range of GMC and cluster observables, we develop a semi-analytic model for the sinking of massive stars to cluster centers and their merger into a massive quasi-star. We find:

1. The mass profile of YMCs "at formation" (centered on local peaks, as there can still be substructure) can be described by a double power-law with steep, near-isothermal inner slopes common (which flatten at later times as the inner regions dynamically relax). This means that some runaway merging can occur early even in clusters with relatively low mean densities and long relaxation times (e.g., $M_{\rm cl} \sim 10^5 - 10^6\,{\rm M}_{\odot}$, $r_{\rm h} \sim 1 - 10\,$pc, with relaxation times $t_{\rm rlx} \gtrsim 100\,$Myr). The runaway ceases at $\sim 1 - 3\,$Myr, regardless of the details of the quasi-star evolution.

2. Over the parameter space of greatest interest (where massive, dense stellar systems are observed), our predictions can be approximated with a simple scaling, with the total mass of massive stars which sink to the center and could potentially merge, M_q, scaling as $M_q \propto V_{\rm eff}^{1.5}$, where $V_{\rm eff}$ is a characteristic circular velocity (Eq. 2.4).

3. Although some runaway merging is predicted in nearly all clusters (Fig. 2.6), the actual masses of IMBH relics predicted in our model for observed globulars

and typical dense star clusters are quite modest, $\sim 100 - 1000\,M_\odot$. For relic mass $M_{\rm BH} \lesssim 0.3\,M_q$ (expected allowing for mass-loss, imperfect merging, quasi-star evolution, etc.), our predictions are consistent with even the most stringent upper limits (to our knowledge) on central IMBH mass in all clusters for which such constraints exist. The most constraining clusters for our models at present are M15 and NGC6388; the only well-studied cluster where our model predicts $M_{\rm BH} \gtrsim 1000\,M_\odot$ is G1.

4. In more massive systems such as nuclear star clusters, ultra-compact dwarfs, and the centers of compact ellipticals, the central object mass could reach $M_q \sim 10^4 - 10^5\,M_\odot$, an interesting range for initial seeds of super-massive BHs. However for *any* system with velocity dispersion $\gtrsim 10\,{\rm km\,s^{-1}}$, the SMBHs on the various observed SMBH-host scaling relations (e.g., $M_{\rm BH}-\sigma$) are far more massive than even the most optimistic IMBH masses resulting from runaway merging. Thus runaway merging does not significantly reduce the need for subsequent accretion to super-massive BH masses.

Our models are intentionally simplified in order to survey a wide parameter space efficiently and guide intuition and predictions for future models. Using the models here to identify the most interesting parameter space, in future work we hope to consider explicit N-body simulations of the merging process in cluster centers (necessarily limited to a small number of realizations). In the systems where merging occurs most rapidly, it is also possible that mergers occur even *as* stars are still forming in the cluster, potentially before massive protostellar cores even complete their pre-main sequence evolution. Exploring this will require fully hydrodynamic+N-body simulations of star formation which can resolve the stellar IMF self-consistently and follow mergers as they occur "live." Considerable uncertainties also still surround the actual dynamics of massive stellar mergers (including complicated effects not followed here, such as the effect of resolved binaries and hierarchical multiples on merger efficiency) and the evolution (especially as it grows via rapid merging) of the (proto) quasi-star. In addition, if such a system forms, a variety of processes may allow for rapid growth even after it collapses to an IMBH, as it could accrete tidally-disrupted lower-mass stars which sink on longer timescales (e.g., $m \sim 2 - 8\,M_\odot$), or stellar mass-loss products from AGB stars that can remain gravitationally bound in the cluster potential. All of these remain important subjects for future study.

Chapter 3

HYPER-EDDINGTON ACCRETION: CAN IT HAPPEN?

Shi, Y. et al. (Jan. 2023). "Hyper-Eddington black hole growth in star-forming molecular clouds and galactic nuclei: can it happen?" MNRAS 518.3, 3606–3621. DOI: 10.1093/mnras/stac3245. arXiv: 2208.05025 [astro-ph.GA].

Abstract

Formation of supermassive black holes (BHs) remains a theoretical challenge. In many models, especially beginning from stellar relic "seeds," this requires sustained super-Eddington accretion. While studies have shown BHs can violate the Eddington limit on accretion disk scales given sufficient "fueling" from larger scales, what remains unclear is whether or not BHs can actually capture sufficient gas from their surrounding ISM. We explore this in a suite of multi-physics high-resolution simulations of BH growth in magnetized, star-forming dense gas complexes including dynamical stellar feedback from radiation, stellar mass-loss, and supernovae, exploring populations of seeds with masses $\sim 1-10^4\,M_\odot$. In this initial study, we neglect feedback from the BHs: so this sets a strong upper limit to the accretion rates seeds can sustain. We show that stellar feedback plays a key role. Complexes with gravitational pressure/surface density below $\sim 10^3\,M_\odot\,\mathrm{pc}^{-2}$ are disrupted with low star formation efficiencies so provide poor environments for BH growth. But in denser cloud complexes, early stellar feedback does not rapidly destroy the clouds but does generate strong shocks and dense clumps, allowing $\sim 1\%$ of randomly-initialized seeds to encounter a dense clump with low relative velocity and produce runaway, hyper-Eddington accretion (growing by orders of magnitude). Remarkably, mass growth under these conditions is almost independent of initial BH mass, allowing rapid IMBH formation even for stellar-mass seeds. This defines a necessary (but perhaps not sufficient) set of criteria for runaway BH growth: we provide analytic estimates for the probability of runaway growth under different ISM conditions.

3.1 Introduction

Observations have demonstrated the existence of supermassive black holes (BHs) with masses $M_{\rm bh} \sim 10^9 \mathrm{M}_\odot$ in quasars at very high redshift ($z \gtrsim 7$) when the Universe was less than a billion years old (e.g., Fan et al., 2001; Wang et al., 2021),

which implies that these BHs must accrete rapidly from their "seeds" (Inayoshi et al., 2020). The physical origin of these seeds remains deeply uncertain, but popular models including direct collapse of super-massive stars with masses $\sim 10^4 - 10^6\,M_\odot$ (e.g., Begelman et al., 2006; Regan et al., 2017; Corbett Moran et al., 2018; Chon and Omukai, 2020), runaway mergers in globular clusters (e.g., Portegies Zwart et al., 2004; Boco et al., 2020; Alister Seguel et al., 2020; Kremer et al., 2020; Rizzuto et al., 2021; Shi et al., 2021; Fragione et al., 2022), remnants from Population III stars (e.g., Madau and Rees, 2001; Ryu et al., 2016), and relics of "standard" stellar evolution (e.g., Population II) stars generally produce seeds with masses $\ll 10^4\,M_\odot$. Given that the e-folding time of a BH growing at the Eddington limit[1] with a canonical radiative efficiency of ~ 0.1 is $\sim 50\,$Myr, almost all of these models require a sustained period of super or hyper-Eddington accretion in the early Universe to be viable (e.g., Pezzulli et al., 2016). This is especially important at masses $\ll 10^5\,M_\odot$, as various studies have shown that once larger "super-massive" mass scales are reached, the gravity of the BH can capture gas from larger radii and lead to runaway growth (Li et al., 2007; Di Matteo et al., 2008; Li, 2012; Johnson et al., 2013; Weinberger et al., 2018; Huang et al., 2018; Zhu et al., 2020; Anglés-Alcázar et al., 2021). But unless one invokes exotic formation mechanisms, a sustained rapid accretion phase is necessary to grow BHs from the stellar ($\sim 10-100\,M_\odot$) to super-massive ($\gg 10^4\,M_\odot$) mass scale (Li, 2012; Valiante et al., 2016)

There is a well-established and rapidly-growing body of work demonstrating that compact objects can, in fact, exceed the naive "Eddington accretion rate" $\dot{M}_{\rm Edd}$ by large factors (up to $\gtrsim 1000$) on scales of the accretion disk itself (recently, see e.g., theoretical arguments by Inayoshi et al. 2016; Jiang et al. 2019; Park et al. 2020; Kitaki et al. 2021; Botella et al. 2022, empirical arguments in Berdina et al. 2021; Tortosa et al. 2022, or for reviews, Pezzulli et al. 2016; Mayer 2019; Smith and Bromm 2019; Brightman et al. 2019 and references therein). But these studies generally assume a constant hyper-Eddington ($\sim 10^3\,\dot{M}_{\rm Edd}$) influx of gas from larger scales onto the accretion disk as their "outer boundary condition." What remains deeply unclear is whether or not a seed BH – especially at stellar mass scales – could actually capture gas from the interstellar medium at a sufficient rate to sustain this accretion, and for long enough that the total mass supplied would be able to grow the

[1]Throughout, we will follow standard convention and define the Eddington *luminosity* as the usual $L_{\rm Edd} = 3.2\times10^4\,L_\odot\,(M_{\rm bh}/M_\odot)$, and the "Eddington mass-accretion rate" as the accretion rate which would produce $L_{\rm Edd}$ given a canonical reference radiative efficiency $\epsilon_r = 0.1$ ($L = \epsilon_r\,\dot{M}\,c^2$), so $\dot{M}_{\rm Edd} \approx M_{\rm bh}/(45\,{\rm Myr})$.

BH by many e-foldings. There has been some theoretical work on the topic, but it has generally either considered idealized models where the gas around the seed sits in a common potential well and accretes instead of being multi-phase and turbulent, rapidly forming stars (see e.g. Takeo et al., 2020; Park et al., 2022), or considered only galactic ($\gg$ pc) scales (e.g. Massonneau et al., 2023) where especially with BHs already $\gg 10^4\,M_\odot$, sustaining super-Eddington inflow to a nuclear region at least appears viable (Huang et al., 2018; Regan et al., 2019; Zhu et al., 2020; Anglés-Alcázar et al., 2021).

The problem is that in the realistic ISM, order-of-magnitude estimates such as those in Johnson et al. (2013) suggest that the rate of gravitational capture of gas from the surrounding ISM – the Bondi-Hoyle rate (Hoyle and Lyttleton, 1939; Bondi, 1952) – should be extremely small unless the seed is already super-massive. Consider the standard expression

$$\dot{M}_{\rm Bondi} \approx \frac{4\pi\,G^2\,M_{\rm bh}^2\,\rho}{(c_{\rm s}^2+\delta V^2)^{3/2}}. \tag{3.1}$$

where ρ, $c_{\rm s}$, and δV are the density, sound speed, and gas-BH relative velocity. In the diffuse/warm ISM, this gives $\dot{M}_{\rm Bondi}/\dot{M}_{\rm Edd} \sim 10^{-6}\,(M_{\rm bh}/10\,M_\odot)\,(n/{\rm cm^{-3}})$ – vastly sub-Eddington. In dense ($n \gtrsim 100\,{\rm cm^{-3}}$) cold molecular gas (sound speed $\sim 0.1\,{\rm km\,s^{-1}}$), $\dot{M}_{\rm Bondi}$ would be much larger *if the gas were laminar and the BH stationary* – this is akin to the idealized non-turbulent models above. The problem is that realistic cold molecular gas in the ISM is clumpy and dynamical and turbulent, with star formation and stellar feedback generating large random motions – i.e. large δV (Larson, 1981; Goodman et al., 1998; Evans, 1999; Stanimirovic et al., 1999; Elmegreen and Scalo, 2004). As we show below, assuming relative velocities are of order typical gravitational/virial velocities in the cloud then gives $\dot{M}_{\rm Bondi}/\dot{M}_{\rm Edd} \sim 10^{-4}\,(\langle n_{\rm cl}\rangle/100\,{\rm cm^{-3}})^{1/2}\,(M_{\rm bh}/10\,M_\odot)\,(10^6\,M_\odot/M_{\rm cl})$ – once again, vastly sub-Eddington. Previous analytic and simulation models of this "turbulent Bondi-Hoyle problem" in idealized driven turbulence have argued that vorticity and turbulent magnetic fields will suppress the *average* accretion rates even relative to this (pessimistic) result (Krumholz et al., 2006; Burleigh et al., 2017).

However, it is also clear from many studies of star formation that turbulence in dense gas also promotes the existence of extremely dense shocks and clumps in the gas (see e.g. Klessen, 2000; Elmegreen, 2002; Vázquez-Semadeni et al., 2003; Mac Low and Klessen, 2004; Federrath et al., 2008; Goodman et al., 2009; Federrath et al., 2010; Hopkins, 2013a; Squire and Hopkins, 2017), which can have low internal velocity

dispersions and play a crucial role in turbulent fragmentation and star formation (McKee and Ostriker, 2007; Hennebelle and Chabrier, 2008; Hopkins, 2012a; Hopkins, 2012b; Hopkins, 2013d; Hopkins, 2013c; Hopkins, 2013b; Guszejnov et al., 2018b; Murray et al., 2017). So it is possible that a more realistic model might allow for hyper-Eddington accretion in rare (but not impossible) cases in these environments. In this study, we therefore extend the series of simulations of dense, star forming environments used previously to study star and star cluster formation in Grudić et al., 2018b; Guszejnov et al., 2018b; Grudić et al., 2018a; Grudić and Hopkins, 2019; Grudić et al., 2019b; Grudić et al., 2019a; Shi et al., 2021, to explore BH seed growth in dynamic, star-forming environments akin to dense giant molecular clouds (GMCs) and galactic nuclei.

In this first study, we neglect feedback from the accreting BHs themselves. This is obviously a major simplification, especially for BHs accreting above the Eddington limit – however, the form and strength of feedback from BHs in this regime remain highly uncertain (see references above), and we wish to identify whether or not sustaining hyper-Eddington accretion is even remotely possible on these scales. Clearly, accretion *without* BH feedback represents a relatively strong upper limit to the maximum possible BH seed growth. We can then use the conditions identified here as necessary for such accretion to run simulations including BH feedback, with various parameterizations.

In § 3.2, we describe our simulation methods. Then in § 3.3 we present results, including BH mass evolution in different clouds and its dependence on different initial conditions (ICs). In § 3.4, we analyze the effects of different physics and simulation ICs, give simple analytic formulae for the conditions required for runaway accretion, and discuss some major caveats of our work in § 3.5. Finally, we conclude in § 3.6.

3.2 Simulations

Our simulation numerical methods are identical to those described and tested fully in Grudić et al. (2018b), Grudić et al. (2018a), Hopkins et al. (2018a), Grudić et al. (2021b), and Grudić et al. (2021a), modulo the addition of BH seeds described below, so we briefly summarize here. We use the code GIZMO[2] (Hopkins, 2015) in Meshless Finite Mass (MFM) mode, with magnetohydrynamics (MHD) solved as in Hopkins and Raives (2016) and Hopkins (2016), self-gravity with adaptive

[2] A public version of GIZMO is available at `http://www.tapir.caltech.edu/~phopkins/Site/GIZMO.html`

$\bar{\Sigma}_0$ [$M_\odot$/pc^2]	$R_{\rm cl}$ [pc]	$M_{\rm cl}$ [$M_\odot$]	$t_{\rm ff,\,c}$ [Myr]	$m_{\rm gas}$ [$M_\odot$]	$\epsilon^{\rm star}_{\rm soft}$ [pc]	$\epsilon^{\rm bh}_{\rm soft}$ [pc]
130	5	10^4	2	0.005	0.04	0.04
130	5	10^4	2	0.04	0.09	0.09 [a]
130	50	10^6	6	0.5	0.21	0.21
130	500	10^8	20	50	0.96	0.31
1300	5	10^5	0.6	0.4	0.19	0.19
1300	50	10^7	2	40	0.89	0.31
1300	500	10^9	6	500	2.06	0.31
13000	5	10^6	0.2	0.5	0.21	0.21
13000	5	10^6	0.2	4	0.41	0.31 [b]
13000	50	10^8	0.6	6	0.48	0.31 [c]
13000	50	10^8	0.6	50	0.96	0.31
13000	50	10^8	0.6	400	1.91	0.31 [d]
13000	500	10^{10}	2	40000	8.89	0.31

[a] No-feedback (low-resolution) variant. [b] Varied metallicity test series. [c] Highest resolution; $M_{\rm bh} \in (10, 100)\,M_\odot$. [d] Varied BH seed number test series.

Table 3.1: Initial conditions (ICs) of our "fiducial" reference simulations. Here we show three groups of simulations with low, medium, and high initial mean surface density ($\bar{\Sigma}_0$). In each group, the clouds have radii ($R_{\rm cl}$) of 5, 50, and 500 pc. Subsequent columns give the approximate initial total cloud mass ($M_{\rm cl}$), initial free-fall time ($t_{\rm ff,\,c}$), gas cell mass/resolution ($m_{\rm gas}$), Plummer-equivalent force softening for star particles ($\epsilon^{\rm star}_{\rm soft}$), and for BHs ($\epsilon^{\rm bh}_{\rm soft}$), and additional notes.

Lagrangian force-softening, radiative cooling from $1 - 10^{10}$ K, including molecular, metal-line, fine-structure, photo-electric, ionization and other processes as well as star formation in dense, locally-self-gravitating gas (Hopkins et al., 2013; Grudić et al., 2018b), and stellar feedback following the FIRE-2 implementation of the Feedback In Realistic Environments (FIRE[3]) physics (Hopkins et al., 2018a; Hopkins et al., 2023). In these models "star particles" each repreent IMF-averaged ensembles of stars (rather than resolving individual stars and proto-stars as in Grudić et al. 2021b; Guszejnov et al. 2021), which evolve along standard stellar evolution models to return mass, metals, momentum, and energy to the ISM in the form of supernovae and O/B and AGB winds (Hopkins et al., 2018b) as well as acting on the gas via radiative heating, photo-ionization, and radiation pressure (Hopkins et al., 2020b). Simulations with these methods have been previously used to study many properties of GMCs, galactic nuclei, and star clusters, including their observed star formation efficiencies, cluster dynamics and mass profiles, young massive cluster

[3] http://fire.northwestern.edu

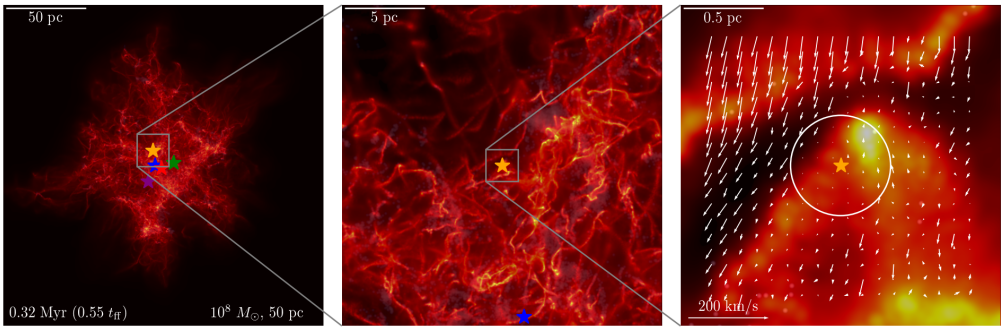

Figure 3.1: An example visualization of the simulations at different scales. The simulation starts with a massive dense gas complex of $M_{\rm cl} = 10^8$ M$_\odot$, $R_{\rm cl} = 50$ pc, and 256^3 resolution, and we choose the snapshot where the seeds have the highest accretion rate. Here we show the distribution of the gas surface density as the black-red-orange color map. As stars, we show the BH seeds that undergo most significant growth. **Left**: Visualization of the whole complex; we see the BHs that accrete most are located at the dense region near the center of the system. **Middle**: 10 times zoom-in centered on the BH that shows the most significant mass growth at this time. **Right**: Further zoom-in of the region near the BH and the velocity field of gas (vectors, length proportional to magnitude of $|\mathbf{v}_{\rm bh} - \mathbf{v}_{\rm gas}|$) in the vicinity of the BH. Here the circle denotes the sink radius. We see a dense clump intersecting the sink radius, with a the relative velocity that is quite small near the BH.

internal structure, globular cluster demographics, and gas emission properties (see references above and e.g. Grudić et al., 2018b; Grudić et al., 2018a; Grudić et al., 2021b; Grudić et al., 2021a; Fukushima and Yajima, 2021).

We extend these simulations by adding a population of "seed" BHs (sink particles) to the ICs, which can accrete gas from the surrounding medium, but otherwise feel only gravitational dynamics (we do not model BH feedback or BH-BH mergers).

Black hole accretion

Our BH seeds/sink particle prescription is a simplified version of that numerically presented in Grudić et al. (2021b). Gas is accreted onto a sink if it meets three criteria:

1. It is within the sink radius $r_{\rm sink}$ of the BH: $r = |\mathbf{r}_{\rm gas} - \mathbf{r}_{\rm bh}| < r_{\rm sink}$.
2. It is bound to the BH, including kinetic, thermal, and magnetic support: $u_{\rm thermal} + (1/2)\, v_{\rm A}^2 + (1/2)\, \delta V^2 < G\, M_{\rm sink}/r$, where $u_{\rm thermal}$ is the specific thermal energy, $v_{\rm A}$ the Alfvén speed, and $\delta V^2 \equiv |\mathbf{v}_{\rm gas} - \mathbf{v}_{\rm bh}|^2$.

3. Its angular momentum is insufficient to support a circular orbit with radius larger than $r_{\rm sink}$ (Bate et al., 1995), i.e. $j_{\rm gas} < \sqrt{G\,M_{\rm sink}\,r_{\rm sink}}$ where $j_{\rm gas}$ is the specific angular momentum of the gas cell (evaluated at its center-of-mass location).

If a gas cell somehow meets all these criteria with two BHs simultaneously, it will accrete onto whichever is closer.

We must choose $r_{\rm sink}$ in each simulation. This is usually set to something like the simulation resolution (typical inter-cell separation δr), and would ideally resolve the Bondi radius, $R_{\rm Bondi} \sim G\,M_{\rm bh}/(c_{\rm s}^2 + \delta V^2)$, i.e. $r_{\rm sink} \sim R_{\rm Bondi} \gtrsim \delta r$. But in our Lagrangian, dynamical simulations (1) the spatial resolution is not fixed, but scales as $\delta r \sim (\rho/m_{\rm gas})^{1/3}$, and (2) the Bondi radius fluctuates dramatically (as we will show), and varies between seeds. In the "worst case" scenario, assume accretion is coming from the low-density diffuse intra-cloud medium (density $\rho \sim \langle\rho\rangle \sim 3\,M_{\rm cl}/4\pi\,R_{\rm cl}^3$) with virial or free-fall level relative velocities $\delta V \sim v_{\rm cl} \sim (G\,M_{\rm cl}/R_{\rm cl})^{1/2} \gg c_s$. This would give $R_{\rm Bondi} \sim (M_{\rm bh}/M_{\rm cl})\,R_{\rm cl}$, so resolving the Bondi radius ($\delta r \lesssim R_{\rm Bondi}$ in the same diffuse mean-density gas) would require a prohibitive number of cells $N_{\rm cells} \sim (R_{\rm cl}/\delta r)^3 \gtrsim (M_{\rm cl}/M_{\rm bh})^3$. However, as we noted above and will show more rigorously below, the accretion rates from such diffuse gas are orders-of-magnitude below Eddington, and (even if well-resolved) would contribute essentially nothing to the total BH accretion in our simulations. Therefore consider instead the "best-case" scenario for accretion: since the turbulence in the molecular clouds has rms Mach numbers $\mathcal{M}_{\rm cl} \sim v_{\rm cl}/c_s \sim 10-100$, radiative shocks can produce regions with very high densities $\rho \sim \langle\rho\rangle\,\mathcal{M}_{\rm cl}^2$, and low relative velocities $\delta V \lesssim c_s$ (Vazquez-Semadeni, 1994; Padoan et al., 1997; Mac Low and Klessen, 2004). Under these conditions, the Bondi radii will be well-resolved ($\delta r \lesssim R_{\rm Bondi}$) so long as $N \gtrsim \mathcal{M}^{-8}\,(M_{\rm cl}/M_{\rm bh})^3$ – a huge relief ($\propto \mathcal{M}^8$) in resolution requirements (which would be easily satisfied by every simulation in this paper). As we will show, regions akin to this idealized example dominate the actual accretion in the simulations.

In practice, we choose a sink radius by estimating a "characteristic" Bondi radius $b_{\rm c}$ by assuming $M_{\rm bh,\,c} = 100\,{\rm M}_\odot$, and considering two limits: $\delta V \lesssim c_{\rm s}$ (assuming a mean temperature of 100 K, typical in our simulations) so $b_1 = G\,M_{\rm bh,\,c}/c_{\rm s}^2$, and $\delta V \sim v_{\rm cl} \gg c_{\rm s}$ so $b_2 \approx (M_{\rm bh}/M_{\rm cl})R_{\rm cl}$, and then take $b_{\rm c} = \min(b_1, b_2)$. We have verified in post-processing that in all cases which produce "interesting" runaway BH growth, the Bondi radii *during the phase where the BH actually accretes rapidly* is at least marginally resolved, as expected from the argument above.

We wish to reminder the readers again that the mass "accreted" in the simulation is not the actual mass swallowed by BHs due to multiple feedback effects (for details see Sec. 3.5). The sink radius $r_{\rm sink}$ is the actual resolution limit for BH accretion, while the physics from $r_{\rm sink}$ to the Schwarzchild radius is not resolved in this simulation, but it does not impact the science goal of this article. For completeness, an estimate considering BH radiative feedback from the previous analytic work (Inayoshi et al., 2016) is included in Sec. 3.4.

Initial conditions

We sample spherical, turbulent, and non-rotating molecular clouds or cloud complexes with different initial mean surface density ($\bar{\Sigma}_0 \equiv M_{\rm cl}/\pi R_{\rm cl}^2 \approx 100,\ 10^3,\ 10^4\,{\rm M}_\odot/{\rm pc}^2$) and initial radius ($R_{\rm cl} = 5,\ 50,\ 500\,{\rm pc}$) following the setup and results of Grudić et al. (2018b), where each group with the same surface density was shown to have similar star formation efficiency. Note that these parameters are motivated by massive, dense star-forming cloud and "clump" complexes seen in high-redshift galaxies and starburst galaxy nuclei, with only the smaller and lowest-$\bar{\Sigma}_0$ clouds analogous to massive GMCs in the Milky Way. Each initial cloud is uniformly magnetized, we also set $E_{\rm turb}/|E_{\rm grav}| = 1$ and $E_{\rm mag}/E_{\rm grav} = 0.1$, where $E_{\rm turb}$, $E_{\rm mag}$, and $E_{\rm grav}$ are the turbulence (kinetic) energy, magnetic field density, and gravitational binding energy respectively. The clouds serve as the mass reservoirs for BH accretion.

We then insert an ensemble of BH seeds into the IC. Typically, for every seed, the mass ranges within $1\,{\rm M}_\odot \leq M_{\rm bh} \leq 10^4\,{\rm M}_\odot$ and are uniformly distributed in $\log M_{\rm bh}$. The initial position of seeds are sampled randomly but statistically uniformly within the cloud. The initial velocity is sampled such that in each dimension it is uniformly distributed in $[-V_{\rm circ}, V_{\rm circ}]$ while the total magnitude is suppressed below $V_{\rm circ}$ to ensure the seeds are bound to the cloud, where $V_{\rm circ}^2 = GM_{\rm cl}(<r)/r$ is the local circular velocity at radius r (assuming uniform mass distribution). We resample seeds which would be within a small distance to the cloud "edge" with an outward radial velocity, since these would trivially escape without interesting dynamics.

Rather than simulating only a few BH seeds in one cloud, we include a large number of seeds in every IC so that we can sample many different seed masses and positions and kinematics. However, to avoid significant interactions among the BHs and heavy computational costs, the number of BH seed is controlled to be either below 10000, or the number such that the total BH mass does not exceed 5% of the cloud

initial mass $M_{\rm cl}$. For low mass clouds, we decrease the lower and upper bounds of BH seed mass sampling to ensure a sufficient number of BH seeds, which also helps ensure the Bondi radii are resolved (e.g., for $M_{\rm cl} = 10^4\,{\rm M}_\odot$, $1\,{\rm M}_\odot \leq M_{\rm bh} \leq 100\,{\rm M}_\odot$; for $M_{\rm cl} = 10^5\,{\rm M}_\odot$, $10\,{\rm M}_\odot \leq M_{\rm bh} \leq 10^3\,{\rm M}_\odot$, for $M_{\rm cl} \gtrsim 10^6\,{\rm M}_\odot$, $10^2\,{\rm M}_\odot \leq M_{\rm bh} \leq 10^4\,{\rm M}_\odot$).

We use adaptive force softening to avoid divergences in our gravity evaluation or extremely small time steps. For the newly formed stars, which have the same mass as gas particles, the minimum softening length is $r_{\rm soft}^{\rm star} \sim (m_{\rm gas}/\rho_{\rm sf})^{1/3}$, where $m_{\rm gas}$ is the mass resolution of the cloud and $\rho_{\rm sf}$ is the numerical minimum density for star formation ($1000\,{\rm cm}^{-3}$ in the simulation). For BHs, the softening radius is set as $r_{\rm soft}^{\rm bh} = \min(r_{\rm soft}^{\rm star}, b_{\rm c})$, where $b_{\rm c}$ is the characteristic Bondi-Hoyle accretion radius (introduced in § 3.2). In the simulation $r_{\rm sink} = r_{\rm soft}^{\rm bh}$, so the setup ensures the code resolves the Bondi-Holye accretion radius and the BHs interact reasonably with star particles.

For reference, we show the initial-conditions in Table 3.1. The clouds are divided into three groups with different initial mean surface density $\bar{\Sigma}_0 = M_{\rm cl}/(\pi R_{\rm cl}^2)$, though within each group the clouds have the same set of initial radii. The fiducial resolution (number of initial gas cells) of our simulations is 128^3, while a few low (64^3) and high (256^3) resolution runs of a subset of clouds are also included for comparison. For each fiducial simulation, the termination time scale is $2\,t_{\rm ff}$, where $t_{\rm ff} = \pi\sqrt{R_{\rm cl}^3/(8GM_{\rm cl})}$ is the initial free-fall time scale of the cloud, while for low-resolution ones the termination time is $5\,t_{\rm ff}$. Finally, BH mergers are disabled since the event rate is not significant.

3.3 Results

In this section we show the major results of the simulations. As a first impression, we present the morphology of one example GMC in Fig. 3.1, which has $M_{\rm cl} = 10^8\,N_\odot$, $R_{\rm cl} = 50\,{\rm pc}$, and resolution of 256^3. After $0.55\,t_{\rm ff}$ of evolution, the GMC has become quite turbulent. We also show the 5 BHs that show the most significant mass growth during the period, which are generally located near the center of the GMC. For the BH that grows most rapidly during the period (the orange star in Fig. 3.1), we show the zoomed-in distribution of gas[4] and its velocity field in the middle and right-hand panels. Near the BH's sink radius (0.313 pc), there is a dense gas clump which has very low velocity compared to the gas at the edge of the view ($\sim 50\,{\rm km/s}$); this is

[4]For illustration purposes, the color is scaled nonlinearly with the density field so as to better illustrate its morphology.

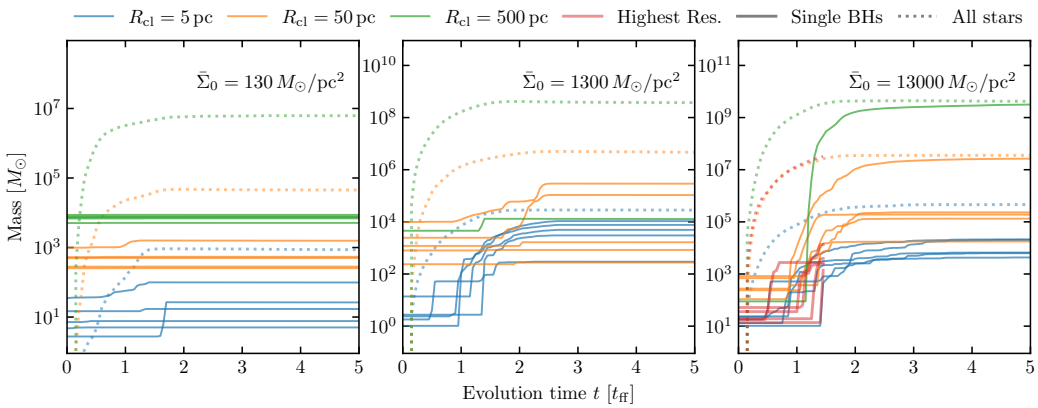

Figure 3.2: Mass growth of the total mass of stars as well as (up to) five BHs that show the most significant mass growth, in the "default" simulations from Table 3.1, as a function of time (in units of the initial homogeneous-cloud free-fall time $t_{\rm ff}$). Here solid lines representing the mass growth of individual BHs, dotted lines representing the total mass growth of all stars summed. We show properties of complexes with different radii/masses ($r_{\rm cl}$): 5 pc (blue), 50 pc (orange), 500 pc (green); and different initial mean surface density ($\bar{\Sigma}_0$): $130\,{\rm M}_\odot/{\rm pc}^2$ (left), $1300\,{\rm M}_\odot/{\rm pc}^2$ (middle), $13000\,{\rm M}_\odot/{\rm pc}^2$ (right). We also show the highest-resolution run with $M_{\rm cl} = 10^8\,{\rm M}_\odot$ and $R_{\rm cl} = 50$ pc (red lines in the right panel). The low-density complexes feature almost no BH growth. Higher-density systems generally feature a small number of seeds which "run away" and can grow by orders of magnitude.

rapidly accreted in the time between the snapshot shown and the next simulation snapshot.

This essentially fits our expectations from Bondi-Hoyle theory, applied locally at scales of order the Bondi radius: high gas density and low relative velocity between the BH and nearby gas create the ideal conditions for growth.

Seed growth in different clouds

As described in the previous section, in each cloud we sampled a large number of BH seeds to study their mass growth. In Fig. 3.2 we present the mass evolution of (up to) 5 BHs in each simulation that show the most significant mass growth. As we show below, these are *not* necessarily the most massive seeds in the ICs.

For clouds with low initial surface density ($\bar{\Sigma}_0 = 127\,{\rm M}_\odot/{\rm pc}^2$) the mass growth is modest: essentially no BHs grow by more than a factor $\sim 2-3$, and in general even the most-rapidly growing only increase in mass by tens of percent. At the larger surface densities we sample, the mass of the most-rapidly-growing BHs typically increases by at least two orders of magnitude.

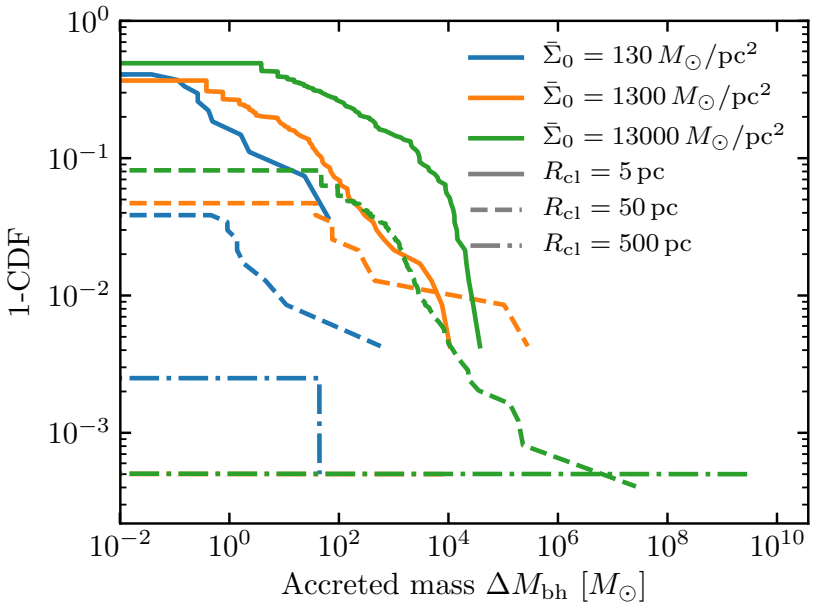

Figure 3.3: Distribution of fractional mass growth in different ICs: we plot the cumulative fraction of the BH seeds which accreted some amount of mass. We denote initial surface density with color, and initial cloud radius/mass with linestyle (as labeled). Most BHs do not accrete significantly (see lower-end cutoffs). But the most high-density, massive clouds generally feature a very small number of seeds which runaway to enormous masses.

Ignoring the low surface density complexes, if we consider clouds with fixed $\bar{\Sigma}_0$ but different sizes $R_{\rm cl}$ (or equivalently, masses $M_{\rm cl} \equiv \pi\,\bar{\Sigma}_0\,R_{\rm cl}^2$), we see that the final masses of the single most-rapidly-growing BHs increase with the total cloud mass, reaching as high as $\sim 3-10\%$ of the total cloud mass. Interestingly, for the lower-mass complexes, we often see several BHs exhibiting similar growth, while for the most massive complexes ($R_{\rm cl} = 500\,{\rm pc}$), one BH runs away early and then proceeds to accrete a huge amount of gas, "stealing" the gas supply from other seeds in the cloud.

From the same plot, we also see that the BHs typically grow their mass quickly in a short range of time ($\Delta t \lesssim t_{\rm ff}$) starting at some time near $t \sim t_{\rm ff}$. However, for clouds with higher surface density, we see the time range becomes slightly longer; the BHs in those clouds also start to grow somewhat earlier. Moreover, as we will show below in more detail in some illustrative examples, BH growth always *follows* the formation of a significant mass of stars. All these features inspire us to study the effect of star formation and stellar feedback in different clouds, which is discussed

in § 3.4.

As a different way to study the probability of mass growth, we show the cumulative distribution of the final-initial mass difference for all the BHs in Fig. 3.3. For most of the BHs there is no large significant mass growth except for a small fraction ($\lesssim 10\%$) of them, which we will discuss in more detail below.

Dependence on ICs

In Fig. 3.4 we show the dependence of mass growth ($\Delta M_{\rm bh}$) on the initial mass of the BH seeds. As we showed above, most seeds did not grow significantly. But more strikingly – and perhaps surprisingly, given the strong dependence of the Bondi-Hoyle rate on $M_{\rm bh}$ – we see that there is almost no correlation between the initial seed mass and BH mass growth. The particular simulation here considers seeds from $10^2 - 10^4\,{\rm M}_\odot$, but we find the same (in the extended tests described below) for initial seed masses down to $\sim 10\,{\rm M}_\odot$.

In Fig. 3.5, we present the initial velocity magnitude (relative to the cloud center-of-mass), initial position, and mass growth for all BHs in the simulation. As we can see, there is no strong dependence on either the initial position or velocity magnitude, *provided* the BH is (a) reasonably bound to the cloud (initial velocity not larger than $\sim v_{\rm cl} \sim (G\,M_{\rm cl}/R_{\rm cl})^{1/2}$), and (b) the BH does not begin too close to the edge of the cloud with a velocity directed away from the (irregular) centers of collapse (in which case the BH tends to drift away from the dense regions, rather than interact with them).

Another factor that could change the result is the initial metallicity Z, which self-consistently alters the cooling physics, stellar evolution tracks, and radiative feedback (opacities) in the simulations. We test this simulating GMCs with $M_{\rm cl} = 10^6\,{\rm M}_\odot$ and $R_{\rm cl} = 5\,{\rm pc}$ (from the high surface density group) with varying initial Z in Fig. 3.6. By comparing the distribution functions of BH final-initial mass difference, we see that all those clouds produce statistically similar results for runaway BH accretion, independent of Z. We note that there are caveats regarding uncertainties in stellar evolution and treatment of molecular chemistry at extremely low metallicities in these models – these are reviewed in detail in Grudić et al. (2018b) – but for all but truly metal-free clouds (where Pop-III evolution may be quite different) we regard this as robust. We also note that Corbett Moran et al. (2018) showed that the fragmentation and turbulent clumping in even metal-free clouds under high-density conditions like those of interest here are quite similar, independent of different

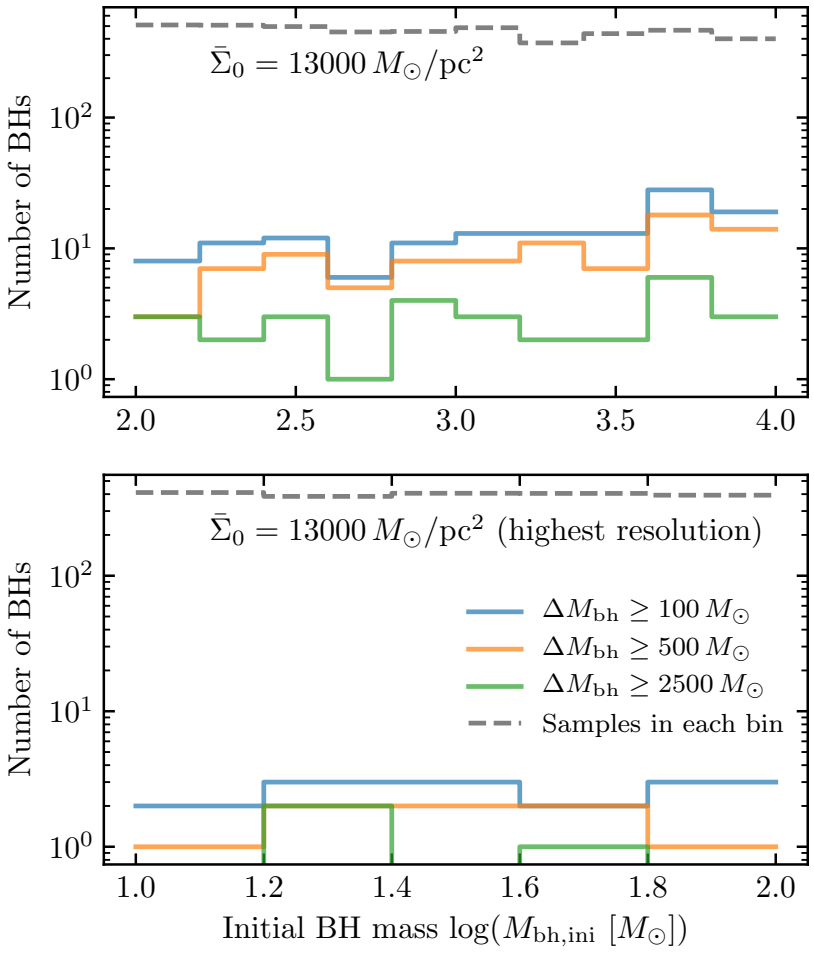

Figure 3.4: Dependence of BH growth on initial seed BH mass. *Top*: We aggregate all seeds in the three fiducial runs ($R_{\rm cl}$ = 5, 50, 500 pc) for our highest-density clouds, and plot both the total number of BHs in different ~ 0.1 dex-wide bins of initial BH mass (~ 1000 per bin, summing across the simulations), and the number in each bin which capture/accrete a mass $\Delta M_{\rm bh}$ in excess of some fixed amount. The probability of runaway accretion depends only very weakly on initial seed mass, over this range. *Bottom*: Same as above, but for the highest resolution cloud ($M_{\rm cl} = 10^8$ M$_\odot$, $R_{\rm cl}$ = 50 pc) which has lighter seeds (10–100 M$_\odot$). Again, there is shallow dependence on the initial seed mass.

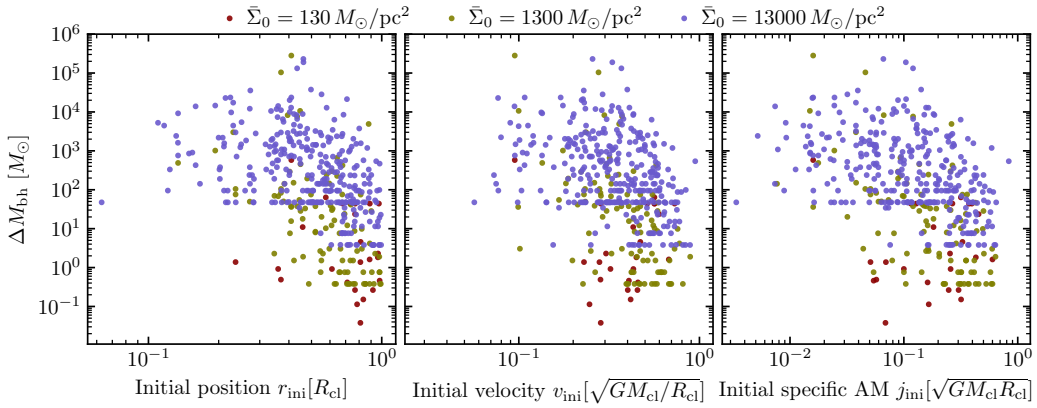

Figure 3.5: Initial value of the BH seed velocity $v_{\rm ini} = |\mathbf{v}_{\rm bh}|$ (relative to the initial complex center-of-mass velocity, in units of the characteristic gravitational velocity of the complex $v_{\rm cl} = \sqrt{G\,M_{\rm cl}/R_{\rm cl}}$), initial position $r_{\rm ini} = |\mathbf{r}_{\rm bh}|$ (relative to the initial complex center-of-mass, in units of its radius $R_{\rm cl}$), and initial value of the specific angular momentum $j_{\rm ini} = |\mathbf{r}_{\rm BH} \times \mathbf{v}_{\rm BH}|$, for all seeds in clouds of a given initial surface density (aggregating the three different-mass/size runs). All these quantities are compared with the amount of mass growth (final-to-initial mass difference) for each BH. As long as the seeds do not begin too close to the "edge" of the cloud or with too large an initial velocity (in which case they tend to "drift away" rather than accrete), or with too large specific angular momentum, there is no strong preference for e.g., seeds to be at the cloud center for runaway accretion to occur.

molecular chemistry networks used for the thermochemistry.

The result does not mean the metallicity is not important for the actual accretion flow onto BHs, but is only valid for larger-scale accretion flows to the BH+disk system. Due to complexities of physics below our resolution limit ($r_{\rm sink}$), e.g., high metallicity may enhace the radiative force due to BH feedback and thus suppress accretion (Yajima et al., 2017; Toyouchi et al., 2019).

We also change the number of BH seeds in the ICs ($N_{\rm bh,tot}$) and check the number of seeds that undergo significant mass growth, in Fig. 3.7. Here we use different criteria to denote "significant": the final-initial mass ratio of the BH is above a constant r and $r = 100, 500, 2500$. If we simulate an initial number of seeds $N_{\rm bh,\,ini} \lesssim 64$, it becomes unlikely to see even a single seed undergo runaway growth, while for $N_{\rm bh,\,ini} \gtrsim 100$, we are essentially guaranteed that at least one seed will experience runaway growth. We find the same applying a more limited version of this test to other clouds. Thus there appears to be a threshold $\sim 1\%$ probability for a randomly-drawn seed to undergo runaway growth. However, if we increase the number of

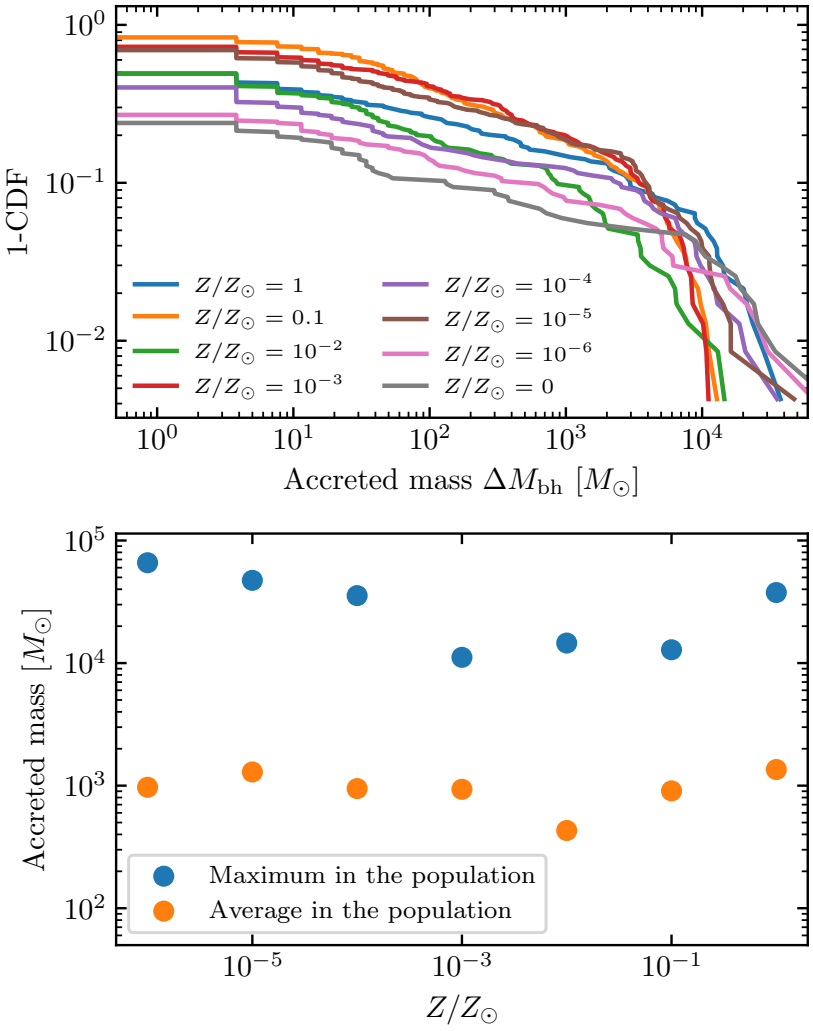

Figure 3.6: Metallicity effects on accretion. We show the cumulative accreted mass distribution for all BHs as Fig. 3.3, but for a set of $M_{\rm cl} = 10^6\,{\rm M}_\odot$ and $R_{\rm cl} = 5\,{\rm pc}$ systems simulated at low resolution systematically varying the initial metallicity. There is no strong systematic metallicity dependence.

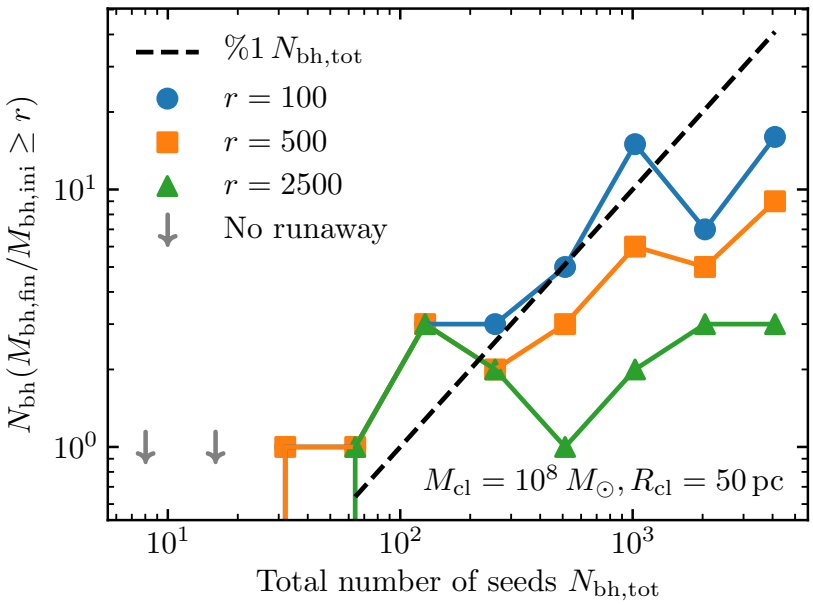

Figure 3.7: Number of BHs which exceed some final-to-initial mass ratio r (as a proxy for "runaway" growth), in simulations of an otherwise identical complex (with properties labeled) where we vary the initial seed number systematically. We require $\sim 50-100$ seeds before there is reliably at least one seed that undergoes runaway growth. Increasing the seed number further, the fraction of seeds which experience at least *some* significant growth is $\sim 1\%$, but we see that typically no more than one to a few BHs run away most dramatically (regardless of the seed number provided it is sufficient).

seeds further, the absolute number of BHs undergoing runaway accretion clearly saturates at a finite value, of $\sim$a few to ten with factor $10-100$ growth and ~ 1 with extreme runaway growth. Thus a given cloud can only support at most a few runaway BHs.

3.4 Discussion

Effects stellar feedback & global cloud properties

Intuitively, stellar feedback can alter BH accretion in two ways. i) Feedback expels gas, which makes it harder for BHs to capture that gas. ii) Feedback can make the cloud more turbulent and create more dense regions. As an example, we include low-resolution simulations with and without feedback physics for the same ICs in Fig. 3.8. As we see, for this low-surface density cloud, feedback effectively blows gas away after two free-fall time scales. As a result, feedback suppresses both BH accretion and star formation – BH growth in particular is suppressed by more than

an order of magnitude, the difference between there being a few versus essentially no "runaway" BHs.

Star formation and stellar feedback in GMCs have been well studied in previous simulations that are related to this work (e.g., Grudić et al. 2018b), as well as similar studies with different numerical methods which have reached very similar conclusions for star formation (e.g., Li et al. 2019). One important conclusion of these studies is that the integrated star formation efficiency, and effects of feedback, depend strongly on $\bar{\Sigma}_0$. Briefly: a young stellar population of mass M_* produces a net feedback momentum flux (from the combination of radiation and stellar winds) $\dot{P} \sim \langle \dot{p}/m_* \rangle \, M_{\rm cl,\,*} \sim 10^{-7}\,{\rm cm\,s^{-2}}\, M_{\rm cl,\,*}$, while the characteristic gravitational force of the cloud on its gas is $F_{\rm grav} \sim G\, M_{\rm cl,\,tot}\, M_{\rm cl,\,gas}/R_{\rm cl}^2 \sim G\, M_{\rm cl,\,gas}\, \bar{\Sigma}_0$. So the gas reservoir of a cloud is rapidly unbound and ejected when its stellar mass exceeds $M_{\rm cl,\,ast}/M_{\rm cl,\,gas} \gtrsim G\,\bar{\Sigma}_0/\langle \dot{p}/m_* \rangle \sim \bar{\Sigma}_0/(1000\,{\rm M_\odot\,pc^{-2}})$. So for our low-$\bar{\Sigma}_0$ clouds, almost all of the gas is rapidly un-bound after just a small fraction of the GMC forms into stars, preventing it from being accreted by BHs.

We can see this reflected in Fig. 3.9, which shows the gas rms bulk velocity $\langle |\mathbf{v}_{\rm gas}|^2 \rangle^{1/2}$, gas sound speed $\langle c_{\rm s} \rangle$, and BH rms velocity $\langle |\mathbf{v}_{\rm bh}|^2 | \rangle^{1/2}$ as a function of time in different ICs, in units of the characteristic cloud gravitational velocity $v_{\rm cl} \sim (G\, M_{\rm cl}/R_{\rm cl})^{1/2}$. Not surprisingly, the rms velocity of BHs remains of order the gravitational velocities. The gas bulk velocities are dominated by gravity at first so remain of order $v_{\rm cl}$, but when feedback begins to disrupt the cloud they increase in magnitude by a factor ~ 10. This effect depends primarily on $\bar{\Sigma}_0$, as expected from the argument above.

Similarly, the sound speed of the clouds initially drops extremely quickly owing to cooling until it reaches molecular temperatures (we arbitrarily start from higher temperature, but this has no effect on our results), with $c_{\rm s} \ll v_{\rm cl}$, but then rises once feedback disrupts the cloud owing to a combination of (1) photo-ionization, (2) shocks from stellar winds bubbles, and (3) lower gas densities increasing the cooling time. Since e.g., the characteristic photo-ionized $c_{\rm s} \sim 10\,{\rm km\,s^{-1}}$ is roughly constant, the importance of this effect depends primarily on $v_{\rm cl}$, which ranges from $\sim 3\,{\rm km\,s^{-1}}$ in our lowest-mass, lowest-density simulation, to $\sim 300\,{\rm km\,s^{-1}}$ in our highest-mass, highest-density simulation.

In our low-density, low-mass clouds, we see disruption occurs very early (less than $\sim 2\,t_{\rm ff}$), with the gas bulk velocities and sound speeds reaching $\gg v_{\rm cl}$. This makes gravitational capture of gas by seeds nearly impossible. For the intermediate-density

clouds, we see the disruption is significantly delayed, and the magnitude of the post-disruption velocities is reduced (with $c_s \lesssim v_{cl}$ even during disruption). For the highest-density clouds, there is no real disruption but just dispersal of some residual gas after star formation completes.

We have also considered the impact of stellar feedback on the volume and mass fraction in dense clumps (Fig. 3.10). Specifically, we calculated the volume and mass (in units of the initial cloud volume and total mass) of regions/clumps within the cloud that satisfy $\rho > 100\,\langle\rho\rangle_0$ (where $\langle\rho\rangle_0 \equiv 3\,M_{cl}/(4\pi\,R_{cl}^3)$ is the initial mean cloud density). The volume/mass of dense clumps increases in all cases rapidly at early times as the cloud collapses, but in the low-density clouds it is rapidly truncated by feedback. In contrast, we see in the higher-density clouds a sustained "lifetime" of dense gas: this is driven by shocks and turbulence from feedback from the stars that have formed, but have insufficient power to completely disrupt the cloud. In the highest-density case we even see dense clumps re-emerge several times after $t \gtrsim 3\,t_{ff}$ due to large-scale stellar feedback events – these correspond to large wind/HII region shells colliding to form dense regions (see e.g., Ma et al. 2020 for more detailed discussion).

Another obvious requirement for runaway BH growth to "interesting" IMBH or even SMBH masses is that the total cloud mass is sufficiently large, such that the mass of dense "clumps" accreted is interesting. As we show below, the characteristic gas clump masses at high densities which meet the conditions for runaway BH growth are typically $\sim 1\%$ of the cloud mass, neatly explaining the maximum final BH masses seen in § 3.3. This requires a total cloud mass $\gtrsim 10^5 - 10^6\,M_\odot$ for growth to true IMBH (let alone SMBH) scales. Interestingly, since $v_{cl} \sim 15\,{\rm km\,s^{-1}}\,(M_{cl}/10^6\,M_\odot)^{1/4}\,(\bar{\Sigma}_0/10^3\,M_\odot\,{\rm pc^{-2}})^{1/4}$, this plus the surface density condition above simultaneously ensure that complexes are not over-heated or disrupted by photo-ionized gas.

How does runaway growth occur?

We now consider the local conditions for runaway growth. In a small "patch" of cloud on scales $\sim r_{sink}$ (small compared to the cloud but large compared to the BH accretion disk), it is not unreasonable to approximate the rate of gravitational capture of gas by a sink via the Bondi formula (Eq. (3.1)), given the local value of ρ, δV, and c_s.

Recall, from § 3.1 and § 3.2, that if we consider the typical or diffuse/volume-filling

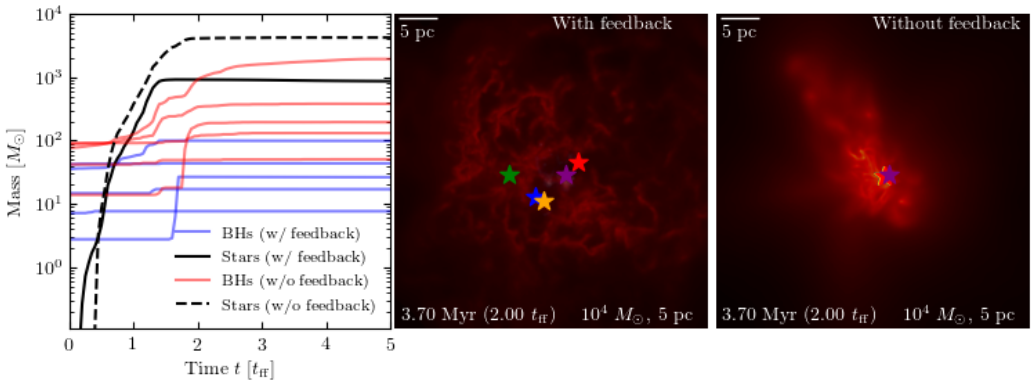

Figure 3.8: Effects of stellar feedback on gas morphology and seed BH mass growth. We show two low-resolution runs of a low-density, low-mass cloud with $M_{\rm cl} = 10^4$ M$_\odot$, $R_{\rm cl} = 5$ pc cloud, including (middle) and excluding (right) stellar feedback effects, as Fig. 3.1. Gas is more concentrated near the center for the no-feedback run while most gas is expelled by stellar winds in the feedback run. We show the cumulative BH and stellar mass growth for these runs as Fig. 3.2 (left): BH growth and star formation are both suppressed at the order-of-magnitude level in these lower-density clouds.

conditions within the cloud, i.e. $\rho \sim \langle\rho\rangle_0 \sim 3\,M_{\rm cl}/4\pi\,R_{\rm cl}^3$ and $\delta V \sim v_{\rm cl} \gg c_{\rm s}$, we would obtain

$$\langle \dot{M}_{\rm bh}\rangle_{\rm diffuse} \sim \frac{G^2 M_{\rm bh}^2 \rho}{\delta V^3} \sim \frac{G^{1/2}\,M_{\rm bh}^2}{M_{\rm cl}^{1/2}\,R_{\rm cl}^{3/2}} \sim \left(\frac{\langle n_{\rm cl}\rangle}{\rm cm^{-3}}\right)\left(\frac{M_{\rm bh}}{M_{\rm cl}}\right)\dot{M}_{\rm Edd} \tag{3.2}$$

where $\langle n_{\rm cl}\rangle = \langle\rho\rangle_0/m_p$. If we further assume that the timescale for accretion Δt is of order the cloud lifetime, $\sim t_{\rm eff} \sim \sqrt{R_{\rm cl}^3/GM_{\rm cl}}$, then the total mass accreted $\sim \dot{M}_{\rm bh}\,\Delta t$ would be

$$\Delta M_{\rm bh} \sim \langle \dot{M}_{\rm bh}\rangle_{\rm diffuse}\,t_{\rm ff} \sim \frac{M_{\rm bh}}{M_{\rm cl}}\,M_{\rm bh} \tag{3.3}$$

In other words, unless the "seed" is already a large fraction of the entire GMC complex mass (i.e. is not really a seed in any sense), then the diffuse accretion will be highly sub-Eddington and the BH will grow only by a tiny fractional amount. This immediately explains why *most* of the seeds we simulate indeed grow negligibly.

However, in a highly turbulent cloud we argued above that two effects that may boost the mass growth: i) the dense clumps appear with $\rho \gg \langle\rho\rangle_0$, and ii) the turbulence velocity contributes to the relative velocity $\delta\mathbf{V}$ so locally, low δV is possible.

In Fig. 3.11 we follow one particular but representative example of a sink which undergoes runaway growth, considering how the relevant factors in the local Bondi

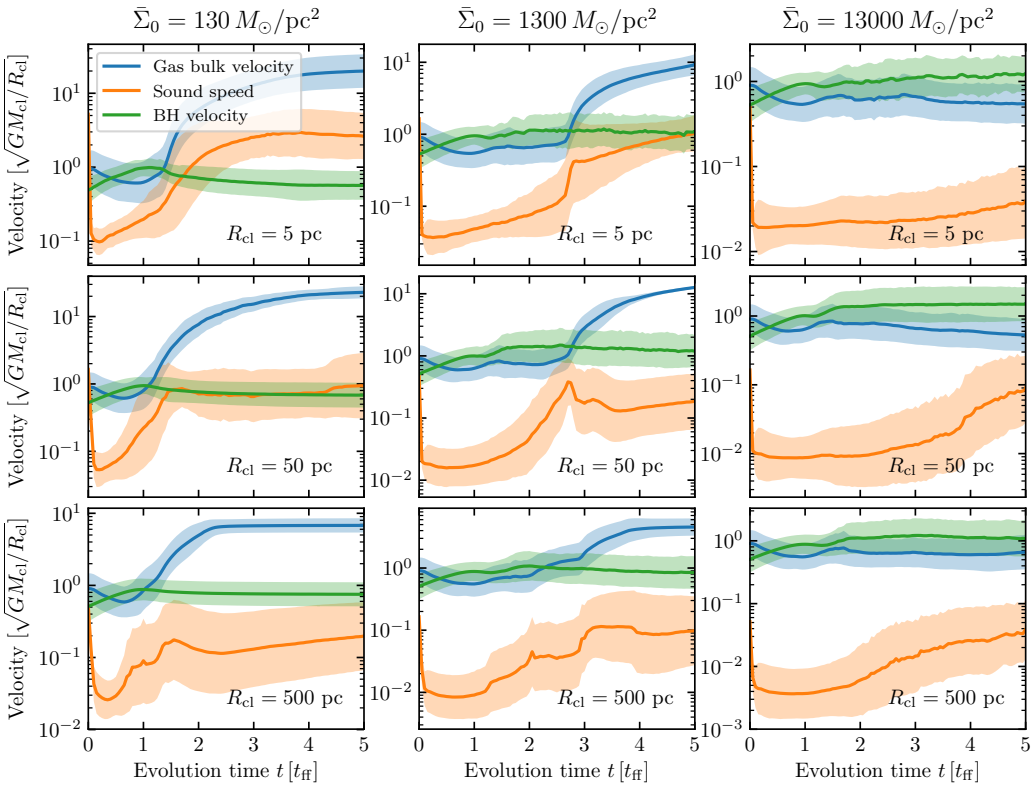

Figure 3.9: Behavior of the rms gas bulk velocity dispersion ($\equiv |\mathbf{v}_{\rm gas} - \langle \mathbf{v}_{\rm gas} \rangle|$), sound speeds ($c_{\rm s}$), and BH seed particle velocity dispersions relative to the complex center-of-mass ($\equiv |\mathbf{v}_{\rm bh} - \langle \mathbf{v}_{\rm gas} \rangle|$), all in units of the characteristic gravitational/circular velocity of the complex ($v_{\rm circ} = v_{\rm cl} = \sqrt{G\,M_{\rm cl}/R_{\rm cl}}$), as a function of time (in units of the initial complex free-fall time ($t_{\rm ff}$). We compare the fiducial runs with different surface density (left-to-right) and radii (top-to-bottom). For each we show the median-absolute-value (line) and 14 – 86% inclusion interval (shaded). Low-density, low-mass clouds are rapidly disrupted by stellar feedback producing large gas bulk velocities and high sound speeds. This is suppressed in high-density, high-mass systems, enabling continued BH accretion.

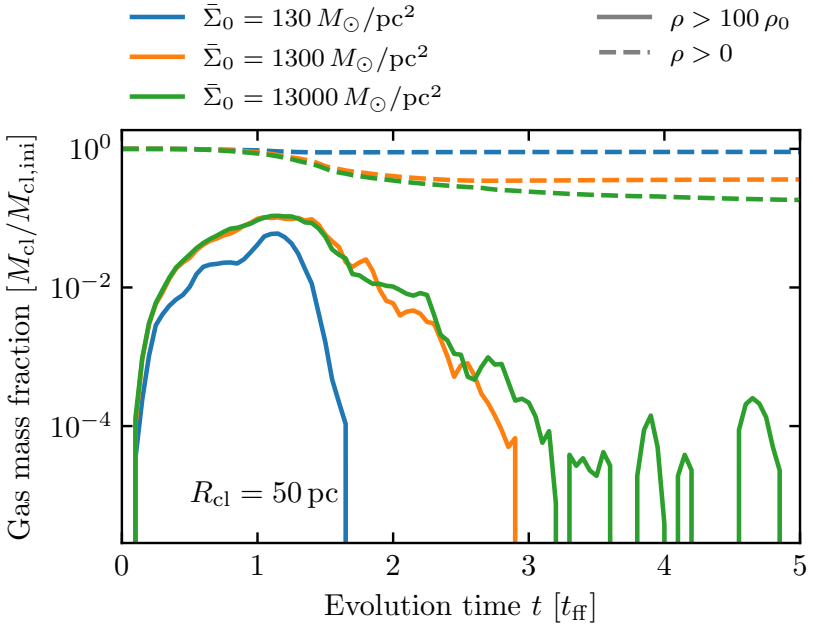

Figure 3.10: Evolution of the abundance of dense clumps in the simulations. We compare complexes with different initial mean surface density $\bar{\Sigma}_0$ (different colors; only $R_{\rm cl} = 50\,\mathrm{pc}$ shown for simplicity). For each, we measure the total gas mass (in units of the initial mass $M_{\rm cl}$) with a local gas density exceeding $\rho > 100\,\langle\rho\rangle_0$ (where $\langle\rho\rangle_0 \equiv 3\,M_{\rm cl}/4\pi\,R_{\rm cl}^3$ is the initial mean density). In all cases this rises rapidly as gravitational collapse and turbulence develop. In low-density systems, it almost immediately drops to zero after stellar feedback unbinds the gas. In higher-density systems, the presence of dense gas is sustained and even rejuvenated later in the system evolution owing to the presence of strong shocks.

rate evolve in the immediate vicinity of the sink. The thermal sound speed is negligible at basically all times in the cold molecular phases compared to δV, as expected. Runaway growth therefore occurs when the BH happens to encounter a region which simultaneously features a strong local density enhancement, $\rho \sim 10^3 - 10^4\,\langle\rho\rangle_0$, and low relative velocity $\delta V \lesssim 0.1\,v_{\rm cl}$, below the escape velocity of gas from the sink radius (so it is indeed captured). This boosts the local Bondi accretion rate by a factor of $\sim 10^7$, compared to our estimate above for the "diffuse" cloud medium. Visual examination shows this resembles Fig. 3.1 – the BH happens (essentially by chance) to be moving with a very low relative velocity to a dense clump created nearby by intersecting shock fronts (with Mach $\sim 30-100$ shocks, i.e. $v_{\rm shock} \sim 10\,\mathrm{km\,s^{-1}}$, producing the large density enhancement), and begins accreting it extremely rapidly. Since the Bondi rate scales as $\propto M_{\rm sink}^2$, this runs away and most of the clump mass ($\sim 10^5\,\mathrm{M}_\odot$) is rapidly accreted and the clump is tidally disrupted

and then captured before it fragments internally to form stars. Examination show this pattern is typical of the seeds which experience runaway accretion in the simulations.

Analytically, therefore, let us assume that during evolution, a BH encounters a dense clump with local density ρ_c, clump radius r_c, mass δM_c, at relative velocity δV_c (and define $C^2 = \delta V_c^2 + c_s^2$, where we can generally assume $C \sim \delta V_c \gtrsim c_s$, even in regions where δV_c is relatively low), and accretes in Bondi-Hoyle-like fashion. Fig. 3.12 summarizes the resulting accretion for various assumptions. Integrating the Bondi accretion rate for some time Δt (assuming the background is constant), we have

$$\frac{1}{M_{\rm bh,0}} - \frac{1}{M_{\rm bh,final}} = \frac{1}{M_{\rm bh,0}} - \frac{1}{M_{\rm bh,0}+\Delta M_{\rm bh}} \sim \frac{4\pi\, G^2 \rho_c}{C^3}\Delta t \tag{3.4}$$

where $M_{\rm bh,\,0}$ is the "initial" BH mass. This diverges (formally $\Delta M_{\rm bh} \rightarrow \infty$), so in practice the entire clump will be accreted ($\Delta M_{\rm BH} \rightarrow M_c$), in a finite time $\Delta t \rightarrow t_{\rm acc} \sim C^3/(4\pi\, G^2\, \rho_c\, M_{\rm bh,0})$. In practice, the time Δt will be limited by the shortest of either the dense clump lifetime (usually not shorter than its freefall time $t_{\rm ff,\,c} \sim 1/\sqrt{G\,\rho_c}$), the timescale for the clump to fragment and form stars (also no shorter than $t_{\rm ff,\,c}$), or the crossing time $t_{\rm cross} \sim r_c/\delta V_c$ for the mutual interaction. A simple calculation shows that the ratio $t_{\rm cross}/t_{\rm ff,\,c} \sim (\delta M_c/M_{\rm cl})^{1/3}\,(\rho_c/\langle\rho\rangle_0)^{1/6}\,(v_{\rm cl}/\delta V_c)$. Inserting numbers or considering Fig. 3.12 shows that for the conditions of greatest interest for rapid accretion ($\delta V_c \ll v_{\rm cl}$, $\rho_c \gg \langle\rho\rangle_0$, and clump masses δM_c not incredibly small compared to the mass of the cloud so large BH growth is possible), we usually expect $t_{\rm cross} \gtrsim t_{\rm ff,\,c}$. So considering a "worst-case" scenario, then, accretion can run away to accrete the entire clump when $t_{\rm acc} \lesssim t_{\rm ff,\,c}$, which in turn requires:

$$\frac{\delta V_c}{v_{\rm cl}} \lesssim 0.1 \left(\frac{M_{\rm bh,\,0}}{10^{-5}\,M_{\rm cl}}\right)^{1/3} \left(\frac{\rho_c}{100\,\langle\rho\rangle_0}\right)^{1/6} \tag{3.5}$$

This corresponds reasonably well to the conditions where, in the simulations, we indeed see runaway growth – regions with enhanced ρ_c, and (crucially here), low local δV_c. This also naturally explains why we see only a very weak dependence on initial BH mass – provided this condition is met (which does not depend strongly on $M_{\rm bh,\,0}$), then the "growth limiter" is not the BH mass or Bondi rate (which depends strongly on $M_{\rm BH}$), but the mass of the clump M_c (which is, of course, entirely independent of the mass of the BH). Moreover, accretion events can occur sequentially, so once a BH "jumps" in mass by accreting a clump, its "effective" mass will be larger making it easier to accrete subsequent clumps (in an extreme form of competitive accretion).

Still, if the BHs were truly extremely small (e.g., $\ll 10\,M_\odot$), or the clouds extremely massive, then the probability of such an event would become small rapidly – this may explain, in part, why for the most massive complexes we see fewer BHs grow (but those that do grow, grow to even larger masses).

Finally, in Appendix 3.A, we use this to make an order-of-magnitude estimate of the probability of a seed encountering a "patch" (i.e. clump) of gas meeting the criteria above. Assuming e.g., uncorrelated Gaussian velocity fields and lognormal density fields, we estimate that the probability of seeds encountering dense clumps is not low, but the probability of such an encounter also having low relative velocity meeting the condition above is, giving a net probability in the range $\sim 0.001 - 0.01$. This is remarkably similar (given the simplicity of these assumptions) to our estimate of ~ 0.01 from the simulations where we varied the number of seeds systematically, as discussed above.

Hyper-Eddington accretion

Here we want to assess if the mass accretion onto BHs is hyper-Eddington. For this simulation without feedback, the mass flow onto BHs should already be enormous, which is a sufficient (though not necessary) condition for hyper-Eddington accretion. We first check this condition in Fig. 3.13. For each BH in the simulation, we can estimate its average mass accretion rate $\langle \dot{M}_{\rm BH} \rangle$ from neighboring snapshots. We define the Eddington ratio as $f_{\rm Edd} \equiv \langle \dot{M}_{\rm BH} \rangle / \dot{M}_{\rm Edd}$, and check the maximum $f_{\rm Edd}$ for each BH in its history. We then show the distribution of the maximum $f_{\rm Edd}$ for all BHs. There is a fraction of simulated BHs undergoing hyper-Eddington accretion (e.g., the fraction of BH with $f_{\rm Edd} \gtrsim 10^3$ is $\sim 2\%$ for GMCs with $\bar{\Sigma}_0 = 13000\,M_\odot/{\rm pc}^2$, and $\sim 0.5\%$ for those with $\bar{\Sigma}_0 = 1300\,M_\odot/{\rm pc}^2$). For BHs in GMCs with higher initial surface density, the possibility of hyper-Eddington accretion is also higher, in the same way as discussed in § 3.3.

Feedback from black holes, especially the radiative feedback will play a negative role in mass accretion (details to be expanded in § 3.5). Although in this study BH feedback is not included, we can infer the availability of hyper-Eddington accretion from theoretical studies. Inayoshi et al. (2016) predicted that the critical density for hyper-Eddington accretion (with the accretion rate of $\gtrsim 5000 L_{\rm Edd}/c^2$) is

$$n_\infty \gtrsim 10^5 \left(\frac{M_{\rm BH}}{10^4\,M_\odot}\right)^{-1} \left(\frac{T_\infty}{10^4\,{\rm K}}\right)^{3/2} {\rm cm}^{-3}.$$

Here n_∞ and T_∞ are the density and temperature near the BH. For each BH with

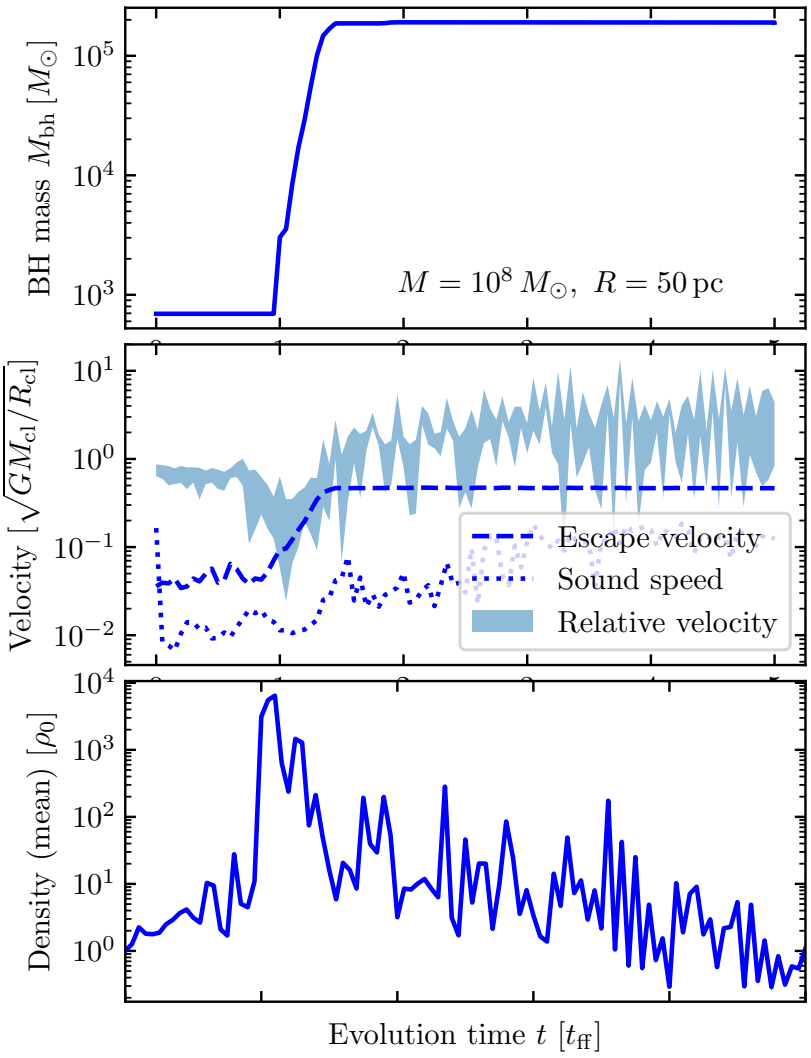

Figure 3.11: A representative case study of the environment around one BH seed which undergoes runaway growth (complex properties labeled). *Top:* BH/sink particle mass versus time (in units of the initial complex free-fall time $t_{\rm ff}$). *Middle:* Median sound speed (c_s; dotted), and 5 – 90% range of relative gas bulk velocities ($|\mathbf{v}_{\rm gas} - \mathbf{v}_{\rm bh}|$; shaded) of all gas cells which fall within the sink radius $r_{\rm sink}$, and the escape velocity from the sink ($\sim \sqrt{G\,M_{\rm sink}/r_{\rm sink}}$). Velocities are in units of the characteristic complex gravitational velocity $v_{\rm cl} = \sqrt{G\,M_{\rm cl}/R_{\rm cl}}$. *Bottom:* Mean density of gas within the sink radius, in units of the initial complex mean density $\langle\rho\rangle_0 \equiv 3\,M_{\rm cl}/4\pi\,R_{\rm cl}^3$. The runaway growth occurs when the BH intercepts an overdense clump $\rho \gtrsim 100\,\langle\rho\rangle_0$, with a low relative velocity $\delta V \lesssim 0.1\,v_{\rm cl}$ so that it is gravitationally captured. Thermal pressure support/sound speed is relatively unimportant, since this is occurring in cold molecular gas.

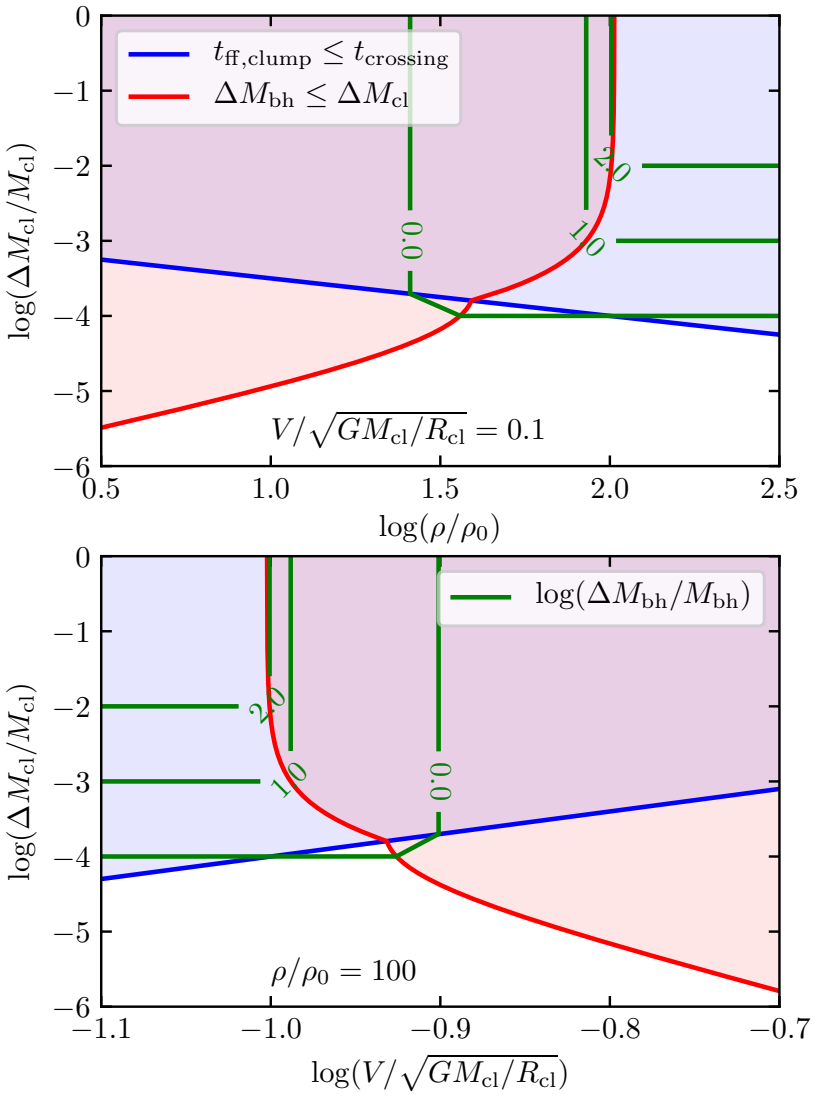

Figure 3.12: Illustrative analytic predictions for BH accretion, based on a simple model of Bondi-Hoyle accretion in encounters with sub-clumps that have local density $\rho_{\rm c}$, mass $\delta M_{\rm c}$, and relative BH-clump velocity $\delta V_{\rm c}$. Here we assume the initial seed mass $M_{\rm bh} = 10^{-4}\,M_{\rm cl}$. *Top:* Assuming a fixed $\delta V_{\rm c}$ (in units of $v_{\rm cl}$), we plot behavior as a function of $\delta M_{\rm c}$ and $\rho_{\rm c}$. *Bottom:* Behavior as a function of $\delta M_{\rm c}$ and $\delta V_{\rm c}$, at fixed ρ_c. The blue shaded region denotes where the internal free-fall time of the clump ($t_{\rm ff,\,clump}$) is shorter than the clump-BH crossing timescale ($t_{\rm crossing}$), so will be the rate-limiting timescale for accretion. Red shaded range shows where the total mass accreted ($\Delta M_{\rm bh}$) over the shorter of $\Delta t = \min(t_{\rm ff,\,clump},\ t_{\rm crossing})$ would be less than the clump mass ($\delta M_{\rm c}$), so the accretion does not fully "run away." Green lines show contours where $\log_{10}(\Delta M_{\rm bh}/M_{\rm bh,\,0})$ is constant and equal to the value shown. The region where $\Delta M_{\rm bh}/M_{\rm bh}$ contour is horizontal denotes "runaway," defined by where the BH will accrete the entire clump mass.

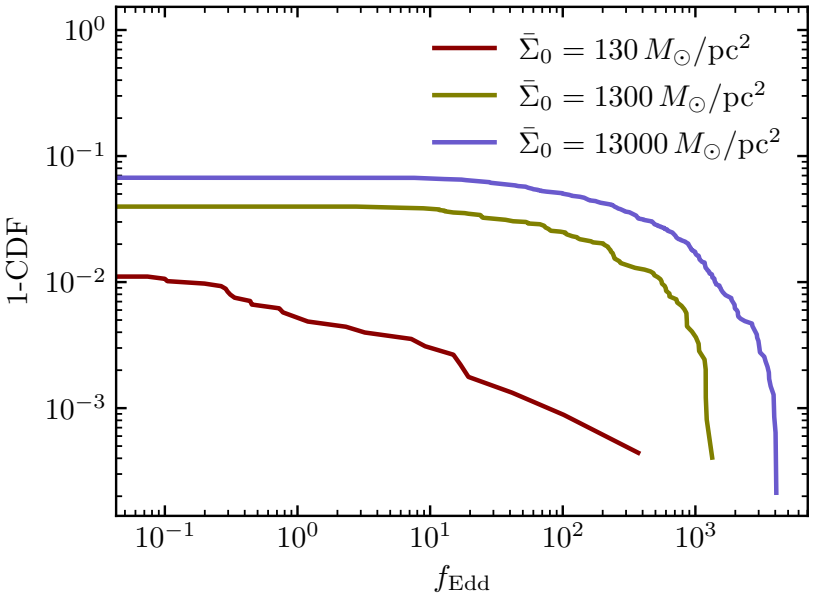

Figure 3.13: Distribution of the Eddington ratio $f_{\rm Edd}$ for BHs in different groups of GMCs. Here for each BH, $f_{\rm Edd}$ is estimated in its fastest-accreting stage. For GMCs with high surface density, there are $\sim 2\%$ BHs reaching hyper-Eddington accretion with $f_{\rm Edd} \gtrsim 1000$.

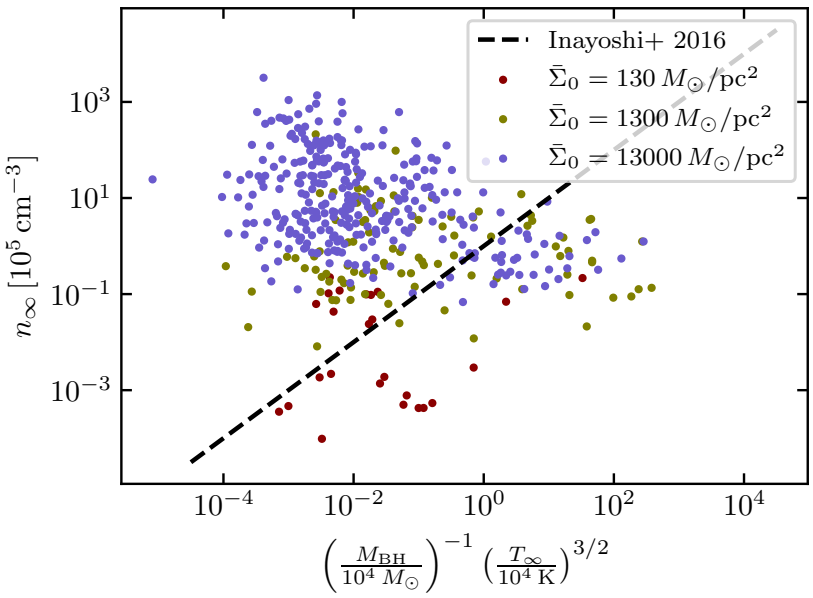

Figure 3.14: Comparing the simulation with the critical density for hyper-Eddington accretion predicted by Inayoshi et al. (2016). Most BHs in the simulation, especially for those in GMCs with $\bar{\Sigma}_0 = 13000\,\mathrm{M}_\odot/\mathrm{pc}^2$, are above the critical density.

mass accretion in our simulation, we track the time when the BH reaches the fastest accretion rate through its history, and measure the nearby gas density and temperature. We compare our simulation data with Inayoshi et al. (2016) in Fig. 3.14. We find that for most BHs the nearby density is above the critical density that allows hyper-Eddington accretion even if there is radiative feedback. For GMCs with higher surface density, the fraction of BHs above the critical density is also higher.

Effects of numerical parameters

At the end of the discussion section, we include the effects of several numerical parameters in the simulation.

Mass & Force Resolution

Resolution could influence our results both directly and indirectly. Ideally we would wish to ensure $m_{\rm gas} \ll M_{\rm bh}$, and that the Bondi radii are resolved (see § 3.2), but there are of course physics we cannot hope to resolve in our larger cloud complexes, such as the formation of individual stars (e.g., predicting the IMF itself). Nonetheless, we have tested our results for several clouds at different resolution levels: 64^3, 128^3, and 256^3 (See Appendix 3.B). For most clouds (especially those with high initial mean surface density), we see no significant different in our statistical/qualitative conclusions across these resolution levels. Similarly, we have re-run two of our clouds (one low and one high density) with factor ~ 3 different force-softening values for the collisionless (star and BH) particles, and see no significant effect. Thus our conclusions appear robust, but we caution again that qualitatively new physical processes would need to be simulated if we went to higher resolution (which are represented here by our sub-grid models for e.g., IMF-averaged stellar evolution).

BH Sink Radii

As noted above, in the simulation the sink radius for BH accretion is set as the smaller value of the Bondi-Hoyle accretion radius with either $\delta V \sim c_{\rm s}$ or $\delta V \sim v_{\rm cl}$. Analysis of our simulation shows that runaway accretion almost always occurs in regions where $\delta V \sim c_{\rm s} \lesssim 0.1\,v_{\rm cl}$, with enhanced densities $\gtrsim 100\,(3\,M_{\rm cl}/4\pi\,R_{\rm cl}^3)$, where (as noted above) the Bondi radii are orders-of-magnitude larger than one would calculate for the diffuse GMC gas with low relative velocities. As a result the simulations relatively easily resolve the Bondi radius where accretion is relevant. Nonetheless we have re-run a small subset varying $r_{\rm sink}$ by more than an order

of magnitude in either direction. If we make $r_{\rm sink}$ much too small – significantly smaller than the rms inter-cell separation (spatial resolution in the gas) at the highest cloud densities ($\gtrsim 100\,(3\,M_{\rm cl}/4\pi\,R_{\rm cl}^3)$), then we artificially see suppressed accretion (simply because we require the separation between BH and gas cell center-of-mass be $< r_{\rm sink}$ for capture). If we make the sink radius more than an order of magnitude larger than our default value, we see spurious accretion, usually in the very early timesteps of the simulations (before turbulence is fully-developed), where diffuse gas with low relative velocities is rapidly accreted. But for more reasonable variations in $r_{\rm sink}$, even spanning an order of magnitude, our results are robust. And as we show below, the accretion corresponds fairly well with analytic post-processing expectations, further lending confidence to this estimate.

Initial BH Velocities

We have considered some limited experiments where we add a systematic "boost" or arbitrarily increase the initial velocities of the BH seeds in the initial conditions (for details see Appendix 3.C). As expected, if the seeds are moving well in excess of the escape velocity relative to the cloud, they escape rapidly and never capture a large amount of gas. So the rms velocities of "interesting" BH seeds can only exceed $v_{\rm cl}$ by a modest (at most order-one) factor. On the other hand, reducing the BH seed velocities to zero has very little effect (other than introducing some spurious transient accretion in the first few timesteps when there is no relative gas-BH motion), because they quickly acquire random velocities of order the gravitational velocity $v_{\rm cl}$ from the fragmenting cloud potential.

Connections with observations

Given that this is really a theoretical "proof of concept" and we do not yet include these crucial physics (which we expect may change the key conclusions), we hesitate to make specific observational predictions. Nonetheless, even if BH feedback did nothing to further suppress runaway BH growth, there are some important conclusions we can draw regarding observations of both active (star-forming) clouds and "relic" star clusters.

1. Runaway accretion would not occur in Milky Way/Local Group GMCs or cloud complexes: the necessary conditions much more closely resemble starburst galaxy nuclei and the most massive dense star-forming clumps observed in high-redshift massive galaxies.

2. As a result, the "relic" star clusters from regions which could produce runaway accretion will not be typical star clusters or globular clusters. They are much more akin to nuclear star clusters (at the low-mass end) and dense galactic bulges (at the high-mass end). Even if the high-redshift clumps are off-center, these complexes would quickly spiral to the center of the galaxies to form proto-bulges (Noguchi, 1999; Dekel et al., 2009), which is important for SMBH seed formation mechanisms as it is almost impossible for seeds of the masses we predict here to "sink" to galaxy centers via dynamical friction in a Hubble time at high redshift, if they are not "carried" by more massive star cluster complexes (Ma et al., 2021).

3. Regardless of which clusters could have hosted this runaway process, we again find the probability is low on a "per seed" basis. Therefore, whether we expect an IMBH/SMBH "relic" in the descendants depends fundamentally on the population of seeds and their dynamics. While we find stellar-mass seeds are viable, it is not obvious if these could come from the stars forming in the cloud itself (e.g., from the relics of the stars formed during the process). Most stellar-mass seeds form relatively late after star formation ($\gtrsim 30\,$Myr), in explosions (which could disrupt the cloud), and have large natal kicks (excessive relative velocity). It is possible, if kicks were somehow avoided, that the most massive stars which reach the end of the main sequence more rapidly (at $\sim 3\,$Myr) and collapse directly to BHs could be viable seeds, but then these are much more rare. Alternatively, the seeds could come from the "pre-existing" background of stars, as especially in e.g., galactic nuclei or $\sim$kpc-scale clump complexes in massive galaxies we expect a very large population of background stellar-mass BHs. The key then is their kinematics (i.e. whether a sufficient number can be "captured" to locally interact as we model).

4. Almost by definition, the required conditions make it very difficult to observe this process "in action." Complexes which meet the criteria above are, by definition, Compton-thick (and since the accretion occurs in over-dense sub-regions, these are even more heavily obscured). Moreover, if the maximum luminosity of accreting BHs (even if they are undergoing hyper-Eddington accretion) is not much larger than the traditional Eddington limit (as most models predict; see § 3.1), then the bolometric and even X-ray luminosities of the clouds/complexes will be dominated by the stars (not the runaway

accreting BHs), unless the BH accretes an enormous fraction ($\sim 10\%$) of the entire cloud mass.

5. Even if such enormous accretion were to occur (or if the luminosity could exceed Eddington), by the time the BH luminosity could "outshine" even a fraction of the stellar luminosity of the complex, its luminosity would be so large that it would not be a ULX-type source. Rather (especially, again, recalling that the complexes of interest are generally in or around distant galactic nuclei), it would much more closely resemble an off-center, obscured AGN (or a dual AGN, if the galaxy already has an accreting SMBH). Large populations of such AGN sources are, of course, well-known, and there are much more mundane ways to produce them (via galaxy mergers or irregular kinematics), but it is perhaps conceivable that a small fraction of them could be systems like what we simulate here.

3.5 Caveats

Feedback from accreting black holes

The most important caveat of this study is that we did not include any "sub-grid" model for BH accretion or feedback in the simulations. So "BH accretion rate" here should really be understood to be "rate of gravitational capture of gas by the BH-disk system" (akin to "Bondi-Hoyle-like mass inflow rate") and "BH mass" or "sink mass" represents a sum of the actual BH mass and its bound/captured material (whether that material has actually formed an accretion disk is another question itself).

This is not, of course, because we expect feedback to be unimportant for the BHs which rapidly capture gas: indeed, models of super-Eddington accretion disks (models whose "outer boundary condition" is something like the sink radii or "inner boundary condition" of our simulations) predict both strong radiative (luminosities near or somewhat above the Eddington luminosity) and kinetic (broad-angle MHD outflows from the disk) feedback (see references in § 3.1). While it is conceivable that under sufficiently-dense conditions, the surrounding material could continue to accrete (see e.g., Quataert and Gruzinov 2000; Takeo et al. 2018; Regan et al. 2019), this could also completely shut down BH growth and even star formation in the surrounding cloud (Schawinski et al., 2006).

However, crucial details of such accretion and feedback processes remain deeply uncertain. This includes (i) the rate at which material can go from being "gravita-

tionally captured" to actually accreted onto the BH (which determines the luminosity and other feedback); (ii) whether star formation and/or fragmentation occurs in the captured disk material if too much mass is captured; and (iii) for a given accretion rate, the radiated spectrum and energy, and the energy and momentum and mass and opening angle of accretion-disk winds. Our intention here is therefore to first identify a set of *necessary*, but perhaps not sufficient, pre-conditions for runaway hyper-Eddington seed growth in on ISM scales. Clearly, if a BH cannot sustain super-Eddington gravitational capture rates of sufficient total mass in the first place, then it is unlikely that adding feedback would do anything other than further decrease the (already minimal) accretion. This allows us to already rule out large segments of parameter space as viable locations for hyper-Eddington accretion (e.g., Milky Way-like low-density or low-mass clouds, systems with insufficient statistical sampling of "seeds," highly-unbound seeds). In future work (in preparation), we will use this study as the basis for a follow-up set of simulations which do include BH feedback, systematically surveying parameterized models for the major uncertainties described above, but using the results of this study to specifically begin from conditions where we know that, *absent* BH feedback, rapid accretion is possible.

Other caveats

There are also of course other caveats in our simulations themselves. While we survey a factor of ~ 100 in mass resolution and see robust results, we are certainly not able to "converge" in a strict sense, especially given some ISM micro-physics where the relevant dynamics occur on sub-au scales. We cannot resolve or predict the IMF or stellar evolution tracks of individual stars, let alone their late-stage evolution and potential collapse into BH relics. This is especially unfortunate as one might imagine one source of "seed" BHs bound to the cloud would be extremely massive stars that form in that cloud with very short lifetimes that might implode or collapse directly to massive BH remnants, rather than exploding as SNe. A new generation of simulations like STARFORGE might be able to address some of these, but the resolution required has thus far limited their explicit simulations to precisely the low-density, low-mass clouds of least interest here (Grudić et al., 2021b; Grudić et al., 2021a).

It is also possible that physics we neglect plays an important role. For example, on galactic scales, cosmic rays can influence the ISM significantly, although many have argued that because of their diffusive nature (smooth CR density gradients), they play little dynamical role (except perhaps via ionization) in the dense ISM clouds

of interest here (Farber et al., 2018; Hopkins et al., 2020a; Hopkins et al., 2022b; Bustard and Zweibel, 2021).

More realistic initial conditions and boundary conditions for clouds (embedded in a full ISM, for example) could also be important (Lane et al., 2022). This is perhaps especially relevant for our most massive complexes. When we simulate regions with $R_{\rm cl} \sim 500\,{\rm pc}$ and $\bar{\Sigma}_0 \sim 10^4\,{\rm M_\odot\,pc^{-2}}$ – i.e. gas masses as large as $\sim 10^{10}\,{\rm M_\odot}$, these are not really "clouds" as we think of GMCs in the Milky Way. Rather, these values are motivated by typical sizes and densities observed in systems like starburst and/or ultra-luminous infrared galaxy nuclei (see e.g. Kennicutt, 1998; Gao and Solomon, 2004; Narayanan et al., 2008; Bigiel et al., 2008), and seen in the common massive clump-complexes or nuclei of high-redshift massive galaxies (Tacconi et al., 2010; Krumholz and Dekel, 2010; Narayanan et al., 2011; Orr et al., 2018). But under these conditions, there is usually also a large pre-existing stellar population and dark matter halo, defining the potential of the nuclear gas – properly simulating these regimes would really require full galaxy-formation simulations. It is likely that this added potential would make the starburst even less able to disrupt, leaving behind a dense nuclear bulge (e.g. Sanders et al., 1988; Tacconi et al., 2002; Rothberg and Joseph, 2004; Hopkins et al., 2008a; Hopkins et al., 2008b; Hopkins et al., 2009a; Hopkins et al., 2009b; Hopkins and Quataert, 2011).

3.6 Conclusions

We have simulated populations of dynamic, accreting BH seeds with masses $\sim 10^1 - 10^4\,{\rm M_\odot}$ in massive cloud complexes (meant to resemble the most massive GMCs, high-redshift and starburst galaxy nuclei), with self-gravity, realistic cooling, detailed models for star formation and stellar feedback in the form of radiation, outflows, and supernovae, but neglecting the feedback from the BHs themselves. Our goal is to identify whether, under any conditions, such seeds can capture gas from the dense, cold ISM at the rates required to power hyper-Eddington accretion, and whether this can be sustained for long enough periods that it is conceivable such BHs could grow to IMBH or even SMBH mass scales. This forms a necessary, but not sufficient, condition for hyper-Eddington growth models for the origin of IMBHs and SMBHs.

Based on our analysis above, we can draw the following conclusions (again, absent BH feedback):

1. Sustained hyper-Eddington gravitational capture from the ISM can occur,

under specific conditions (detailed below). This occurs when BH seeds coincidentally find themselves in regions with locally enhanced densities (local densities well in excess of ~ 100 times the complex-mean), with (by chance) very low relative velocities (less than $\sim 10\%$ of the characteristic gravitational velocity of the complex). The dense clump is then captured extremely quickly (on less than its internal dynamical time), which can set of a "runaway" of competitive accretion by which the seed grows even more massive (reaching up to $\sim 1\%$ of the complex gas mass).

2. Provided the right conditions are met, this process is only very weakly dependent on the initial seed mass, even for stellar-mass seeds in the $\sim 10-100\,M_\odot$ range. Thus, the "seed" does not need to already be an IMBH.

3. Much like with star formation, stellar feedback plays a dual role. Stellar feedback overall suppresses star formation and unbinds gas, suppressing BH growth (especially in lower-density clouds). But in higher-density, more-massive complexes, feedback produces regions like colliding shocks/shells which promote exactly the conditions needed for runaway BH growth.

For this runaway accretion to occur, we show that there are several necessary "global" criteria the molecular complex must meet, including:

1. The complex must have a high surface density/gravitational pressure, $\bar{\Sigma}_0 \gtrsim 1000\,M_\odot\,pc^{-2}$. Otherwise, stellar feedback disrupts the medium too efficiently, both reducing the time available for accretion but also unbinding dense gas instead of allowing it to remain trapped and thus potentially creating situations with low relative velocities.

2. The complex must also be sufficiently high-mass, $M_{cl} \gtrsim 10^6\,M_\odot$. This is to ensure both that there is sufficient total mass supply that if hyper-Eddington accretion occurs, the final mass is "interesting" (reaching IMBH, let alone SMBH mass scales), but also required, along with the $\bar{\Sigma}_0$ criterion, to ensure that the escape velocity of the cloud will be large enough that ionizing radiation does not rapidly unbind material or disrupt the complex and prevent accretion.

3. The BH seeds must be "trapped" by the complex, with systematic relative velocities not significantly larger than the characteristic gravitational velocity of the cloud. This means, for example, that a BH moving isotropically in the

background galaxy bulge, intersecting a cloud, would be unable to accrete, while BHs with small relative velocities to the cloud are viable.

4. We require at least ~ 100 seeds, in complexes meeting all the criteria above, to have an order-unity probability of one showing sustained hyper-Eddington accretion. Thus even when all the criteria are met, the conditions are "rare" on a per-seed basis. Once the number of seeds is sufficiently large, the finite number of locations where runaway can occur, plus the competitive accretion dynamics noted above, mean that the number which actually do experience runaway growth saturates at one to a few.

In future work, we will use this preliminary study to inform a more focused study which does include BH feedback, systematically exploring the uncertainties in BH feedback models but focused on cloud conditions where – at least in the absence of said feedback – we find runaway growth is possible.

3.A Estimating the probability of a runaway accretion event

Based on arguments in 3.4, we try here to estimate the probability of a runaway BH accretion event. Specifically, from § 3.4, we want to estimate the probability of a random BH seed encountering a "clump" in a turbulent cloud complex which meets the conditions defined in Eq. 3.5. For simplicity (although somewhat motivated by simulations, see e.g., Burkhart et al. (2009)) we will assume uncorrelated density and velocity fields, with Gaussian velocity statistics and lognormal density statistics as is usually assumed in supersonic turbulence.

First consider the probability of a seed encountering a clump which is overdense in the manner of Figs. 3.1 & 3.11, or Eq. 3.5. Assume the seeds have an rms velocity dispersion $\langle \mathbf{v}_{\rm bh}^2 \rangle^{1/2}$ of order the gravitational velocity of the complex $v_{\rm cl}$, as does the gas, and that the complex is filled with some number density of clumps $n_{\rm c}$ with effective cross-section $\sigma_{\rm c} \sim {\rm Vol}_{\rm c}/r_{\rm c}$, where ${\rm Vol}_{\rm c}$ is the volume of a typical clump. Assume the seeds randomly move through the complex (uniformly sampling the volume) over its lifetime $\Delta t = \tau\, t_{\rm ff,\,cl}$ (where for the massive complexes of interest, $\tau \sim$ a few, and $t_{\rm ff,\,cl} \equiv R_{\rm cl}/v_{\rm cl}$). The average number of dense clumps encountered is therefore $\langle N_{\rm cl} \rangle \sim \tau\, n_{\rm c}\, \sigma_{\rm c}\, v_{\rm cl}\, t_{\rm ff,\,cl} \sim \tau\, (R_{\rm cl}/r_{\rm c})\, f_{\rm V,\,c}$. We are interested in dense clumps or shocks, which simulations show tend to have a characteristic size/width of order the sonic scale, $r_{\rm c} \sim R_{\rm cl}/\mathcal{M}_{\rm comp}^2$ (where $\mathcal{M}_{\rm comp}$ is the compressive Mach number of the cloud; see e.g., Passot et al. 1988; Vazquez-Semadeni 1994; Scalo et al. 1998). We can also estimate $f_{\rm V,\,c}$ by integrating the standard volume-weighted

lognormal density PDF for supersonic turbulence (Gaussian in $\ln(\rho/\langle\rho\rangle_0)$, with mean $= -S/2$ required by continuity, and variance $S \approx \ln[1+\mathcal{M}_{\rm comp}^2]$) above some critical $\rho \gtrsim \rho_{\rm c} \sim 100\,\langle\rho\rangle_0$. Plugging in numbers, we can see that $\langle N_{\rm cl}\rangle \gtrsim 1$ so long as $\mathcal{M}_{\rm comp} \gtrsim 10$, which is easily satisfied in cold molecular gas for the massive, high-density complexes of interest.

So it is not particularly rare for a BH to encounter a dense clump over a duration of several free-fall times in the massive, dense complexes of interest. What is less common is for such an encounter to feature a low relative velocity $\delta V = |\mathbf{v}_{\rm bh} - \mathbf{v}_{\rm gas}|$. Let us assume, similar to the above, that the BH velocity is drawn from an isotropic Gaussian distribution with 1D dispersion $\sigma_{\rm v,\,bh} \sim v_{\rm cl}/\sqrt{3}$ in each dimension, and the gas or clump velocity is drawn from an independent isotropic Gaussian with similar 1D dispersion in each dimension $\sigma_{\rm v,\,gas} = \alpha_v\,\sigma_{\rm v,\,bh}$ (where α_v is an arbitrary order-unity constant). The velocity difference $\delta\mathbf{V}$ is therefore also Gaussian-distributed, and integrating we obtain the probability

$$P_v(\delta V < \epsilon\,v_{\rm cl}) = {\rm erf}\left(\frac{q}{\sqrt{2}}\right) - \sqrt{\frac{2}{\pi}}\,q\,\exp\left(-\frac{q^2}{2}\right)\,, \tag{3.6}$$

$$q \equiv \frac{\sqrt{3}\,\epsilon}{\sqrt{1+\alpha_v^2}} \tag{3.7}$$

Assuming $\alpha_v \sim 1$, and $\epsilon \sim 0.1$ from Eq. 3.5, we obtain $P_v \sim 5\times10^{-4}$; multiplying by $\langle N_{\rm cl}\rangle \sim$ a few (for our massive cloud complexes), this gives a probability of $\sim 10^{-3} - 10^{-2}$ of an "interesting" event, per seed.

We stress that this is only intended as a guide for intuition – we have ignored a wide range of effects which modify the statistics, the fact that the density and velocity statistics are probably correlated (see e.g. Konstandin et al., 2012; Squire and Hopkins, 2017), the fact that strong shocks and feedback tend to produce large local deviations from Gaussianity (Hopkins, 2013a; Beattie et al., 2022), gravitational focusing (which probably significantly increases the rate of "coincidences" in velocity-density space), the size spectrum of different density structures (Guszejnov and Hopkins, 2016; Guszejnov et al., 2018a), and more. Ultimately, capturing all of these effects is only possible in the full simulations, but the simple arguments here can provide some very approximate guide to the typical behaviors in the simulations.

3.B Resolution convergence

In Fig. 3.15 we show the cumulative distribution of BH final-to-initial mass difference (same as Fig. 3.3) for simulations in different resolutions. Here we choose

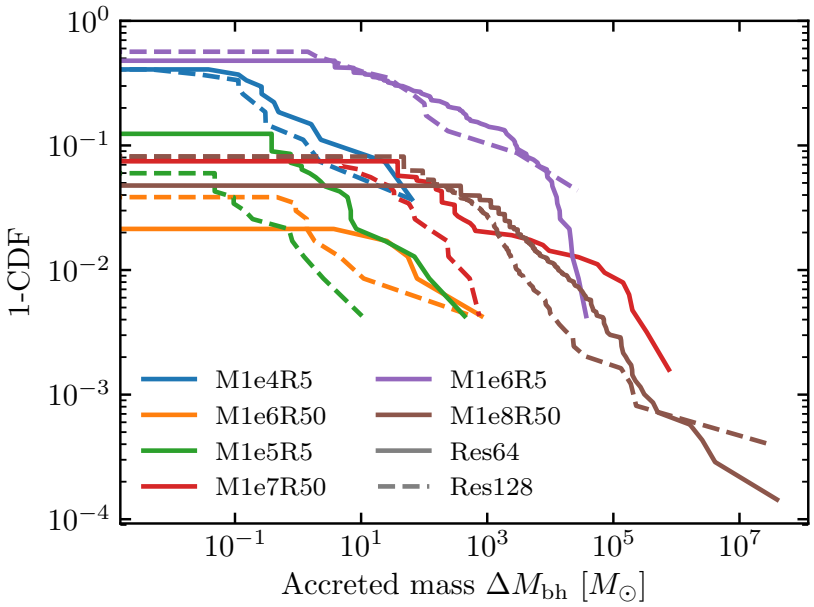

Figure 3.15: Cumulative distribution of accreted mass as a resolution convergence test. Here we show clouds with initial radius $R_{\rm cl} \leq 50\,$pc. Each cloud is simulated with resolutions of 64^3 (solid) and 128^3 (dashed). We see general good agreement for simulations in different resolution for most clouds.

clouds with $R_{\rm cl} \leq 50\,$pc, such that all clouds weigh $M_{\rm cl} \leq 10^8\,{\rm M}_\odot$ and the condition $m_{\rm gas} \ll M_{\rm bh}$ is more likely to be satisfied. We see that for low (`M1e4R5`[5] and `M1e6R50`) and high (`M1e6R5` and `M1e8R50`) surface density clouds, there is good agreement in the CDFs under high (`Res128`) and low (`Res64`) resolutions. The resolution convergence is worse for the medium surface density group: for `M1e7R50` we see the same cut-off but different span of CDFs, while for `M1e7R50` there is a systematic difference. One possible reason might be the uncertainties in these near-breakup clouds.

As a summary for the test, we find good quantitative resolution convergence for most clouds, especially dense ones where there is significant BH accretion (`M1e6R5` and `M1e8R50`). There are indeed some clouds with systematic offsets under different resolutions, but they fall into a “less-interesting" category in terms of BH accretion and will not qualitatively change our conclusions.

[5]In this section, we use the template `M%eR%d` to denote a cloud with its mass (in $\rm M_\odot$) and radius (in pc).

3.C Initial velocity dependence

Due to considerations in computational costs, we made some confinements in the initial velocity distribution in order to capture BH accretion events more efficiently in a limited suite of simulations. In the main text the fiducial choice is to have all BH initial velocity $v_{\rm ini}$ below the circular velocity $v_{\rm cl} \equiv (GM_{\rm cl}/R_{\rm cl})^{1/2}$. Inevitably this will miss some BHs that are still bounded to the GMC, and possibly overestimate (or underestimate) the possibility of runaway accretion in a more general BH seed population. In this section we inspect the issue with a test.

In Fig. 3.16 we show the initial-velocity depends and cumulative distributions of BH accretion (featured by the mass accreted by each BH, $\Delta M_{\rm BH}$), for three cutoffs in the initial velocity magnitude: fiducial ($v_{\rm ini} \leq v_{\rm cl}$), "critically bounded" ($v_{\rm ini} \leq \sqrt{2}v_{\rm cl}$, which means some BHs may reach $v_{\rm ini} \lesssim \sqrt{2}v_{\rm cl}$), and "unbounded" ($v_{\rm ini} \leq \sqrt{2}v_{\rm cl}$). For each test, other quantities like the initial position and velocity direction for each BH are the same. Compared with the fiducial case, there are a few ($\sim$ 5) BHs of above $v_{\rm cl}$ accreting at least one gas cell, for both the "crucially bounded" and "unbounded" group. We also note that above $\sqrt{2}v_{\rm cl}$, no BH accretes more than one gas cell, which is not runaway accretion.

From the cutoff of the CDF, we see that the fraction of BH seed with accretion events in the "critically bounded" and "unbounded" groups are lower, but still in the same order of magnitude. The maximum mass accretion for the three tests are also similar: although the cutoff of the orange line is higher, the general trend of the three lines at the high-mass end are very close if excluding the "lucky" BH.

In conclusion, we find that most of BH accretion events happens when $v_{\rm ini} \leq v_{\rm cl}$. Our BH population in the main text overestimated these events, but still well within the same order of magnitude.

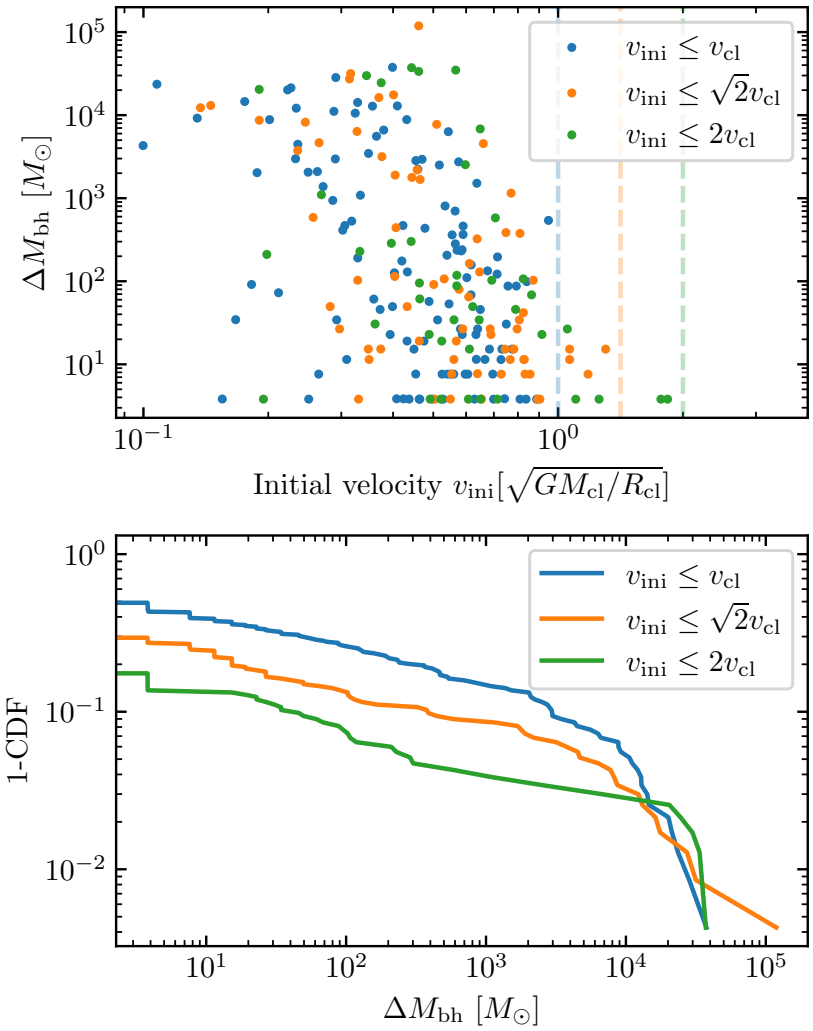

Figure 3.16: A test of the dependence on the initial velocity distribution of BHs. In the fiducial case we confine $v_{\rm ini} \leq v_{\rm cl}$, where $v_{\rm cl} = \sqrt{GM_{\rm cl}/R_{\rm cl}}$, and there are tests with different cutoffs ($\sqrt{2}v_{\rm cl}$ and $2v_{\rm cl}$).

Chapter 4

HYPER-EDDINGTON ACCRETION: FEEDBACK SELF-REGULATIONS

Abstract

The existence of supermassive black holes (SMBHs) observed in high-redshift luminous quasars may require a phase of fast accretion. In our previous work, we showed that such phases of so-called "hyper-Eddington" accretion may be possible for black hole seeds inside star-forming giant molecular clouds (GMCs) with high surface density ($\sim 10^4\,\mathrm{M_\odot\,pc^{-2}}$), where dense clumps driven by turbulence and stellar feedback can provide sufficient gas supply to support hyper-Eddington phases. In this article, we explore the effects of feedback from accreting black holes on this process, including radiation, mechanical jets, and highly-relativistic cosmic rays (CRs). We run a suite of numerical simulations to explore the parameter space of BH feedback processes, including mass transfer from disk to BH, feedback energy efficiency, mass loading factor, and GMC metallicity. We assume all BH seeds are embedded in GMCs with high surface density. Using slim-disk models with radiatively-inefficient accretion flows, we find that hyper-Eddington accretion is still achievable. We find the maximum mass accreted by the black hole seeds $\Delta M_{\rm BH}^{\rm max}$ are regulated by the feedback efficiency $\epsilon \equiv L/(\dot{M}_{\rm BH}c^2)$, which can be fitted with the relation $\Delta M_{\rm BH}^{\rm max} = M_\star/[1+(\epsilon/\epsilon_\star)^\gamma]$, where $M_\star$, γ, and $\epsilon_\star$ are constants. In the strong feedback limit ($\epsilon \gg \epsilon_\star$), we find $\Delta M_{\rm BH}^{\rm max} \propto \epsilon^{-\gamma}$ and $\gamma \approx 1$ for radiative and CR feedback, while $\gamma \approx 0.5$ for mechanical feedback. We find these relations can be well explained semi-analytically with momentum deposition from BHs. We also study the effects of other free parameters and how BH feedback may suppress star formation in the strong feedback limit.

4.1 Introduction

Formation of supermassive black holes (SMBHs), especially those weighing $\sim 10^9\,\mathrm{M_\odot}$ at very high redshift like $z \gtrsim 7$ (e.g., recent observations by Bañados et al., 2018; Yang et al., 2020; Wang et al., 2021), has long been an intriguing astrophysical problem (e.g., recent reviews by Inayoshi et al., 2020; Volonteri et al., 2021). Observations have shown that these SMBHs grow from lighter "seed" BHs (Yu and Tremaine, 2002). The seeds, typically in the mass range of intermediate-

mass black holes (IMBHs; $\sim$ 100 – $10^6\,M_\odot$), are proposed to form in multiple astrophysical scenarios like the direct collapse of the pristine gas (e.g., Bromm and Loeb, 2003; Latif et al., 2022), Population III star remnants (e.g. Madau and Rees, 2001; Ryu et al., 2016), stellar-mass BHs that undergo hyper-Eddington accretion (e.g., Lupi et al., 2016; Pezzulli et al., 2016; Shi et al., 2023b), and runaway stellar mergers in dense star clusters (e.g., Portegies Zwart et al., 2004; Kremer et al., 2020; Shi et al., 2021). If we use a reference radiative efficiency of 0.1, the e-folding time scale at the Eddington accretion rate is $\sim$ 45 Myr; on the other hand, due to the limited time allowed for SMBH formation (especially for $z \gtrsim 7$ quasars that formed only $\lesssim 10^9$ yr after the Big Bang), a sustained phase of fast accretion is inevitable, possibly at super- or hyper-Eddington ($\gtrsim 500\,\dot{M}_{\rm Edd}$) accretion rates (Inayoshi et al., 2020).[1]

A number of theoretical works on small-scale BH accretion physics have shown that super-Eddington accretion is achievable and sustainable (Begelman, 1979; Quataert and Gruzinov, 2000; Blandford and Begelman, 2004; Inayoshi et al., 2016). This is also supported by simulations with RHD (Ohsuga et al., 2005), RMHD (Jiang et al., 2014; Jiang et al., 2019) and GRMHD (Sądowski et al., 2015). However, these simulations typically embed the BH inside a gas reservoir with a sufficiently high mass supply rate ($\gtrsim 10^3\dot{M}_{\rm Edd}$). This is not essentially true in more realistic star-forming astrophysical environments, since the gas medium may fragment due to self-gravity and result in star formation; feedback from newly-formed stars, including radiative pressure, photoionization/heating, and winds, will develop turbulence or bulk motion in the medium (e.g., see star formation simulations Grudić et al., 2018a; Grudić et al., 2021b). Strong stellar feedback near an accreting BH may deplete the available fuel and challenge the feasibility of super-Eddington accretion (Dubois et al., 2015; Habouzit et al., 2017; Bower et al., 2017). Light seeds, like IMBHs or stellar-mass BHs, are especially prone to the accretion challenges inherent to these environments since regimes influenced/dominated by their gravity (i.e., Bondi-Hoyle radius, Hoyle and Lyttleton, 1939; Bondi, 1952) are small compared with galactic scales.

This problem is addressed in the recent work by the authors (Shi et al., 2023b), which is based on simulations of star formation and feedback in giant molecular clouds (GMCs) as that in Grudić et al., 2018a, while omitting the BH feedback.

[1] Throughout the article, we define the Eddington accretion rate by assuming a reference radiative efficiency of $\epsilon = 0.1$, thus the Salpeter time is $t_{\rm Sal} = \epsilon\sigma_{\rm T}c/(4\pi G\,m_p) \approx 45\,{\rm Myr}$ and $\dot{M}_{\rm Edd} \equiv M_{\rm BH}/t_{\rm Sal}$.

Although the stellar feedback makes the GMC uneven and turbulent, it also generates dense clumps and shocks (Klessen, 2000), which may have low internal velocity dispersion (Mac Low and Klessen, 2004; McKee and Ostriker, 2007) and are optimal environments for accretion if they are gravitationally bounded to the BH (analytically this is described with the Bondi-Hoyle accretion, see Hoyle and Lyttleton, 1939; Bondi, 1952). Similar to the star formation efficiency explored in the literature (Grudić et al., 2018a; Kim et al., 2018; He et al., 2019; Fukushima et al., 2020; Grudić et al., 2021b; Kim et al., 2021; Chevance et al., 2022), BH accretion wherein is also regulated by the surface density ($\Sigma_0 \equiv M_{\rm cl}/R_{\rm cl}^2$) of the cloud: higher Σ_0 means higher self-gravity which keeps the cloud bound rather than disrupted by stellar feedback. Shi et al., 2023b also found that for clouds with high surface density ($\Sigma_0 \approx 10^4\,{\rm M_\odot\,pc^{-2}}$), gas supply reaching the BH's accretion disk is sufficient to support hyper-Eddington accretion with $f_{\rm Edd} \equiv \dot{M}_{\rm BH}/\dot{M}_{\rm Edd} \sim 1000$ after considering the density and temperature criterion presented in Inayoshi et al., 2016.

More realistically, BH feedback mechanisms, like electromagnetic radiation (Fabian, 2012; Hopkins et al., 2016), winds/jets (Silk and Rees, 1998; Murray et al., 2005; Di Matteo et al., 2005; Sądowski et al., 2016; Torrey et al., 2020; Hu et al., 2022; Massonneau et al., 2023), and cosmic rays (CRs; Sijacki et al., 2008; Guo and Mathews, 2012; Zweibel, 2017; Su et al., 2021; Ishibashi and Fabian, 2023) will deposit energy and mechanical momentum back to the gas reservoir. The energy and momentum heat and deplete the gas fuel, or even prevent its infall to the BH (Dubois et al., 2013), potentially challenging the hyper-Eddington accretion scenario. Still, close to the BH ($\lesssim 1000\,r_{\rm Sch}$), at sufficiently high accretion rates and opacities, photons are effectively trapped with the inflow, which means the radiated energy (Watarai et al., 2000; Madau et al., 2014, and many other references in the second paragraph) will only grow sub-linearly with the accretion rate (measured as $\dot{M}_{\rm BH}/\dot{M}_{\rm Edd}$). This is also true for the mass outflow powered by radiation (Hu et al., 2022). As a result, the feedback strength at high accretion rates is suppressed and hyper-Eddington accretion remains possible.

Though BH feedback is not included in simulations of Shi et al., 2023b, there is an estimate in terms of radiative feedback based on the density criteria for hyper-Eddington accretion predicted by Inayoshi et al., 2016:

$$n_\infty \gtrsim 10^5 (M_{\rm BH}/10^4\,{\rm M_\odot})^{-1} (T_\infty/10^4\,{\rm K})^{3/2}\,{\rm cm^{-3}},$$

where n_∞ and T_∞ are the density and temperature of gas "near" the BH (at sub-pc scales). For BH samples in our simulations, especially those inside GMCs

with $\Sigma_0 \approx 10^4\,M_\odot\,pc^{-2}$, the ambient gas density is above this critical value, which suggests hyper-Eddington accretion may be achievable even if there is radiative feedback. Still, there is a necessity to include BH radiative feedback in simulations like Shi et al., 2023b for completeness since BH feedback may still affect GMC behaviors at larger scales. The influence of other forms of BH feedback, namely, mechanical feedback and cosmic rays on accretion is also to be determined.

In this article, we extend the discussion of Shi et al., 2023b and explore the impact of multiple BH feedback mechanisms, including radiation, mechanical outflow, and CRs. In particular, we are interested in how the BH feedback mechanisms determine the maximum mass a BH can reach from accretion, and how they scale in different GMCs. To reach the goal, we run a suite of numerical simulations by keeping the basic setups/physics involved in Shi et al., 2023b, but with a new sub-grid BH accretion and feedback model, as well as related physics.

The article is organized as follows. In § 4.2, we introduce the background and implementations of BH accretion and feedback in numerical simulations, as well as the simulation's initial condition and setups. In § 4.3 , we present the result with the fiducial feedback setups and explore the effects of different accretion/feedback physics. In § 4.4, we develop discussions and introduce caveats of our simulation. Finally, we conclude in § 4.5.

4.2 Background and method

Our simulation follows the same numerical framework for star formation and feedback as that in previous star-formation simulations (Grudić et al., 2018b; Grudić et al., 2018a; Grudić et al., 2021a) and the previous study of this series (Shi et al., 2023b). As a short summary, we use the meshless, Lagrangian, Godunov MHD code GIZMO[2] (Hopkins, 2015; Hopkins, 2016; Hopkins and Raives, 2016) in its Meshless Finite Mass (MFM) mode, including physics like self-gravity, radiative cooling, star formation, and feedback. In particular, star formation and feedback are based on the FIRE-2 implementation of the Feedback In Realistic Environments[3] (FIRE) framework (Hopkins et al., 2018a; Hopkins et al., 2023). Each "star" particle in the simulation represents an IMF-averaged ensemble of stars (more recent development based on GIZMO, the STARFORGE framework, is able to resolve single-star formation, evolution, and dynamics: Grudić et al., 2021b; Guszejnov et al., 2021), which evolves and deposits mass outflow, metals, and radiation back

[2] http://www.tapir.caltech.edu/~phopkins/Site/GIZMO.html
[3] http://fire.northwestern.edu/

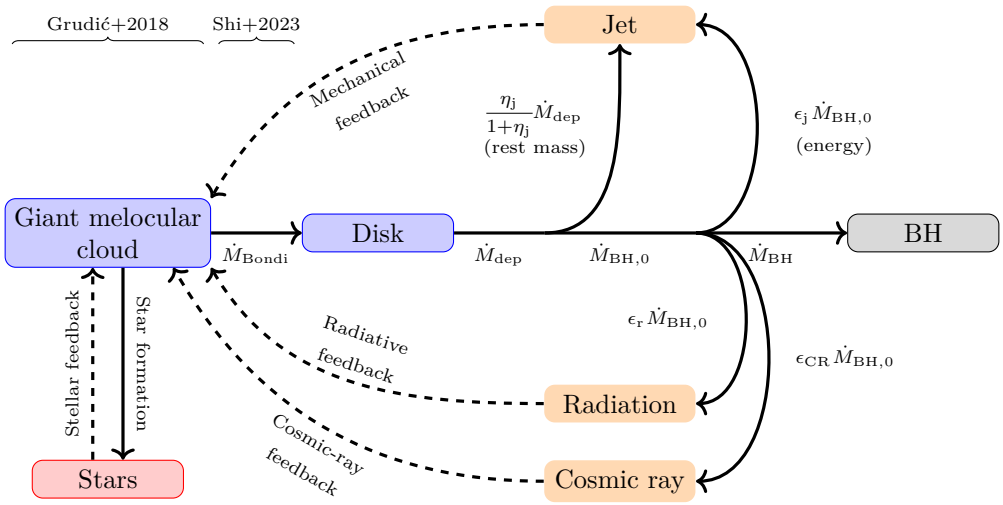

Figure 4.1: Mass and energy flow of BH accretion and feedback. This study is based on the framework of star formation in Grudić et al. (2018b) and BH accretion without feedback in Shi et al. (2023b). To implement BH feedback, we use a model of mass transfer from the disk to the BH. With only a fraction of the accretion flow going to the BH, other portions are deposited back to the GMC in the form of radiation, jets, and cosmic rays.

to the ISM as its feedback (Hopkins et al., 2018b). This treatment is proven successful in recovering the properties of star formation GMCs, like the star formation efficiency, star cluster dynamics, and cluster mass distribution and statures (Grudić et al., 2018b; Grudić et al., 2018a; Grudić et al., 2021a).

$M_{\rm cl}$ [$\rm M_\odot$]	$R_{\rm cl}$ [pc]	$t_{\rm ff}$ [Myr]	$m_{\rm gas}$ [$\rm M_\odot$]	$r_{\rm soft}^{\rm star}$ [pc]	$r_{\rm soft}^{\rm BH}$ [pc]	$\epsilon_{\rm j,c}$	$v_{\rm j,c}$ [km/s]	$N_{\rm BH}$	$M_{\rm BH}^{\rm ini}$ [$\rm M_\odot$]	Notes
10^6	5	0.19	3.8	0.41	0.31	9.6×10^{-7}	420	234	$10 - 10^3$	Low resolution
10^6	5	0.19	0.48	0.21	0.21	9.6×10^{-7}	420	234	$10 - 10^3$	High resolution
10^8	50	0.59	380	1.9	0.31	9.6×10^{-4}	13000	2000	$10^2 - 10^4$	Low resolution
10^8	50	0.59	48	0.96	0.31	9.6×10^{-4}	13000	2000	$10^2 - 10^4$	High resolution

Table 4.1: Properties of GMCs involved in this study. We chose some clouds in the "high surface-density" ($\Sigma_0 = 13000\,\rm M_\odot\,pc^{-2}$) group of Shi et al. (2023b), with the initial radius ($R_{\rm cl}$) of 5 pc or 50 pc. Each kind of GMC is simulated at high or low resolution. Starting from the third column, we show the initial free-fall time ($t_{\rm ff}$), gas mass resolution ($m_{\rm gas}$), softening radius for stars ($r_{\rm soft}^{\rm star}$) and BHs ($r_{\rm soft}^{\rm BH}$), characteristic jet energy efficiency ($\epsilon_{\rm j,c}$) and velocity ($v_{\rm j,c}$) derived from Eq. (4.4), number of BH seeds ($N_{\rm BH}$), and initial BH mass ($M_{\rm BH}^{\rm ini}$) for different kinds of simulations.

The simulation also follows the same scheme for BH accretion from gravitational capture as that in Shi et al., 2023b (a more delicate version is also in Grudić et al., 2021b): gas cells are captured by a BH if (i) they are within a preset "sink radius" near the BH, (ii) they are gravitationally bounded to the BH, and (iii) their individual Keplerain orbit is within the sink radius (Bate et al., 1995). Moreover, we choose the softening radius of BHs to be the same as its sink radius and set the value to make sure that the Bondi-Hoyle accretion radius is resolved (i.e., greater than the sink radius) for fast-accreting BHs, which is extensively discussed in Shi et al., 2023b.

For this study, we extend the BH accretion scheme with a sub-grid model of BH accretion to account for BH feedback. To help explain this, we present a schematic view of the simulation in Fig. 4.1. Accretion onto a BH can be decomposed into two successive phases: (i) the Bondi-Hoyle accretion of gas from the GMC (as a reservoir), or from $\sim$ pc to sub-pc scales, as studied in Shi et al., 2023b; (ii) the mass transfer from the BH accretion disk (as a secondary reservoir) to the event horizon, or from sub-pc to $\sim$ km (or $r_{\rm Sch}$) scales. Along with the accretion, gravitational energy is transformed into other forms of energy, like the internal energy and radiation.

At the second phase (smaller scales), not all of the mass/energy flows reach the BH: (i) some fraction of the accretion flow will be powered by kinetic/radiative pressure and form jets/winds; (ii) some fraction of the energy "leaks" from the disk and is deposited into the GMC, in the form of radiation and CRs. As a result, intuitively BH feedback mechanisms typically serve as negative factors that suppress the BH accretion in both two ways: (i) reducing the final mass transfer rate onto the BH due to energy and mass loss; (ii) preventing additional gas in GMC from infalling.

Moreover, there is thus a huge mismatch among the scales and physics involved, and the second process is beyond the resolution limit (~ 0.1 pc) of our MHD simulation. So a proper way is the sub-grid model, which synthesizing analytic expressions of the mass/energy outflow from theory or simulations of the second phase (e.g., Watarai et al., 2000; Sądowski, 2009; Madau et al., 2014; Sądowski et al., 2016; Hu et al., 2022). We add some sub-structures to the simple BH sink particle in Shi et al., 2023b: the BH sink particle accretes gas from the GMC by the Bondi-Hoyle accretion and store the mass inside a gas reservoir (or disk), then transfer the mass to the BH at a rate $\dot{M}_{\rm dep}$, which is also used to calculate mass and energy flow rates for different feedback mechanisms.

Details of the sub-grid model are expanded below, following the "order" of mass flow from the disk to the BH shown in Fig. 4.1. However, we note that the "order" is only

for the definition of quantities like the mass loading factor and energy efficiency, which is not in the chronological sense. Moreover, since the energy efficiency (defined as the ratio between the outflow energy and $\dot{M}_{\rm BH}c^2$) is typically very small (≤ 0.1) in the simulation, we treat $\dot{M}_{\rm BH,0}$ and $\dot{M}_{\rm BH}$ interchangeably in the simulation and the text (though $\dot{M}_{\rm dep}$ is indeed different from the two), without impacting our results at least in the order-of-magnitude sense.

Sub-grid models for BH accretion and feedback

Disk mass depletion

As shown in the flowchart Fig. 4.1, the mass flow from the GMC first arrives at the BH system at $\dot{M}_{\rm Bondi}$ and flows towards the central BH along the accretion disk. We assume the mass of the disk to be $M_{\rm d}$, and a BH system is a sink particle in the simulation, so $M_{\rm sink} = M_{\rm BH} + M_{\rm d}$. The characteristic disk-to-BH mass depletion time scale is $t_{\rm dep}$, so the mass depletion time scale is then given by $\dot{M}_{\rm dep} = M_{\rm d}/t_{\rm dep}$.

The classical way to describe the BH accretion disk is the thin disk model (Shakura and Sunyaev, 1973), where the accretion rate follows

$$\dot{M} \sim 2\pi\alpha \frac{\Sigma_{\rm d} c_{\rm s}^2}{\Omega_{\rm K}}. \tag{4.1}$$

Here $\Sigma_{\rm d}$, $c_{\rm s}$, and $\Omega_{\rm K}$ are respectively the surface density, sound speed, and Keplerian frequency at a certain radius of the disk; α is a dimensionless constant that is linear to the viscosity.

In our simulation, once a gas cell is bound to the BH, its mass will be added to the disk mass $M_{\rm d}$. We assume that in the sub-grid model, the mass elements spirals to the BH from the sink radius $r_{\rm sink}$. Since $\Sigma_{\rm d} \cdot \pi R^2 \sim M_{\rm d}$, with Eq. (4.1) we set

$$t_{\rm dep} = \frac{1}{2\pi\alpha} t_{\rm dyn,sink}. \tag{4.2}$$

Note that we redefined α by absorbing the factor of $(\Omega_{\rm K} r_{\rm sink}/c_{\rm s})^2$ and other constants. Here $t_{\rm dyn,sink} \equiv [r_{\rm sink}^3/G(M_{\rm BH} + M_{\rm d})]^{1/2}$ is the dynamical time scale of at the sink radius, which is the fastest possible mass-depletion time. By varying α we may bracket different conditions including slow and fast mass depletion rates.

We caution that for realistic BH accretion, the mass inflow rate can be dependent on the radius since there is mass outflow in the form of winds (Blandford and Begelman, 1999; Hu et al., 2022). Although in Eq. (4.1) we actually assume a scale-independent mass inflow rate, the effect of BH wind feedback is indeed considered

(the next subsection), where we assume only a fraction of the mass can reach the BH while the remaining are deposited back to the GMC in the form of wind and jet.

In the simulation, we also add other constraints on the BH mass transfer. We first set the maximum mass of the accretion disk, which is quantified by the upper limit of $M_{\rm d}/M_{\rm BH}$: once $M_{\rm d}$ reach the limit, no gas cells will be absorbed by the BH in the next time step. Secondly, there is also an upper limit on the Eddington ratio which is defined as $f_{\rm Edd} \equiv \dot{M}_{\rm BH}/\dot{M}_{\rm Edd}$. All these factors will have instant impacts on the BH accretion. In our parameter surveys, we vary the upper limit of $M_{\rm d}/M_{\rm BH}$ to study the effect of disk mass. Due to our particular interest in hyper-Eddington accretion which is predicted to be extreme (Inayoshi et al., 2020), we fix the upper limit of $f_{\rm Edd}$ to be 1000.

Mechanical feedback

In this simulation, we treat the mass and energy flow as shown in Fig. 4.1. A portion of the mass flows $\dot{M}_{\rm dep}$ will contribute to the rest mass of jets, while the rest is labeled as $\dot{M}_{\rm BH,0}$. We define the jet mass loading factor as $\eta_{\rm j} \equiv \dot{M}_{\rm j}/\dot{M}_{\rm BH,0}$, where $\dot{M}_{\rm j}$ is the jet mass outflow rate, which also follows $\dot{M}_{\rm j} = \dot{M}_{\rm dep} \cdot \eta_{\rm j}/(1+\eta_{\rm j})$.

On the other hand, the jet luminosity can be parameterized with a coefficient $\epsilon_{\rm j}$, such that $L_{\rm jet} = \epsilon_{\rm j}\dot{M}_{\rm BH,0}c^2$. The jet luminosity is also related to its outflow velocity $v_{\rm j}$. Under non-relativistic condition $L_{\rm j} = M_{\rm j}v_{\rm j}^2/2$, we find $v_{\rm j} = c\sqrt{2\epsilon_{\rm j}/\eta_{\rm j}}$.

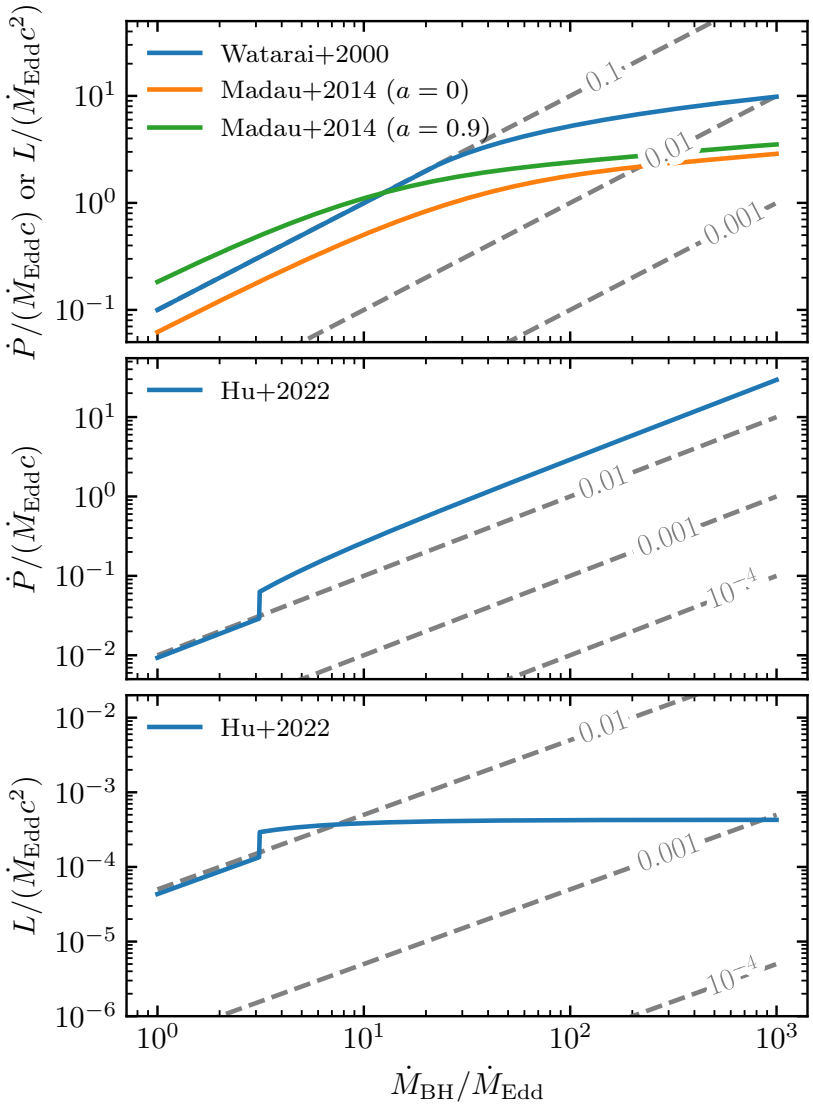

Figure 4.2: Sub-grid models for radiative feedback (top panel) and mechanical feedback (bottom two panels). *Top*: energy and momentum ejection rates as a function of accretion rates, the number on each dashed line is the radiative efficiency ($\epsilon_{\rm r} \equiv L/(\dot{M}_{\rm BH}c^2)$). For realistic models the feedback strength grows sub-linearly. *Middle and bottom*: energy and momentum ejection rates for mechanical feedback, here the number on each line is the jet velocity $v_{\rm j}/c$. In particular, we show the model in Hu et al. (2022), where the luminosity is almost constant but momentum grows linearly.

Physical process	Quantity	Fiducial setup	Variations	Notes
Disk mass depletion	α	0.1	0.01, 1	Effective viscosity
	$\sup(M_{\rm d}/M_{\rm BH})$	10	1	Disk mass threshold
Radiative feedback	$\epsilon_r' \equiv L_{\rm bol}/(\dot{M}_{\rm BH,0}c^2)$	"log-form" models	10^{-9} – 0.1	Radiative efficiency
	$Z/Z_\odot$	1	10^{-2}, 10^{-4}, 10^{-6}	GMC's initial metallicity
Mechanical feedback	$\epsilon_{\rm j} \equiv L_{\rm j}/(\dot{M}_{\rm BH,0}c^2)$	$\epsilon_{\rm j,c}$ (see Eq. 4.4)	10^{-8} – 0.1, Hu et al., 2022	Jet energy efficiency
	$\eta_{\rm j} \equiv \dot{M}_{\rm j}/\dot{M}_{\rm BH,0}$	1	9, 99	Jet mass-loading factor
Cosmic-ray feedback	$\epsilon_{\rm CR} \equiv L_{\rm CR}/\dot{M}_{\rm BH,0}$	0	10^{-8} – 0.1	CR energy efficiency

Table 4.2: Free parameters in our BH feedback sub-grid model. Along with the fiducial setup, we also study the impact of different physical processes by varying the corresponding quantities. "Log-form" models mean Watarai et al., 2000 or Madau et al., 2014.

To set up jet outflow velocities in the simulation, we consider a critical condition where the mechanical feedback energy is capable to disrupt the whole cloud, i.e., the accumulated jet energy fills the potential well of the GMC:

$$\int \epsilon_{\rm j} \dot{M}_{\rm BH,0} c^2 {\rm d}t \sim \frac{G M_{\rm cl}^2}{R_{\rm cl}}. \tag{4.3}$$

Treating $\epsilon_{\rm j}$ as a constant, we integrate over BH accretion history and find the LHS turns into $\epsilon_{\rm j} \Delta M_{\rm BH,0} c^2$, where $\Delta M_{\rm BH,0}$ is the total mass of gas reaching near the event horizon. We choose a characteristic value that $\Delta M_{\rm BH,c} = 10^4\,{\rm M}_\odot$. Then we define a characteristic coefficient of

$$\epsilon_{\rm j,c} = \frac{G M_{\rm cl}^2}{R_{\rm cl} \Delta M_{\rm BH,c} c^2} = \frac{M_{\rm cl}}{\Delta M_{\rm BH,c}} \left(\frac{v_{\rm cl}}{c}\right)^2. \tag{4.4}$$

Here $v_{\rm cl}^2 = G M_{\rm cl}/R_{\rm cl}$ is the characteristic circular velocity of the cloud. Following the energy argument we assumed above, if $\epsilon_{\rm j} \ll \epsilon_{\rm j,c}$ then the mechanical feedback is insignificant; while if $\epsilon_{\rm j} \gg \epsilon_{\rm j,c}$ then the strong mass outflow may disrupt the GMC quickly. It also implies the critical jet velocity at the critical jet luminosity: $v_{\rm j,c} = v_{\rm cl}\sqrt{M_{\rm cl}/\Delta M_{\rm BH,c}}$.

In our simulations, our default assumption is fixing energy efficiency $\epsilon_{\rm j}$ for all BHs for all periods in the simulation, which follows the same form as Sądowski et al., 2016, though they further proposed that $\epsilon_{\rm j} = 1.3 f_{\rm MAD} a^2$ where a is the BH spin and $0 \leq f_{\rm MAD} \leq 1$ is a prefactor from the magnetically arrested accretion disk (MAD) model. Alternatively, Hu et al., 2022 proposed a sub-grid model for super-Eddington accretion ($\dot{M}_{\rm BH}/\dot{M}_{\rm Edd} \gg 10$) where the mass outflow velocity and mass loading factor are dependent on the actual BH accretion rate: [4]

$$\eta_{\rm j} = \dot{m} - 1, \qquad v_{\rm j} = 3 \times 10^{-2}\, c \dot{m}^{-1}. \tag{4.5}$$

Here $\dot{m} \equiv \dot{M}_{\rm BH}/\dot{M}_{\rm Edd}$ (but note the original equations are in term of $\dot{m}_0 = \dot{M}_{\rm dep}/\dot{M}_{\rm Edd}$, and $\dot{m}_0 \doteq \dot{m}^2$). With the setup we $L_{\rm j}$ is almost a constant in the hyper-Eddington regime ($\dot{m}_0 \gg 10$ or $\dot{m} \gg \sqrt{10} \approx 3$), though the momentum ejection rate $\dot{M}_{\rm j} v_{\rm j}$ is still linear. In this study, we also include this variety when $\dot{m}_0 \geq 10$ for completeness. For the regime of $\dot{m}_0 \leq 10$, we choose the fiducial setup $\eta_{\rm j} = 1$ and fix $v_{\rm j} = 0.01\,c$. See Fig. 4.2 for the comparison of different models.

Our simulation includes mechanical feedback in the form of bipolar, collimated, and constant-velocity jets from BHs. We evaluate and save the mass for ejection after

[4] We made some approximations like $17^2 \approx 17.5^2 \approx 300$ without changing orders of magnitude.

each time step. Once that mass exceeds a preset characteristic mass $2m_{\rm jet}$, two new gas cells (each with mass $m_{\rm jet}$, and $m_{\rm jet} \lesssim m_{\rm gas}$ for all simulations) are created and spawned in opposite directions which are determined by the angular momentum of the ambient gas. The implementation is described in Torrey et al., 2020 and also applied to other studies like AGN jets (Su et al., 2021) and protostellar jets (Grudić et al., 2021b).

Radiative feedback

Radiation is another form of feedback that may affect the surrounding gas medium by heating and momentum deposition. In our simulations, BH radiative feedback effects include HII heating (Hopkins et al., 2018b), Compton heating (Hopkins et al., 2016), and photon momentum (Hopkins et al., 2018b).

The strength of the radiative feedback for a BH is described by the bolometric luminosity $L_{\rm bol}$. To further quantify $L_{\rm bol}$ with the BH accretion rate, we defined the radiative efficiency $\epsilon_{\rm r}' \equiv L_{\rm bol}/(\dot{M}_{\rm BH,0}c^2)$. In literature, the radiative efficiency can also be defined with the Eddington accretion rate: $\epsilon_{\rm r} \equiv L_{\rm bol}/(\dot{M}_{\rm Edd}c^2)$. Analytical studies and simulations have shown that due to the photon-trapping effect on small scales near BHs, the bolometric luminosity grows slowly with increasing accretion rate (can be rescaled as $\dot{m} \equiv \dot{M}_{\rm BH,0}/\dot{M}_{\rm Edd}$), typically in a logarithm form. Due to this reason, super-Eddington accretion is not limited by the radiative energy loss (Madau et al., 2014).

In our simulation, we choose two kinds of “realistic" radiative efficiency forms from the literature. The first one by Watarai et al., 2000 is analytically derived from the thin disk model, which features a linear $\epsilon_{\rm r}$ at low $\dot{m}$ (equivalently $\epsilon_{\rm r}' = 0.1$) and a logarithm form at high $\dot{m}$. Another form is fitted by Madau et al., 2014 from original simulations of relativistic slim disks in Sądowski, 2009, which also features dependence on the BH spin parameter a. We set $a = 0$ for this variety in our simulation since Madau et al., 2014 also found that the super-Eddington accretion e-folding time is nearly independent of a. Moreover, we also include constant $\epsilon_{\rm r}'$'s to study the scaling of the BH radiative feedback.

Cosmic ray

Cosmic rays are relativistic charged particles that stream and diffuse inside the gaseous medium, which affects the medium through scattering and Lorentz force, which may produce strong winds in the ISM (e.g., Zweibel, 2017). Previous

simulations also demonstrated the importance of CR-driven jets/winds produced by AGNs (Sijacki et al., 2008; Guo and Mathews, 2012; Su et al., 2021). In addition, CRs also lose energy due to Coulomb interactions, ionization, and catastrophic losses, which also heat the gas (e.g., Guo and Oh, 2008). This can thus be another limiting factor of BH accretion.

In this study, we simulate CRs based on implementations described in Hopkins et al., 2022a, while simpler implementations of the zeroth-moment CR transport are introduced in Chan et al., 2019; Hopkins et al., 2020a. We assume that CR particles are ultra-relativistic, resulting in an adiabatic index $\gamma_{\rm CR} = 4/3$. The CR streaming and diffusion are determined by a set of two-moment equations with an additional closure equation similar to the M1 closure approximation, and keeps the leading terms of $O(u/c)$ (where u is the typical speed of gas), as described in Hopkins et al., 2022a. The governing equations used for our simulation are further integrated over the CR momentum spectrum (Hopkins et al., 2022a) for considerations in computational costs, thus there is no CR spectral evolution. We input a fiducial effective diffusion coefficient of $\kappa_{\rm CR} \sim 10^{29}\,{\rm cm}^2/{\rm s}$ to quantify the scattering rates. CR heating effects are also implemented in the simulation.

In our simulations, CR feedback from BHs is coupled alongside the mechanical feedback (i.e., the newly spawned jet cells). We vary the strength of the BH CR feedback through its energy-loading coefficient $\epsilon_{\rm CR}$, defined from $L_{\rm CR} = \epsilon_{\rm CR}\dot{M}_{\rm BH,0}c^2$. Additionally, for each simulation with the BH CR feedback, we set a constant CR energy ejection rate of 10% for supernovae to account for the CR feedback from stars. This particular effect is not considered in other sets of simulations without CRs.

Simulation setups

Similar to that in Shi et al., 2023b we run a suite of simulations of BH accretion in GMCs, but there is feedback physics as mentioned above. We also follow the same initial condition (IC) for GMCs as Shi et al., 2023b, but only choose GMCs with the highest initial surface density ($\Sigma_0 = 13,000\,M_\odot/{\rm pc}^2$) with different radii (5 or 50 pc) and therefore, different masses (10^6 or $10^8\,{\rm M}_\odot$). The clouds are initially with the solar metallicity ($Z_\odot$) in the fiducial case. The ICs are listed in Table 4.1. The time limit for each simulation is $2.5\,t_{\rm ff}$, where $t_{\rm ff} = [R_{\rm cl}^3/(8GM_{\rm cl})]^{1/2}$ is the initial free-fall time of the cloud. For each mass group, there are low (initially with 64^3 equal-mass gas cells) and high (128^3) resolution runs. Setups of the softening radius are described in Shi et al., 2023b.

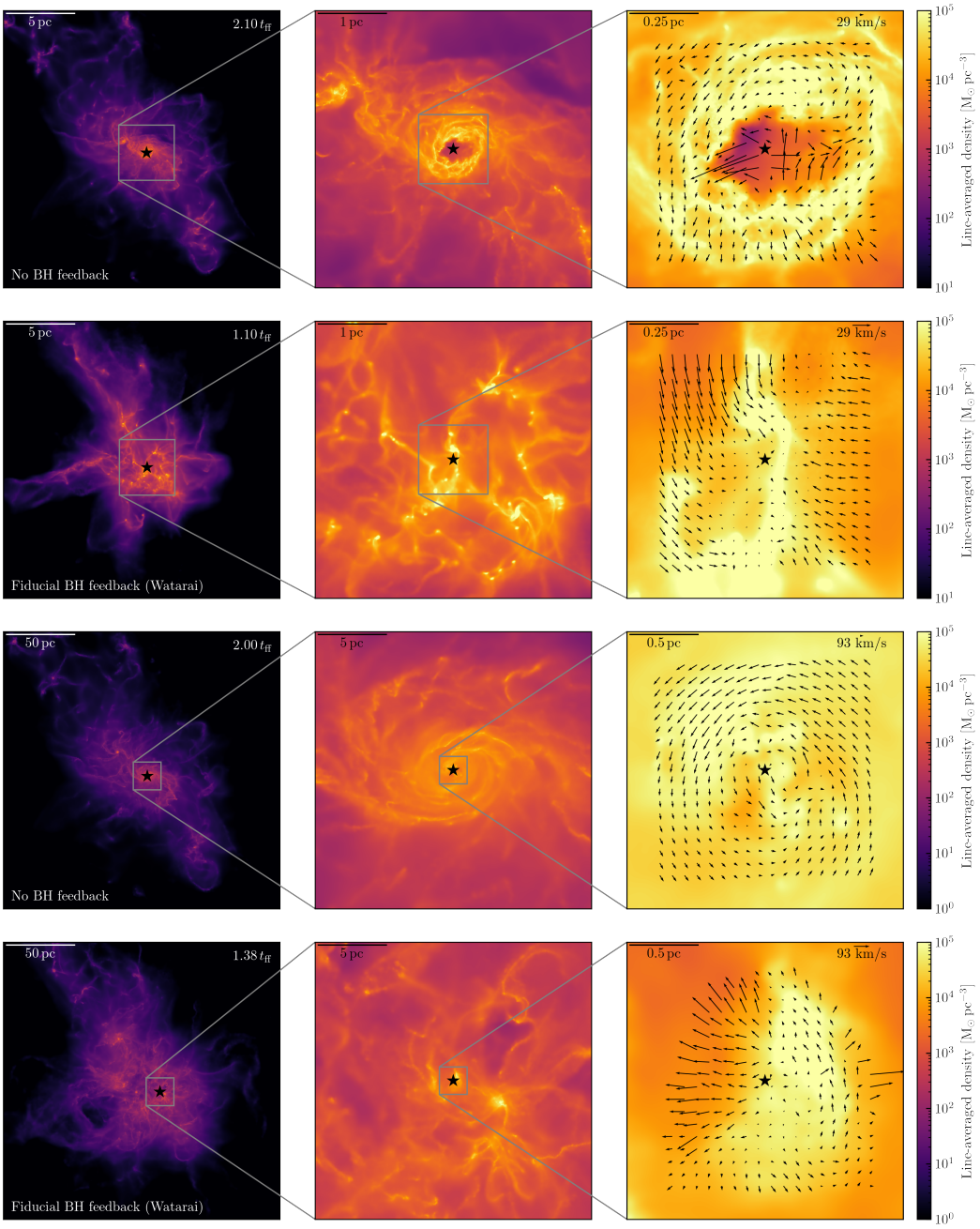

Figure 4.3: Comparisons between simulations with and without BH feedback physics. *Top two rows*: Gas morphology for the $10^6\,M_\odot$ GMCs with or without BH feedback. From left to right, we zoom in at a BH undergoing hyper-Eddington accretion. As the smallest scale, we also show the velocity field near the BH, with the circular velocity ($\sqrt{GM_{\rm cl}/R_{\rm cl}}$) presented for reference. *Bottom two rows*: the same as the first two rows, but for the $10^8\,M_\odot$ GMC.

Each simulation initializes with a number of BH seeds with random mass, position, and velocity, which are sampled following the same way as Shi et al., 2023b: BHs are randomly distributed following uniform spatial distribution within the volume; the initial velocity magnitude is confined below the local circular velocity (for discussions of these choices, see Shi et al., 2023b). In particular, the BH mass follows log-uniform distribution within 10 (100) – 1000 $M_\odot$ (10^4 $M_\odot$) for the 10^6 $M_\odot$ (10^8 $M_\odot$) cloud, which covers the range of stellar-mass BHs and IMBHs.

The independent parameters to quantify the BH feedback are listed in Table 4.2. For each parameter, we set a fiducial value as the baseline, which assumes the radiative-inefficient accretion model of Watarai et al., 2000 and generates the "fiducial" result of this paper. Moreover, there are also several variations to reflect the impact of the related physics. These variations are run mainly with low-resolution simulations as shown in Tab. 4.1, they will compose the "parameter survey" part of our results. For each parameter survey, we only vary the corresponding parameter while keeping others with their fiducial values.

4.3 Results

Fiducial results: radiative-inefficient models

In this section, we compare the two conditions with and without BH feedback, which connects this work with the previous one (Shi et al., 2023b). To "disable" BH feedback and reproduce the setup in Shi et al., 2023b, we set very small energy efficiency for all mechanisms, i.e., $\epsilon_\mathrm{r} = 10^{-5}$, $\epsilon_\mathrm{j}/\epsilon_\mathrm{j,c} = 10^{-5}$, and $\epsilon_\mathrm{CR} = 0$. However, there is still a slight difference due to the subgrid model: in these new runs, we distinguish $\dot{M}_\mathrm{sink}$ and $\dot{M}_\mathrm{BH}$, which was disregarded in our previous work.

As the first impression, Fig. 4.3 shows the gas morphology at different scales. From left to right, we zoom in at a BH experiencing significant mass accretion. The particular BH accreted the most mass throughout the simulation time range, and the snapshot to be shown is also chosen when the BH is in its fastest-accreting phase. Each panel shows the line-averaged density, which is defined as $(\int \rho(s)\mathrm{d}s)/L$, where L is along the line-of-sight direction and equals 1.5 times the field of view (FOV) of the panel. At the smallest scales (panels in the right column), we evaluate $\mathbf{v}_\mathrm{gas} - \mathbf{v}_\mathrm{BH}$ and show the velocity field within a thin layer of 1/8 FOV (centered at the BH) on top of the density field.

As was also suggested in Shi et al., 2023b, the fast-growing BH seed is near a dense clump of the GMC ($\rho \sim 10^5$ $M_\odot/\mathrm{pc}^3$, typically more than 100 multiples denser than

the mean density). Overall, there is also $|\mathbf{v}_{\rm gas} - \mathbf{v}_{\rm BH}| < |\mathbf{v}_{\rm BH}|$ which ensures efficient gravitational capture of gas. Despite feedback from BHs, these features are also observed in corresponding simulations of both $10^6\,{\rm M}_\odot$ and $10^8\,{\rm M}_\odot$ GMC, which also fit the expectations of the Bondi-Hoyle theory (Bondi, 1952; Shi et al., 2023b).

In the absence of BH feedback, the gas in the simulations is relatively condensed. Additionally, near the accreting BH without feedback (see the first and third row of Fig. 4.3), there are features like disks and spiral arms at $\sim$ pc scales at late times, which means that there is coherent gas inflow due to the potential well of the GMC. At this time, there is also star formation in the $10^6\,{\rm M}_\odot$ GMC near the BH, creating a cavity in the gas distribution (see the first row of Fig. 4.3), though not observed in the $10^8\,{\rm M}_\odot$ GMC through the simulation time. In contrast, when feedback turned is on, additional bubbles and dispersions appear and the inflow is relatively incoherent.

We quantify the BH accretion in Fig. 4.4. For each simulation, we first track the mass evolution of each BH seed and define the accreted mass as $\Delta M(t) = M(t) - M_{\rm BH,ini}$, where $M(t)$ can either be the BH-only mass or the sink-particle mass (BH+disk). Then we check the evolution of the BH with the most significant mass growth ($\Delta M^{\rm max}$), as well as the mean accreted mass of all the BHs ($\Delta M^{\rm mean}$, to count the "overall" BH accretion). Similar to that in Shi et al., 2023b, single BHs acquire steep mass growth when they encounter dense clumps, while the accretion rate is low in most of the evolution. The mean mass accretion is more steady after synergizing the evolution of all BHs. There is also $\Delta M^{\rm max} \approx N_{\rm BH}\Delta M^{\rm mean}$ at the final stage of the evolution, which means that mass accretion in the BH seed population is dominated by the one with the most significant contribution.

When there is BH feedback, we see little difference in $\Delta M^{\rm mean}_{\rm sink}$ at the early stage of the evolution when the BH accretion rate is low. Once the BH feedback is strong, the overall mass accretion is then suppressed. Due to the timescale for mass transfer from the disk to the BH, there is a "phase lag" between $\Delta M_{\rm BH}$ and $\Delta M_{\rm sink}$. At the late time, for a single BH, if there is no further accretion from the cloud onto the sink we see $\Delta M_{\rm BH}$ and $\Delta M_{\rm sink}$ converge.

For single BHs, we present BH mass accretion rates $\dot{M}_{\rm BH}$ (the actual accretion rate arriving at the BH) in Fig. 4.5. We scale the rate in the unit of the Eddington rate for each BH. Here we only show 5 BHs with the most amount of mass accretion for each simulation. These samples typically reach hyper-Eddington accretion abruptly at some time in their evolution and maintain the status for a short period of time ($\sim 0.1\,t_{\rm ff}$), which is capped by the upper limit set in the code. Once the fast

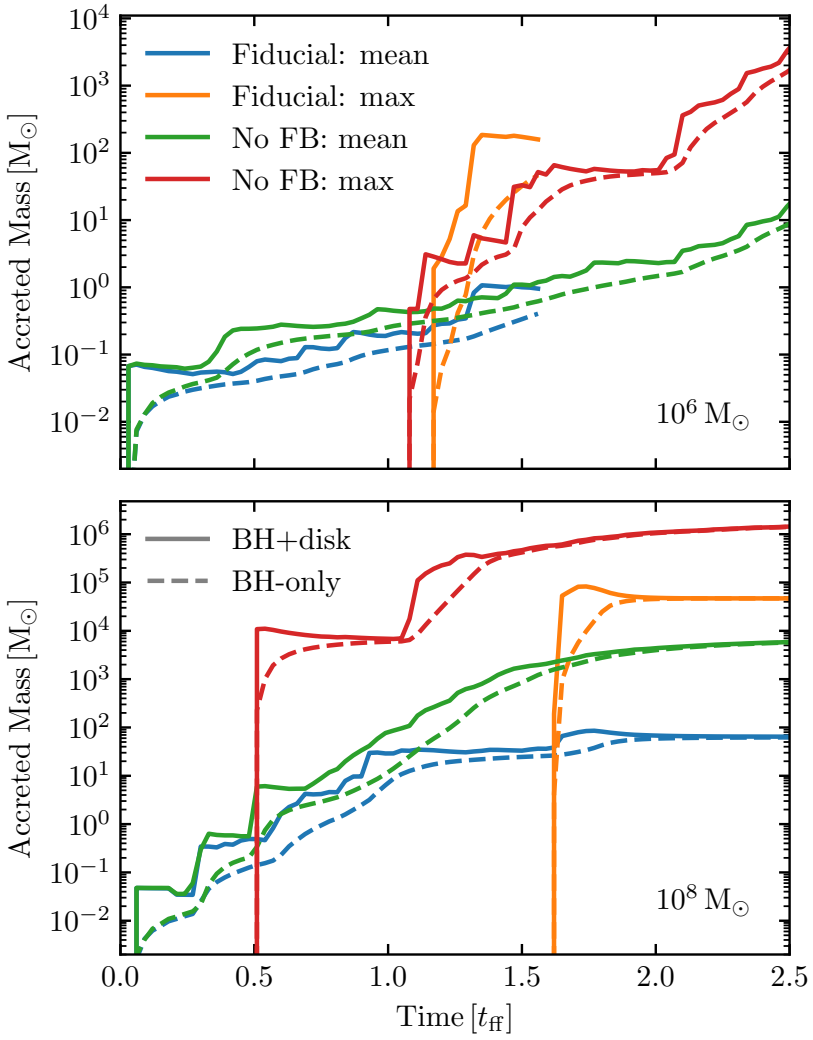

Figure 4.4: Mass evolution for BH particles in different GMCs. In each panel, we show the accreted mass of average BHs and a single BH with the most significant mass growth. We also distinguish between the mass arriving at the BH system (BH+disk, solid lines) and the BH itself (dashed lines).

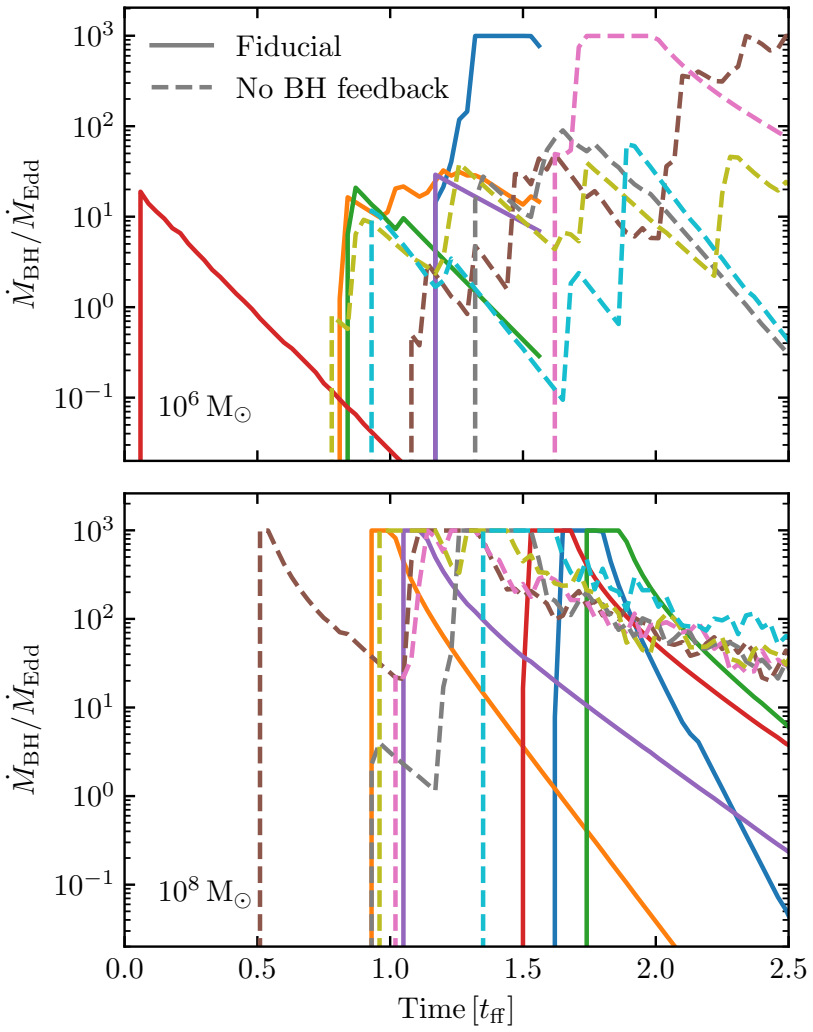

Figure 4.5: Eddington ratios for BH in different GMCs and feedback setups. Here we choose 5 BHs with the most significant mass growth in each simulation.

accretion phase is terminated, the mass transfer from the disk to the BH remains with the characteristic scale of t_{dep} as defined in § 4.2.

We also find that the Eddington ratio for BHs with feedback is lower than those without feedback. Especially at the late phase of the simulation, the no-feedback case has a period with sustaining Eddington ratio of $\sim$ 10 – 100, which is due to gas inflow under GMC's self-gravity and BHs' gravity. This is also visualized in Fig. 4.3.

Thus, from Fig. 4.5, there is evidence that hyper-Eddington accretion is achievable for BHs in the dense GMCs we simulated, even if a BH feedback model (radiative-

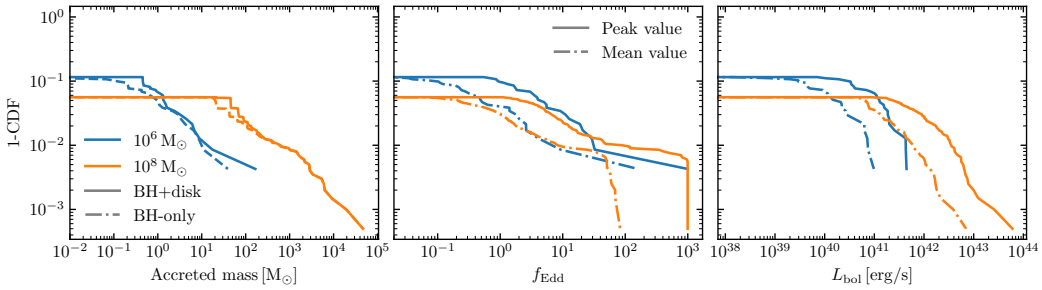

Figure 4.6: Cumulative distribution function (CDF) of the accreted mass, Eddington ratio, and bolometric luminosity for BH populations in simulations. Only simulations with the fiducial BH feedback setups are shown here. In the right two panels, we show the distribution of both peak and time-averaged values throughout the evolution.

inefficient accretion flow, "intermediate" kinetic outflow, no cosmic-ray feedback). However, the BH feedback indeed has a negative impact on accretion. We will quantify the impact through a series of experiments in § 4.3.

In Fig. 4.6 we show the cumulative distribution function (CDF) of $\Delta M_{\rm BH}$ and $\Delta M_{\rm sink}$ measured from simulations. Since the mass resolution is fixed at $m_{\rm gas}$ in the simulation, it also set a cutoff at the horizon axis of the CDF (in parallel, this is also because the radius of gravitational influence for BH without fast accretion is also not resolved beyond the scale resolution limit). The number of BH seeds, on the other hand, determines another cutoff in the vertical axis. Within the resolution of the simulations, only a small fraction ($\lesssim 10\%$) of BH seeds have mass accretion. Comparing the two GMCs, we find that BHs in the 10^8 M$_\odot$ GMC have much more significant mass growth.

We then check other properties, like the Eddington ratio $f_{\rm Edd}$ (what was partly displayed in Fig. 4.5). We present both the peak and time-average values. We find that the difference between the two GMCs is not significant in this comparison: $\sim 1\%$ of BH seeds reach the preset cap (1000). When averaged over the evolution history, there are still $\sim 1\%$ BHs reaching a high Eddington ratio (~ 100).

We also check the bolometric luminosity from radiative feedback, defined as $L_{\rm bol} = \epsilon_{\rm r}(f_{\rm Edd})\dot{M}_{\rm BH}c^2$. As expected from the first panel, there is a significant difference between BHs in the two GMCs. For the 10^6 M$_\odot$ GMC, BHs with accretion typically emit radiation at $\sim 10^{41}$ erg/s through their evolution, while the value can be $\sim 10^{43}$ – 10^{44} erg/s for the 10^8 M$_\odot$ GMC.

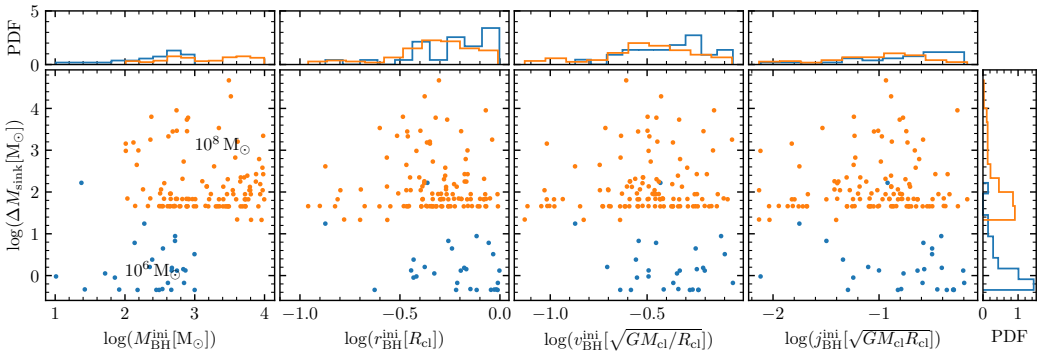

Figure 4.7: Dependence of BH accretion on initial conditions of BHs. From the left to the right, we plot BHs with accretion in a phase space of the accreted mass ($M_{\rm sink}$) versus The initial mass ($M_{\rm BH,ini}$), distance to the GMC center ($r_{\rm BH,ini}$), velocity ($v_{\rm BH,ini}$), and specific angular momentum ($j_{\rm BH,ini}$), in the unit of GMC quantities. The data is from the fiducial BH accretion/feedback setups but different initial masses (10^6 M$_\odot$ and 10^8 M$_\odot$). We note that for BH accretion is stochastic because of the turbulent nature of GMC evolution, and there is only shallow dependence (if any) on initial conditions studied here.

For BHs in these two GMCs, despite that the CDFs of $\Delta M_{\rm BH}$ and $L_{\rm bol}$ are significantly different, CDFs of $f_{\rm Edd}$ are similar. As a result, we infer that BHs in the two GMCs have a similar level of super-Eddington accretion, while other differences in the initial conditions, like BH seeds' initial masses (seeds in the 10^6 M$_\odot$ GMC is typically one order of magnitude lighter) and GMC's dynamical time (characterized with $t_{\rm ff}$) determines the difference in the mass growth.

In the previous work (Shi et al., 2023b), we demonstrated with experiments that there is shallow dependence on the initial properties of BH seeds, like their initial mass, position, and velocity magnitude. Similarly, we present such dependence for our new simulations by checking $\Delta M_{\rm sink}$ for each BH at the end of the simulation. In each panel of Fig. 4.7, we list BH's initial mass, radii from the GMC's center, velocity magnitude, and the specific angular momentum. Again, for both the 10^6 M$_\odot$ and 10^8 M$_\odot$ cloud, there is no (or little) correlation with $\Delta M_{\rm sink}$. The result means that BH accretion in a turbulent environment is stochastic and much information from the initial condition is smeared in the process.

Parameter survey: effects of different physics

To check the effects of different physics, we perform a parameter survey by varying parameters in our sub-grid model, as listed in Tab. 4.2. Due to considerations in computational costs, we perform these simulations with low resolution (see Tab. 4.1).

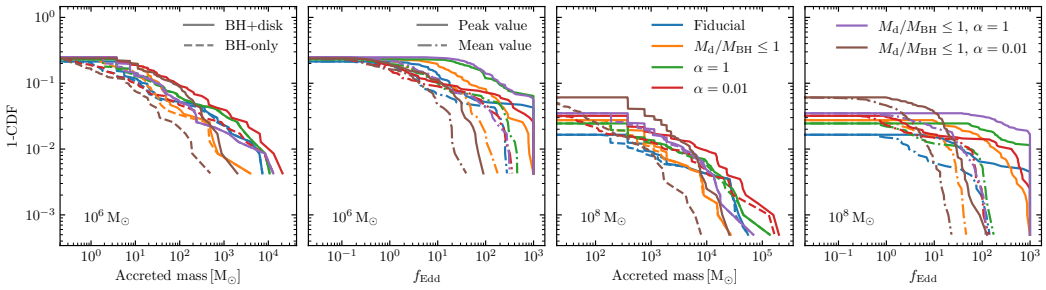

Figure 4.8: Parameter survey of the α-disk model. Here we vary the α parameter and the upper limit of disk mass. In the fiducial case, $\alpha = 0.1$ and $M_{\rm d}/M_{\rm BH} \leq 10$.

For the fiducial setups, we still choose the radiative-inefficient models but switch to Madau et al., 2014 with fixed $a = 0$, which is in a less feedback-dominated regime than Watarai et al., 2000 (as will be shown later in this section), thus feedback effects from jets and cosmic rays can be better identified.

Disk mass depletion

In Fig. 4.8 we show the effect of free parameters in the disk mass depletion: the upper limit of $M_{\rm d}/M_{\rm BH}$, and the effective α parameter for viscosity. In this plot, we show the CDF of the change in BH+disk and the BH-only mass, as well as the CDF of the Eddington ratio for BHs through evolution. Comparing the fiducial case, with $M_{\rm d}/M_{\rm BH} \leq 1$ the accreted mass is lower by a factor of ~ 10, and fewer BHs can reach hyper-Eddington accretion. This is a natural consequence of the smaller disk mass, which means that less mass can reach the BH+disk system.

Then we test higher (1) or lower (0.01) values of the α parameter, in contrast with the fiducial one (0.1). As shown in Eq. (4.1), smaller α means slower mass transfer from the disk to the BH, this is true in our tests: by fixing $M_{\rm d}/M_{\rm BH} \leq 10$, there is a larger deviation between the BH+disk curve and the BH-only curve in the mass CDF once α is smaller, and the Eddington ratio is typically lower for smaller α. The trend is also true for tests with fixed $M_{\rm d}/M_{\rm BH} \leq 1$.

The parameter α also affects the mass accretion onto the BH+disk system in the simulation. If α is low, the feedback is also weaker due to less mass reaching the BH; if α is high, mass depletion from the disk is efficient and the disk mass can be supplemented quickly in a very gas-rich environment. Both effects are positive factors for accumulating more mass in the BH+disk system. This argument is also reflected in Fig. 4.8 when comparing tests with different α, where $\alpha = 1$ and

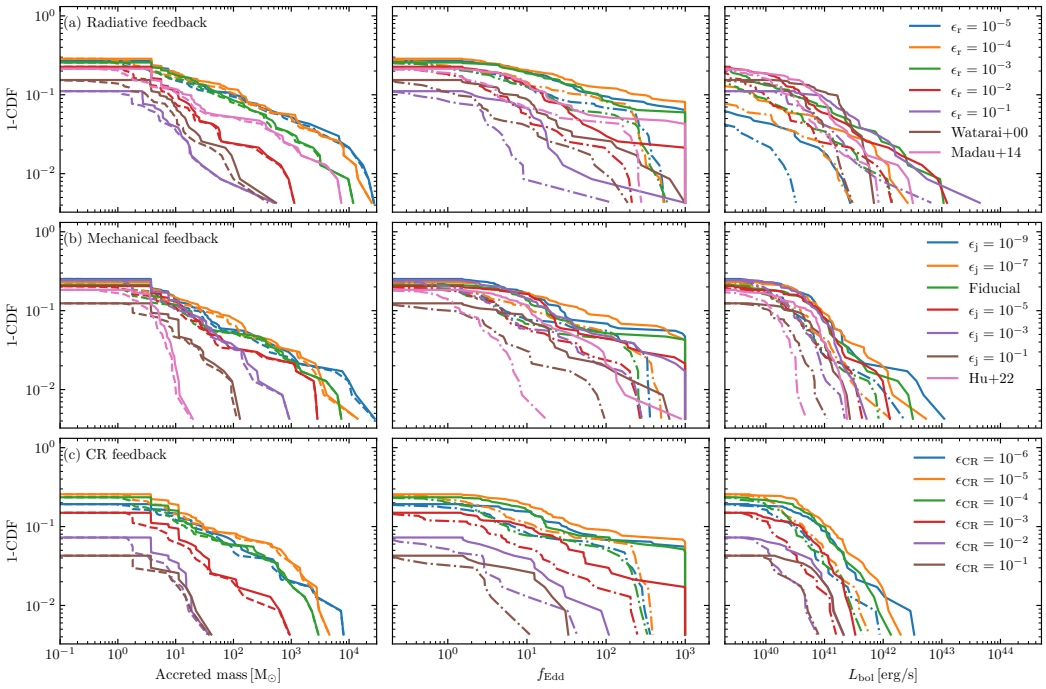

Figure 4.9: Parameter survey of the energy efficiency in different feedback mechanisms based on experiments with the $10^6\,M_\odot$ GMC. From left to right, the three columns show the CDF of accreted mass (solid: BH+disk, dashed: BH-only), $f_{\rm Edd}$ (solid and dot-dashed for maximum and average values through the evolution, respectively), and $L_{\rm bol}$ (line styles are defined the same way as $f_{\rm Edd}$). Each row is for a set of simulations of a specific feedback mechanism (labeled in each left panel), with legends shown in each right panel.

$\alpha = 0.01$ tests sometimes have more mass accretion than the fiducial $\alpha = 0.1$ case.

Radiative feedback

We study the effect of radiative feedback by varying its energy efficiency $\epsilon_{\rm r}$. As our fiducial setup, we include two "log-form" radiative-inefficient models from Watarai et al., 2000 and Madau et al., 2014, then set fixed $\epsilon_{\rm r}$ at 10^{-9} – 0.1. Similar to the layout of Fig. 4.6, the top panels of Fig. 4.9 and Fig. 4.10 show the CDF of accreted mass, the Eddington ratio, and the bolometric luminosity of the BH population.

Comparing fixed-value energy efficiencies, there is a clear trend that once $\epsilon_{\rm r} \gtrsim 10^{-3}$ (10^{-1}) for the $10^6\,M_\odot$ ($10^8\,M_\odot$) GMC, the accretion onto BHs is suppressed. The same behavior appears in the Eddington ratio. Despite relatively strong feedback, there are 1% of BHs reaching the preset cap in the Eddington ratio in many simulations, while the fraction of these BHs drops when the feedback is strong. Finally,

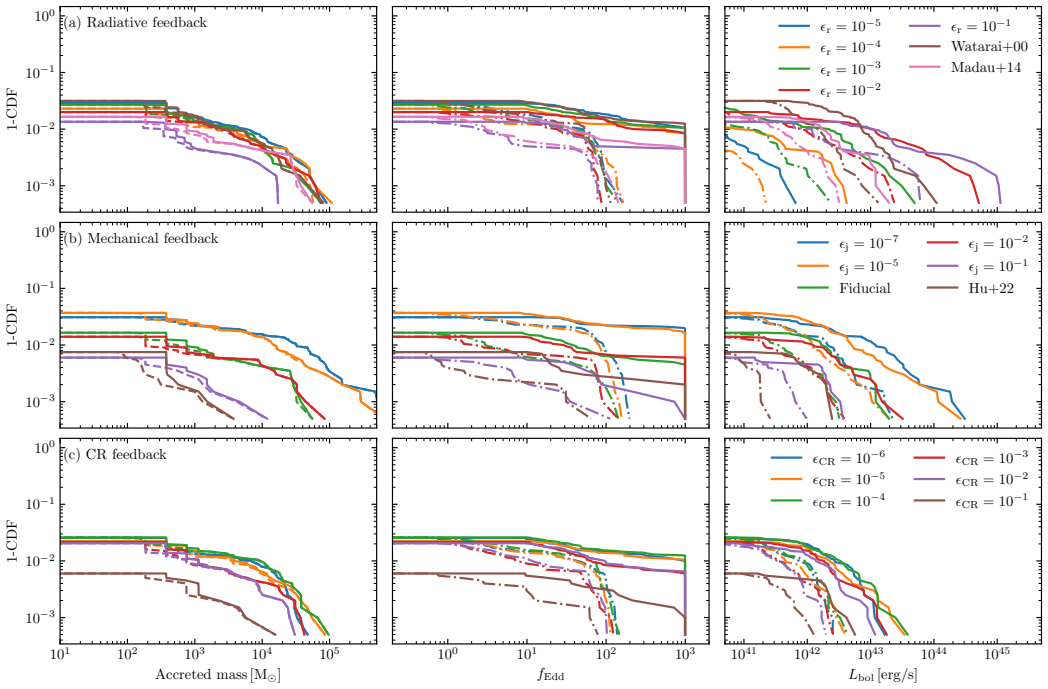

Figure 4.10: Parameter survey of the energy efficiency in different feedback mechanisms based on experiments with the 10^8 $M_\odot$ GMC. Conventions are the same as that in Fig. 4.9.

the luminosity of BHs typically increases with radiative efficiency as expected.

As also shown in Fig. 4.2, the radiative efficiency at high accretion rates ($f_{\rm Edd}$ = 1000) can be as low as 3×10^{-2} for Madau et al., 2014 and 10^{-2} for Watarai et al., 2000. Comparing simulations with fixed-value efficiencies, we find that these radiative-inefficient models behave closely like those with fixed $\epsilon_{\rm r} = 10^{-3}$ and $\epsilon_{\rm r} = 10^{-2}$ respectively. The feedback strength is thus mainly dominated by the hyper-Eddington regime for these models. As the result, the Madau et al., 2014 model is less feedback-dominated.

We further study the impact of the GMC's initial metallicity. In the no-BH-feedback limited studied in Shi et al., 2023b, experiments with different initial metallicity found no (or little) correlation between BH accretion and the initial metallicity. However, higher metallicity means tighter coupling between the radiation and wind due to more dust grains in the ISM, which may imply stronger radiative pressure (e.g., Larson and Starrfield, 1971), which is one of the radiative feedback mechanisms (alongside with heating and photoionization) implemented in the simulation. In this study, we vary the initial metallicity for two kinds of radiative models: the

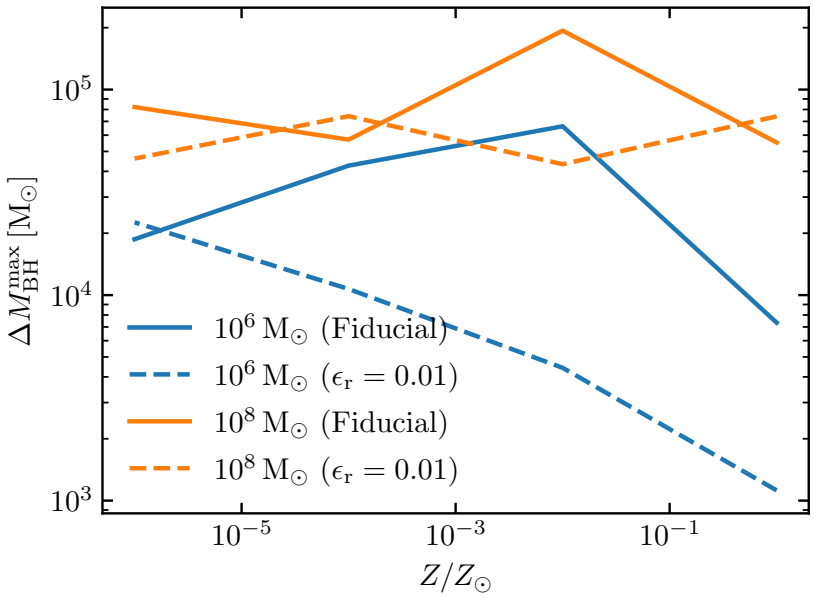

Figure 4.11: The impact of the initial metallicity on BH accretion. The initial metallicity is varied from 10^{-6} $Z_\odot$ to $Z_\odot$ in simulations with different GMC masses and BH radiative-feedback models.

fiducial Madau et al., 2014 model and the fixed-value $\epsilon_{\rm r} = 0.01$ model (which is in the strong feedback limit). In Fig. 4.11, we plot the maximum accretion in the BH population as a function of the initial metallicity. For most possible combinations of the initial GMC masses and feedback models, there is still no strong dependence on the metallicity. One exception is the 10^6 M$_\odot$ GMC with fixed $\epsilon_{\rm r} = 0.01$, there is a clear trend that BH accretion drops as the metallicity increases.

This can be explained with the aid of Fig. 4.9 and Fig. 4.10. For the 10^8 M$_\odot$ GMC, both radiative-feedback models above are in the weak-feedback limit even at the solar metallicity (since the CDF of BH mass accretion is close to that with $\epsilon_{\rm r} = 10^{-6}$). However, for the 10^6 M$_\odot$ GMC, the $\epsilon_{\rm r} = 0.01$ model is in a "strong" feedback limit as its CDF of mass accretion significantly deviates from the fiducial case. As a result, the GMC metallicity becomes important for that condition.

Mechanical feedback

Mechanical feedback is also presented in the second rows of Figs. 4.9 and 4.10. For models with fixed mass loading factoring $\eta_{\rm j} = 1$, we again see the trend that the accretion onto black holes is suppressed once the energy efficiency is high, this happens at $\epsilon_{\rm j} \gtrsim 10^{-5}$ for both GMCs. These "transition points" happen at lower

energy than in the radiative feedback simulations. In terms of $f_{\rm Edd}$, we find the BHs can not reach the maximum value once $\epsilon_{\rm j} \approx 1$. All these simulations assume the radiative feedback efficiency following Madau et al., 2014, we find the bolometric luminosity decreases when the mechanical feedback is stronger, as expected.

The model presented in Hu et al., 2022 is special. Although its energy efficiency is $10^{-3} - 10^{-2}$ depending on the accretion rate, the accretion rate is highly suppressed: the maximum accretion ($\Delta M_{\rm BH}^{\rm max}$) is even lower than the strong-feedback case with $\epsilon_{\rm j} = 0.1$. Despite that the energy efficiency is relatively low, the model has a strong momentum outflow that scales like $\dot{P} \geq 0.01 f_{\rm Edd} \dot{M}_{\rm Edd} c$ (see Fig. 4.2), resulting very strong BH feedback. Moreover, the fraction of mass flow reaching the BH is low ($1/f_{\rm Edd}$ in the hyper-Eddington phase), making the BH hard to grow. Instead, a much more significant fraction of the material is ejected as mechanical outflow.

Given the fiducial radiative feedback model (Madau et al., 2014), we estimate the bolometric luminosity. The typical luminosity is $10^{41} - 10^{42}$ erg/s for BHs in the 10^6 M$_\odot$ GMC, and $10^{42} - 10^{44}$ erg/s for the 10^8 M$_\odot$ GMC. The BH luminosity is especially suppressed for the Hu et al., 2022 model.

Another important quantity in the mechanical feedback model is the jet loading factor $\eta_{\rm j}$, which determines the fraction of mass flow that goes into the BH ($f_{\rm acc} = 1/(1+\eta_{\rm j})$). We present the result of this experiment in Fig. 4.12, where we vary $\eta_{\rm j}$ among 1, 9, and 99, corresponding to $f_{\rm acc}$ equals to 0.5, 0.1, and 0.01. For both GMCs, we find that the fraction of BHs with mass accretion (with the mass resolution of gas) is almost unchanged despite different $\eta_{\rm j}$, while the maximum accreted mass ($\Delta M_{\rm BH}^{\rm max}$) differs. As a rough estimate, $\Delta M_{\rm BH}^{\rm max} \propto f_{\rm acc}$. Since $f_{\rm acc}$ is proportional to the mass transfer rate from the disk to the BH, larger $\eta_{\rm j}$ means more obvious deviations in the CDF of change in BH sink and BH-only masses, which is also reflected in Fig. 4.12.

Cosmic ray

To visualize the cosmic ray feedback we show Fig. 4.13. We choose simulations with high CR energy efficiency (a 10^6 M$_\odot$ GMC with $\epsilon_{\rm CR} = 10^{-3}$ and a 10^8 M$_\odot$ GMC with $\epsilon_{\rm CR} = 10^{-2}$), and zoom in toward a fast-accreting BH. As also suggested in Fig. 4.3, the BH is located at a dense clump in the GMC. Due to strong CR feedback, there is also strong outflow near the BH. Along with the density field, we also show the CR energy density field. Due to CR feedback, there is a high-energy CR "bubble" near the BH, whose energy density is comparable with CRs generated

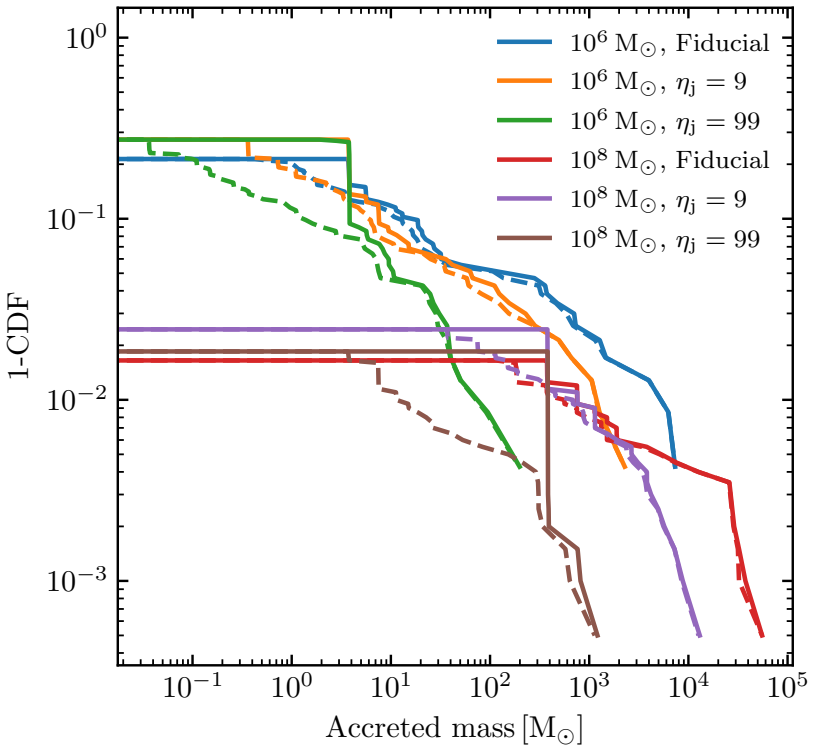

Figure 4.12: The effect of jet mass loading factor (η_j) variations. Here we show the CDF of BH sink particle mass (solid lines) and BH-only mass (dashed lines) based on experiments with different GMCs and different values of η_j. The fiducial value of η_j is 1 in all other simulations.

through stellar feedback. However, these bubbles are of the size of ~ 0.25 pc to ~ 2.5 pc, significantly smaller than the scale of stellar CRs (typically $\sim R_{cl}$). As a result, there is a higher energy (pressure) gradient from the high-energy CR bubbles near the BH, which may then expel gaseous material from the BH or even disrupt the whole GMC.

From Figs. 4.9 and 4.10 we find that BH CR feedback can be important for BH accretion in these dense GMCs we simulated if the energy efficiency is high. For example, BH accretion is significantly suppressed when $\epsilon_{CR} \gtrsim 10^{-3}$ for the 10^6 $M_\odot$ GMC, or $\epsilon_{CR} \gtrsim 10^{-1}$ for the 10^8 $M_\odot$ GMC. We also see a similar trend in f_{Edd} and L_{bol}. Despite that CR feedback from SNe is also included in this set of simulations, we find no clear difference when comparing the $\epsilon_{CR} = 10^{-6}$ run and the run with fiducial setups (without SNe CR feedback), which means this new stellar feedback mechanism does not bring new effects to BH accretion/feedback.

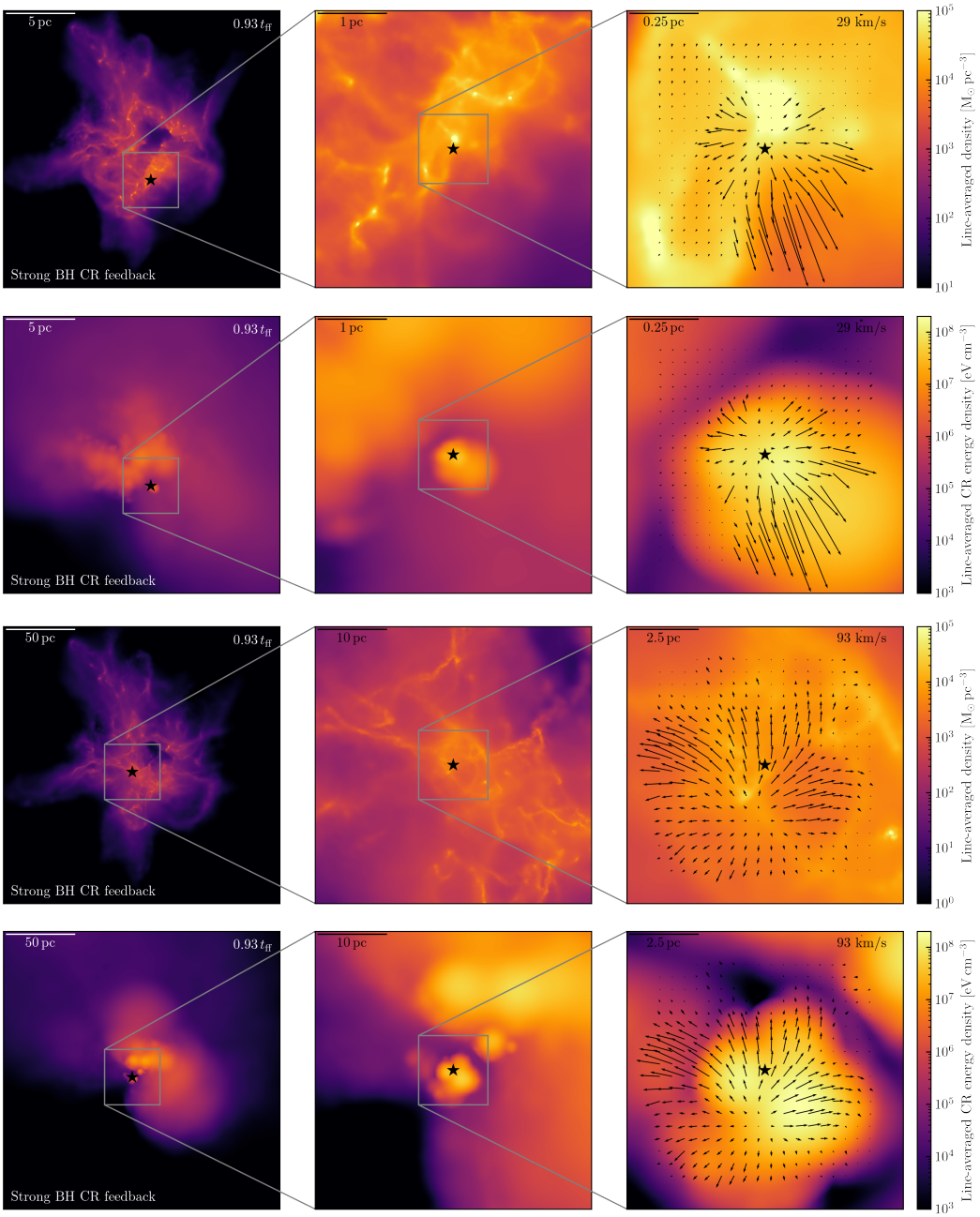

Figure 4.13: Visualization of the GMCs at strong cosmic-ray feedback. *Top two rows*: the line-averaged mass density and CR energy density near a BH undergoing runaway accretion, based on a 10^6 $M_\odot$ GMC. We zoom in near the BH, from the left to the right panel, similar to that in Fig. 4.3. The line-averaged density is evaluated within the box of each panel. We see a high-energy CR bubble generated by the BH. *Bottom two rows*: the same as the top two rows, but embedded in the 10^8 $M_\odot$ GMC.

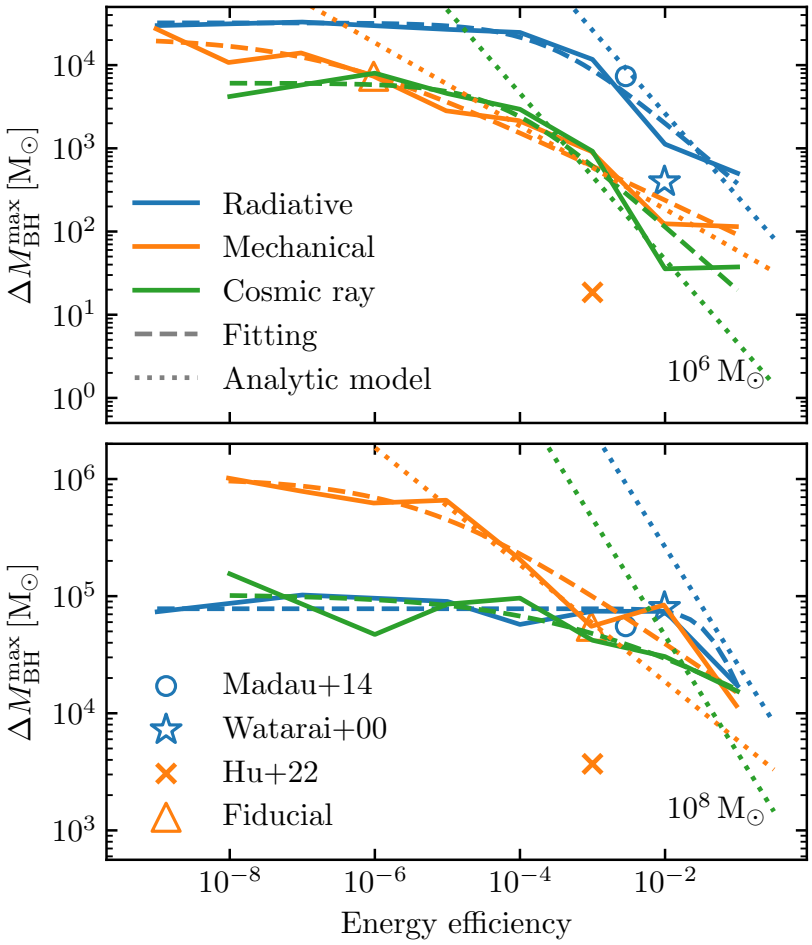

Figure 4.14: Dependence of BH accretion on the energy efficiency of specific feedback mechanisms for the 10^6 M$_\odot$ (top panel) and 10^8 M$_\odot$ (bottom panel) GMCs. We summarize experiments with fixed-value energy efficiencies (solid lines) and show the fitted relation (dashed lines) based on Eq. (4.6). Moreover, we show analytic models at the strong-feedback limit (dotted lines), calculated with Eqs. (4.7), (4.8), and (4.9). Several more sophisticated sub-grid models are also displayed for reference, for each the energy efficiency is calculated at the hyper-Eddington regime of $f_{\rm Edd} = 1000$. The grey shaded regions represent that BH feedback energy is less than the binding energy of the GMC, where BH feedback is insufficient to disrupt the whole GMC.

Feedback Type	$M_{\rm cl}$ [$M_\odot$]	$\log(M_{\rm c}$ [$\rm M_\odot$])	$\log \epsilon_\star$	γ
Radiative	10^6	4.51	-3.58	0.75
	10^8	4.89	-1.31	1.80
Mechanical	10^6	4.33	-6.68	0.42
	10^8	6.01	-5.25	0.43
Cosmic-ray	10^6	3.78	-4.24	0.77
	10^8	5.02	-3.19	0.34

Table 4.3: Fitted parameters following Eq. (4.6) for $\Delta M_{\rm sink}^{\rm max}$ as a function of feedback energy efficiency. Here $\Delta M_{\rm sink}^{\rm max}$ is the greatest amount of mass accretion for the BH seed population in a simulation with various feedback efficiency; $\epsilon_\star$ is the characteristic feedback efficiency and $-\gamma$ is the scaling at the strong-feedback limit.

4.4 Discussions

BH Feedback and BH accretion

For all the feedback mechanisms simulated, a naive conclusion is that BH feedback suppresses BH accretion. To further quantify the effect of feedback, we show the relationship between the feedback strength (indicated by energy efficiencies $\epsilon_{\rm r}$, $\epsilon_{\rm j}$, and $\epsilon_{\rm CR}$) and the maximum of the accreted mass of the BH population in Fig. 4.14. Besides the fixed-value models, we also show some specific sub-grid models for reference, in which energy efficiency is estimated at the hyper-Eddington regime (at $f_{\rm Edd} = 1000$). We find that the two radiative-feedback models (Watarai et al., 2000; Madau et al., 2014) are approximately aligned with the fixed-value models, while the mechanical-feedback model Hu et al., 2022 deviates from the relation.

For all mechanisms, there is a plateau at the weak-feedback (low energy-efficiency) end, while when feedback is stronger, there is a drop in $\Delta M_{\rm BH}^{\rm max}$. We then fit the data points with the equation

$$\Delta M_{\rm BH}^{\rm max} = \frac{M_{\rm c}}{1 + (\epsilon/\epsilon_\star)^\gamma}. \tag{4.6}$$

The equation has a characteristic efficiency $\epsilon_\star$, which describes the transition from the weak-feedback limit to the strong-feedback limit. The power index γ describes how the BH accretion is regulated by feedback.

The fitted parameters are summarized in Table 4.3. From the data in Fig. 4.14, we find that for the radiative and CR feedback experiments on the $10^8\,\rm M_\odot$ GMC, $\Delta M_{\rm BH}^{\rm max}$ almost does not change, which means the simulations are generally in a weak-feedback regime and fittings for $\epsilon_\star$ and γ then becomes unreliable. Otherwise,

we find that with BH radiative and CR feedback $\gamma \approx 1$ and with BH mechanical feedback $\gamma \approx 0.5$.

Strong feedback limit: momentum outflow suppresses BH accretion

The BH feedback mechanism can be described by different arguments based on energy-driven (e.g., Silk and Rees, 1998) or momentum-driven (e.g., Murray et al., 2005) winds. In the context of our problem, the former model assumes the (energy-conserving) outflow disrupts the GMC when its energy deposition covers the GMC's binding energy, while the latter compares the momentum deposition rate versus the GMC's self-gravity. Here we bring out an order-of-magnitude semi-analytical explanation of BH feedback behaviors we observed in simulations and find that the momentum argument can well describe the behavior of mass accretion.

As shown before, the BH feedback will impact the final accreted mass through its energy efficiency ϵ, which can be fitted with Eq. (4.6). We also showed that at the strong feedback regime, $\Delta M_{\rm BH/sink} \propto \epsilon^{-\gamma}$. This can be explained by the balance between the "feedback force" (in the form of radiation pressure, ram pressure, CR diffusion, etc.) and the self-gravity of the cloud. In general, as shown in the previous work Shi et al., 2023b, self-gravity can keep the cloud in a bound state and keep the dense environment, which is the necessary condition for BH runaway accretion. Different from that in Shi et al., 2023b, stellar feedback becomes unimportant to challenge the self-gravity since only clouds with high surface density ($\sim 10^4\,{\rm M}_\odot/{\rm pc}^2$) are simulated in this work.

The self gravity can be scaled as $F_{\rm g} \sim GM_{\rm cl}^2/R_{\rm cl}^2 \sim \pi G\Sigma_0 \cdot M_{\rm cl}$. The "feedback force" is different for different kinds of feedback physics.

Radiative feedback The radiative feedback can be described with the momentum carried by photons, whose time variation results in a force $F_{\rm r} \sim \epsilon_{\rm r}\dot{M}_{\rm BH}c$. At the hyper-Eddington phase, we assume that $\dot{M}_{\rm BH} = f_{\rm Edd}M_{\rm BH}/t_{\rm Sal}$. From the simulations, we also note that $\Delta M_{\rm BH}^{\rm max} \sim M_{\rm BH}^{\rm max}$ for BHs with significant mass accretion. Equating the feedback and self-gravity, we find that

$$\begin{aligned}\Delta M_{\rm BH}^{\rm max} \sim M_{\rm BH}^{\rm max} &\sim \frac{\pi G\Sigma M_{\rm cl} t_{\rm Sal}}{f_{\rm Edd} c\epsilon_{\rm r}} \\ &\sim 263\left(\frac{M_{\rm cl}}{10^6\,{\rm M}_\odot}\right)^2\left(\frac{R_{\rm cl}}{5\,{\rm pc}}\right)^{-2}\left(\frac{f_{\rm Edd}}{1000}\right)^{-1}\left(\frac{\epsilon_{\rm r}}{0.1}\right)^{-1}{\rm M}_\odot. \end{aligned} \tag{4.7}$$

From the simulation, BHs with significant mass accretion can reach $f_{\rm Edd} \sim 1000$. With this number, we show the analytic scaling ration in Fig. 4.14. Compared with the strong-feedback regime, we find good agreement in both the magnitude and slope with the data and fitting.

Mechanical feedback For jets, the mechanical feedback is the ram pressure, which can be approximated with $F_{\rm m} \sim \eta_{\rm j} \dot{M}_{\rm BH} v_{\rm j}$. Note that $\epsilon_{\rm j} = \eta_{\rm j}(v_{\rm j}/c)^2/2$, so $F_{\rm m} \sim \dot{M}_{\rm BH} c (2\epsilon_{\rm j}\eta_{\rm j})^{1/2}$. Comparing and equating $F_{\rm m}$ with $F_{\rm g}$, we find that

$$\begin{aligned}\Delta M_{\rm BH}^{\rm max} \sim M_{\rm BH}^{\rm max} &\sim \frac{\pi G \Sigma M_{\rm cl} t_{\rm Sal}}{\sqrt{2} f_{\rm Edd} c \eta_{\rm j}^{1/2} \epsilon_{\rm j}^{1/2}} \\ &\sim 58 \eta_{\rm j}^{-1/2} \left(\frac{M_{\rm cl}}{10^6\,{\rm M}_\odot}\right)^2 \left(\frac{R_{\rm cl}}{5\,{\rm pc}}\right)^{-2} \left(\frac{f_{\rm Edd}}{1000}\right)^{-1} \left(\frac{\epsilon_{\rm j}}{0.1}\right)^{-1/2} {\rm M}_\odot. \end{aligned} \tag{4.8}$$

In our experiments, we fix $\eta_{\rm j} = 1$. We find good agreement between the data and this simple analytic relation in the strong-feedback regime, as shown in Fig. 4.14. We argue that Eq. (4.8) gives $\Delta M_{\rm BH}^{\rm max} \propto \eta_{\rm j}^{-1/2}$ at fixed $\epsilon_{\rm j}$, but this does not essentially imply a contradiction with the experiments of varying $\eta_{\rm j}$ as described in § 4.3 and Fig. 4.12 where $\Delta M_{\rm BH}^{\rm max} \propto f_{\rm acc} = 1/(1+\eta_{\rm j})$. In that experiment, we fix $v_{\rm j}$ and vary $\eta_{\rm j}$, so $\epsilon_{\rm j} \propto \eta_{\rm j}$ and $\Delta M_{\rm BH}^{\rm max} \propto \eta_{\rm j}^{-1}$. This is very close to $1/(1+\eta_{\rm j})$.

Cosmic-ray feedback Since we consider relativistic CRs, we have $\gamma_{\rm CR} = 4/3$ which also implies $p_{\rm CR} = (\gamma_{\rm CR} - 1) u_{\rm CR} = u_{\rm CR}/3$ where $u_{\rm CR}$ is the CR energy density. At the critical limit, for gas element, there is force equilibrium between the CR pressure gradient and the self-gravity of the cloud, which means $\nabla p_{\rm CR}/\rho \sim \pi G \Sigma_0$. We then approximate the gradient with a characteristic scale $l_{\rm c}$, such that $\nabla p_{\rm CR} \sim u_{\rm CR}/(3 l_{\rm c})$. Thus

$$\frac{\nabla p_{\rm CR}}{\rho} \sim \frac{u_{\rm CR}}{3 l_{\rm c}} \frac{V_l}{\rho V_l} \sim \frac{E_{\rm CR}}{3 l_{\rm c} M_l} \sim \frac{\epsilon_{\rm CR} \Delta M_{\rm BH} c^2}{3 M_{\rm cl} l_{\rm c}} \frac{R_{\rm cl}^3}{\alpha_\rho l_{\rm c}^3}.$$

In the intermediate step, the volume $V_l = 4\pi l_{\rm c}^3/3$ is the characteristic volume of the high-energy CR bubble. We note that ρ is the density of the dense clump where the BH resides, we then define $\alpha_\rho = \rho/\bar{\rho}$ to quantify the density in terms of the mean density $\bar{\rho} = 3M_{\rm cl}/(4\pi R_{\rm cl}^3)$. Comparing this pressure gradient term with the

self-gravity acceleration $\pi G\Sigma_0$, we find

$$\Delta M_{\rm BH}^{\rm max} \sim M_{\rm BH}^{\rm max} \sim \frac{3\pi\alpha_\rho G M_{\rm cl}\Sigma_0 l_{\rm c}^4}{\epsilon_{\rm CR} c^2 R_{\rm cl}^3}$$
$$\sim 5\left(\frac{M_{\rm cl}}{10^6\,{\rm M}_\odot}\right)^2\left(\frac{R_{\rm cl}}{5\,{\rm pc}}\right)^{-1}\left(\frac{l_{\rm c}}{0.2\,R_{\rm cl}}\right)^4\left(\frac{\alpha_\rho}{10^4}\right)\left(\frac{\epsilon_{\rm CR}}{0.1}\right)^{-1}{\rm M}_\odot. \quad (4.9)$$

When choosing reasonable numbers inferred from the simulation, like $l_{\rm c} = 0.2\,R_{\rm cl}$ (implied by assuming $l_{\rm c} \propto 1/\rho_{\rm cl}$) and $\alpha_\rho = 10^4$ (e.g., from Fig. 4.13), we find good agreement with data for the $10^6\,{\rm M}_\odot$ GMC (see Fig. 4.14). For the $10^8\,{\rm M}_\odot$ GMC, the magnitude also agrees well with the data.

Though the argument fits the experiments at the order-of-magnitude level, we caution that there are still many uncertainties in the CR feedback. For example, in the analytic argument, we assumed a tight coupling between the CR and the gas, as well as a smooth characteristic diffusive scale $l_{\rm c}$, resulting in a very steep dependence on $l_{\rm c}$. This is possibly not true for more realistic conditions, where the CR interaction with gas is complicated. A more sophisticated but expensive simulation is probably needed to resolve these uncertainties.

Despite that momentum outflow models can explain the behavior of BH mass accretion at different feedback strengths (energy efficiency), it is still essential to check if the outflow indeed carries enough energy to disrupt the GMC. This can be characterized by an energy efficiency $\epsilon_{\rm E}$, at which the energy deposited from the BH ($\epsilon_{\rm E}\Delta M_{\rm BH}^{\rm max}c^2$) is equal to the binding energy of the GMC ($\sim GM_{\rm cl}^2/R_{\rm cl}$). At the weak feedback limit, we may choose typical values of $\Delta M_{\rm BH}^{\rm max}$ ($10^4\,{\rm M}_\odot$ for the $10^6\,{\rm M}_\odot$ GMC, and $10^6\,{\rm M}_\odot$ for the $10^8\,{\rm M}_\odot$ GMC) and present the region with $\epsilon \lesssim \epsilon_{\rm E}$ in Fig. 4.14. There is $\epsilon_{\rm E} < \epsilon_\star$. At the strong feedback limit, with some calculation, we find $\epsilon_{\rm E} = (\epsilon_{\rm E0}\epsilon_\star^\gamma)^{1/(1+\gamma)} < \epsilon_\star$ (where $\epsilon_{\rm E0}$ is the value of $\epsilon_{\rm E}$ at the weak feedback limit), which means the momentum outflow always carries sufficient energy.

Despite the argument being simple, we find it a good agreement with the experiments varying the BH feedback energy efficiency, and it demonstrates that the feedback mechanisms are momentum-driven. However, we also note that some assumptions we made, like $\Delta M_{\rm BH}^{\rm max} \sim M_{\rm BH}^{\rm max}$, fail at very high energy efficiency, though the agreement is still acceptable at the order-of-magnitude level. Another limiting factor is $f_{\rm Edd}$, which can't achieve its maximum value (1000 in our simulations) when the feedback efficiency is high. From experiments, we find that under such conditions, "extreme" or hyper-Eddington accretion is not possible, but the Eddington factor can still reach 10 – 100 for a short period (see middle columns of Figs. 4.9 and 4.10).

Effects of different feedback mechanisms

The relative importance or "sensitivity" of different feedback mechanisms can be quantified with the fitted parameters $\epsilon_\star$ and γ of Eq. (4.6): small $\epsilon_\star$ means the BH growth is regulated by feedback even if the energy efficiency is just over $\epsilon_\star$, steep γ means that BH growth is highly suppressed and sensitively dependent on the energy efficiency.

From our simulation experiments and analytic models based on momentum outflow, we find that mechanical feedback has the smallest $\epsilon_\star$, which means its impact is effective even if the energy efficiency is small. However, for models with fixed mass loading factor (η_j), we find $\gamma \sim 0.5$, which is shallower than other mechanisms. A very special case is the Hu et al., 2022 model with very strong mass outflow which has the most significant suppression and kills to hope of runaway BH accretion in the dense environments we simulated.

We also find that the feedback from relativistic CRs is strong since it has a smaller $\epsilon_\star$ than that from radiation. Different from mechanical feedback, CR (as well as radiative) feedback features a steeper γ, which means that their feedback impact can be strong and dominates over the mechanical one.

Finally, we find that radiative feedback is typically not important for BH accretion for the $10^8\,M_\odot$ GMC since both the Watarai et al., 2000 and Madau et al., 2014 models are at the weak feedback regime with $\epsilon \lesssim \epsilon_\star$. Instead, BH accretion in this series of simulations is regulated by the fiducial mechanical feedback model (the triangle in Fig. 4.14). However, these two models show a significant difference in simulations with the $10^6\,M_\odot$ GMC, as also expected in our analytic argument in Eq. (4.7). This also means exact models of such radiative-inefficient accretion flows should still be further inspected.

From the simulations, we again confirm that in GMCs with high surface density ($\sim 10^4\,M_\odot/pc^2$), stellar formation/feedback fragment the GMC and general dense clumps, which are instantaneous reservoirs for BH accretion. This is also true even if a new mechanism, the cosmic-ray feedback from stars, is considered. This can be inferred from Fig. 4.14. For the $10^6\,M_\odot$ GMC, at weak CR feedback from BHs, the accreted mass is regulated by the fiducial mechanical feedback model (the triangle in the upper panel), while there is no further suppression. This is also true for the $10^8\,M_\odot$ GMC.

BH feedback and star formation

BH feedback may also challenge star formation in the GMC due to strong strong outflow, which expels gas away from the galaxy center. This is well-discussed in the AGN literature from both theoretical/numerical (e.g., Silk and Rees, 1998; Fabian, 1999; Murray et al., 2005; King, 2010; Su et al., 2021; Mercedes-Feliz et al., 2023) and observational aspects (e.g., Page et al., 2012; Harrison, 2017). Motivated by these studies, we also inspect how BH feedback affects star formation in our simulations, which is at a much smaller scale than typical galaxies.

In Fig. 4.15 we present the star formation efficiency (SFE, defined as the ratio between the stellar mass at the end of the simulation and the initial GMC mass) for different kinds of feedback mechanisms and various energy efficiencies. When the energy efficiency is sufficiently low, we find that in both the $10^6\,M_\odot$ and $10^8\,M_\odot$ GMCs, the SFE is ~ 0.3. This is expected since the two GMCs have the same initial mean surface density (Grudić et al., 2018b, and more citations in § 4.1). Then once the energy efficiency increase beyond $\sim 10^{-3}$, the SFE for the $10^6\,M_\odot$ GMC drops below 0.1. However, the impact on the $10^8\,M_\odot$ is not significant.

A very special case is the $\epsilon_{\rm CR} = 0.1$ run, in which the SFE drops to a very low value ($< 10^{-3}$). With further inspection of the run, we find that the cloud was disrupted by strong CR winds at $\sim 0.3\,t_{\rm ff}$, which is much shorter than the characteristic time scale of star formation at the low-BH-feedback limit (from simulations it is $t^{\rm SF}_{1/2} \sim 1.25\,t_{\rm ff}$, defined as the time when the SFE reaches half of the final value). As a result, the SFE almost freezes at the (extremely low) star-formation level at the time of GMC's disruption.

We may roughly explain this quantitatively. From our simulations, BH growth history is dominated by a few "bursty" super-Eddington accretions which happen in a short period of time (typically less than $0.05\,t_{\rm ff}$). At a time scale much longer than the bursty growth, the BH mass is then anticipated to be $M_{\rm BH} \sim M^{\rm ini}_{\rm BH} \exp(\langle f_{\rm Edd}\rangle t/t_{\rm Sal})$. Applying this to the BH with the most significant mass growth, we find the disruption time of the GMC due to strong BH feedback to be

$$t_{\rm d} \sim \frac{t_{\rm Sal}}{\langle f_{\rm Edd}\rangle} \ln\left(1 + \frac{\Delta M^{\rm max}_{\rm BH}}{M^{\rm ini}_{\rm BH}}\right). \tag{4.10}$$

For each simulation, $M^{\rm max}_{\rm BH}$ and $\langle f_{\rm Edd}\rangle$ are presented in the middle columns of Figs. 4.6, 4.9, and 4.10; and $M^{\rm max}_{\rm BH}$ (or $\Delta M^{\rm max}_{\rm BH}$) is also analytically evaluated from Eqs. (4.7), (4.8), and (4.9). In general, we find that $\langle f_{\rm Edd}\rangle$ is approximately 10

– 100, and there is $M_{\rm BH}^{\rm max} \gg M_{\rm BH}^{\rm ini}$ so $t_{\rm d}$ is generally much larger than the free-fall time of the two GMCs we simulated. However, when there is very strong BH feedback, $\Delta M_{\rm BH}^{\rm max}$ is low. Thus there are chances that $\Delta M_{\rm BH}^{\rm max} \ll M_{\rm BH}^{\rm ini}$ and $t_{\rm d} \sim t_{\rm Sal}\Delta M_{\rm BH}^{\rm max}/(\langle f_{\rm Edd}\rangle M_{\rm BH}^{\rm ini})$ is smaller than (or comparable with) the free-fall time. For the $\epsilon_{\rm CR} = 0.1$ run of the $10^6\,{\rm M}_\odot$ GMC, there is $M_{\rm BH}^{\rm ini} = 702\,{\rm M}_\odot$ and $M_{\rm BH}^{\rm max} = 740\,{\rm M}_\odot$ (thus $\Delta M_{\rm BH}^{\rm max} \approx 0.05$), resulting $t_{\rm d} \sim 2/\langle f_{\rm Edd}\rangle$ Myr. The time scale is comparable to (or substantially smaller than if $\langle f_{\rm Edd}\rangle$ is large) the free-fall time of the GMC (0.19 Myr).

We also note that the argument is dependent on the initial mass of the BH, thus $t_{\rm d}$ is essentially short only when the "lucky" seed BH is initially massive. As a result, the extreme suppression of SFE does not always happen even if the energy efficiency is high, which is true for most experiments in Fig. 4.15 with high energy efficiency.

In summary, we find that BH feedback will not affect the star formation efficiency unless it is in a highly feedback-dominated/regulated regime ($\epsilon \gtrsim 10^{-3}$ for the $10^6\,{\rm M}_\odot$ GMC). The significance of the impact is largely decided by how soon the winds induced by BH feedback "interrupt" star formation (which happens at the free-fall time scale) – in some particular models (e.g., very strong feedback from a massive BH seed), even if BH accretion is limited, the strong BH feedback is still able to disrupt the whole GMC at the very early stage of the star-formation history and result in very low star formation efficiency.

Caveats and outlook

Because of the huge mismatch in scales of the BH accretion/feedback problem (from kpc/pc scale to the Schwarzschild radius), it is difficult to simulate every aspect in great detail. In this study, we concentrate on larger scales, where the gas inflow towards BHs is well simulated with the MHD but dynamics of small scales (gas cells that are considered "gravitationally bounded to the BH") are described by sub-grid models with a few free parameters (as listed in Tab. 4.2). However, the setup is sufficient to answer the question we were asking: whether there is enough fuel from large scales (kpc/pc) reaching small scales (sub-pc) if there is BH feedback since mass and momentum outflow from these small-scale dynamics is counted in a large parameter space. The setup is thus also able to study the impact of different parameters on BH accretion, as an attempt to bridge the dynamics of small and large scales.

Still, the sub-grid models and resolution of our simulations do not connect the

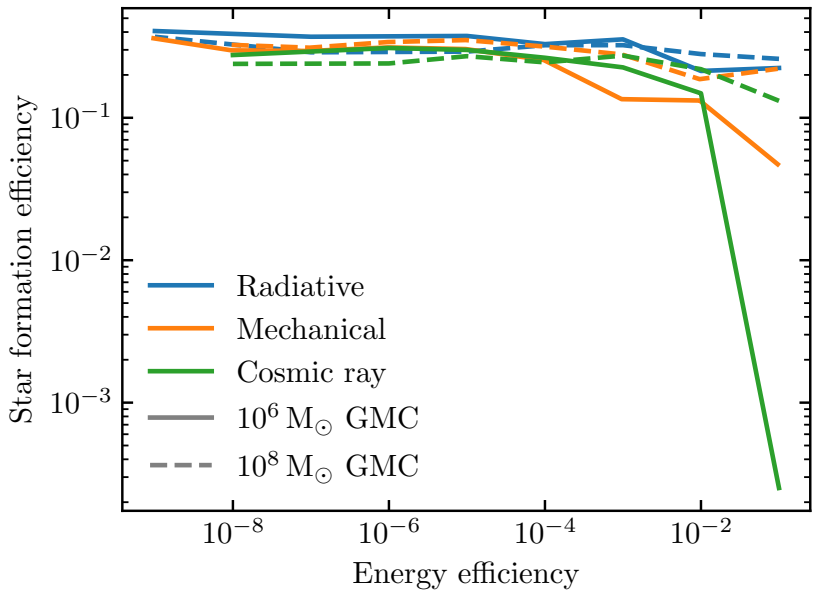

Figure 4.15: The star formation efficiency (SFE) in our experiments with various fixed-value BH-feedback energy efficiencies. For the 10^6 M$_\odot$ GMC, there is (sometimes extreme) suppression of the SFE at high energy efficiency.

large and small scales in great self-consistency. For example, energy efficiencies of different feedback mechanisms are treated as uncorrelated parameters, and these parameters are not dependent on BH ambient boundary conditions like magnetic field and angular momentum flow. There is thus plenty of space for improvement.

Recent zoom-in simulations of BH accretion or feedback can shed light on this problem (e.g., Talbot et al., 2021; Guo et al., 2023), including the most recent implementation in FIRE-3. With the technique of grid-based refinement or super-Lagrangian refinement, the mass/scale resolution of gas increases towards the accreting BHs of interest. More small-scale structures (e.g., BH accretion disk, jets) and dynamics (e.g., the magnetic field in disks, jet launching mechanisms, BH-disk interactions) are thus possible to be simulated at a much higher level of self-consistency. This technique, by narrowing down toward the BH's event horizon, also lifts another caveat of the gravitational capture method used for BH accretion, which may face issues like resolution convergence (see Shi et al., 2023b, for more discussions and tests).

Finally, as also described in Shi et al., 2023b, the STARFORGE physics can also help since it can track single star dynamics (Grudić et al., 2021b; Guszejnov et al., 2021). As a result, dynamics missing in this study, like BH relics from individual

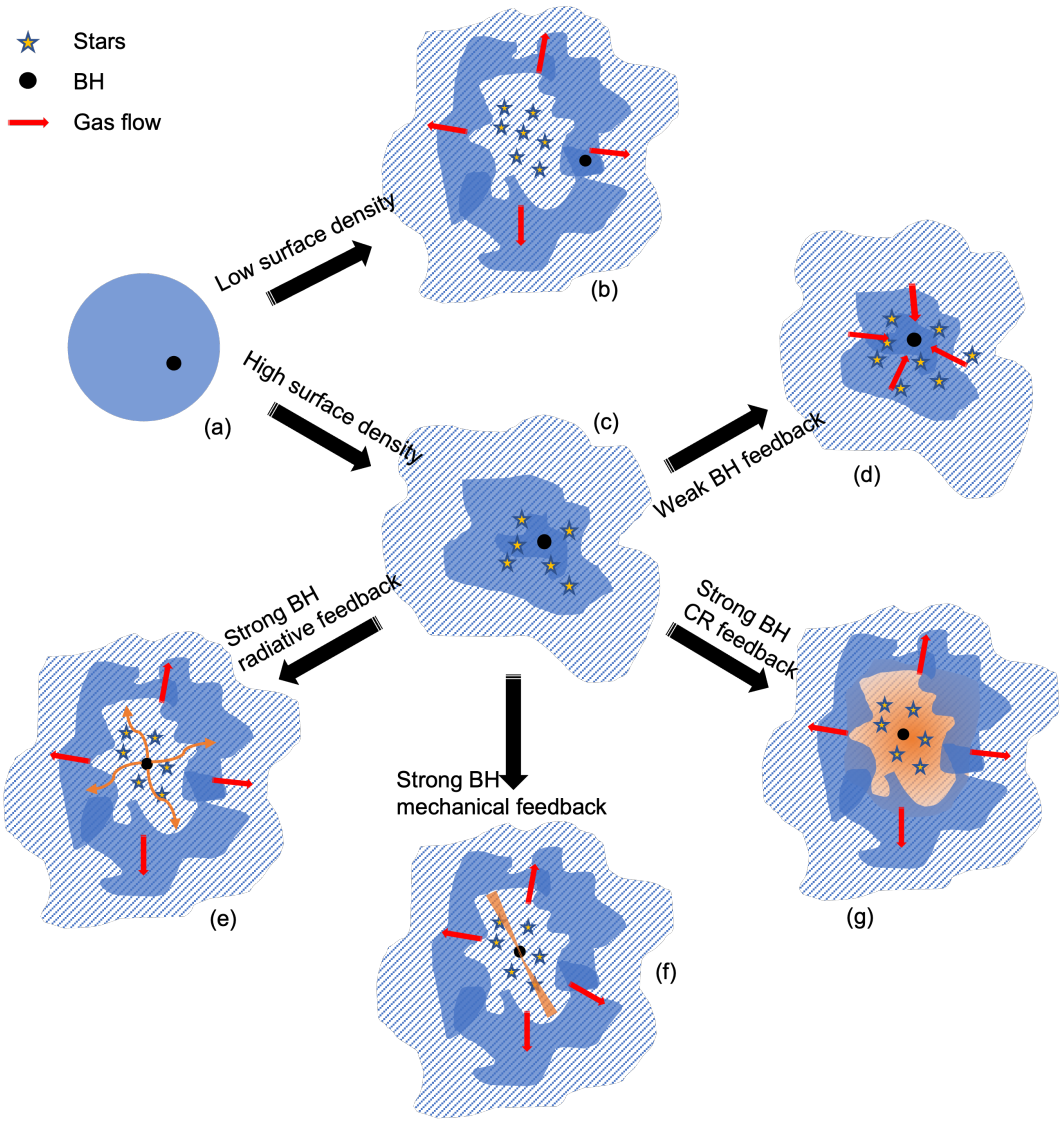

Figure 4.16: A schematic diagram of seed BH accretion and feedback in GMCs. (a) Initial condition, where the seed BH is inside a pre-star-formation, turbulent GMC. (b) If the self-gravity of the GMC (characterized by its mean surface density), star formation and feedback dominate and disrupt the GMC, suppressing BH accretion. (c) If the GMC's self-gravity is strong, gas is kept bound, creating a proper environment for BH accretion and feedback. (d) If the BH feedback is weak, there is steady accretion flow towards the BH if it is at the center of the potential well. (e) (f) (g) Strong feedback in different forms may suppress both BH accretion and star formation, this process is dominated by momentum outflow from BHs and can be described with analytic arguments as in Eqs. (4.7), (4.8), and (4.9).

stars and BH seed formation can be further studied.

4.5 Conclusions

This study is a parameter-space survey of seed BH accretion and feedback in star-forming GMCs, while key parameters are listed in Table 4.2. We focus on high surface-density clouds which are environments for runaway BH accretion at the weak (or on) BH feedback limit (Shi et al., 2023b), and find that BH feedback leaves a negative effect on BH accretion once they are sufficiently strong.

With the simulations and analysis, the major conclusions for our fiducial BH accretion & feedback runs are listed below.

- Even with feedback, the BH accretion scenario is the same as that presented in Shi et al., 2023b. BH accretion happens when there is a small relative velocity between the BH and a dense clump in the GMC. This happens only when the dynamics of both BH and gas are dominated by GMC's self-gravity, under which condition the feedback effects from either BH or stars should be unimportant.

- With the fiducial feedback model (log-form radiative efficiency and critical mechanical feedback efficiency defined in Eq. 4.4), we find there is suppression of BH accretion in both simulations with $10^6\,M_\odot$ and $10^8\,M_\odot$ GMCs. Significant BH accretion is more likely in the $10^8\,M_\odot$ GMC, where BHs grow up to $\sim 5\times10^4\,M_\odot$. There are short phases of hyper-Eddington accretion ($\sim 1000\dot{M}_{\rm Edd}$) for both simulations.

- Like the condition without BH feedback (Shi et al., 2023b), initial information about black holes like initial mass, position, velocity, and angular momentum does not significantly correlate with BH accretion.

We also reach some conclusions from the parameter survey of key free parameters in the sub-grid BH accretion and feedback model. The most important conclusions are from surveys of the energy efficiency $\epsilon \equiv E_{\rm feedback}/(\dot{M}_{\rm BH}c^2)$.

- For feedback physics involved in this study, we find that the maximum possible accreted mass for BHs $\Delta M_{\rm BH}^{\rm max}$ satisfies the relation as shown in Eq. (4.6), which is a function of the energy efficiency ϵ. At the strong feedback limit ($\epsilon > \epsilon_\star$), $\Delta M_{\rm BH}^{\rm max} \propto \epsilon^{-\gamma}$. We find $\gamma \approx 1$ for radiative and CR feedback

(both of which are relativistic), and $\gamma \approx 0.5$ for the mechanical feedback (non-relativistic).

- We argue that since the cooling time of radiation, jets, and cosmic ray is significantly shorter than the free-fall time of the GMC, a momentum-driven feedback model can explain both the magnitude and the slope of $M_{\rm BH}^{\rm max}(\epsilon)$ at the strong feedback limit. These analytic arguments are summarized in Eqs. (4.7), (4.8), and (4.9).

- Mechanical feedback can be impactful for BH accretion. We find that for both the $10^6\,{\rm M}_\odot$ and the $10^8\,{\rm M}_\odot$ GMC, the transition between the weak and strong feedback happens at $\sim 10^{-7}$ and $\sim 10^{-5}$ respectively, which are very small energy coefficients. An extreme case is the Hu et al., 2022 sub-grid model for mechanical feedback, we find that significant BH accretion is largely prohibited.

- Radiative feedback is not a huge limiting factor for runaway accretion in our simulation. This is ensured by "log form" radiative efficiency models like Watarai et al., 2000 and Madau et al., 2014, where the fraction of energy radiated away from the BH is very low at super or hyper-Eddington accretion rates. We find that these models are typically in the weak-feedback limit ($\epsilon_{\rm r} \lesssim 10^{-4}$ for the $10^6\,{\rm M}_\odot$ GMC and $\epsilon_{\rm r} \lesssim 10^{-2}$ for the $10^8\,{\rm M}_\odot$ one). However, our simulations with the $10^6\,{\rm M}_\odot$ GMC show that the two models still have a non-trivially different level of suppression. An effort toward the exact model is thus desired.

- Cosmic rays feedback from BHs can be important since the transition to strong feedback limit happens at the energy efficiency of 10^{-4} for the $10^6\,{\rm M}_\odot$ GMC and 10^{-3} for the $10^8\,{\rm M}_\odot$, higher than that of the radiative feedback. CR feedback effects from stars are not important. We caution that this is based on assumptions of ultra-relativistic and diffusive ($\kappa_{\rm CR} \sim 10^{29}{\rm cm}^2/{\rm s}$) cosmic rays, while there can be uncertainties of these assumptions due to the lack of experimental data.

- Despite that BH accretion overall is suppressed by BH feedback with the energy efficiency is high, there are still short phases of very high accretion rate ($\gtrsim 100\dot{M}_{\rm Edd}$) for a subset of BHs in the simulation (~ 0.1 for the $10^6\,{\rm M}_\odot$ GMC and ~ 0.01 for the $10^8\,{\rm M}_\odot$ one). This generates a bolometric luminosity

of $\sim 10^{42} - 10^{43}$ erg/s for these BHs depending on their masses (Fig. 4.9 and 4.10).

- When varying the BH feedback energy efficiency, we find that star formation efficiency is generally not suppressed by BH feedback unless the feedback efficiency is very high ($\gtrsim 0.01$). We find that significant suppression happens if i) the energy efficiency is very high; ii) a BH reaches hyper-Eddington accretion and deposits strong feedback before $\sim t_{\rm ff}$, which is the characteristic time for star formation. This GMC is disrupted and further star formation is prevented. We argue that this is unlikely in reality since it is hard to reach very high feedback efficiency.

We also experimented with other free parameters that may affect the BH feedback.

- The metallicity of the GMC can affect the strength of the BH radiative feedback through coupling with the ISM. We find that the metallicity importance follows the argument of weak or strong feedback limits. For log-form radiative feedback models, metallicity dependence is not important.
- Other parameters are related to mass flow to the BH, like the effective α, the upper limit of BH accretion rate, and the jet mass loading factor $\eta_{\rm j}$. We find these factors affect the BH accretion inverse-proportionally. There is also a degeneracy between these parameters.

We find similarities with the existing work. For example, Lupi et al. (2016) simulated the super-critical accretion onto stellar-mass BH seeds in gaseous circum-nuclear disks (CNDs), with options of constant $\epsilon_{\rm r} = 0.1$ and the slim disk model (Madau et al., 2014) for radiative efficiency. Pezzulli et al., 2016 studied the growth of the central BH (initially with $\sim 100\,{\rm M}_\odot$ seed mass) of high redshift quasars with the semi-analytic framework including the slim-disk model and AGN wind feedback efficiency of $\sim 10^{-3}$. They both see super-Eddington accretion, where the radiative-inefficient accretion model plays a key role.

Technically, the extension of this work may include more sophisticated sub-grid models of BH accretion, which connect the BH accretion with the properties of the ambient gas. Another direction is to develop zoom-in simulations that attain higher resolution near the BH seed, which is more self-consistent but computationally more expensive. We leave these possibilities for future work.

Chapter 5

IMBH MIGRATION AND EFFICIENT ACCRETION IN CLUSTERS

Abstract

Seed black hole (BH) accretion in dense giant molecular clouds (GMCs) can be amplified due to interactions between stars, BHs, and gas. In this paper, we report a simulation of BH accretion and star formation in a GMC with $\Sigma \sim 10^4\,\mathrm{M_\odot/pc^2}$ and $R_{\rm cl} = 50\,\mathrm{pc}$. Due to the strong self-gravity, stellar feedback is insufficient to disrupt the GMC. Along with star formation, star clusters form and merge hierarchically, creating deep potential wells. BH seeds near the edge can be captured by merging clusters and migrated to the center in approximately one free-fall time. At the late stage of the simulation, a $\sim 10\,\mathrm{pc}$ disk structures form with a convergent gas inspiral, aided by the gravity of the final major cluster and the BH. Due to flux-freezing and differential rotation, a strong toroidal magnetic field ($\lesssim 0.1\,\mathrm{G}$) is formed in the disk. Analysis of the thermodynamics shows that the disk is heated and ionized by feedback from stars. Further star formation is suppressed by the magnetic field. The gas inflow rate can be $\sim 10\,\mathrm{M_\odot/yr}$, creating an optimal condition for efficient seed BH accretion.

5.1 Introduction

The formation of massive black holes is a fascinating problem (Volonteri et al., 2021). Observations of high-redshift ($z \gtrsim 7$, $\sim 0.7\,\mathrm{Gyr}$ since the Big Bang) quasars revealed the existence of supermassive black holes (SMBHs) of $10^9\,\mathrm{M_\odot}$ at the very early stage of the Universe (Fan et al., 2001; Yang et al., 2020; Wang et al., 2021). If these SMBHs grow from accretion like quasars at lower redshift (Yu and Tremaine, 2002), their existence time from the Big Bang is short in view of the classical limit of the accretion, the Eddington accretion rate, which is defined as $\dot{M}_{\rm Edd} = M_{\rm BH}/(\epsilon_{\rm ref} t_{\rm Sal})$, where $t_{\rm Sal} = \kappa_{\rm es} c/(4\pi G) \approx 0.45\,\mathrm{Gyr}$ and $\epsilon_{\rm ref}$ is assumed to be 0.1 (Inayoshi et al., 2020). Seed black holes for SMBHs are thus assumed to fall in the category of intermediate-mass black holes (IMBHs, Volonteri et al., 2021; Wang et al., 2021), with the mass range to be $\sim 10^2$ – $10^6\,\mathrm{M_\odot}$ (Greene et al., 2020).

There are several scenarios to build these IMBHs or seed BHs, like the Population III remnants ($\sim 100\,\mathrm{M_\odot}$, Madau and Rees, 2001), the direct collapse of the pristine gas

($\sim 10^5\,M_\odot$, Bromm and Loeb, 2003), and runaway mergers in dense star clusters ($\sim 10^3\,M_\odot$, Portegies Zwart et al., 2004; Shi et al., 2021). Moreover, super-Eddington accretion of stellar-mass BHs and Population III remnants can also build more massive seed BHs ($\sim 10^5\,M_\odot$) quickly (Inayoshi et al., 2016; Shi et al., 2023b), which is favored from observations of high-redshift quasars (Wang et al., 2021).

Theoretical works on small-scale (sub-pc) accretion physics show that super-Eddington accretion is possible (Begelman, 1979; Blandford and Begelman, 2004; Inayoshi et al., 2016), through the "photon trapping" effect, in which photons are trapped in the strong accretion flow ($\sim 1000\dot{M}_{\rm Edd}$) without radiated away efficiently. This is also demonstrated by numerical simulations (Jiang et al., 2014; Sądowski et al., 2015; Jiang et al., 2019) where a sustainable phase of super-Eddington accretion is observed. Still, there is a need to inspect the availability of super-Eddington accretion in more realistic environments, which is turbulent and star-forming: the actual inflow from parsec-scale may not be enough to feed super-Eddington accretion.

This problem is checked in (Shi et al., 2023b) where we embed BH seeds into star-forming giant molecular clouds (GMCs). We found that significant BH accretion in these turbulent environments happens if a dense clump (pc or sub-pc scale) developed by turbulence and star formation (Klessen, 2000; Mac Low and Klessen, 2004; McKee and Ostriker, 2007) is gravitationally bounded and close (sub-pc) to the BH. The material supply to the BH is also dense and cold enough to make super-Eddington accretion possible (Inayoshi et al., 2016). This "clump accretion" happens if both dynamics of gas and the BH is dominated by the GMC's self-gravity, which is true for GMCs with a high initial surface density (Shi et al., 2023b). The conclusion follows the similar dynamics of the fact that GMC's surface density is important in regulating the strength of stellar feedback and star formation efficiency (Grudić et al., 2018b; Grudić et al., 2021b; Chevance et al., 2022).

BH feedback effects can be important at larger parsec-scales, though sub-pc simulations found radiative feedback is not a huge limiting factor (Jiang et al., 2019), there are other BH feedback effects like winds or jets at different scales (Silk and Rees, 1998; Blandford and Begelman, 1999), and cosmic rays that may drive winds and heat/ionize the ISM (Guo and Oh, 2008; Guo and Mathews, 2012; Zweibel, 2017). We studied these effects in more recent Shi et al., 2023a, where we analyzed and quantified different BH feedback effects. We found the large-scale BH feedback is through momentum-driven winds that compete with the self-gravity. For BH feedback energy efficiency, there is a weak-feedback limit that BH feedback is

unimportant and a strong-feedback limit that BH accretion is inversely correlated with the feedback energy efficiency through a power law.

Still, there is missing physics not covered by Shi et al., 2023b and Shi et al., 2023a about BH accretion in GMCs, which is the interaction between stars and seed BHs. Stars in the simulation form clusters (Grudić et al., 2018b; Shi et al., 2021), which is more massive than most seed BHs considered in the simulation so their gravity can be important. This is especially the case for GMCs with high surface density, where star formation efficiency is high and star clusters are dense and massive. Moreover, it is also worthwhile to check if there is another accretion mode along with the "clump accretion," which is stochastic and typically only a small fraction ($\lesssim 0.01$ depending on GMC properties) of BHs can grow significantly in this way.

In this study, we analyze a simulation with a BH feedback model in the weak-feedback limit and run inside a $10^8\,M_\odot$ and 50 pc GMC (so the surface density is $\sim 10^4\,M_\odot/pc^2$). We find clusters form hierarchically (as also in Guszejnov et al., 2022) while mergers are more violent in this dense GMC. BHs can be captured by clusters and migrate to the central cluster, which also brings a strong inflow. This steady inflow makes BHs grow almost linearly at high rates ($\sim 2\,M_\odot/yr$). We also find a parsec-scale disk structure that is magnetized and non-trivial.

The paper is structured in the following way. We introduce the method briefly in § 5.2, though a more extended description is in (Shi et al., 2023a). Then we study the dynamical interaction between BHs and star clusters in § 5.3, and the magnetized disk in § 5.4. Finally, we conclude and discuss caveats and implementations of the scenario in § 5.5.

5.2 Simulations

The simulation is based on the MHD code GIZMO[1] (Hopkins, 2015; Hopkins and Raives, 2016) in its Meshless Finite Mass (MFM), and follows the same treatment of star formation as previous works (Grudić et al., 2018b; Shi et al., 2021; Shi et al., 2023b; Shi et al., 2023a). Multiple physics are included in the simulation, including self-gravity, radiative cooling and heating, star formation, and feedback. Star formation and feedback are calculated with IMF-averages assemble, which follow the treatment of the FIRE-2 implementation of the Feedback In Realistic Environment (FIRE) framework (Hopkins et al., 2018a). The treatment is proven successful in recovering information about star formation and star cluster dynamics

[1] http://www.tapir.caltech.edu/~phopkins/Site/GIZMO.html

(Grudić et al., 2018b; Grudić et al., 2018a; Grudić et al., 2021a).

BH accretion is evaluated with a sink radius, and only gas cells gravitationally bounded inside the radius will be considered to be accreted by the BH (Bate et al., 1995; Shi et al., 2023b). This treatment follows the actual process that happens at parsec scales where gravity dominates. We also implemented a BH feedback sub-grid model, where mass that is captured from the previous step is stored in a secondary "disk" reservoir, and flow toward the BH in a timescale proportional to the dynamic time at the sink radius, in analogy to the α prescription in the standard accretion disk model (Shakura and Sunyaev, 1973). Only a fraction $f_{\rm acc}$ of the mass flow reaches the BH, while the rest is ejected back to the GMC in the form of bipolar jets that follow the angular momentum direction of the ambient gas flow (Torrey et al., 2020; Su et al., 2021), at a velocity $v_{\rm j}$. This implies the mechanical feedback energy efficiency to be $\epsilon_{\rm j} \equiv L_{\rm j}/(\dot{M}_{\rm BH}c^2) = (1 - f_{\rm acc}v_{\rm j}^2/(f_{\rm acc}c^2)$. Some portion ($\epsilon_{\rm r}$) of the rest energy in the remaining inflow will also be extracted as radiative energy.

We implemented a series of simulations covering a large parameter space of GMC properties and the sub-grid BH feedback models, as in Shi et al., 2023a. The simulation of special interest here is in a GMC of $10^8\,{\rm M}_\odot$ and 50 pc. We have $f_{\rm acc} = 1$, $v_{\rm j} = 400\,{\rm km/s}$, and $\epsilon_{\rm r} = 10^{-5}$. All these parameters are in the weak-feedback limit (Shi et al., 2023a). However, it does not mean the choice of these parameters is not physical. For example, more realistic radiative feedback models like Watarai et al., 2000 and Madau et al., 2014 are also in the weak-feedback limit (Shi et al., 2023a).

In Fig. 5.1, we show the gas morphology (the column density in logarithmic scales) of the GMC at different evolution stages in the simulation: the initial condition (0 Myr), the free-fall time ($t_{\rm ff}$, 0.6 Myr), and the simulation time limit ($3t_{\rm ff}$, 1.8 Myr). The simulation starts with a smooth density profile while initial turbulence is seeded. Then gravitational collapses happen and the medium becomes more turbulent, creating dense clumps, shocks, and filaments in the space. Star formation is also initialized significantly before the first free-fall time. At later times, as the right panel shows, the GMC is not disrupted by stellar feedback. Instead, there is a convergent inflow toward the center of the cloud. With further zoom-in, the inflow builds up into disk structure with a size of ~ 10 pc from rough estimates. On top of the gas density, we present the magnetic field lines in the zoom-in panel, which have strong toroidal components.

Along with the gas, we also present two BHs with the most significant accretion.

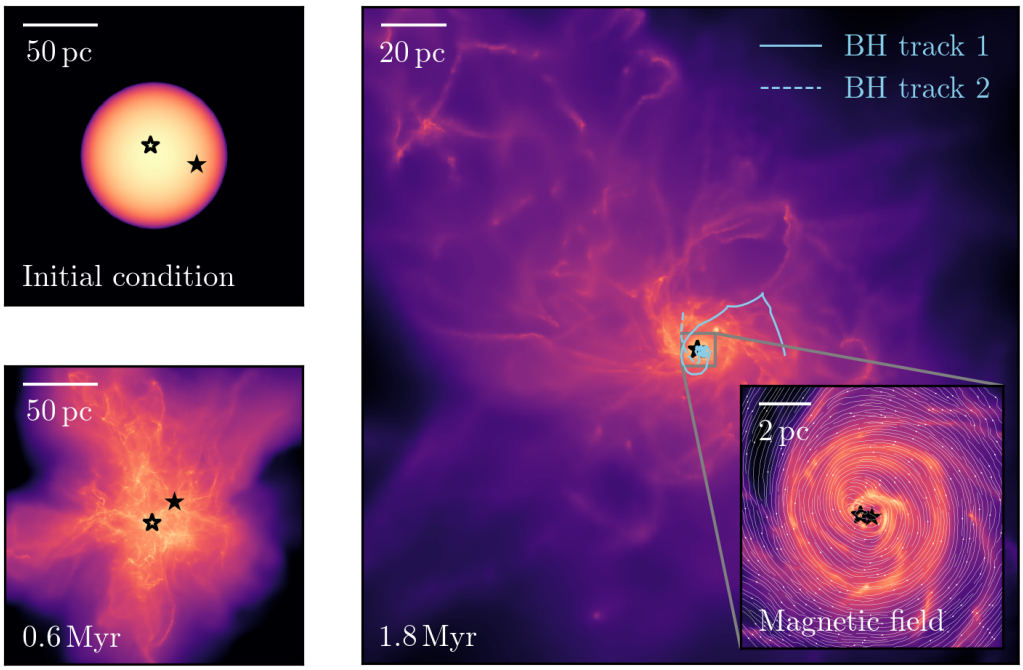

Figure 5.1: Visualization of the simulation. We show the gas morphology (column density in logarithmic scales) and position of two selected BHs (black stars) at different stages of the simulation (initial condition, free-fall time, and simulation time limit). The inserted zoom-in panel shows the convergent inflow and disk structure near the BHs (adapted to the face-on direction), along with magnetic field lines with a strong toroidal component. Trajectories of the two BHs (cyan lines) suggest their migration to the center.

By checking their positions, we find that both BHs migrate to the center where the gas converges. More interestingly, the trajectory of the BH has a sharp turn before it spirals to the center. We expand more details of the BH migration and the disk structure in the next two sections.

5.3 BH migration and accretion

Clusters form hierarchically in the GMC (Guszejnov et al., 2022). Moreover, for the dense GMC we simulated, the gravitational force is dominant over feedback, which means that gravitational interactions between stars can be more significant. To build a merger history, we first identify gravitationally bounded star clusters in each snapshot[2]. To check the inheritance relationship between cluster i in one snapshot and cluster j in another one, we use a "similarity measure" which is defined as $s_{ij} = [n_{ij}/\min(n_i, n_j)] \cdot [2\sqrt{n_i n_j}/(n_i + n_j)]$, where n_i (n_j) is the number of particles

[2] https://github.com/mikegrudic/Phinder

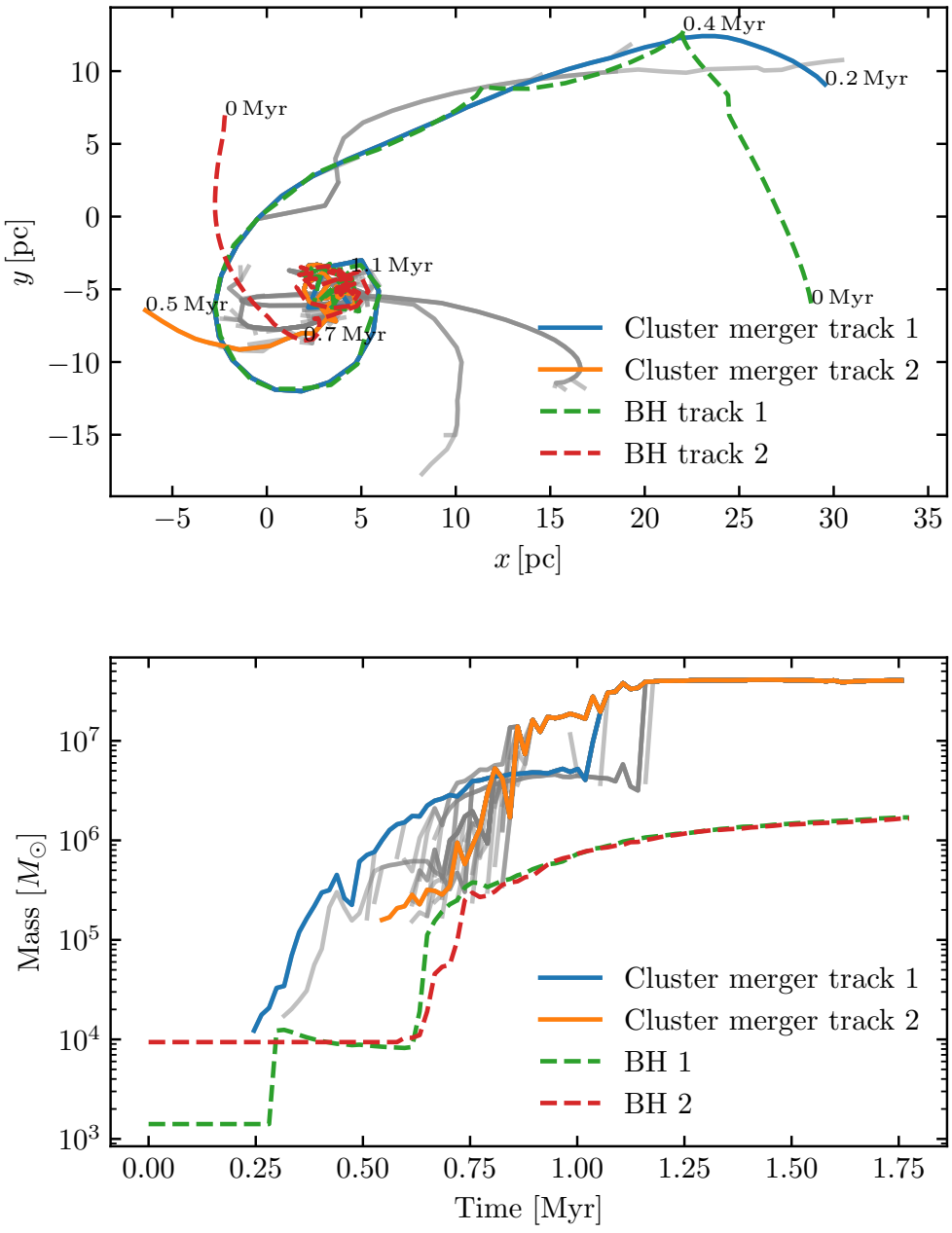

Figure 5.2: Cluster mergers in the simulation. **Top**: trajectories of clusters and BHs. Among mergers and migration of clusters (solid lines), we highlight two clusters that are associated with the evolution of two BHs (dashed lines). We note that each BH is captured by its companion cluster before migrating to the center. **Bottom**: mass evolution of clusters and BHs. Clusters acquire mass through mergers, while the final cluster mass stops growth after ~ 1 Myr. The two BHs grow almost linearly at $\sim 2\,M_\odot/\mathrm{yr}$ after ~ 0.75 Myr.

in the cluster i (j), and n_{ij} is the number of common particles between the two clusters. For a cluster in one snapshot, we iterate over clusters in the next snapshot to rank and determine the most possible successor (above a preset threshold). A "merger tree" is constructed after iterating over all clusters in the simulation.

In Fig. 5.2 we show the trajectories of clusters (i.e., trajectories of their centers) following their merger history. There is an overall trend that clusters merge after their formation, and they migrate to the center. We also plot trajectories of two BHs with the most significant mass accretion (same as those in Fig. 5.1), and highlight cluster merger tracks that interact with them. There is clear evidence that BH 1 encounters cluster merger track 1 at $\sim 0.4\,\mathrm{Myr}$ and becomes captured; it then oscillates along the cluster's trajectory before settling down in the cluster. The BH-cluster pair then migrate to the center at $\sim 1.1\,\mathrm{Myr}$. It also happens for the second pair of BH and cluster, though the capture happens at $\sim 0.7\,\mathrm{Myr}$ and is much closer to the center. These two clusters later merge at $\sim 1.1\,\mathrm{Myr}$.

The merger history of clusters is also reflected in their mass evolution, as shown in the bottom panel of Fig. 5.2. The two clusters merge into a very massive cluster ($\sim 4\times10^7\,\mathrm{M}_\odot$) at $\sim 1\,\mathrm{Myr}$, while the cluster stalls mass growth since then. We also plot the mass evolution of the two BHs. The two BHs reaches $\sim 10^4\,\mathrm{M}_\odot$ before $\sim 0.5\,\mathrm{Myr}$, while BH 1 grows significantly at $\sim 0.25\,\mathrm{Myr}$. This accretion happens when a dense clump is gravitationally bounded to the BH, as shown in previous studies (Shi et al., 2023b). After $\sim 0.75\,\mathrm{Myr}$, the two BHs grow almost linearly in time, at a rate of $\sim 2\,\mathrm{M}_\odot/\mathrm{yr}$. They finally both reach $\sim 2\times10^6\,\mathrm{M}_\odot$ at the end of the simulation.

Through evolution, each cluster changes its mass M_c and half-mass radius r_h (the radius which encloses half of the mass). For the two clusters we highlighted in Fig. 5.2, they build up their masses and deepen their potential wells to capture BHs. This is illustrated in Fig. 5.3, where we track the relative distance ($\mathbf{r}_\mathrm{rel} \equiv \mathbf{r}_\mathrm{BH}-\mathbf{r}_\mathrm{cluster}$), velocity ($\mathbf{v}_\mathrm{vel} = d\mathbf{r}_\mathrm{rel}/dt$), and specific angular momentum ($\mathbf{j}_\mathrm{rel} \equiv \mathbf{r}_\mathrm{rel}\times\mathbf{v}_\mathrm{vel}$) of the two BH-cluster pairs. Since clusters keep evolving, we rescale each quantity with characteristic units, i.e., r_h, $\sqrt{GM_\mathrm{c}/r_\mathrm{h}}$, and $\sqrt{GM_\mathrm{c}r_\mathrm{h}}$. We find that each BH sinks to the companion cluster's center after $\sim 1\,\mathrm{Myr}$.

We highlight that the capture is not only due to an encounter between a BH and its companion cluster but largely amplified by the deepening of the cluster's potential well. In the bottom panel of Fig. 5.3, we rescale the relative velocity with the escape velocity of the potential well at the BH's position, which is defined as

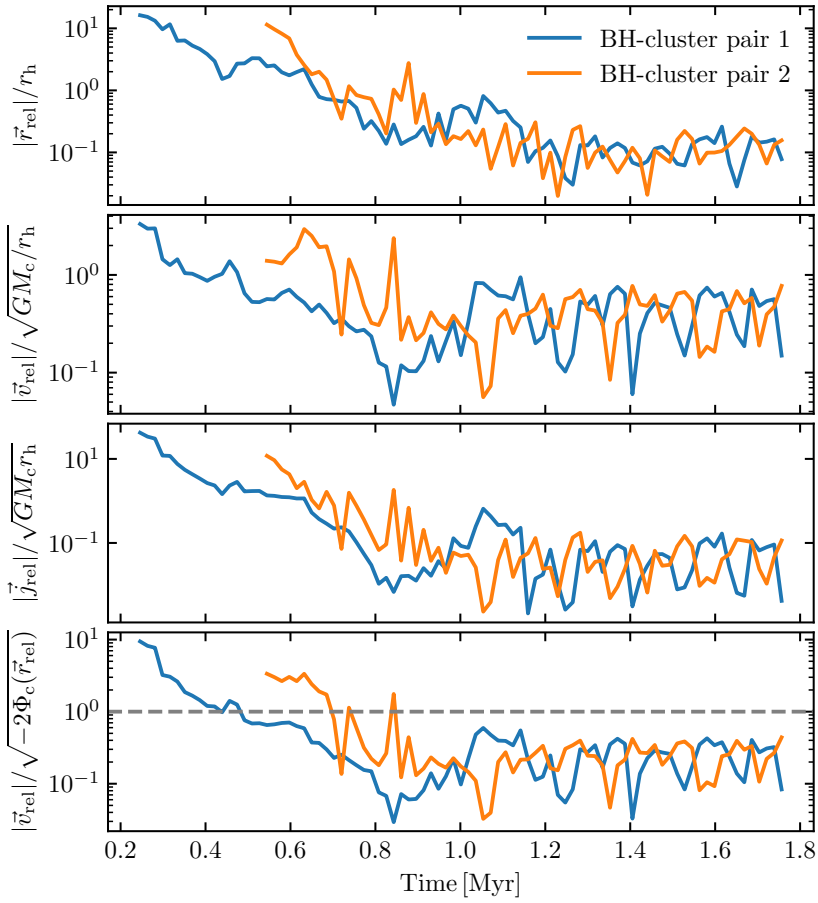

Figure 5.3: Sinking of BHs in their evolving parent cluster. From top to bottom, we show the relative distance, velocity, and specific angular momentum between the BH and the cluster, all rescaled with cluster mass profiles which are also evolving. Despite the absolute value of kinetic energy and angular momentum of each BH do not change significantly, BHs become bound and sink to clusters through the evolution of clusters.

$v_{\rm esc} = \sqrt{-2\Phi_{\rm c}(\mathbf{r}_{\rm rel})}$, where $\Phi_{\rm c}(\mathbf{r}) = -\sum_i Gm_i/|\mathbf{r} - \mathbf{r}_i|$ is the gravitational potential due to all star particles in the cluster. The two BH-cluster pairs are not gravitationally bounded at the beginning, but the ratio of kinetic energy over potential energy is lower than 1 at $\sim 0.4\,$Myr and $\sim 0.7\,$Myr respectively, which is approximately the time when the BH got captured by the companion cluster in Fig. 5.2. However, the actual relative velocity between the BH and the cluster grows from $\sim 50\,$km/s to $\sim 200\,$km/s at the late time, meaning that the mass assembly history of clusters is important.

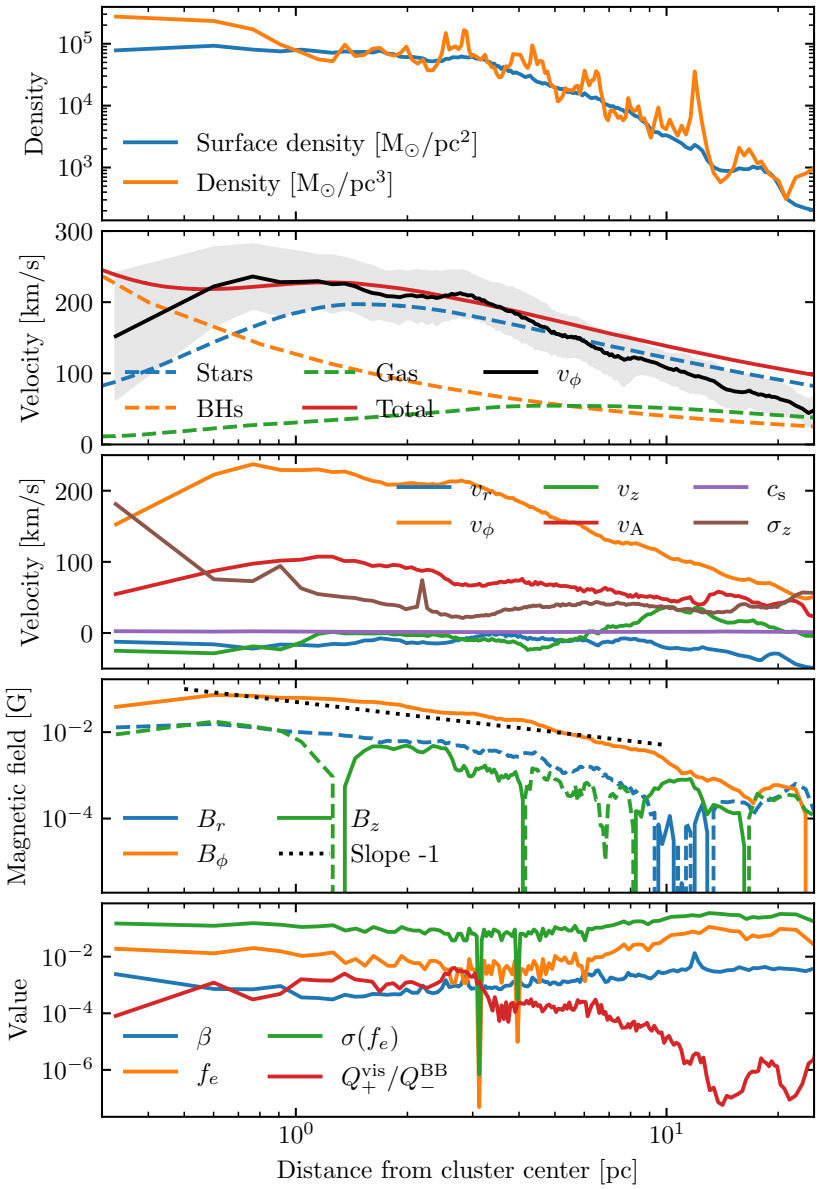

Figure 5.4: Dynamics and magnetic field of the disk. **Panel 1** (from top to bottom): surface density and mid-plane mean density of the profile of the disk. **Panel 2**: circular velocity v_ϕ of the disk and the Keplerian velocity fitting from stars, BHs, and gas. **Panel 3**: the radial, circular, and perpendicular velocity components of the gas inflow in the disk, and characteristic speeds for different physics including magnetic field (v_A), thermal pressure (c_s), and turbulence (σ_z). **Panel 4**: strength of the radial, toroidal, and poloidal magnetic field (dashed lines if negative). **Panel 5**: plasma beta (β), electron fraction (f_e, including its scattering), and the ratio between viscous heating (Q_+^{vis}) and blackbody cooling rates (Q_-^{BB}).

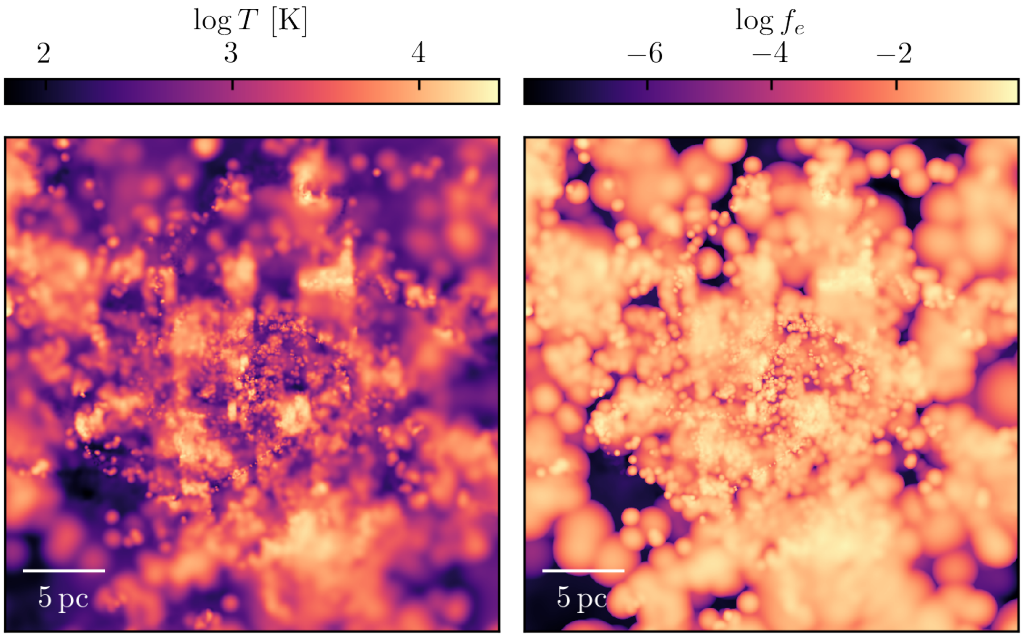

Figure 5.5: Maps of temperature and electron fraction of the disk. These maps are centered at the disk center. They show clumps with high-temperature contrast and bubbles with high ionization fractions from point sources, which means the disk is heated and ionized by feedback from stars.

5.4 The magnetized disk heated by stellar feedback

An unexplained behavior in § 5.3 is the linear mass accretion for BHs shown in Fig. 5.2. We find that it is due to the convergent inflow of gas that arrives at the center of the cluster, while the BHs are embedded in the disk structure presented in Fig. 5.1. In this section, we study the dynamics, magnetic field, and thermodynamics of the disk.

We summarize the dynamics and magnetic field of the disk in Fig. 5.4, where all quantities are measured from the simulation as a function of the relative distance from the final major cluster's center, at the simulation time limit. From the top panel, the surface density of the gas in the disk reaches $\sim 10^5\,\mathrm{M}_\odot/\mathrm{pc}^2$, while the mid-plane density can be $\sim 3\times10^5\,\mathrm{M}_\odot/\mathrm{pc}^3$ at the center. Comparing the two curves, we find that the effective thickness of the disk is ~ 1 pc. Moreover, both the density and surface density drop following a power law of roughly r^{-2}, once the distance is above ~ 4 pc.

There are three sources of gravity in the system: BHs, stars in the cluster, and gas. In the second panel of Fig. 5.4, we fit the measured circular velocity v_ϕ (i.e.,

the rotation curve) with Keplerian contributions from different components. When the radius is small ($\lesssim$ 0.5pc), gravity is dominated by BHs near the center (note that multiple BHs migrated to the center at the end of the simulation); when the radius gets larger, the cluster dominates. Comparing the Keplerian fitting and the measurement, there is a relatively good fit in the 0.5 pc – 5 pc regime. We note that at the inner radius, the rotation curve has a larger scattering, and the Keplerian fitting deviates. This is because of the lack of resolution at these small scales, and the scale is comparable to or smaller than the gravitational softening length of black holes (0.3 pc) in the simulation. Deviations in the outer region can be explained by gas infalling, which requires sub-Keplerian orbits. Another reason is the support from the toroidal magnetic field, which we will discuss later.

We then compare different velocities involved in the simulation in the third panel of Fig. 5.4. For decompositions under cylinder coordinates, we find that the circular velocity is the most dominant one, there is also a negative radial velocity which accounts for the inward mass flows. The z-component velocity is mostly insignificant and close to zero. There are also some characteristic velocities related to different physics. The Alfven speed $v_{\rm A} \equiv B/\sqrt{4\pi\rho}$ is the characteristic velocity of MHD waves, the sound speed $c_{\rm s}$ determines the importance of thermal pressure, and σ_z (velocity dispersion along the z-direction) is a measure of the turbulence velocity. From the disk in our simulation, we find that $v_\phi > v_{\rm A} \gtrsim \sigma_z \gg c_{\rm s}$. This implies that the magnetic field is very important to support the disk, while thermal pressure is negligible, unlike the standard disk model (Shakura and Sunyaev, 1973). We find that turbulence is also important, and even trans-Alfvenic at the outer boundary. This implies that the disk can be fluffy since $H/R \sim v_{\rm turb}/v_\phi \sim \sigma_z/v_\phi$, which is also observed from an edge-on view of the disk in our simulation.

The illustration for the magnetic field is presented in the fourth panel of Fig. 5.4, where we measure the radial (B_r), toroidal (B_ϕ), and poloidal (B_z) components of the magnetic field. The toroidal component is the strongest of the three, while there is also a negative radial component. The poloidal component is frequently flipping its sign at different radii, which means there are some threadings crossing the disk. We fit the slope of B_r and B_ϕ and find that they both grow as r^{-1} towards the center of the disk. At the inner radii of the disk, the toroidal magnetic field is as strong as $\sim$ 0.1G, which the initial magnetic field strength is about 400 μG, which accounts for 10% of the gravitational binding energy of the GMC.

We argue that the growth of the magnetic field is due to flux-freezing. This can

be demonstrated with the induction equation, which is $\partial\mathbf{B}/\partial t = \nabla \times (\mathbf{v} \times \mathbf{B})$ (we intentionally ignored the resistance term as it is unimportant, we will cover this later in this chapter). With the toroidal field, $B_\phi \gg B_r$, we find the dominant term for the induction equation in the toroidal direction is $\partial B_\phi/\partial r = -(1/v_r) \cdot \partial(v_r B_\phi)/\partial r$, which implies $\partial B_\phi/\partial r = -B_\phi \cdot (\partial \ln v_r/\partial r)/2$. We note that $2\pi\Sigma v_r = \dot{M}$ where $\dot{M}$ is the mass inflow rate which is (almost) constant (in the simulation, it is $\sim 10\,\mathrm{M}_\odot/\mathrm{yr}$). In the simulation, we find $\Sigma \propto r^{-2}$ for r in $\sim 0.5 - 10\,\mathrm{pc}$, which is the same regime of B_ϕ fitting (see Fig. 5.4). This further implies that $(\partial \ln v_r/\partial r)/2 = 1/r$ and $B_\phi \propto r^{-1}$, self-consistently explaining what we see in the simulation.

The strong toroidal magnetic field provides support to the disk. This can be evaluated with the Lorentz force $\rho\mathbf{f} = (\nabla \times \mathbf{B}) \times \mathbf{B}/4\pi$. For the toroidal component, we have

$$\mathbf{f} = -\frac{B_\phi}{4\pi\rho}\frac{\partial(rB_\phi)}{\partial r}\hat{\mathbf{r}} - \frac{1}{4\pi\rho}\frac{\partial B_\phi^2}{\partial z}\hat{\mathbf{z}}. \tag{5.1}$$

For moderate radii of the disk, $B^\phi \propto r^{-1}$ so the Lorentz force is negligible in the disk plane, while a significant outward force can be important once $r \gtrsim 10\,\mathrm{pc}$ since B_ϕ has a steep dependence on r (Fig. 5.4). This well explains the deviation of the Keplerian fitting to the rotational curve in Fig. 5.4. In the vertical direction, the gradient term provides a support force to the gas in the disk, which balances gravity. Turbulence support can be less important since $v_\mathrm{A} > \sigma_z$.

Finally, we study the thermodynamics of the disk. We first check the plasma beta, which is defined as $\beta \equiv u_\mathrm{thermal}/u_\mathrm{magnetic} = 8\pi n k_\mathrm{B} T/B^2$. From the simulation, we find the temperature of the disk is $\sim 400\,\mathrm{K}$ for most of the region outside the radii of $\sim 3\,\mathrm{pc}$, while it can increase to $\sim 1500\,\mathrm{K}$ at the center. As shown in the last panel of Fig. 5.4, the plasma beta is $\sim 10^{-3}$ for the disk, which again demonstrates that the disk is magnetically supported.

Still, there are some aspects to check, for example, whether the ideal MHD utilized in the simulation is still applicable to the disk, and whether the disk is heated by viscous heating like the standard disk model (Shakura and Sunyaev, 1973). The first issue arises since the disk scale ($\sim$ pc) is between galactic/AGN disks and sub-parsec protostellar disks. For the latter, the ionization fraction is low such that the resistance η is typically not negligible, non-ideal MHD effects are thus important. The second issue is also important to further understanding of the disk.

We measure the electron fraction f_e of the disk. As shown in the last panel of Fig. 5.4, the electron fraction is typically high in the disk ($\sim 10^{-2}$), while there is

a huge scattering that even reaches ~ 0.1. This means that ionization in the disk is even: some gas cells in the simulation are highly ionized but some are only ionized negligibly. Still, the overall high ionization fraction means that the ideal MHD treatment used in our simulations is proper.

We also check the second issue of heating/cooling of the disk. Cooling of optically thick disks (like this disk, as suggested in the top panel of Fig. 5.4) is dominated by blackbody radiation, while heating is primarily due to viscosity that transforms gravitational energy into heat in the standard disk model (Shakura and Sunyaev, 1973). In equilibrium, cooling per unit area $Q_{-}^{\rm BB} \sim \sigma_{\rm SB} T^4$ equals to the viscous heating rate per unit area $Q_{+}^{\rm vis} \sim \dot{M}\Omega^2$, as also assumed in the standard disk model. We check the ratio $Q_{+}^{\rm vis}/Q_{-}^{\rm BB}$ of the disk, and find the ratio is very low ($\lesssim 10^{-3}$). Viscous heating is thus not sufficient to heat the gas to $\sim 400\,{\rm K}$ or even higher as observed in the disk.

We argue that both the issues with the ionization fraction and heating sources are reconciled by stellar feedback. This is demonstrated in Fig. 5.5, where we show the map of the disk temperature and electron fraction, centered at the disk center. Both maps show no disk structures. Instead, there are hot clumps and ionization bubbles in the disk. A further comparison confirms that both the clumps and bubbles are in alignment with the position of the stars. Feedback from stars not only heats the disk through HII heating and Compton heating but also ionizes the gas through photoionization.

The magnetic-supported and feedback-heated disk creates a sufficient amount of inflow for the BH at the center ($\sim 10\,{\rm M}_\odot/{\rm yr}$ as measured in the simulation). The inflow is also steady since $\sim 0.75\,{\rm Myr}$. BH accretion near the center can be described with the Bondi accretion (Bondi, 1952), in which the gas inside the radius of gravitational influence is bounded to the BH. The radius is proportional to the BH mass (Bondi, 1952; Krumholz et al., 2006), which means more massive BH will have a higher accretion rate. This also explains the mass evolution of the two BHs presented in Fig. 5.2: since they both have a mass of $\sim 10^4\,{\rm M}_\odot$ when they migrate to the center, it is not surprising that they have similar mass accretion and growth history after $\sim 0.75\,{\rm Myr}$. This is also true for a few other BHs with less significant mass accretion.

Another underlying effect of the magnetic field and feedback heating/ionization is the suppression of star formation after $\sim 1,{\rm Myr}$, which is reflected by the mass evolution of the cluster (Fig. 5.2), which almost does not change at late times.

The suppression happens because of the strong magnetic field support that prevents gravitational collapses and fragmentation, while ionization and heating can be less important since $v_{\rm A} \gg c_{\rm s}$ (though they also prevent star formation). These effects also conserve the gas material and provide more fuel for BH accretion.

5.5 Conclusions and discussions

From the simulation, we find a scenario of BH accretion in star-forming GMCs, in which BHs first get gravitationally captured by evolving star clusters. After that, the BHs migrate along with their companion clusters until they settle down at the center of the major massive cluster after mergers. A convergent gas flow to the cluster's center then happens, creating a preferred condition for BH accretion. Major conclusions are summarized below.

1. Before and after the gravitational capture of BHs, the absolute values of their relative velocities and specific angular momentum do not change significantly. Instead, the capture is due to the evolution (mass build-up and potential well deepening) of clusters.

2. The gas inflow creates a disk structure of scale $\sim 10\,{\rm pc}$, surface density $\sim 10^5\,{\rm M_\odot/pc^2}$, and scale height $\sim 1\,{\rm pc}$. The dynamics of the gas are largely dominated by the massive central cluster.

3. The gaseous disk is turbulent/fluffy ($H/R \sim 0.1$), and highly magnetized ($\beta \sim 10^{-3}$) with a strong toroidal magnetic field ($B_\phi \lesssim 0.1\,{\rm G}$) from flux freezing. The magnetic field also supports the disk, while the thermal support is negligible.

4. The disk has an overall high ionization fraction ($f_e \sim 0.01$) and an warm temperature ($\sim 400\,{\rm K}$). Both ionization and heating are from stellar feedback, while viscous heating is negligible.

One caveat for this scenario is the mechanical feedback from BHs since the simulation is in the weak-feedback limit (as mentioned in § 5.2). If BH feedback is strong, the GMC can be disrupted earlier due to the accretion of dense clumps in the GMC (Shi et al., 2023b), preventing further star cluster formation and mergers. We argue that the scenario is still possible even with a strong BH feedback model since the possibility of clump accretion is low (~ 0.01, Shi et al., 2023b), there is still a very

large window for BHs to sink to the cluster center. The sustainability of the later phase of disk accretion is probably affected by BH feedback.

It is also worth mentioning another GMC of $10^6\,M_\odot$ and 5 pc which we simulated at the weak-feedback limit. The GMC has the same initial surface density ($\sim 10^4\,M_\odot$) as the $10^8\,M_\odot$ GMC studied in this paper. In this GMC, we also observed a disk structure at the late time of the simulation, which is also induced by the final central cluster, and BHs trapped at the center grow linearly, as also shown here. The difference is that the disk in the $\sim 10^6\,M_\odot$ is not as typical as the one shown here. Instead, it is even more fluffy. Stellar feedback from stars at the cluster's center also cleared part of the gas at the center (though the disk is not disrupted), generating a torus shape. Still, despite that some other factors (like the cluster or GMC mass) can affect the dynamics of this scenario, they are sub-dominant while the surface density is more important.

In high-redshift galaxies, cosmological simulations also show that dense GMCs of similar size and mass can exist (e.g., FIRE-2 zoom-in simulations of high-redshift galaxies, Ma et al., 2018; Ma et al., 2019; Ma et al., 2020; Wetzel et al., 2023). There are thus some implementations of this scenario. For example, for protoglactic nuclei that have high surface density, cluster formation may capture existing seed BHs (either as Population III remnants or stellar-mass BHs as a result of stellar evolution in the cluster), and hierarchical mergers and migration can move the BH to the center of the nucleus. The seed, after accretion and possibly mergers with other BHs, can be the seed for the central SMBH of the galaxy. If the dense GMC is off-nucleus, BH seeds might migrate to the central cluster formed from the GMC. The cluster plus BH complex is much more massive than a bare BH seed, making it more possible to sink to the galactic center within a reasonable time ($\lesssim$ Gyr) to be the seed of the central SMBH (Ma et al., 2021).

We find the dynamics of disk formation in this study is in analogy with the disk formation of galaxies, which is also due to a potential well that drags gas toward the center, though feedback-inefficient stars play the role of "dark matter". BHs at the center, as "sink particles" that swallow gas, can be also important for disk formation in this study, since the secondary cluster at the end of the simulation also hosts a clump of gas, but no BH is captured by the cluster and there is no disk.

Flux freezing of the magnetic field can form a very strong toroidal component. This is observed in this study but can be more extreme in high-redshift AGNs. Recent zoom-in simulations of AGNs with FIRE-3 and STARFORGE physics (Grudić et

al., 2021b; Guszejnov et al., 2021) in Hopkins, 2023b and Hopkins, 2023a use the super-refinement technique to narrow down the resolution near the BHs from sub-Mpc to the au-scale. The simulation found even more extreme plasma $\beta \sim 10^{-6}$ near the BH, which means the disk is magnetically supported. Star formation also stalls due to the magnetic field near the AGN. The strong toroidal magnetic field in disks can be prevalent in the Universe from flux freezing as suggested by simulations at vastly different scales.

There is apparently a co-evolution between the cluster and the BH since the cluster brings a huge amount of gas to feed the seed BH. We find that the BH-cluster pair is below the $M_{\rm BH} - \sigma_\star$ relation for galaxies: at the late time, the cluster velocity dispersion is $\sim 200\,{\rm km/s}$, while the BH mass is $\sim 10^6\,{\rm M}_\odot$ (or few multiple if seeds in the simulation merge later). This is significantly below the $M_{\rm BH} - \sigma_\star$ relation as in Kormendy and Ho, 2013.

Observational signals for the scenario can be tricky. The Eddington luminosity of a $10^6\,{\rm M}_\odot$ BH is $L_{\rm Edd} = 3.2 \times 10^{10}\,{\rm L}_\odot$, while the star mass is $\sim 4 \times 10^7\,{\rm M}_\odot$, resulting the total luminosity of $\sim 4 \times 10^{10}\,{\rm L}_\odot$ if the light-to-mass ratio for young stars is $\sim 1000\,{\rm L}_\odot/{\rm M}_\odot$. This means the BH accretion can be overshined by light from stars if the system is at a high redshift. Acquiring other information, like the spectroscopic signature might be helpful to provide an observational prediction.

BIBLIOGRAPHY

Abbott, R. et al. (Sept. 2020). "Properties and Astrophysical Implications of the 150 $M_{\odot}$ Binary Black Hole Merger GW190521." ApJ 900.1, L13, L13. DOI: 10.3847/2041-8213/aba493. arXiv: 2009.01190 [astro-ph.HE].

Abramowicz, M. A. et al. (Sept. 1988). "Slim Accretion Disks." ApJ 332, 646. DOI: 10.1086/166683.

Abramowicz, M. A. and P. C. Fragile (Jan. 2013). "Foundations of Black Hole Accretion Disk Theory." *Living Reviews in Relativity* 16.1, 1, 1. DOI: 10.12942/lrr-2013-1. arXiv: 1104.5499 [astro-ph.HE].

Abramowicz, M. A. and O. Straub (Aug. 2014). "Accretion discs." *Scholarpedia* 9, 2408. DOI: 10.4249/scholarpedia.2408.

Alessandrini, E. et al. (Nov. 2014). "Dynamical Friction in Multi-component Evolving Globular Clusters." ApJ 795.2, 169, 169. DOI: 10.1088/0004-637X/795/2/169. arXiv: 1409.4987 [astro-ph.SR].

Alister Seguel, P. J. et al. (Apr. 2020). "Formation of SMBH seeds in Population III star clusters through collisions: the importance of mass loss." MNRAS 493.2, 2352–2362. DOI: 10.1093/mnras/staa456. arXiv: 1912.01737 [astro-ph.GA].

Anglés-Alcázar, D. et al. (Aug. 2021). "Cosmological Simulations of Quasar Fueling to Subparsec Scales Using Lagrangian Hyper-refinement." ApJ 917.2, 53, 53. DOI: 10.3847/1538-4357/ac09e8. arXiv: 2008.12303 [astro-ph.GA].

Ball, W. H. et al. (July 2011). "The structure and evolution of quasi-stars." MNRAS 414.3, 2751–2762. DOI: 10.1111/j.1365-2966.2011.18591.x. arXiv: 1102.5098 [astro-ph.HE].

Bañados, E. et al. (Jan. 2018). "An 800-million-solar-mass black hole in a significantly neutral Universe at a redshift of 7.5." Nature 553.7689, 473–476. DOI: 10.1038/nature25180. arXiv: 1712.01860 [astro-ph.GA].

Barmby, P. et al. (June 2007). "Structural Parameters for Globular Clusters in M31 and Generalizations for the Fundamental Plane." AJ 133.6, 2764–2786. DOI: 10.1086/516777. arXiv: 0704.2057 [astro-ph].

Bate, M. R., I. A. Bonnell, and N. M. Price (Nov. 1995). "Modelling accretion in protobinary systems." MNRAS 277.2, 362–376. DOI: 10.1093/mnras/277.2.362. arXiv: astro-ph/9510149 [astro-ph].

Baumgardt, H. (Jan. 2017). "N -body modelling of globular clusters: masses, mass-to-light ratios and intermediate-mass black holes." MNRAS 464.2, 2174–2202. DOI: 10.1093/mnras/stw2488. arXiv: 1609.08794 [astro-ph.GA].

Baumgardt, H. and M. Hilker (Aug. 2018). "A catalogue of masses, structural parameters, and velocity dispersion profiles of 112 Milky Way globular clusters." MNRAS 478.2, 1520–1557. DOI: 10.1093/mnras/sty1057. arXiv: 1804.08359 [astro-ph.GA].

Baumgardt, H. et al. (May 2003). "A Dynamical Model for the Globular Cluster G1." ApJ 589.1, L25–L28. DOI: 10.1086/375802. arXiv: astro-ph/0301469 [astro-ph].

Beattie, J. R. et al. (Dec. 2022). "The density distribution and physical origins of intermittency in supersonic, highly magnetized turbulence with diverse modes of driving." MNRAS 517.4, 5003–5031. DOI: 10.1093/mnras/stac3005. arXiv: 2109.10470 [astro-ph.GA].

Begelman, M. C. (Apr. 1979). "Can a spherically accreting black hole radiate very near the Eddington limit?" MNRAS 187, 237–251. DOI: 10.1093/mnras/187.2.237.

Begelman, M. C. (Feb. 2010). "Evolution of supermassive stars as a pathway to black hole formation." MNRAS 402.1, 673–681. DOI: 10.1111/j.1365-2966.2009.15916.x. arXiv: 0910.4398 [astro-ph.CO].

Begelman, M. C., M. Volonteri, and M. J. Rees (July 2006). "Formation of supermassive black holes by direct collapse in pre-galactic haloes." MNRAS 370.1, 289–298. DOI: 10.1111/j.1365-2966.2006.10467.x. arXiv: astro-ph/0602363 [astro-ph].

Berdina, L. A., V. S. Tsvetkova, and V. M. Shulga (Jan. 2021). "Super-Eddington accretion in the Q2237+0305 quasar?" A&A 645, A78, A78. DOI: 10.1051/0004-6361/202039379. arXiv: 2012.12025 [astro-ph.HE].

Bigiel, F. et al. (Dec. 2008). "The Star Formation Law in Nearby Galaxies on Sub-Kpc Scales." AJ 136.6, 2846–2871. DOI: 10.1088/0004-6256/136/6/2846. arXiv: 0810.2541 [astro-ph].

Binney, J. and S. Tremaine (2008). *Galactic Dynamics: Second Edition*.

Bjoernsson, G. et al. (Aug. 1996). "Hot Accretion Disks Revisited." ApJ 467, 99. DOI: 10.1086/177587.

Blandford, R. D. and R. L. Znajek (May 1977). "Electromagnetic extraction of energy from Kerr black holes." MNRAS 179, 433–456. DOI: 10.1093/mnras/179.3.433.

Blandford, R. D. and M. C. Begelman (Feb. 1999). "On the fate of gas accreting at a low rate on to a black hole." MNRAS 303.1, L1–L5. DOI: 10.1046/j.1365-8711.1999.02358.x. arXiv: astro-ph/9809083 [astro-ph].

– (Mar. 2004). "Two-dimensional adiabatic flows on to a black hole - I. Fluid accretion." MNRAS 349.1, 68–86. DOI: 10.1111/j.1365-2966.2004.07425.x. arXiv: astro-ph/0306184 [astro-ph].

Boco, L., A. Lapi, and L. Danese (Mar. 2020). "Growth of Supermassive Black Hole Seeds in ETG Star-forming Progenitors: Multiple Merging of Stellar Compact Remnants via Gaseous Dynamical Friction and Gravitational-wave Emission." ApJ 891.1, 94, 94. DOI: 10.3847/1538-4357/ab7446. arXiv: 2002.03645 [astro-ph.GA].

Böker, T. et al. (Jan. 2004). "A Hubble Space Telescope Census of Nuclear Star Clusters in Late-Type Spiral Galaxies. II. Cluster Sizes and Structural Parameter Correlations." AJ 127.1, 105–118. DOI: 10.1086/380231. arXiv: astro-ph/0309761 [astro-ph].

Bondi, H. (Jan. 1952). "On spherically symmetrical accretion." MNRAS 112, 195. DOI: 10.1093/mnras/112.2.195.

Botella, I. et al. (Apr. 2022). "Structure of the super-Eddington outflow and its impact on the cosmological scale." PASJ 74.2, 384–397. DOI: 10.1093/pasj/psac001. arXiv: 2202.13805 [astro-ph.GA].

Bower, R. G. et al. (Feb. 2017). "The dark nemesis of galaxy formation: why hot haloes trigger black hole growth and bring star formation to an end." MNRAS 465.1, 32–44. DOI: 10.1093/mnras/stw2735. arXiv: 1607.07445 [astro-ph.GA].

Bozzo, E. et al. (Nov. 2011). "IGR J17361-4441: a possible new accreting X-ray binary in NGC 6388." A&A 535, L1, L1. DOI: 10.1051/0004-6361/201118022. arXiv: 1109.5719 [astro-ph.HE].

Brightman, M. et al. (May 2019). "Breaking the limit: Super-Eddington accretion onto black holes and neutron stars." BAAS 51.3, 352, 352. DOI: 10.48550/arXiv.1903.06844. arXiv: 1903.06844 [astro-ph.HE].

Bromm, V. and R. B. Larson (Sept. 2004). "The First Stars." ARA&A 42.1, 79–118. DOI: 10.1146/annurev.astro.42.053102.134034. arXiv: astro-ph/0311019 [astro-ph].

Bromm, V. and A. Loeb (Oct. 2003). "Formation of the First Supermassive Black Holes." ApJ 596.1, 34–46. DOI: 10.1086/377529. arXiv: astro-ph/0212400 [astro-ph].

Burkhart, B. et al. (Mar. 2009). "Density Studies of MHD Interstellar Turbulence: Statistical Moments, Correlations and Bispectrum." ApJ 693.1, 250–266. DOI: 10.1088/0004-637X/693/1/250. arXiv: 0811.0822 [astro-ph].

Burleigh, K. J. et al. (June 2017). "Bondi-Hoyle accretion in a turbulent, magnetized medium." MNRAS 468.1, 717–727. DOI: 10.1093/mnras/stx439.

Bustard, C. and E. G. Zweibel (June 2021). "Cosmic-Ray Transport, Energy Loss, and Influence in the Multiphase Interstellar Medium." ApJ 913.2, 106, 106. DOI: 10.3847/1538-4357/abf64c. arXiv: 2012.06585 [astro-ph.HE].

Chabrier, G. (July 2003). "Galactic Stellar and Substellar Initial Mass Function." PASP 115.809, 763–795. DOI: 10.1086/376392. arXiv: astro-ph/0304382 [astro-ph].

Chan, T. K. et al. (Sept. 2019). "Cosmic ray feedback in the FIRE simulations: constraining cosmic ray propagation with GeV γ-ray emission." MNRAS 488.3, 3716–3744. DOI: 10.1093/mnras/stz1895. arXiv: 1812.10496 [astro-ph.GA].

Chevance, M. et al. (Mar. 2022). "The Life and Times of Giant Molecular Clouds." *arXiv e-prints*, arXiv:2203.09570, arXiv:2203.09570. DOI: 10.48550/arXiv.2203.09570. arXiv: 2203.09570 [astro-ph.GA].

Chon, S. and K. Omukai (May 2020). "Supermassive star formation via super competitive accretion in slightly metal-enriched clouds." MNRAS 494.2, 2851–2860. DOI: 10.1093/mnras/staa863. arXiv: 2001.06491 [astro-ph.GA].

Corbett Moran, C., M. Y. Grudić, and P. F. Hopkins (Mar. 2018). "The effects of metallicity and cooling physics on fragmentation: implications on direct-collapse black hole formation." *arXiv e-prints*, arXiv:1803.06430, arXiv:1803.06430. DOI: 10.48550/arXiv.1803.06430. arXiv: 1803.06430 [astro-ph.GA].

Cseh, D. et al. (Aug. 2010). "Radio observations of NGC 6388: an upper limit on the mass of its central black hole." MNRAS 406.2, 1049–1054. DOI: 10.1111/j.1365-2966.2010.16726.x. arXiv: 1003.4604 [astro-ph.HE].

Dekel, A., R. Sari, and D. Ceverino (Sept. 2009). "Formation of Massive Galaxies at High Redshift: Cold Streams, Clumpy Disks, and Compact Spheroids." ApJ 703.1, 785–801. DOI: 10.1088/0004-637X/703/1/785. arXiv: 0901.2458 [astro-ph.GA].

Devecchi, B. and M. Volonteri (Mar. 2009). "Formation of the First Nuclear Clusters and Massive Black Holes at High Redshift." ApJ 694.1, 302–313. DOI: 10.1088/0004-637X/694/1/302. arXiv: 0810.1057 [astro-ph].

Di Matteo, T., V. Springel, and L. Hernquist (Feb. 2005). "Energy input from quasars regulates the growth and activity of black holes and their host galaxies." Nature 433.7026, 604–607. DOI: 10.1038/nature03335. arXiv: astro-ph/0502199 [astro-ph].

Di Matteo, T. et al. (Mar. 2008). "Direct Cosmological Simulations of the Growth of Black Holes and Galaxies." ApJ 676.1, 33–53. DOI: 10.1086/524921. arXiv: 0705.2269 [astro-ph].

Dijkstra, M. et al. (Dec. 2008). "Fluctuations in the high-redshift Lyman-Werner background: close halo pairs as the origin of supermassive black holes." MNRAS 391.4, 1961–1972. DOI: 10.1111/j.1365-2966.2008.14031.x. arXiv: 0810.0014 [astro-ph].

Dubois, Y. et al. (Feb. 2013). "Blowing cold flows away: the impact of early AGN activity on the formation of a brightest cluster galaxy progenitor." MNRAS 428.4, 2885–2900. DOI: 10.1093/mnras/sts224. arXiv: 1206.5838 [astro-ph.CO].

Dubois, Y. et al. (Sept. 2015). "Black hole evolution - I. Supernova-regulated black hole growth." MNRAS 452.2, 1502–1518. DOI: 10.1093/mnras/stv1416. arXiv: 1504.00018 [astro-ph.GA].

Eckart, A. et al. (Apr. 2002). "Stellar orbits near Sagittarius A*." MNRAS 331.4, 917–934. DOI: 10.1046/j.1365-8711.2002.05237.x. arXiv: astro-ph/0201031 [astro-ph].

Elmegreen, B. G. (Sept. 2002). "Star Formation from Galaxies to Globules." ApJ 577.1, 206–220. DOI: 10.1086/342177. arXiv: astro-ph/0207114 [astro-ph].

Elmegreen, B. G. and J. Scalo (Sept. 2004). "Interstellar Turbulence I: Observations and Processes." ARA&A 42.1, 211–273. DOI: 10.1146/annurev.astro.41.011802.094859. arXiv: astro-ph/0404451 [astro-ph].

Elson, R. A. W., S. M. Fall, and K. C. Freeman (Dec. 1987). "The Structure of Young Star Clusters in the Large Magellanic Cloud." ApJ 323, 54. DOI: 10.1086/165807.

Evans Neal J., I. (Jan. 1999). "Physical Conditions in Regions of Star Formation." ARA&A 37, 311–362. DOI: 10.1146/annurev.astro.37.1.311. arXiv: astro-ph/9905050 [astro-ph].

Event Horizon Telescope Collaboration et al. (Apr. 2019). "First M87 Event Horizon Telescope Results. I. The Shadow of the Supermassive Black Hole." ApJ 875.1, L1, L1. DOI: 10.3847/2041-8213/ab0ec7. arXiv: 1906.11238 [astro-ph.GA].

Event Horizon Telescope Collaboration et al. (May 2022). "First Sagittarius A* Event Horizon Telescope Results. I. The Shadow of the Supermassive Black Hole in the Center of the Milky Way." ApJ 930.2, L12, L12. DOI: 10.3847/2041-8213/ac6674.

Evstigneeva, E. A. et al. (Apr. 2007). "Internal Properties of Ultracompact Dwarf Galaxies in the Virgo Cluster." AJ 133.4, 1722–1740. DOI: 10.1086/511958. arXiv: astro-ph/0612483 [astro-ph].

Fabian, A. C. (Oct. 1999). "The obscured growth of massive black holes." MNRAS 308.4, L39–L43. DOI: 10.1046/j.1365-8711.1999.03017.x. arXiv: astro-ph/9908064 [astro-ph].

– (Sept. 2012). "Observational Evidence of Active Galactic Nuclei Feedback." ARA&A 50, 455–489. DOI: 10.1146/annurev-astro-081811-125521. arXiv: 1204.4114 [astro-ph.CO].

Fan, X. et al. (Dec. 2001). "A Survey of z>5.8 Quasars in the Sloan Digital Sky Survey. I. Discovery of Three New Quasars and the Spatial Density of Luminous Quasars at z≂6." AJ 122.6, 2833–2849. DOI: 10.1086/324111. arXiv: astro-ph/0108063 [astro-ph].

Farber, R. et al. (Apr. 2018). "Impact of Cosmic-Ray Transport on Galactic Winds." ApJ 856.2, 112, 112. DOI: 10.3847/1538-4357/aab26d. arXiv: 1707.04579 [astro-ph.HE].

Farrell, S. A. et al. (July 2009). "An intermediate-mass black hole of over 500 solar masses in the galaxy ESO243-49." Nature 460.7251, 73–75. DOI: 10.1038/nature08083. arXiv: 1001.0567 [astro-ph.HE].

Federrath, C. et al. (Mar. 2010). "Comparing the statistics of interstellar turbulence in simulations and observations. Solenoidal versus compressive turbulence forcing." A&A 512, A81, A81. DOI: 10.1051/0004-6361/200912437. arXiv: 0905.1060 [astro-ph.SR].

Federrath, C., R. S. Klessen, and W. Schmidt (Dec. 2008). "The Density Probability Distribution in Compressible Isothermal Turbulence: Solenoidal versus Compressive Forcing." ApJ 688.2, L79. DOI: 10.1086/595280. arXiv: 0808.0605 [astro-ph].

Fragione, G., I. Ginsburg, and B. Kocsis (Apr. 2018). "Gravitational Waves and Intermediate-mass Black Hole Retention in Globular Clusters." ApJ 856.2, 92, 92. DOI: 10.3847/1538-4357/aab368. arXiv: 1711.00483 [astro-ph.GA].

Fragione, G. and F. A. Rasio (Feb. 2023). "Demographics of Hierarchical Black Hole Mergers in Dense Star Clusters." *arXiv e-prints*, arXiv:2302.11613, arXiv:2302.11613. DOI: 10.48550/arXiv.2302.11613. arXiv: 2302.11613 [astro-ph.GA].

Fragione, G. et al. (Mar. 2022). "Repeated Mergers, Mass-gap Black Holes, and Formation of Intermediate-mass Black Holes in Dense Massive Star Clusters." ApJ 927.2, 231, 231. DOI: 10.3847/1538-4357/ac5026. arXiv: 2107.04639 [astro-ph.GA].

Fukushima, H. and H. Yajima (Oct. 2021). "Radiation hydrodynamics simulations of massive star cluster formation in giant molecular clouds." MNRAS 506.4, 5512–5539. DOI: 10.1093/mnras/stab2099. arXiv: 2104.10892 [astro-ph.GA].

Fukushima, H. et al. (Sept. 2020). "Star cluster formation and cloud dispersal by radiative feedback: dependence on metallicity and compactness." MNRAS 497.3, 3830–3845. DOI: 10.1093/mnras/staa2062. arXiv: 2005.13401 [astro-ph.GA].

Gao, Y. and P. M. Solomon (May 2004). "HCN Survey of Normal Spiral, Infrared-luminous, and Ultraluminous Galaxies." ApJS 152.1, 63–80. DOI: 10.1086/383003. arXiv: astro-ph/0310341 [astro-ph].

Gebhardt, K., R. M. Rich, and L. C. Ho (Dec. 2005). "An Intermediate-Mass Black Hole in the Globular Cluster G1: Improved Significance from New Keck and Hubble Space Telescope Observations." ApJ 634.2, 1093–1102. DOI: 10.1086/497023. arXiv: astro-ph/0508251 [astro-ph].

Gebhardt, K. et al. (Aug. 2000). "A Relationship between Nuclear Black Hole Mass and Galaxy Velocity Dispersion." ApJ 539.1, L13–L16. DOI: 10.1086/312840. arXiv: astro-ph/0006289 [astro-ph].

Geha, M., P. Guhathakurta, and R. P. van der Marel (Dec. 2002). "Internal Dynamics, Structure, and Formation of Dwarf Elliptical Galaxies. I. A Keck/Hubble Space Telescope Study of Six Virgo Cluster Dwarf Galaxies." AJ 124.6, 3073–3087. DOI: 10.1086/344764. arXiv: astro-ph/0206153 [astro-ph].

Ghez, A. M. et al. (Apr. 2003). "The First Measurement of Spectral Lines in a Short-Period Star Bound to the Galaxy's Central Black Hole: A Paradox of Youth." ApJ 586.2, L127–L131. DOI: 10.1086/374804. arXiv: astro-ph/0302299 [astro-ph].

Gieles, M. et al. (Aug. 2018a). "Concurrent formation of supermassive stars and globular clusters: implications for early self-enrichment." MNRAS 478.2, 2461–2479. DOI: 10.1093/mnras/sty1059. arXiv: 1804.04682 [astro-ph.GA].

Gieles, M. et al. (Feb. 2018b). "Mass models of NGC 6624 without an intermediate-mass black hole." MNRAS 473.4, 4832–4839. DOI: 10.1093/mnras/stx2694. arXiv: 1709.06874 [astro-ph.GA].

Giersz, M. et al. (May 2013). "MOCCA code for star cluster simulations - II. Comparison with N-body simulations." MNRAS 431.3, 2184–2199. DOI: 10.1093/mnras/stt307. arXiv: 1112.6246 [astro-ph.GA].

Goodman, A. A. et al. (Sept. 1998). "Coherence in Dense Cores. II. The Transition to Coherence." ApJ 504.1, 223–246. DOI: 10.1086/306045.

Goodman, A. A. et al. (Jan. 2009). "A role for self-gravity at multiple length scales in the process of star formation." Nature 457.7225, 63–66. DOI: 10.1038/nature07609.

Goodman, J. and J. C. Tan (June 2004). "Supermassive Stars in Quasar Disks." ApJ 608.1, 108–118. DOI: 10.1086/386360. arXiv: astro-ph/0307361 [astro-ph].

Greene, J. E., L. C. Ho, and A. J. Barth (Nov. 2008). "Black Holes in Pseudobulges and Spheroidals: A Change in the Black Hole-Bulge Scaling Relations at Low Mass." ApJ 688.1, 159–179. DOI: 10.1086/592078. arXiv: 0810.1972 [astro-ph].

Greene, J. E., J. Strader, and L. C. Ho (Aug. 2020). "Intermediate-Mass Black Holes." ARA&A 58, 257–312. DOI: 10.1146/annurev-astro-032620-021835. arXiv: 1911.09678 [astro-ph.GA].

Greif, T. H. et al. (Aug. 2011). "Simulations on a Moving Mesh: The Clustered Formation of Population III Protostars." ApJ 737.2, 75, 75. DOI: 10.1088/0004-637X/737/2/75. arXiv: 1101.5491 [astro-ph.CO].

Grudić, M. Y. and P. F. Hopkins (Sept. 2019). "The elephant in the room: the importance of the details of massive star formation in molecular clouds." MNRAS 488.2, 2970–2975. DOI: 10.1093/mnras/stz1820. arXiv: 1809.08344 [astro-ph.GA].

Grudić, M. Y. et al. (Nov. 2018a). "From the top down and back up again: star cluster structure from hierarchical star formation." MNRAS 481.1, 688–702. DOI: 10.1093/mnras/sty2303. arXiv: 1708.09065 [astro-ph.GA].

Grudić, M. Y. et al. (Apr. 2018b). "When feedback fails: the scaling and saturation of star formation efficiency." MNRAS 475.3, 3511–3528. DOI: 10.1093/mnras/sty035. arXiv: 1612.05635 [astro-ph.GA].

Grudić, M. Y. et al. (Sept. 2019a). "On the nature of variations in the measured star formation efficiency of molecular clouds." MNRAS 488.2, 1501–1518. DOI: 10.1093/mnras/stz1758. arXiv: 1809.08348 [astro-ph.GA].

Grudić, M. Y. et al. (Mar. 2019b). "The maximum stellar surface density due to the failure of stellar feedback." MNRAS 483.4, 5548–5553. DOI: 10.1093/mnras/sty3386. arXiv: 1804.04137 [astro-ph.GA].

Grudić, M. Y. et al. (Sept. 2021a). "A model for the formation of stellar associations and clusters from giant molecular clouds." MNRAS 506.3, 3239–3258. DOI: 10.1093/mnras/stab1894. arXiv: 2008.04453 [astro-ph.GA].

Grudić, M. Y. et al. (Sept. 2021b). "STARFORGE: Towards a comprehensive numerical model of star cluster formation and feedback." MNRAS 506.2, 2199–2231. DOI: 10.1093/mnras/stab1347. arXiv: 2010.11254 [astro-ph.IM].

Gualandris, A. and S. Portegies Zwart (Mar. 2007). "A hypervelocity star from the Large Magellanic Cloud." MNRAS 376.1, L29–L33. DOI: 10.1111/j.1745-3933.2007.00280.x. arXiv: astro-ph/0612673 [astro-ph].

Gültekin, K. et al. (Jan. 2019). "The Fundamental Plane of Black Hole Accretion and Its Use as a Black Hole-Mass Estimator." ApJ 871.1, 80, 80. DOI: 10.3847/1538-4357/aaf6b9. arXiv: 1901.02530 [astro-ph.HE].

Guo, F. and W. G. Mathews (Sept. 2012). "The Fermi Bubbles. I. Possible Evidence for Recent AGN Jet Activity in the Galaxy." ApJ 756.2, 181, 181. DOI: 10.1088/0004-637X/756/2/181. arXiv: 1103.0055 [astro-ph.HE].

Guo, F. and S. P. Oh (Feb. 2008). "Feedback heating by cosmic rays in clusters of galaxies." MNRAS 384.1, 251–266. DOI: 10.1111/j.1365-2966.2007.12692.x. arXiv: 0706.1274 [astro-ph].

Guo, M. et al. (Mar. 2023). "Toward Horizon-scale Accretion onto Supermassive Black Holes in Elliptical Galaxies." ApJ 946.1, 26, 26. DOI: 10.3847/1538-4357/acb81e. arXiv: 2211.05131 [astro-ph.HE].

Gürkan, M. A., M. Freitag, and F. A. Rasio (Apr. 2004). "Formation of Massive Black Holes in Dense Star Clusters. I. Mass Segregation and Core Collapse." ApJ 604.2, 632–652. DOI: 10.1086/381968. arXiv: astro-ph/0308449 [astro-ph].

Guszejnov, D. and P. F. Hopkins (June 2016). "Star formation in a turbulent framework: from giant molecular clouds to protostars." MNRAS 459.1, 9–20. DOI: 10.1093/mnras/stw619. arXiv: 1507.06678 [astro-ph.SR].

Guszejnov, D., P. F. Hopkins, and M. Y. Grudić (July 2018a). "Universal scaling relations in scale-free structure formation." MNRAS 477.4, 5139–5149. DOI: 10.1093/mnras/sty920. arXiv: 1707.05799 [astro-ph.GA].

Guszejnov, D. et al. (Oct. 2018b). "Isothermal Fragmentation: Is there a low-mass cut-off?" MNRAS 480.1, 182–191. DOI: 10.1093/mnras/sty1847. arXiv: 1804.08574 [astro-ph.GA].

Guszejnov, D. et al. (Feb. 2020). "Evolution of giant molecular clouds across cosmic time." MNRAS 492.1, 488–502. DOI: 10.1093/mnras/stz3527. arXiv: 1910.01163 [astro-ph.GA].

Guszejnov, D. et al. (Apr. 2021). "STARFORGE: the effects of protostellar outflows on the IMF." MNRAS 502.3, 3646–3663. DOI: 10.1093/mnras/stab278. arXiv: 2010.11249 [astro-ph.GA].

Guszejnov, D. et al. (Sept. 2022). "Cluster assembly and the origin of mass segregation in the STARFORGE simulations." MNRAS 515.1, 167–184. DOI: 10.1093/mnras/stac1737. arXiv: 2201.01781 [astro-ph.GA].

Habouzit, M., M. Volonteri, and Y. Dubois (July 2017). "Blossoms from black hole seeds: properties and early growth regulated by supernova feedback." MNRAS 468.4, 3935–3948. DOI: 10.1093/mnras/stx666. arXiv: 1605.09394 [astro-ph.GA].

Haiman, Z. and A. Loeb (May 2001). "What Is the Highest Plausible Redshift of Luminous Quasars?" ApJ 552.2, 459–463. DOI: 10.1086/320586. arXiv: astro-ph/0011529 [astro-ph].

Hansen, B. M. S. and M. Milosavljević (Aug. 2003). "The Need for a Second Black Hole at the Galactic Center." ApJ 593.2, L77–L80. DOI: 10.1086/378182. arXiv: astro-ph/0306074 [astro-ph].

Harris, W. E. (Oct. 1996). "A Catalog of Parameters for Globular Clusters in the Milky Way." AJ 112, 1487. DOI: 10.1086/118116.

Harrison, C. M. (July 2017). "Impact of supermassive black hole growth on star formation." *Nature Astronomy* 1, 0165, 0165. DOI: 10.1038/s41550-017-0165. arXiv: 1703.06889 [astro-ph.GA].

Haşegan, M. et al. (July 2005). "The ACS Virgo Cluster Survey. VII. Resolving the Connection between Globular Clusters and Ultracompact Dwarf Galaxies." ApJ 627.1, 203–223. DOI: 10.1086/430342. arXiv: astro-ph/0503566 [astro-ph].

He, C.-C., M. Ricotti, and S. Geen (Oct. 2019). "Simulating star clusters across cosmic time - I. Initial mass function, star formation rates, and efficiencies." MNRAS 489.2, 1880–1898. DOI: 10.1093/mnras/stz2239. arXiv: 1904.07889 [astro-ph.GA].

Heger, A. and S. E. Woosley (Mar. 2002). "The Nucleosynthetic Signature of Population III." ApJ 567.1, 532–543. DOI: 10.1086/338487. arXiv: astro-ph/0107037 [astro-ph].

Heger, A. et al. (July 2003). "How Massive Single Stars End Their Life." ApJ 591.1, 288–300. DOI: 10.1086/375341. arXiv: astro-ph/0212469 [astro-ph].

Heger, A., B. Müller, and I. Mandel (Apr. 2023). "Black holes as the end state of stellar evolution: Theory and simulations." *arXiv e-prints*, arXiv:2304.09350, arXiv:2304.09350. DOI: 10.48550/arXiv.2304.09350. arXiv: 2304.09350 [astro-ph.HE].

Hénault-Brunet, V. et al. (Jan. 2020). "On the black hole content and initial mass function of 47 Tuc." MNRAS 491.1, 113–128. DOI: 10.1093/mnras/stz2995. arXiv: 1908.08538 [astro-ph.GA].

Hennebelle, P. and G. Chabrier (Sept. 2008). "Analytical Theory for the Initial Mass Function: CO Clumps and Prestellar Cores." ApJ 684.1, 395–410. DOI: 10.1086/589916. arXiv: 0805.0691 [astro-ph].

Hilker, M. et al. (Feb. 2007). "Dynamical masses of ultra-compact dwarf galaxies in Fornax." A&A 463.1, 119–130. DOI: 10.1051/0004-6361:20066429. arXiv: astro-ph/0612484 [astro-ph].

Hills, J. G. (Feb. 1988). "Hyper-velocity and tidal stars from binaries disrupted by a massive Galactic black hole." Nature 331.6158, 687–689. DOI: 10.1038/331687a0.

Holley-Bockelmann, K. et al. (Oct. 2008). "Gravitational Wave Recoil and the Retention of Intermediate-Mass Black Holes." ApJ 686.2, 829–837. DOI: 10.1086/591218. arXiv: 0707.1334 [astro-ph].

Hopkins, P. F. (July 2012a). "An excursion-set model for the structure of giant molecular clouds and the interstellar medium." MNRAS 423.3, 2016–2036. DOI: 10.1111/j.1365-2966.2012.20730.x. arXiv: 1111.2863 [astro-ph.GA].

– (July 2012b). "The stellar initial mass function, core mass function and the last-crossing distribution." MNRAS 423.3, 2037–2044. DOI: 10.1111/j.1365-2966.2012.20731.x. arXiv: 1201.4387 [astro-ph.GA].

– (Apr. 2013a). "A general theory of turbulent fragmentation." MNRAS 430.3, 1653–1693. DOI: 10.1093/mnras/sts704. arXiv: 1210.0903 [astro-ph.CO].

– (Apr. 2013b). "A model for (non-lognormal) density distributions in isothermal turbulence." MNRAS 430.3, 1880–1891. DOI: 10.1093/mnras/stt010. arXiv: 1211.3119 [astro-ph.GA].

Hopkins, P. F. (July 2013c). "Variations in the stellar CMF and IMF: from bottom to top." MNRAS 433.1, 170–177. DOI: 10.1093/mnras/stt713. arXiv: 1204.2835 [astro-ph.GA].

– (Jan. 2013d). "Why do stars form in clusters? An analytic model for stellar correlation functions." MNRAS 428.3, 1950–1957. DOI: 10.1093/mnras/sts147. arXiv: 1202.2122 [astro-ph.GA].

– (June 2015). "A new class of accurate, mesh-free hydrodynamic simulation methods." MNRAS 450.1, 53–110. DOI: 10.1093/mnras/stv195. arXiv: 1409.7395 [astro-ph.CO].

– (Oct. 2016). "A constrained-gradient method to control divergence errors in numerical MHD." MNRAS 462.1, 576–587. DOI: 10.1093/mnras/stw1578. arXiv: 1509.07877 [astro-ph.IM].

– (June 2023a). "FORGE'd in FIRE II: The Formation of Magnetically-Dominated, Rapidly-Cooling Quasar Accretion Disks from Cosmological Initial Conditions." *in prep.*

– (June 2023b). "FORGE'd in FIRE: Resolving the End of Star Formation and Structure of AGN Accretion Disks from Cosmological Initial Conditions." *in prep.*

Hopkins, P. F., T. J. Cox, and L. Hernquist (Dec. 2008a). "Dissipation and the Fundamental Plane: Observational Tests." ApJ 689.1, 17–48. DOI: 10.1086/592105. arXiv: 0806.3974 [astro-ph].

Hopkins, P. F., D. Narayanan, and N. Murray (July 2013). "The meaning and consequences of star formation criteria in galaxy models with resolved stellar feedback." MNRAS 432.4, 2647–2653. DOI: 10.1093/mnras/stt723. arXiv: 1303.0285 [astro-ph.CO].

Hopkins, P. F. and E. Quataert (Feb. 2011). "An explanation for the slopes of stellar cusps in galaxy spheroids." MNRAS 411.1, L61–L65. DOI: 10.1111/j.1745-3933.2010.00995.x. arXiv: 1011.3045 [astro-ph.CO].

Hopkins, P. F. and M. J. Raives (Jan. 2016). "Accurate, meshless methods for magnetohydrodynamics." MNRAS 455.1, 51–88. DOI: 10.1093/mnras/stv2180. arXiv: 1505.02783 [astro-ph.IM].

Hopkins, P. F., J. Squire, and I. S. Butsky (Jan. 2022a). "A consistent reduced-speed-of-light formulation of cosmic ray transport valid in weak- and strong-scattering regimes." MNRAS 509.3, 3779–3797. DOI: 10.1093/mnras/stab2635. arXiv: 2103.10443 [astro-ph.HE].

Hopkins, P. F. et al. (May 2008b). "Dissipation and Extra Light in Galactic Nuclei. I. Gas-Rich Merger Remnants." ApJ 679.1, 156–181. DOI: 10.1086/587544. arXiv: 0802.0508 [astro-ph].

Hopkins, P. F. et al. (Mar. 2009a). "Dissipation and Extra Light in Galactic Nuclei. II. "Cusp" Ellipticals." ApJS 181.1, 135–182. DOI: 10.1088/0067-0049/181/1/135. arXiv: 0805.3533 [astro-ph].

Hopkins, P. F. et al. (Feb. 2009b). "Dissipation and Extra Light in Galactic Nuclei. IV. Evolution in the Scaling Relations of Spheroids." ApJ 691.2, 1424–1458. DOI: 10.1088/0004-637X/691/2/1424. arXiv: 0807.2868 [astro-ph].

Hopkins, P. F. et al. (Jan. 2010). "A maximum stellar surface density in dense stellar systems." MNRAS 401.1, L19–L23. DOI: 10.1111/j.1745-3933.2009.00777.x. arXiv: 0908.4088 [astro-ph.CO].

Hopkins, P. F. et al. (May 2016). "Stellar and quasar feedback in concert: effects on AGN accretion, obscuration, and outflows." MNRAS 458.1, 816–831. DOI: 10.1093/mnras/stw289. arXiv: 1504.05209 [astro-ph.GA].

Hopkins, P. F. et al. (Oct. 2018a). "FIRE-2 simulations: physics versus numerics in galaxy formation." MNRAS 480.1, 800–863. DOI: 10.1093/mnras/sty1690. arXiv: 1702.06148 [astro-ph.GA].

Hopkins, P. F. et al. (June 2018b). "How to model supernovae in simulations of star and galaxy formation." MNRAS 477.2, 1578–1603. DOI: 10.1093/mnras/sty674. arXiv: 1707.07010 [astro-ph.GA].

Hopkins, P. F. et al. (Mar. 2020a). "But what about...: cosmic rays, magnetic fields, conduction, and viscosity in galaxy formation." MNRAS 492.3, 3465–3498. DOI: 10.1093/mnras/stz3321. arXiv: 1905.04321 [astro-ph.GA].

Hopkins, P. F. et al. (Jan. 2020b). "Radiative stellar feedback in galaxy formation: Methods and physics." MNRAS 491.3, 3702–3729. DOI: 10.1093/mnras/stz3129. arXiv: 1811.12462 [astro-ph.GA].

Hopkins, P. F. et al. (Nov. 2022b). "First predicted cosmic ray spectra, primary-to-secondary ratios, and ionization rates from MHD galaxy formation simulations." MNRAS 516.3, 3470–3514. DOI: 10.1093/mnras/stac1791. arXiv: 2109.09762 [astro-ph.HE].

Hopkins, P. F. et al. (Feb. 2023). "FIRE-3: updated stellar evolution models, yields, and microphysics and fitting functions for applications in galaxy simulations." MNRAS 519.2, 3154–3181. DOI: 10.1093/mnras/stac3489. arXiv: 2203.00040 [astro-ph.GA].

Hosokawa, T. et al. (Dec. 2013). "Formation of Primordial Supermassive Stars by Rapid Mass Accretion." ApJ 778.2, 178, 178. DOI: 10.1088/0004-637X/778/2/178. arXiv: 1308.4457 [astro-ph.SR].

Hoyle, F. and R. A. Lyttleton (Jan. 1939). "The effect of interstellar matter on climatic variation." *Proceedings of the Cambridge Philosophical Society* 35.3, 405. DOI: 10.1017/S0305004100021150.

Hu, H. et al. (Aug. 2022). "Long-term Evolution of Supercritical Black Hole Accretion with Outflows: A Subgrid Feedback Model for Cosmological Simulations." ApJ 934.2, 132, 132. DOI: 10.3847/1538-4357/ac75d8. arXiv: 2203.14994 [astro-ph.HE].

Huang, K.-W. et al. (Aug. 2018). "BLUETIDES simulation: establishing black hole-galaxy relations at high redshift." MNRAS 478.4, 5063–5073. DOI: 10.1093/mnras/sty1329. arXiv: 1801.04951 [astro-ph.GA].

Inayoshi, K., Z. Haiman, and J. P. Ostriker (July 2016). "Hyper-Eddington accretion flows on to massive black holes." MNRAS 459.4, 3738–3755. DOI: 10.1093/mnras/stw836. arXiv: 1511.02116 [astro-ph.HE].

Inayoshi, K., E. Visbal, and Z. Haiman (Aug. 2020). "The Assembly of the First Massive Black Holes." ARA&A 58, 27–97. DOI: 10.1146/annurev-astro-120419-014455. arXiv: 1911.05791 [astro-ph.GA].

Ishibashi, W. and A. C. Fabian (Feb. 2023). "AGN cool feedback and analogy with X-ray binaries: from radiation pressure to cosmic ray-driven outflows." MNRAS 519.2, 1931–1940. DOI: 10.1093/mnras/stac3638. arXiv: 2212.06199 [astro-ph.HE].

Jiang, Y.-F., J. M. Stone, and S. W. Davis (Dec. 2014). "A Global Three-dimensional Radiation Magneto-hydrodynamic Simulation of Super-Eddington Accretion Disks." ApJ 796.2, 106, 106. DOI: 10.1088/0004-637X/796/2/106. arXiv: 1410.0678 [astro-ph.HE].

– (Aug. 2019). "Super-Eddington Accretion Disks around Supermassive Black Holes." ApJ 880.2, 67, 67. DOI: 10.3847/1538-4357/ab29ff. arXiv: 1709.02845 [astro-ph.HE].

Johnson, J. L. et al. (July 2013). "Supermassive Seeds for Supermassive Black Holes." ApJ 771.2, 116, 116. DOI: 10.1088/0004-637X/771/2/116. arXiv: 1211.0548 [astro-ph.CO].

Kaaret, P., H. Feng, and T. P. Roberts (Aug. 2017). "Ultraluminous X-Ray Sources." ARA&A 55.1, 303–341. DOI: 10.1146/annurev-astro-091916-055259. arXiv: 1703.10728 [astro-ph.HE].

Kamann, S. et al. (Apr. 2016). "MUSE crowded field 3D spectroscopy of over 12 000 stars in the globular cluster NGC 6397. II. Probing the internal dynamics and the presence of a central black hole." A&A 588, A149, A149. DOI: 10.1051/0004-6361/201527065. arXiv: 1602.01643 [astro-ph.SR].

Kennicutt Robert C., J. (May 1998). "The Global Schmidt Law in Star-forming Galaxies." ApJ 498.2, 541–552. DOI: 10.1086/305588. arXiv: astro-ph/9712213 [astro-ph].

Kim, J.-G., W.-T. Kim, and E. C. Ostriker (May 2018). "Modeling UV Radiation Feedback from Massive Stars. II. Dispersal of Star-forming Giant Molecular Clouds by Photoionization and Radiation Pressure." ApJ 859.1, 68, 68. DOI: 10.3847/1538-4357/aabe27. arXiv: 1804.04664 [astro-ph.GA].

Kim, J.-G., E. C. Ostriker, and N. Filippova (Apr. 2021). "Star Formation Efficiency and Dispersal of Giant Molecular Clouds with UV Radiation Feedback: Dependence on Gravitational Boundedness and Magnetic Fields." ApJ 911.2, 128, 128. DOI: 10.3847/1538-4357/abe934. arXiv: 2011.07772 [astro-ph.GA].

King, A. R. (Mar. 2010). "Black hole outflows." MNRAS 402.3, 1516–1522. DOI: 10.1111/j.1365-2966.2009.16013.x. arXiv: 0911.1639 [astro-ph.CO].

Kirsten, F. and W. H. T. Vlemmings (June 2012). "No evidence for a central IMBH in M 15." A&A 542, A44, A44. DOI: 10.1051/0004-6361/201218928. arXiv: 1204.4457 [astro-ph.GA].

Kitaki, T. et al. (Apr. 2021). "The origins and impact of outflow from super-Eddington flow." PASJ 73.2, 450–466. DOI: 10.1093/pasj/psab011.

Kızıltan, B., H. Baumgardt, and A. Loeb (Feb. 2017). "An intermediate-mass black hole in the centre of the globular cluster 47 Tucanae." Nature 542.7640, 203–205. DOI: 10.1038/nature21361. arXiv: 1702.02149 [astro-ph.GA].

Klessen, R. S. (June 2000). "One-Point Probability Distribution Functions of Supersonic Turbulent Flows in Self-gravitating Media." ApJ 535.2, 869–886. DOI: 10.1086/308854. arXiv: astro-ph/0001379 [astro-ph].

Koliopanos, F. (June 2017). "Intermediate Mass Black Holes: A Review." In: *XII Multifrequency Behaviour of High Energy Cosmic Sources Workshop (MULTIF2017)*, 51, 51. DOI: 10.22323/1.306.0051. arXiv: 1801.01095 [astro-ph.GA].

Konstandin, L. et al. (Feb. 2012). "Statistical properties of supersonic turbulence in the Lagrangian and Eulerian frameworks." *Journal of Fluid Mechanics* 692, 183–206. DOI: 10.1017/jfm.2011.503. arXiv: 1111.2748 [physics.flu-dyn].

Kormendy, J. and L. C. Ho (Aug. 2013). "Coevolution (Or Not) of Supermassive Black Holes and Host Galaxies." ARA&A 51.1, 511–653. DOI: 10.1146/annurev-astro-082708-101811. arXiv: 1304.7762 [astro-ph.CO].

Kormendy, J. et al. (May 2009). "Structure and Formation of Elliptical and Spheroidal Galaxies." ApJS 182.1, 216–309. DOI: 10.1088/0067-0049/182/1/216. arXiv: 0810.1681 [astro-ph].

Kremer, K. et al. (Nov. 2020). "Populating the Upper Black Hole Mass Gap through Stellar Collisions in Young Star Clusters." ApJ 903.1, 45, 45. DOI: 10.3847/1538-4357/abb945. arXiv: 2006.10771 [astro-ph.HE].

Kroupa, P. (Apr. 2001). "On the variation of the initial mass function." MNRAS 322.2, 231–246. DOI: 10.1046/j.1365-8711.2001.04022.x. arXiv: astro-ph/0009005 [astro-ph].

Krumholz, M. R. (Nov. 2015). "Notes on Star Formation." *arXiv e-prints*, arXiv:1511.03457, arXiv:1511.03457. DOI: 10.48550/arXiv.1511.03457. arXiv: 1511.03457 [astro-ph.GA].

Krumholz, M. R. and A. Dekel (July 2010). "Survival of star-forming giant clumps in high-redshift galaxies." MNRAS 406.1, 112–120. DOI: 10.1111/j.1365-2966.2010.16675.x. arXiv: 1001.0765 [astro-ph.CO].

Krumholz, M. R., C. F. McKee, and R. I. Klein (Feb. 2006). "Bondi-Hoyle Accretion in a Turbulent Medium." ApJ 638.1, 369–381. DOI: 10.1086/498844. arXiv: astro-ph/0510410 [astro-ph].

Lane, H. B. et al. (Mar. 2022). "Less wrong: a more realistic initial condition for simulations of turbulent molecular clouds." MNRAS 510.4, 4767–4778. DOI: 10.1093/mnras/stab3739. arXiv: 2110.14816 [astro-ph.GA].

Lanzoni, B. et al. (June 2013). "The Velocity Dispersion Profile of NGC 6388 from Resolved-star Spectroscopy: No Evidence of a Central Cusp and New Constraints on the Black Hole Mass." ApJ 769.2, 107, 107. DOI: 10.1088/0004-637X/769/2/107. arXiv: 1304.2953 [astro-ph.SR].

Larson, R. B. (Mar. 1981). "Turbulence and star formation in molecular clouds." MNRAS 194, 809–826. DOI: 10.1093/mnras/194.4.809.

Larson, R. B. and S. Starrfield (July 1971). "On the formation of massive stars and the upper limit of stellar masses." A&A 13, 190.

Latif, M. A. et al. (July 2022). "Turbulent cold flows gave birth to the first quasars." Nature 607.7917, 48–51. DOI: 10.1038/s41586-022-04813-y. arXiv: 2207.05093 [astro-ph.GA].

Lauer, T. R. et al. (July 2007). "The Centers of Early-Type Galaxies with Hubble Space Telescope. VI. Bimodal Central Surface Brightness Profiles." ApJ 664.1, 226–256. DOI: 10.1086/519229. arXiv: astro-ph/0609762 [astro-ph].

Li, H. et al. (July 2019). "Disruption of giant molecular clouds and formation of bound star clusters under the influence of momentum stellar feedback." MNRAS 487.1, 364–380. DOI: 10.1093/mnras/stz1271. arXiv: 1904.11987 [astro-ph.GA].

Li, L.-X. (Aug. 2012). "Accretion, growth of supermassive black holes, and feedback in galaxy mergers." MNRAS 424.2, 1461–1470. DOI: 10.1111/j.1365-2966.2012.21336.x. arXiv: 1205.0363 [astro-ph.CO].

Li, Y. et al. (Aug. 2007). "Formation of z$\backsim$6 Quasars from Hierarchical Galaxy Mergers." ApJ 665.1, 187–208. DOI: 10.1086/519297. arXiv: astro-ph/0608190 [astro-ph].

Liu, T., W.-M. Gu, and B. Zhang (Nov. 2017). "Neutrino-dominated accretion flows as the central engine of gamma-ray bursts." New A Rev. 79, 1–25. DOI: 10.1016/j.newar.2017.07.001. arXiv: 1705.05516 [astro-ph.HE].

Lupi, A. et al. (Mar. 2016). "Growing massive black holes through supercritical accretion of stellar-mass seeds." MNRAS 456.3, 2993–3003. DOI: 10.1093/mnras/stv2877. arXiv: 1512.02651 [astro-ph.GA].

Lützgendorf, N. et al. (Apr. 2013). "Limits on intermediate-mass black holes in six Galactic globular clusters with integral-field spectroscopy." A&A 552, A49, A49. DOI: 10.1051/0004-6361/201220307. arXiv: 1212.3475 [astro-ph.GA].

Lützgendorf, N. et al. (Sept. 2015). "Re-evaluation of the central velocity-dispersion profile in NGC 6388." A&A 581, A1, A1. DOI: 10.1051/0004-6361/201425524. arXiv: 1507.02813 [astro-ph.GA].

Ma, L. et al. (Dec. 2021). "Seeds don't sink: even massive black hole 'seeds' cannot migrate to galaxy centres efficiently." MNRAS 508.2, 1973–1985. DOI: 10.1093/mnras/stab2713. arXiv: 2101.02727 [astro-ph.GA].

Ma, X. et al. (Aug. 2018). "Simulating galaxies in the reionization era with FIRE-2: galaxy scaling relations, stellar mass functions, and luminosity functions." MNRAS 478.2, 1694–1715. DOI: 10.1093/mnras/sty1024. arXiv: 1706.06605 [astro-ph.GA].

Ma, X. et al. (Aug. 2019). "Dust attenuation, dust emission, and dust temperature in galaxies at z ≥ 5: a view from the FIRE-2 simulations." MNRAS 487.2, 1844–1864. DOI: 10.1093/mnras/stz1324. arXiv: 1902.10152 [astro-ph.GA].

Ma, X. et al. (Apr. 2020). "Self-consistent proto-globular cluster formation in cosmological simulations of high-redshift galaxies." MNRAS 493.3, 4315–4332. DOI: 10.1093/mnras/staa527. arXiv: 1906.11261 [astro-ph.GA].

Mac Low, M.-M. and R. S. Klessen (Jan. 2004). "Control of star formation by supersonic turbulence." *Reviews of Modern Physics* 76.1, 125–194. DOI: 10.1103/RevModPhys.76.125. arXiv: astro-ph/0301093 [astro-ph].

Madau, P. (Apr. 1988). "Thick Accretion Disks around Black Holes and the UV/Soft X-Ray Excess in Quasars." ApJ 327, 116. DOI: 10.1086/166175.

Madau, P., F. Haardt, and M. Dotti (Apr. 2014). "Super-critical Growth of Massive Black Holes from Stellar-mass Seeds." ApJ 784.2, L38, L38. DOI: 10.1088/2041-8205/784/2/L38. arXiv: 1402.6995 [astro-ph.CO].

Madau, P. and M. J. Rees (Apr. 2001). "Massive Black Holes as Population III Remnants." ApJ 551.1, L27–L30. DOI: 10.1086/319848. arXiv: astro-ph/0101223 [astro-ph].

Mann, C. R. et al. (Apr. 2019). "A Multimass Velocity Dispersion Model of 47 Tucanae Indicates No Evidence for an Intermediate-mass Black Hole." ApJ 875.1, 1, 1. DOI: 10.3847/1538-4357/ab0e6d. arXiv: 1807.03307 [astro-ph.GA].

Massonneau, W. et al. (Feb. 2023). "How the super-Eddington regime regulates black hole growth in high-redshift galaxies." A&A 670, A180, A180. DOI: 10.1051/0004-6361/202243170. arXiv: 2201.08766 [astro-ph.GA].

Mayer, L. (2019). "Super-Eddington accretion; flow regimes and conditions in high-z galaxies." In: *Formation of the First Black Holes*. Ed. by M. Latif and D. Schleicher, 195–222. DOI: 10.1142/9789813227958_0011.

McCrady, N. and J. R. Graham (July 2007). "Super Star Cluster Velocity Dispersions and Virial Masses in the M82 Nuclear Starburst." ApJ 663.2, 844–856. DOI: 10.1086/518357. arXiv: 0704.0478 [astro-ph].

McKee, C. F. and E. C. Ostriker (Sept. 2007). "Theory of Star Formation." ARA&A 45.1, 565–687. DOI: 10.1146/annurev.astro.45.051806.110602. arXiv: 0707.3514 [astro-ph].

Mercedes-Feliz, J. et al. (Jan. 2023). "Local positive feedback in the overall negative: the impact of quasar winds on star formation in the FIRE cosmological simulations." *arXiv e-prints*, arXiv:2301.01784, arXiv:2301.01784. DOI: 10.48550/arXiv.2301.01784. arXiv: 2301.01784 [astro-ph.GA].

Merloni, A., S. Heinz, and T. di Matteo (Nov. 2003). "A Fundamental Plane of black hole activity." MNRAS 345.4, 1057–1076. DOI: 10.1046/j.1365-2966.2003.07017.x. arXiv: astro-ph/0305261 [astro-ph].

Mezcua, M. (Jan. 2017). "Observational evidence for intermediate-mass black holes." *International Journal of Modern Physics D* 26.11, 1730021, 1730021. DOI: 10.1142/S021827181730021X. arXiv: 1705.09667 [astro-ph.GA].

Miller, B. P. et al. (Jan. 2015). "X-Ray Constraints on the Local Supermassive Black Hole Occupation Fraction." ApJ 799.1, 98, 98. DOI: 10.1088/0004-637X/799/1/98. arXiv: 1403.4246 [astro-ph.GA].

Mottram, J. C. et al. (Apr. 2011). "The RMS Survey: The Luminosity Functions and Timescales of Massive Young Stellar Objects and Compact H II Regions." ApJ 730.2, L33, L33. DOI: 10.1088/2041-8205/730/2/L33. arXiv: 1102.4702 [astro-ph.GA].

Murray, D. W. et al. (Feb. 2017). "Collapse in self-gravitating turbulent fluids." MNRAS 465.2, 1316–1335. DOI: 10.1093/mnras/stw2796. arXiv: 1509.05910 [astro-ph.GA].

Murray, N., E. Quataert, and T. A. Thompson (Jan. 2005). "On the Maximum Luminosity of Galaxies and Their Central Black Holes: Feedback from Momentum-driven Winds." ApJ 618.2, 569–585. DOI: 10.1086/426067. arXiv: astro-ph/0406070 [astro-ph].

Narayan, R., I. V. Igumenshchev, and M. A. Abramowicz (Dec. 2003). "Magnetically Arrested Disk: an Energetically Efficient Accretion Flow." PASJ 55, L69–L72. DOI: 10.1093/pasj/55.6.L69. arXiv: astro-ph/0305029 [astro-ph].

Narayan, R. and I. Yi (June 1994). "Advection-dominated Accretion: A Self-similar Solution." ApJ 428, L13. DOI: 10.1086/187381. arXiv: astro-ph/9403052 [astro-ph].

Narayanan, D., T. J. Cox, and L. Hernquist (July 2008). "The Star Formation Rate-Dense Gas Relation in the Nuclei of Nearby Galaxies." ApJ 681.2, L77. DOI: 10.1086/590342. arXiv: 0805.4019 [astro-ph].

Narayanan, D. et al. (Mar. 2011). "The Kennicutt-Schmidt star formation relation at z~ 2." MNRAS 412.1, 287–294. DOI: 10.1111/j.1365-2966.2010.17903.x. arXiv: 1005.3020 [astro-ph.CO].

Nguyen, D. D. et al. (Feb. 2019). "Improved Dynamical Constraints on the Masses of the Central Black Holes in Nearby Low-mass Early-type Galactic Nuclei and the First Black Hole Determination for NGC 205." ApJ 872.1, 104, 104. DOI: 10.3847/1538-4357/aafe7a. arXiv: 1901.05496 [astro-ph.GA].

Noguchi, M. (Mar. 1999). "Early Evolution of Disk Galaxies: Formation of Bulges in Clumpy Young Galactic Disks." ApJ 514.1, 77–95. DOI: 10.1086/306932. arXiv: astro-ph/9806355 [astro-ph].

Nyland, K. et al. (July 2012). "The Intermediate-mass Black Hole Candidate in the Center of NGC 404: New Evidence from Radio Continuum Observations." ApJ 753.2, 103, 103. DOI: 10.1088/0004-637X/753/2/103. arXiv: 1204.3089 [astro-ph.GA].

Ohsuga, K. et al. (July 2005). "Supercritical Accretion Flows around Black Holes: Two-dimensional, Radiation Pressure-dominated Disks with Photon Trapping." ApJ 628.1, 368–381. DOI: 10.1086/430728. arXiv: astro-ph/0504168 [astro-ph].

Omukai, K. (Jan. 2001). "Primordial Star Formation under Far-Ultraviolet Radiation." ApJ 546.2, 635–651. DOI: 10.1086/318296. arXiv: astro-ph/0011446 [astro-ph].

Orr, M. E. et al. (Aug. 2018). "What FIREs up star formation: the emergence of the Kennicutt-Schmidt law from feedback." MNRAS 478.3, 3653–3673. DOI: 10.1093/mnras/sty1241. arXiv: 1701.01788 [astro-ph.GA].

Padoan, P., A. Nordlund, and B. J. T. Jones (June 1997). "The universality of the stellar initial mass function." MNRAS 288.1, 145–152. DOI: 10.1093/mnras/288.1.145. arXiv: astro-ph/9703110 [astro-ph].

Page, M. J. et al. (May 2012). "The suppression of star formation by powerful active galactic nuclei." Nature 485.7397, 213–216. DOI: 10.1038/nature11096. arXiv: 1310.4147 [astro-ph.CO].

Park, K., G. Chiaki, and J. H. Wise (Sept. 2022). "Accelerated Growth of Seed Black Holes by Dust in the Early Universe." ApJ 936.2, 116, 116. DOI: 10.3847/1538-4357/ac886c. arXiv: 2201.06584 [astro-ph.GA].

Park, K. et al. (Dec. 2020). "Biconical-dominated Accretion Flow onto Seed Black Holes in a Hyperaccretion Regime." ApJ 905.2, 92, 92. DOI: 10.3847/1538-4357/abc336. arXiv: 2006.06781 [astro-ph.GA].

Passot, T., A. Pouquet, and P. Woodward (May 1988). "The plausibility of Kolmogorov-type spectra in molecular clouds." A&A 197.1-2, 228–234.

Perera, B. B. P. et al. (June 2017). "Evidence for an intermediate-mass black hole in the globular cluster NGC 6624." MNRAS 468.2, 2114–2127. DOI: 10.1093/mnras/stx501. arXiv: 1705.01612 [astro-ph.HE].

Peterson, B. M. et al. (Oct. 2005). "Multiwavelength Monitoring of the Dwarf Seyfert 1 Galaxy NGC 4395. I. A Reverberation-based Measurement of the Black Hole Mass." ApJ 632.2, 799–808. DOI: 10.1086/444494. arXiv: astro-ph/0506665 [astro-ph].

Petts, J. A. and A. Gualandris (June 2017). "Infalling young clusters in the Galactic Centre: implications for IMBHs and young stellar populations." MNRAS 467.4, 3775–3787. DOI: 10.1093/mnras/stx296. arXiv: 1701.07440 [astro-ph.GA].

Pezzulli, E., R. Valiante, and R. Schneider (May 2016). "Super-Eddington growth of the first black holes." MNRAS 458.3, 3047–3059. DOI: 10.1093/mnras/stw505. arXiv: 1603.00475 [astro-ph.GA].

Popham, R., S. E. Woosley, and C. Fryer (June 1999). "Hyperaccreting Black Holes and Gamma-Ray Bursts." ApJ 518.1, 356–374. DOI: 10.1086/307259. arXiv: astro-ph/9807028 [astro-ph].

Portegies Zwart, S. F. and S. L. W. McMillan (Sept. 2002). "The Runaway Growth of Intermediate-Mass Black Holes in Dense Star Clusters." ApJ 576.2, 899–907. DOI: 10.1086/341798. arXiv: astro-ph/0201055 [astro-ph].

Portegies Zwart, S. F. et al. (Apr. 2004). "Formation of massive black holes through runaway collisions in dense young star clusters." Nature 428.6984, 724–726. DOI: 10.1038/nature02448. arXiv: astro-ph/0402622 [astro-ph].

Quataert, E. and A. Gruzinov (Aug. 2000). "Convection-dominated Accretion Flows." ApJ 539.2, 809–814. DOI: 10.1086/309267. arXiv: astro-ph/9912440 [astro-ph].

Regan, J. A. et al. (Mar. 2017). "Rapid formation of massive black holes in close proximity to embryonic protogalaxies." *Nature Astronomy* 1, 0075, 0075. DOI: 10.1038/s41550-017-0075. arXiv: 1703.03805 [astro-ph.GA].

Regan, J. A. et al. (July 2019). "Super-Eddington accretion and feedback from the first massive seed black holes." MNRAS 486.3, 3892–3906. DOI: 10.1093/mnras/stz1045. arXiv: 1811.04953 [astro-ph.GA].

Rejkuba, M. et al. (July 2007). "Bright globular clusters in NGC 5128: the missing link between young massive clusters and evolved massive objects." A&A 469.1, 147–162. DOI: 10.1051/0004-6361:20066493. arXiv: astro-ph/0703385 [astro-ph].

Rizzuto, F. P. et al. (Mar. 2021). "Intermediate mass black hole formation in compact young massive star clusters." MNRAS 501.4, 5257–5273. DOI: 10.1093/mnras/staa3634. arXiv: 2008.09571 [astro-ph.GA].

Rothberg, B. and R. D. Joseph (Nov. 2004). "A Deep K-Band Photometric Survey of Merger Remnants." AJ 128.5, 2098–2143. DOI: 10.1086/425049.

Ryon, J. E. et al. (Sept. 2015). "Sizes and shapes of young star cluster light profiles in M83." MNRAS 452.1, 525–539. DOI: 10.1093/mnras/stv1282. arXiv: 1506.02042 [astro-ph.GA].

Ryon, J. E. et al. (June 2017). "Effective Radii of Young, Massive Star Clusters in Two LEGUS Galaxies." ApJ 841.2, 92, 92. DOI: 10.3847/1538-4357/aa719e. arXiv: 1705.02692 [astro-ph.GA].

Ryu, T. et al. (Aug. 2016). "Intermediate-mass black holes from Population III remnants in the first galactic nuclei." MNRAS 460.4, 4122–4134. DOI: 10.1093/mnras/stw1241. arXiv: 1603.08513 [astro-ph.GA].

Sądowski, A. (Aug. 2009). "Slim Disks Around Kerr Black Holes Revisited." ApJS 183.2, 171–178. DOI: 10.1088/0067-0049/183/2/171. arXiv: 0906.0355 [astro-ph.HE].

Sądowski, A. et al. (Feb. 2015). "Global simulations of axisymmetric radiative black hole accretion discs in general relativity with a mean-field magnetic dynamo." MNRAS 447.1, 49–71. DOI: 10.1093/mnras/stu2387. arXiv: 1407.4421 [astro-ph.HE].

Sądowski, A. et al. (Mar. 2016). "Energy flows in thick accretion discs and their consequences for black hole feedback." MNRAS 456.4, 3915–3928. DOI: 10.1093/mnras/stv2854. arXiv: 1510.08845 [astro-ph.HE].

Sakurai, Y. et al. (Dec. 2017). "Formation of intermediate-mass black holes through runaway collisions in the first star clusters." MNRAS 472.2, 1677–1684. DOI: 10.1093/mnras/stx2044. arXiv: 1704.06130 [astro-ph.GA].

Sanders, D. B. et al. (Feb. 1988). "Ultraluminous Infrared Galaxies and the Origin of Quasars." ApJ 325, 74. DOI: 10.1086/165983.

Scalo, J. et al. (Sept. 1998). "On the Probability Density Function of Galactic Gas. I. Numerical Simulations and the Significance of the Polytropic Index." ApJ 504.2, 835–853. DOI: 10.1086/306099. arXiv: astro-ph/9710075 [astro-ph].

Schawinski, K. et al. (Aug. 2006). "Suppression of star formation in early-type galaxies by feedback from supermassive black holes." Nature 442.7105, 888–891. DOI: 10.1038/nature04934. arXiv: astro-ph/0608517 [astro-ph].

Schleicher, D. R. G. et al. (Oct. 2013). "Massive black hole factories: Supermassive and quasi-star formation in primordial halos." A&A 558, A59, A59. DOI: 10.1051/0004-6361/201321949. arXiv: 1305.5923 [astro-ph.CO].

Shakura, N. I. and R. A. Sunyaev (Jan. 1973). "Black holes in binary systems. Observational appearance." A&A 24, 337–355.

Shi, Y., M. Y. Grudić, and P. F. Hopkins (Aug. 2021). "The mass budget for intermediate-mass black holes in dense star clusters." MNRAS 505.2, 2753–2763. DOI: 10.1093/mnras/stab1470. arXiv: 2008.12290 [astro-ph.GA].

Shi, Y., K. Kremer, and P. F. Hopkins (June 2023a). "Hyper-Eddington black hole growth in star-forming molecular clouds and galactic nuclei: feedback self-regulation." *in prep.*

Shi, Y. et al. (Jan. 2023b). "Hyper-Eddington black hole growth in star-forming molecular clouds and galactic nuclei: can it happen?" MNRAS 518.3, 3606–3621. DOI: 10.1093/mnras/stac3245. arXiv: 2208.05025 [astro-ph.GA].

Sijacki, D. et al. (July 2008). "Simulations of cosmic-ray feedback by active galactic nuclei in galaxy clusters." MNRAS 387.4, 1403–1415. DOI: 10.1111/j.1365-2966.2008.13310.x. arXiv: 0801.3285 [astro-ph].

Sikora, M. (July 1981). "Superluminous Accretion Discs." MNRAS 196, 257. DOI: 10.1093/mnras/196.2.257.

Silk, J. and M. J. Rees (Mar. 1998). "Quasars and galaxy formation." A&A 331, L1–L4. DOI: 10.48550/arXiv.astro-ph/9801013. arXiv: astro-ph/9801013 [astro-ph].

Smith, A. and V. Bromm (Apr. 2019). "Supermassive black holes in the early universe." *Contemporary Physics* 60.2, 111–126. DOI: 10.1080/00107514.2019.1615715. arXiv: 1904.12890 [astro-ph.GA].

Sollima, A. and H. Baumgardt (Nov. 2017). "The global mass functions of 35 Galactic globular clusters: I. Observational data and correlations with cluster parameters." MNRAS 471.3, 3668–3679. DOI: 10.1093/mnras/stx1856. arXiv: 1708.09529 [astro-ph.GA].

Spera, M. and M. Mapelli (Oct. 2017). "Very massive stars, pair-instability supernovae and intermediate-mass black holes with the sevn code." MNRAS 470.4, 4739–4749. DOI: 10.1093/mnras/stx1576. arXiv: 1706.06109 [astro-ph.SR].

Squire, J. and P. F. Hopkins (Nov. 2017). "The distribution of density in supersonic turbulence." MNRAS 471.3, 3753–3767. DOI: 10.1093/mnras/stx1817. arXiv: 1702.07731 [astro-ph.GA].

Stanimirovic, S. et al. (Jan. 1999). "The large-scale HI structure of the Small Magellanic Cloud." MNRAS 302.3, 417–436. DOI: 10.1046/j.1365-8711.1999.02013.x.

Su, K.-Y. et al. (Oct. 2021). "Which AGN jets quench star formation in massive galaxies?" MNRAS 507.1, 175–204. DOI: 10.1093/mnras/stab2021. arXiv: 2102.02206 [astro-ph.GA].

Tacconi, L. J. et al. (Nov. 2002). "Ultraluminous Infrared Galaxies: QSOs in Formation?" ApJ 580.1, 73–87. DOI: 10.1086/343075. arXiv: astro-ph/0207405 [astro-ph].

Tacconi, L. J. et al. (Feb. 2010). "High molecular gas fractions in normal massive star-forming galaxies in the young Universe." Nature 463.7282, 781–784. DOI: 10.1038/nature08773. arXiv: 1002.2149 [astro-ph.CO].

Tagawa, H., Z. Haiman, and B. Kocsis (Mar. 2020). "Making a Supermassive Star by Stellar Bombardment." ApJ 892.1, 36, 36. DOI: 10.3847/1538-4357/ab7922. arXiv: 1909.10517 [astro-ph.GA].

Takeo, E., K. Inayoshi, and S. Mineshige (Sept. 2020). "Hyper-Eddington accretion flows on to black holes accompanied by powerful outflows." MNRAS 497.1, 302–317. DOI: 10.1093/mnras/staa1906. arXiv: 2002.07187 [astro-ph.HE].

Takeo, E. et al. (May 2018). "Rapid growth of black holes accompanied with hot or warm outflows exposed to anisotropic super-Eddington radiation." MNRAS 476.1, 673–682. DOI: 10.1093/mnras/sty264. arXiv: 1705.05382 [astro-ph.HE].

Talbot, R. Y., M. A. Bourne, and D. Sijacki (July 2021). "Blandford-Znajek jets in galaxy formation simulations: method and implementation." MNRAS 504.3, 3619–3650. DOI: 10.1093/mnras/stab804. arXiv: 2011.10580 [astro-ph.GA].

Torrey, P. et al. (Oct. 2020). "The impact of AGN wind feedback in simulations of isolated galaxies with a multiphase ISM." MNRAS 497.4, 5292–5308. DOI: 10.1093/mnras/staa2222.

Tortosa, A. et al. (Jan. 2022). "The extreme properties of the nearby hyper-Eddington accreting active galactic nucleus in IRAS 04416+1215." MNRAS 509.3, 3599–3615. DOI: 10.1093/mnras/stab3152. arXiv: 2109.02573 [astro-ph.GA].

Toyouchi, D. et al. (Feb. 2019). "Super-Eddington accretion of dusty gas on to seed black holes: metallicity-dependent efficiency of mass growth." MNRAS 483.2, 2031–2043. DOI: 10.1093/mnras/sty3012. arXiv: 1811.01368 [astro-ph.GA].

Tremou, E. et al. (July 2018). "The MAVERIC Survey: Still No Evidence for Accreting Intermediate-mass Black Holes in Globular Clusters." ApJ 862.1, 16, 16. DOI: 10.3847/1538-4357/aac9b9. arXiv: 1806.00259 [astro-ph.HE].

Valiante, R. et al. (Apr. 2016). "From the first stars to the first black holes." MNRAS 457.3, 3356–3371. DOI: 10.1093/mnras/stw225. arXiv: 1601.07915 [astro-ph.GA].

van der Marel, R. P. and J. Anderson (Feb. 2010). "New Limits on an Intermediate-Mass Black Hole in Omega Centauri. II. Dynamical Models." ApJ 710.2, 1063–1088. DOI: 10.1088/0004-637X/710/2/1063. arXiv: 0905.0638 [astro-ph.GA].

van Dokkum, P. G. et al. (Apr. 2008). "Confirmation of the Remarkable Compactness of Massive Quiescent Galaxies at z ∼2.3: Early-Type Galaxies Did not Form in a Simple Monolithic Collapse." ApJ 677.1, L5. DOI: 10.1086/587874. arXiv: 0802.4094 [astro-ph].

Vazquez-Semadeni, E. (Mar. 1994). "Hierarchical Structure in Nearly Pressureless Flows as a Consequence of Self-similar Statistics." ApJ 423, 681. DOI: 10.1086/173847.

Vázquez-Semadeni, E., J. Ballesteros-Paredes, and R. S. Klessen (Mar. 2003). "A Holistic Scenario of Turbulent Molecular Cloud Evolution and Control of the Star Formation Efficiency: First Tests." ApJ 585.2, L131–L134. DOI: 10.1086/374325. arXiv: astro-ph/0301546 [astro-ph].

Volonteri, M. (July 2010). "Formation of supermassive black holes." A&A Rev. 18.3, 279–315. DOI: 10.1007/s00159-010-0029-x. arXiv: 1003.4404 [astro-ph.CO].

Volonteri, M. and M. C. Begelman (Dec. 2010). "Quasi-stars and the cosmic evolution of massive black holes." MNRAS 409.3, 1022–1032. DOI: 10.1111/j.1365-2966.2010.17359.x. arXiv: 1003.5220 [astro-ph.HE].

Volonteri, M., M. Habouzit, and M. Colpi (Sept. 2021). "The origins of massive black holes." *Nature Reviews Physics* 3.11, 732–743. DOI: 10.1038/s42254-021-00364-9. arXiv: 2110.10175 [astro-ph.GA].

Walcher, C. J. et al. (Jan. 2005). "Masses of Star Clusters in the Nuclei of Bulgeless Spiral Galaxies." ApJ 618.1, 237–246. DOI: 10.1086/425977. arXiv: astro-ph/0409216 [astro-ph].

Wang, F. et al. (Jan. 2021). "A Luminous Quasar at Redshift 7.642." ApJ 907.1, L1, L1. DOI: 10.3847/2041-8213/abd8c6. arXiv: 2101.03179 [astro-ph.GA].

Wang, L. et al. (May 2016). "The DRAGON simulations: globular cluster evolution with a million stars." MNRAS 458.2, 1450–1465. DOI: 10.1093/mnras/stw274. arXiv: 1602.00759 [astro-ph.SR].

Watarai, K.-y. et al. (Feb. 2000). "Galactic Black-Hole Candidates Shining at the Eddington Luminosity." PASJ 52, 133. DOI: 10.1093/pasj/52.1.133.

Webb, N. et al. (Aug. 2012). "Radio Detections During Two State Transitions of the Intermediate-Mass Black Hole HLX-1." *Science* 337.6094, 554. DOI: 10.1126/science.1222779. arXiv: 1311.6918 [astro-ph.HE].

Weinberger, R. et al. (Sept. 2018). "Supermassive black holes and their feedback effects in the IllustrisTNG simulation." MNRAS 479.3, 4056–4072. DOI: 10.1093/mnras/sty1733. arXiv: 1710.04659 [astro-ph.GA].

Wetzel, A. et al. (Apr. 2023). "Public Data Release of the FIRE-2 Cosmological Zoom-in Simulations of Galaxy Formation." ApJS 265.2, 44, 44. DOI: 10.3847/1538-4365/acb99a. arXiv: 2202.06969 [astro-ph.GA].

Yajima, H. et al. (Sept. 2017). "Dusty Gas Accretion onto Massive Black Holes and Infrared Diagnosis of the Eddington Ratio." ApJ 846.1, 3, 3. DOI: 10.3847/1538-4357/aa8269. arXiv: 1704.05567 [astro-ph.GA].

Yang, J. et al. (July 2020). "Pōniuā'ena: A Luminous z = 7.5 Quasar Hosting a 1.5 Billion Solar Mass Black Hole." ApJ 897.1, L14, L14. DOI: 10.3847/2041-8213/ab9c26. arXiv: 2006.13452 [astro-ph.GA].

Yu, Q., Y. Lu, and D. N. C. Lin (Sept. 2007). "On the Origin of the Kinematic Distribution of the Subparsec Young Stars in the Galactic Center." ApJ 666.2, 919–933. DOI: 10.1086/520622. arXiv: 0705.3649 [astro-ph].

Yu, Q. and S. Tremaine (Oct. 2002). "Observational constraints on growth of massive black holes." MNRAS 335.4, 965–976. DOI: 10.1046/j.1365-8711.2002.05532.x. arXiv: astro-ph/0203082 [astro-ph].

– (Dec. 2003). "Ejection of Hypervelocity Stars by the (Binary) Black Hole in the Galactic Center." ApJ 599.2, 1129–1138. DOI: 10.1086/379546. arXiv: astro-ph/0309084 [astro-ph].

Zhu, Q. et al. (Dec. 2020). "The Formation of the First Quasars. I. The Black Hole Seeds, Accretion and Feedback Models." *arXiv e-prints*, arXiv:2012.01458, arXiv:2012.01458. DOI: 10.48550/arXiv.2012.01458. arXiv: 2012.01458 [astro-ph.GA].

Zocchi, A., M. Gieles, and V. Hénault-Brunet (July 2017). "Radial anisotropy in ω Cen limiting the room for an intermediate-mass black hole." MNRAS 468.4, 4429–4440. DOI: 10.1093/mnras/stx316. arXiv: 1702.00725 [astro-ph.GA].

Zweibel, E. G. (May 2017). "The basis for cosmic ray feedback: Written on the wind." *Physics of Plasmas* 24.5, 055402, 055402. DOI: 10.1063/1.4984017.